Synthesis and Characterization of Poly-dentate C_3 Symmetric Ligand Systems in Metal Coordination

Dissertation

zur Erlangung des mathematisch-naturwissenschaftlichen Doktorgrades

” Doctor rerum naturalium “

der Georg-August-Universität Göttingen

im Promotionsprogramm Chemie

der Georg-August-University School of Science (GAUSS)

vorgelegt von

PETER STOLLBERG

aus Bernau

Göttingen, 2018

Thesis Committee

Prof. Dr. Dietmar Stalke	*Institute of Inorganic Chemistry,* *Georg-August-University, Göttingen*
Prof. Dr. Sven Schneider	*Institute of Inorganic Chemistry,* *Georg-August-University, Göttingen*

Members of the Examination Commission

Reviewer

Prof. Dr. Dietmar Stalke	*Institute of Inorganic Chemistry,* *Georg-August-University, Göttingen*

Reviewer

Prof. Dr. Sven Schneider	*Institute of Inorganic Chemistry,* *Georg-August-University, Göttingen*

Additional Members of the Examination Commission

Prof. Dr. Ulf Diederichsen	*Institute of Organic und Biomolecular Chemistry,* *Georg-August-University, Göttingen*
Dr. Christian Sindlinger	*Institute of Inorganic Chemistry,* *Georg-August-University, Göttingen*
Dr. Franziska Thomas	*Institute of Organic und Biomolecular Chemistry,* *Georg-August-University, Göttingen*
Dr. Heidrun Sowa	*Geoscience Center,* *Georg-August-University, Göttingen*

Day of the Oral Examination 10. August 2018

The work described in this doctoral thesis has been carried out under the guidance and supervision of PROF. DR. DIETMAR STALKE at the Institute of Inorganic Chemistry of the Georg-August-University, Göttingen between January 2013 and June 2018.

Synthesis and Characterization of Poly-dentate C_3 Symmetric Ligand Systems in Metal Coordination

to U. R. and L. St.

Publications

1. Roy, S.; Stollberg, P.; Herbst-Irmer, R.; Stalke, D.; Andrada, D. M.; Frenking, G.; Roesky, H. W. Journal of the American Chemical Society **2015**, *137*, 150-153.

2. Roy, S.; Mondal, K. C.; Krause, L.; Stollberg, P.; Herbst-Irmer, R.; Stalke, D.; Meyer, J.; Stückl, A. C.; Maity, B.; Koley, D.; Vasa, S. K.; Xiang, S. Q.; Linser, R.; Roesky, H. W. Journal of the American Chemical Society **2014**, *136*, 16776-16779.

3. Li, Y.; Mondal, K. C.; Stollberg, P.; Zhu, H.; Roesky, H. W.; Herbst-Irmer, R.; Stalke, D.; Fliegl, H. Chemical Communications **2014**, *50*, 3356-3358.

4. Kinauer, M.; Scheibel, M. G.; Abbenseth, J.; Heinemann, F. W.; Stollberg, P.; Wurtele, C.; Schneider, S. Dalton Transactions **2014**, *43*, 4506-4513.

5. Granitzka, M.; Stollberg, P.; Stalke, D. Zeitschrift für Naturforschung B **2014**, *69*, 1429-1440.

6. Scheibel, M. G.; Klopsch, I.; Wolf, H.; Stollberg, P.; Stalke, D.; Schneider, S. European Journal of Inorganic Chemistry **2013**, 3454-3457.

7. Li, Y.; Mondal, K. C.; Roesky, H. W.; Zhu, H.; Stollberg, P.; Herbst-Irmer, R.; Stalke, D.; Andrada, D. M. Journal of the American Chemical Society **2013**, *135*, 12422-12428.

TABLE OF CONTENTS

Abbreviation

Å	Ångstrom
aNHC	abnormal *N*-heterocyclic carbene
amu	atomic mass unit
CCDC	Cambridge Crystallographic Database
CSD	Cambridge Structural Database
*cy*Pr	Cyclopropyl
d	doublet
DCM	Dichloromethane
DMF	Dimethylformamide
DMSO	Dimethyl sulfoxide
EI	Electron ionization
ESI	Electrospray ionization
eq.	equivalents
et al.	*et alii,* and others
Et_2O	Diethyl ether
EtOH	Ethanol
h	hour
*i*Pr	Isopropyl
M	Molar
Me	Methyl
MeCN	Acetonitrile
MeOH	Methanol
Mes	Mesityl (2,4,6-trimethylphenyl)
MHz	Megahertz
MIC	Mesoionic carbene

MS	Mass spectrometry
m/z	mass/charge
NHC	*N*-heterocyclic carbene
NMR	Nuclear Magnetic Resonance
*n*Pr	n-Propyl
Ph	Phenyl
pKs	Acid dissociation constant
ppm	parts per million
R	any substituent if not defined otherwise
rNHC	remote *N*-heterocyclic carbene
rt	room temperature
s	singlet
*t*Bu	*tertiary* Butyl
TEP	Tolman Electronic Parameter
THF	Tetrahydrofuran
tol	Toluene
z	charge

List of Compounds

2.1 Iminophosphorane Ligand Systems

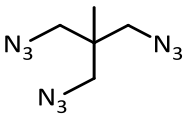

1

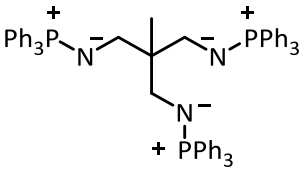

2

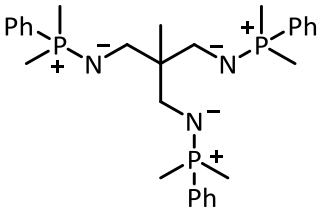

3

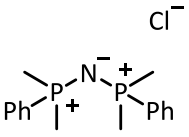

4

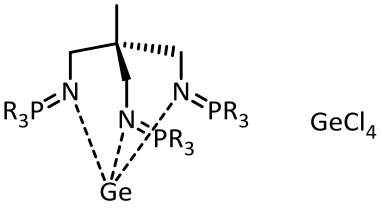

5

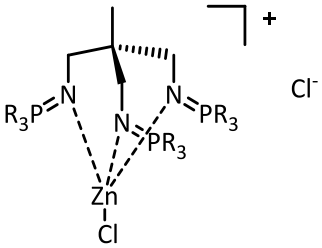

6

2.2 Tripodal Triazolic Ligand Systems with a Bridging Alkyl Backbone

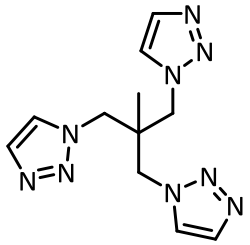

7

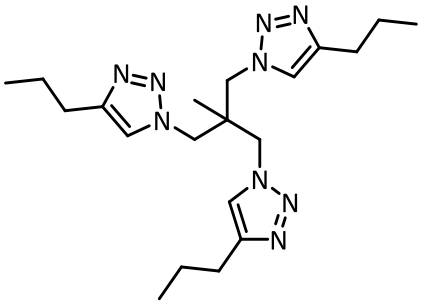

8

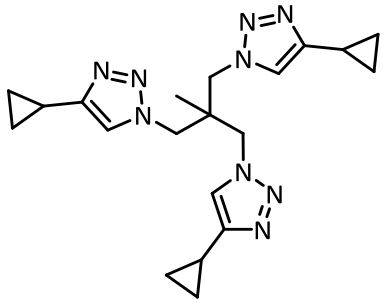

9

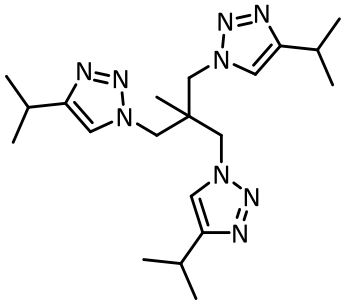

10

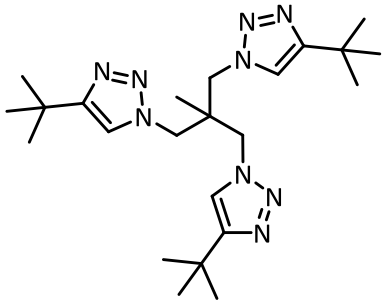

11

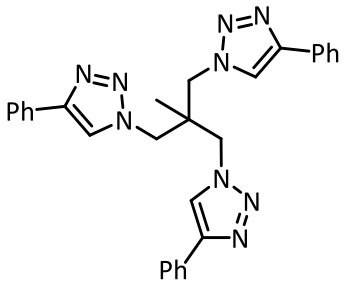

12

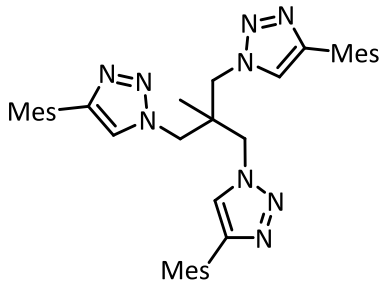

13

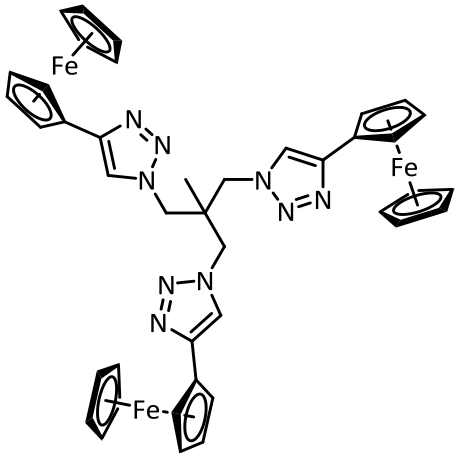

14

2.3 Tripodal Triazolic Ligand Systems with a Bridging π-System

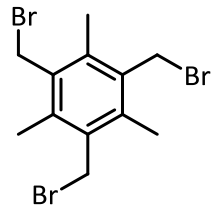

15

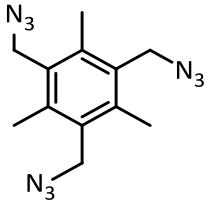

16

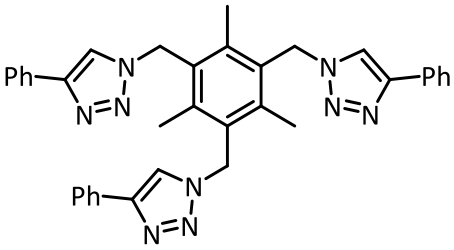

17

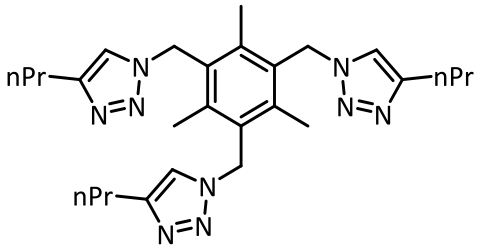

18

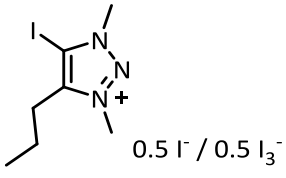

19

2.4.1 Triazolic Ring Activation via a Methylation Reaction

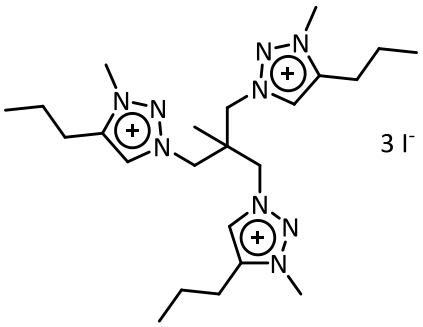

20

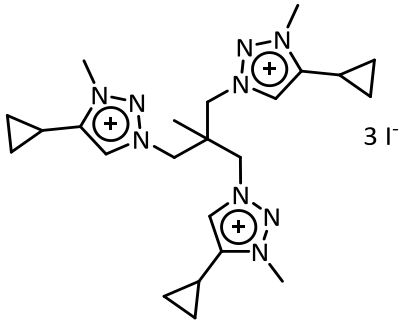

21

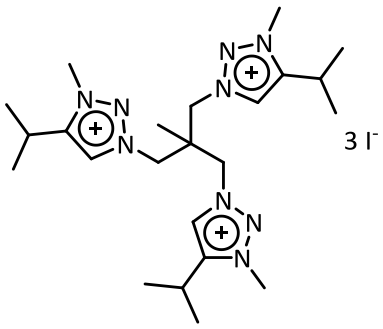

22

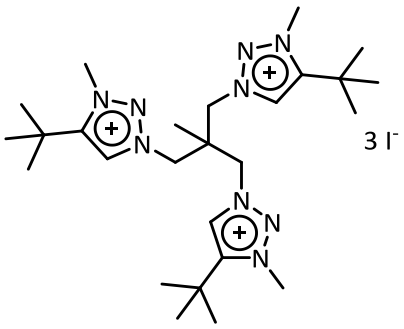

23

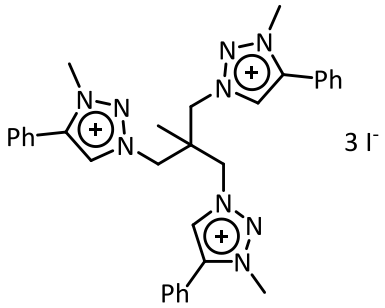

24

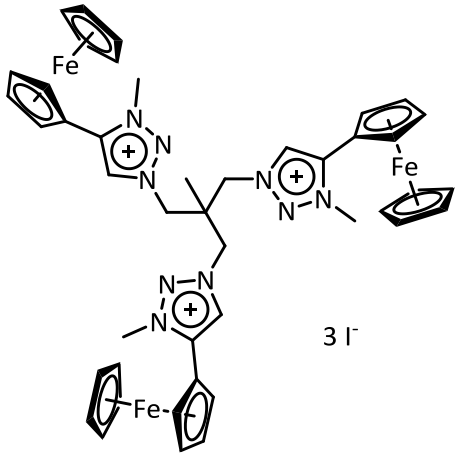

25

2.4.2 Ion Exchange Reactions to Weakly-Coordinating Anions

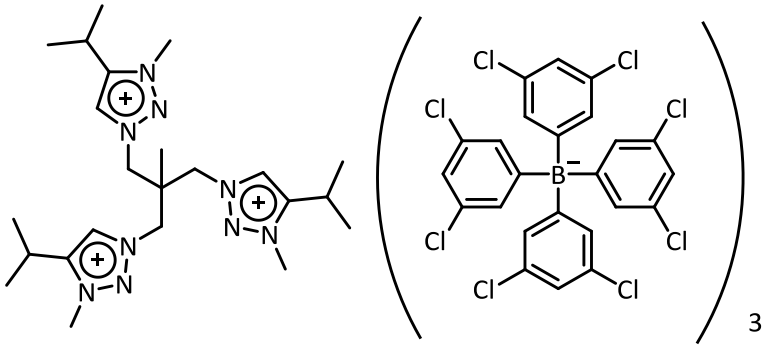

26

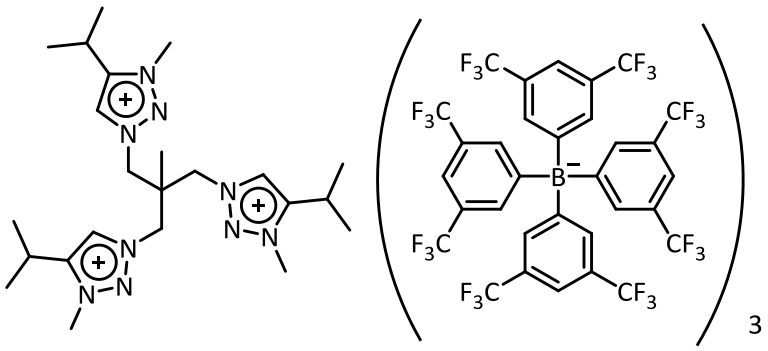

27

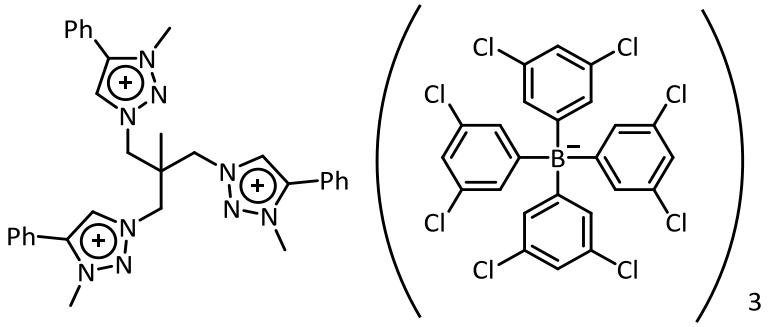

28

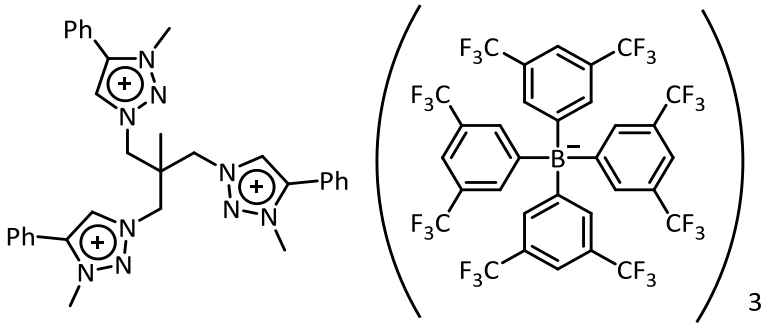

29

2.4.3 Selected Tripodal Triazolic Ligand Systems in Metal Coordination with Coinage Metals (Cu, Ag, Au)

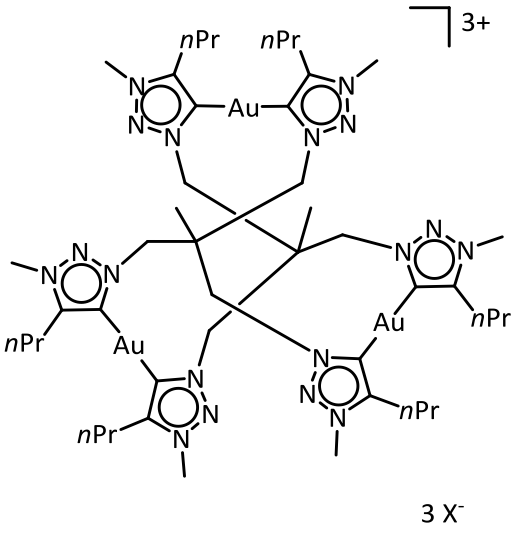

30

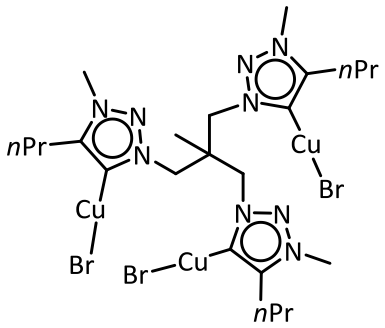

31

2.4.4 Selected Tripodal Triazolic Ligand System in Metal Coordination with Group 10 Transition Metals (Ni, Pd)

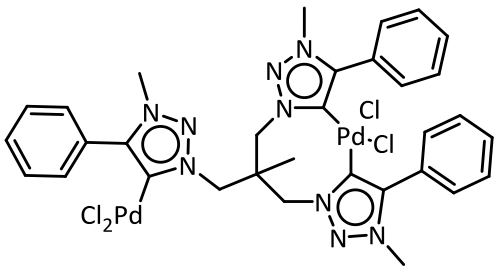

32

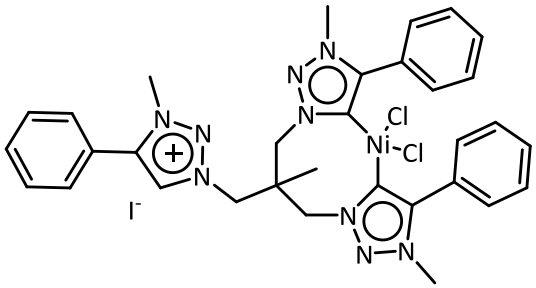

33

INTRODUCTION

1.1 Scope

Tripodal ligand systems with a tridentate coordination sphere can be used in a multitude of chemical reactions. Most prominently these type of systems can be found in classic coordination chemistry and may eventually lead to new achievements in catalyzed reactions.[1] Some examples of these type of compounds are shown in Figure 1.1.1.

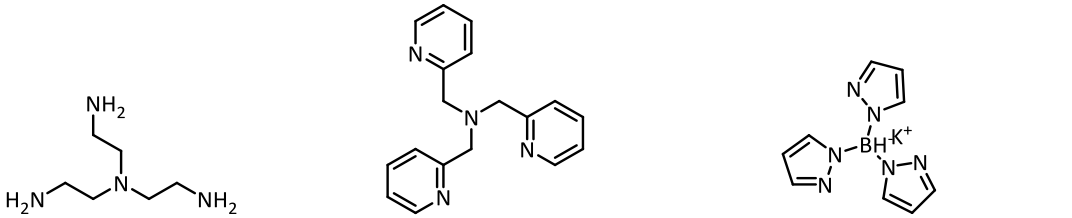

N,*N*-Bis(2-aminoethyl)-1,2-ethanediamine (TREN) | Tris(2-pyridylmethyl)amine (TPMA) | Potassium tri(1H-pyrazol-1-yl)hydroborate (KTp)

Figure 1.1.1: Examples of commonly used tripodal compounds in research and industry.

One prominent feature of this type of ligand system is the possibility to form C_3 symmetric compounds with metal atoms with three to four coordination sites. The coordination of metals with even more coordination sites at the central metal atom is possible but at the expense of the C_3 symmetry. Furthermore, possible coordination patterns featuring metal atoms with less than three coordination sites in a mono- or bidentate fashion are feasible to also enable bimetallic bonding motifs.[2,3,4] Selected examples of this type of bonding is shown in Figure 1.1.2.

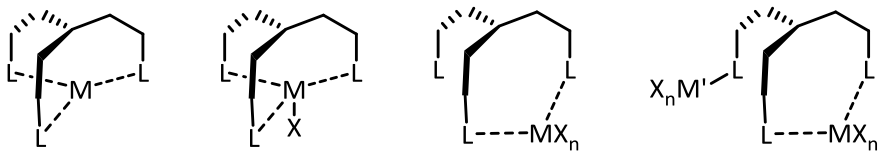

Figure 1.1.2: Selected bonding motifs of tridentate tripodal ligand systems.

With a proper connection of ligand design and coordination chemistry it is possible to tune these features for further uses in coordination chemistry and to get a deeper understanding of the chemistry and coordination patterns observed for these tripodal ligand systems.

As an example, one promising phospholane ligand system is shown in Figure 1.1.3 by GADE *et al.*[5] These system could successfully be transferred to a metal complex bearing three gold atoms and was able to catalyze cyclohydroamination reactions with 94% *ee* much better than the corresponding mono or dimetallic derivatives. Additionally, a *N*-heterocyclic (NHC) derived ligand system presented by MEYER *et al.* and shown in Figure 1.1.3 was employed in the synthesis of a silver carbene complex which revealed substantial π-bonding interactions within the silver carbene unit.[6] This metal complex can be used as a transfer reagent since the free carbene is otherwise unstable.

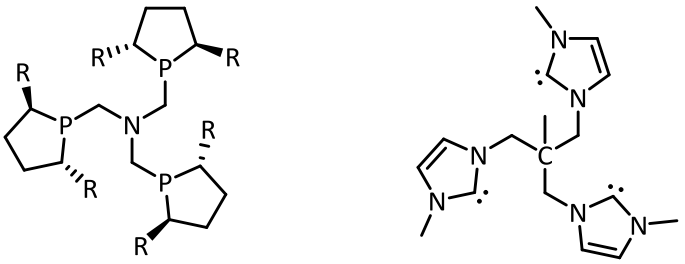

Figure 1.1.3: Phospholane ligand (*left*) by GADE *et al*. and tripodal NHC ligand (*right*) by MEYER *et al*.

Inspired by these findings, which already show a small glimpse into the multiple application possibilitys of tripodal ligand systems, the objective of this work is to achieve a double track approach towards new suitable ligands and possible functionalization options to build multiple ligand systems with an attractive coordination sphere towards catalytically active metals. In particular, a comparison between two well established classes of ligand systems, the iminophosphoranes[7] and mesoionic carbenes (MICs) based on 1,2,3-triacolylidenes[8,9] have been chosen here and are shown in Figure 1.1.4.

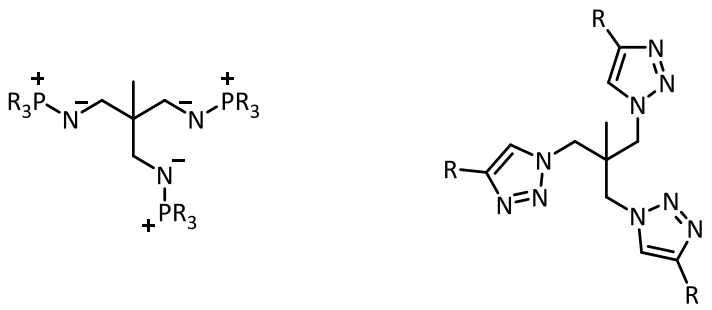

Figure 1.1.4: Base structure of ligand systems used in this work. Iminophosphoranes (*left*) and 1,2,3-triacolylidene (*right*).

While the general coordination chemistry of iminophosphoranes is well known and understood this work aims to transfer that knowledge towards tripodal ligand systems and to get a deeper understanding of the formation of possible metal complexes and their coordination patterns. This should help to project the catalytic potential of the resulting metal complexes and also give insight into possible changes and adaptions of the ligand system itself to complement the goal of a high selectivity towards catalytically active metals which can form C_3 symmetric complexes.

To further broaden the scope of the coordination of possible metal atoms mesoionic carbenes are used besides the iminophosphoranes. Similar to N-heterocyclic carbenes (NHCs) these mesoionic carbenes do not tend to dimerize along the WANZLICK equilibrium.[10] This feature enables a smaller and less sterically demanding ligand design. Due to a reduced amount of heteroatom stabilization these mesoionic carbenes show stronger σ-donor properties than NHCs or their phosphane counterparts also making them less prone to oxidation and protonation reactions and therefore less sensitive to air and moisture enabling new synthetic pathways towards a tripodal ligand system.[7,11,12,13]

After successful synthesis these new ligand systems shall then be used in different metal coordination reactions to get an understanding of their coordination abilities and to pinpoint their distinct characteristics. Among the common analytical methods, the use of single crystal X-ray diffraction should prove to be a viable tool to get insight into the different coordination motifs.

1.2 Tripodal Ligand Systems

Tripodal ligand systems where three separate ligand arm extensions are connected around a central atom are useful systems to form stable metal complexes with a defined ligand and coordination sphere. A major cornerstone in pushing the development and synthesis of tripodal ligand systems was achieved in 1966 by TROFIMENKO with the characterization of tris(1-pyrazolyl)borate shown in Figure 1.2.1.[14,15,16]

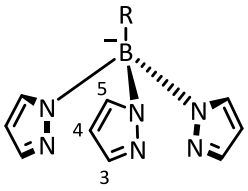

Figure 1.2.1: Tripodal ligand system tris(1-pyrazolyl)borate with a central boron atom by TROFIMENKO *et al.* and numbering scheme.[14,15,16]

This ligand system gained further interest in complexation chemistry since the resulting metal complexes have a higher thermic and hydrolytic stability by comparison with equal polydentate ligands.

By variation of the backbone of the ligand it is also possible to influence the coordination pocket of the ligand towards a metal atom and subsequently influence the symmetry of the resulting complexes, which is an advantageous and highly desired feature with regard to catalytic applications.[17] The features of these ligand systems can furthermore be adapted by introducing different substituents at distinct positions of the ligand arms. Substituents at position 3 or 5 of the pyrazole ring tend to shift the structure of the whole ligand system, electron donating groups at position 4 are useful to change the electron density within the pyrazole ring and therefore its reactivity.[16] Because of these features it has been shown, that the tripodal geometry as well as highly customizable ligand arms are a very useful class of molecules in coordination chemistry.

1.2.1 Effects of Ligand Symmetry and Coordination

Apart from a high efficiency of the catalyst towards a catalyzed reaction it is also of importance to control the stereoselectivity during a reaction. With proper ligand design it is possible to employ polydentate ligand systems which provide a chelating effect and also a shaped coordination sphere. While C_2 symmetric ligands are predominantly used in asymmetric catalysis there are only a few examples of C_3 symmetric ligands currently used in catalysis.[18,19] In 1990 BURK *et al*. came up with a concept to describe the effects of C_3-symmetric ligand systems towards stereoselectivity.[20]

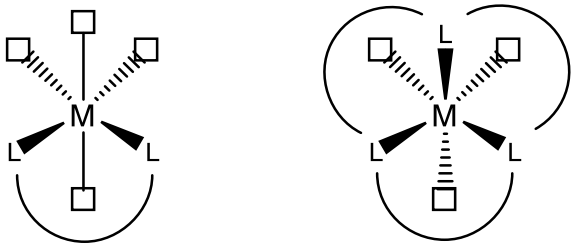

Figure 1.2.2: Symmetry influence towards stereoselectivity by BURK *et al*.[20] bi- (*left*) and tridentante coordination (*right*).

The Figure 1.2.1 shows that in an octahedral transition state of a bidentate ligand there are two diastereotopic bonding points for the substrate while in a tridentate ligand there are three homotopic bonding points. Therefore, a higher denticity should provide a better stereoselectivity than the bidentate systems.[21] This work sparked the interest in these higher dentate compounds as possible precursors for different catalysts.[22] In 1994 DIAS *et al*.[23] isolated the first type of this class of molecules and in 2003 MEYER *et al*. reported a C_3-symmetric system featuring an alkyl backbone[6]

shown in Figure 1.2.3. In 2004 PERIS *et al*. build upon this work to report on rhodium and iridium complexes with these ligands.[24]

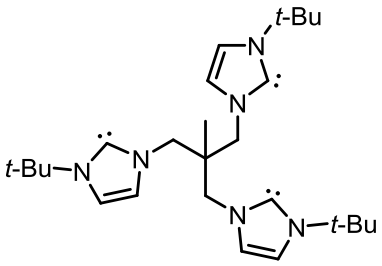

Figure 1.2.3: C_3-symmetric carbene ligand by MEYER *et al*..[6]

1.3 Tripodal Iminophosphorane Ligand Systems

As already mentioned the development of tripodal ligand systems goes back to the tris(1-pyrazolyl)borate presented by TROFIMENKO *et al*. in 1966 and shown in Figure 1.2.1.[14] In these types of molecules one could find boron in a central position defining the whole ligand sphere in combination with the three pyrazole rings. This sphere made it possible for each nitrogen atom with a free electron pair within the pyrazole rings to coordinate to a metal. Depending on the additional substituents on the pyrazole rings it is also possible to steer the reactivity, stability and structure of the whole ligand system.[15] A change of substituents at e. g. position three changes the steric demand and therefore the reactivity of the complex while a change at position four with substituents that reveal a high positive or negative inductive effect can change the electron density of the nitrogen atom which is used for nitrogen-metal-bond. Furthermore the bite angle of the tripodal ligand can be adjusted by implementing substituents on position five of the pyrazole rings.[16]

The prominent C_3 symmetry of the tripodal boron-ligands has been constantly kept in further improvements of these type of systems. GADE *et al*. kept the ligand symmetry by using the same three arms and only changing the backbone atom to nitrogen or silicon. This gave way to the well-known TREN-ligand system which would also have an additional coordination site.[25] Another option is to change the bridging atom connected to the side arms to change the bite angle of those.[26,27] Some selected examples are shown in Figure 1.3.1.

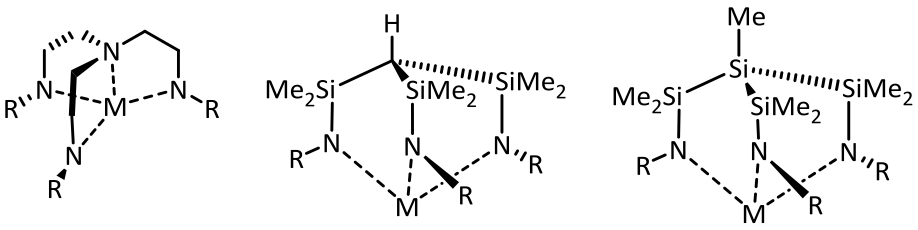

Figure 1.3.1: Tripodal metal complexes with the TREN-ligand (*left*) and adaptations by GADE *et al*. with silicon atoms *(middle, right*).[27]

Further adaptations can be achieved by changing the substituents R to phosphane substituents. Due to the strong electron donating effect from the phosphane substituents at the coordinating nitrogen atom these nitrogen atoms tend to have a strong σ-donor effect. These nitrogen-ylid like transition states can establish stable metal-nitrogen-bonds. Electron density studies have also shown that the nitrogen – phosphorus bond tend to be more like a single bond than a double bond with a negative partial charge at the nitrogen and a positive one at the phosphorus atom forming a typical nitrogen-ylid-compound.[28] Such small adjustments to the base ligand lead to the general tripodal iminophosphorane ligand system shown in Figure 1.3.2 that was used in this work.

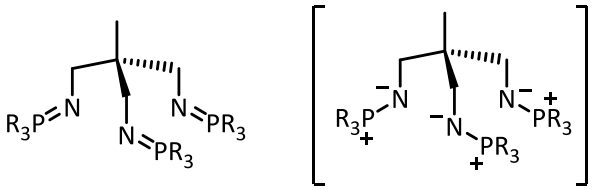

Figure 1.3.2: Structure of a C_3 symmetric tripodal iminophosphorane ligand system (*left*) and its mesomeric form (*right*) examined in this work.

The ligand system itself consists of a carbon atom at the connecting backbone position which bridges the three ligand arms and is further substituted with a methyl-group. While losing a fourth coordination center the change from a nitrogen atom towards this carbon atom with a methyl-group provides a more rigid backbone which should help keeping the C_3 symmetry intact even after a coordination reaction. As a result, the focus in these coordination reactions is shifted more towards metal atoms which coordinate in an up to three- and fourfold coordination sphere. The three ligand arms are each formed by an iminophosphorane group connected to the central carbon atom via a subsequent methylene group. This connection type gives the ligand a claw like appearance and forms the coordination pocket.

Because of the ylid like bond between the nitrogen and the phosphorus the nitrogen gets a negative partial charge further improving its tendency to coordinate towards different metal atoms.[28] The

electronic properties around the nitrogen coordination site as well as the steric demands of the whole ligand can be adjusted by employing different substituents at the phosphorus atom.

1.4 Classic Carbenes

In recent years carbenes especially the NHC type have become a stable reagent in a broad range of chemical reactions, from coupling reactions like the SUZUKI[29], KUMADA[30] or SONOGASHIRA[31] couplings to reactions like the hydrogenation[32,33], hydroformylation[34] and many more. Because of their interesting structural and electronic properties, carbenes themselves are in the focus of many working groups constantly broadening the knowledge and diversity of this subgroup of chemical systems.

For a long time this group of molecules were considered to be a very reactive intermediate which could not be isolated.[35] Early attempts to stabilize and isolate these compounds employed techniques like matrix isolation or by introducing different substituents with various electronic properties. [12,36] This last concept, changing the electronic parameters of a ligand system by introduction of different substituents to the ligand backbone, has since been one of the most favorable ways to stabilize and isolate those compounds.

Following the general definition by IUPAC a carbene is a "*species H_2C: and its derivatives, in which the carbon is covalently bonded to two univalent groups of any kind or a divalent group and bears two nonbonding electrons, which may be spin-paired (singlet state) or spin-non-paired (triplet state)*".[37]

In the case of singlet state carbenes the carbon atom has its two free electrons with opposite spins in an sp^2 hybridized orbital with an empty p_z-orbital. In contrast the electrons of a triplet state carbene are located in the p_y and p_z-orbital with parallel spins while the σ-bond is formed via a sp-hybrid orbital.[38,39] The different orbital states are depicted in Figure 1.4.1.

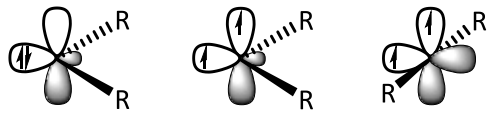

singlet state triplet state triplet state

Figure 1.4.1: Single and triplet states of carbenes.

The energy difference between the two states is rather low with the triplet state being lower than the singlet state and thus being the ground state but π and σ-donor substituents are able to donate electron density into the vacant p orbital and therefore stabilize the singlet state.

Commonly found donor substituents are nitrogen, oxygen and sulfur hence stable carbenes are in a singlet state and thus have a bend structure. Because of the filled and vacant orbitals these carbenes possess an ambiphilic character and can react as nucleophiles or electrophiles depending on the substituents. Strong electron withdrawing groups enhance the electrophilic character while donating groups enhance the nucleophilic one. The singlet carbenes react in a single concerted step which is stereospecific while the triplet carbenes react like diradicals in a step wise reaction which is not stereospecific.

If the electronic effects of the substituents are neglected the sterics alone can be used to dictate the ground-states spin multiplicity. Because of the hybridization demands of the carbon atom, sp^2 for the singlet state and sp for the triplet state, a bent geometry favors the singlet state while a linear one favors the triplet state.[40] By increasing the steric bulk around the carbene atom the bond angle broadens and therefore the triplet state can be forced.[12,41] An example of this behavior is shown in Figure 1.4.2.

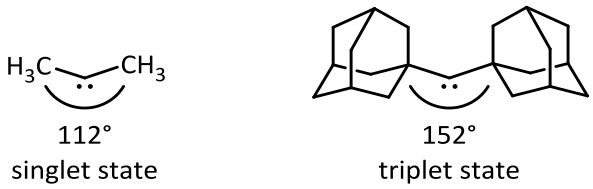

Figure 1.4.2: Steric effects on the ground state multiplicity in comparison between dimethylcarbene[40] and diadamantylcarbene[41].

One of the most common ways to implement both stabilizing effects, sterics and electronics, is to add nitrogen atoms in close proximity to the carbene carbon atom. By doing this the carbene atom gains a stabilizing effect for its singlet state in the form of a "push-pull-stabilization". For one the inductive effect (-I) of the nitrogen atoms pulls on the σ-electrons leading to an increase of the s-character of the σ-non-bonding orbitals and also the mesomeric effect (+M) donates π-electrons into the empty p_π-orbital of the carbene atom.[42] Figure 1.4.3 depicts this behavior.

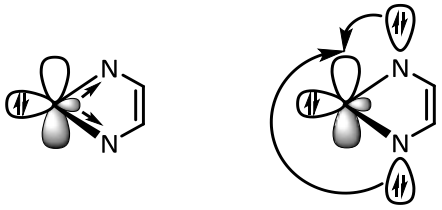

Figure 1.4.3: Push-pull-stabilization of NHCs by inductive (-I, *left*) and mesomeric (+M, *right*) effects.[42]

These features stabilize the singlet state and by also employing bulky substituents close to the carbene atom it became possible to isolate these compounds known as *N*-heterocyclic carbenes (NHCs).

1.5 *N*-Heterocyclic Carbenes (NHCs)

Molecules with a carbene atom which is flanked by two nitrogen atoms in a cycle are called *N*-heterocyclic carbenes. In 1960 WANZLICK *et al*. were able to isolate some of the first NHCs which used nitrogen atoms to stabilize the carbene carbon atom. Unfortunately these compounds were not the desired free NHCs but rather dimers shown in Figure 1.5.1.[43] While the free NHC could not be isolated the reactivity of these compounds could be probed by *in situ* generation of the free NHC which readily reacts with HCl to form the corresponding chloride salt.[10] First metal-NHC complexes could also be synthesized.[44]

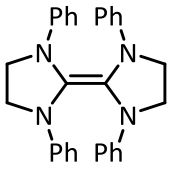

Figure 1.5.1: Carbene-dimer by WANZLICK *et al.*.[43]

To prevent dimerization and less chemical reactions to take place more sterically demanding substituents were introduced to the nitrogen atoms and in 1991 ARDUENGO *et al*. succeeded in isolating the first free carbene by deprotonation of the corresponding imidazolium salt with a strong base.[45] The reaction is shown in Scheme 1.5.1.

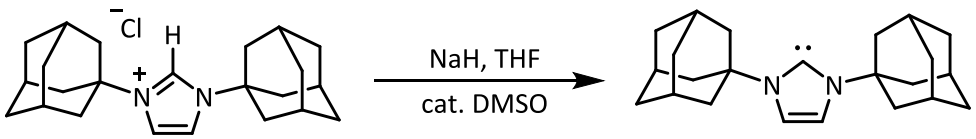

Scheme 1.5.1: First free carbene by Arduengo *et al.*.[45]

Shortly after they were also able to show that the steric hindrance of the substituents is no major factor under normal conditions in stabilizing these molecules but rather the electronic properties of the substituents are much more important.[46] Since then many more different ligand systems could be developed and improved and it could also be shown that nitrogen atoms are not necessarily needed for the stability of the NHC. [47,48,49,50] Figure 1.5.2 shows some selected examples.

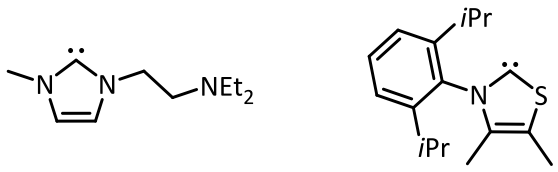

Figure 1.5.2: Different stable carbenes with less steric bulk around the carbene atom by HERRMANN *et al.*[50] (*left*) and a thiazolic carbene by ARDUENGO *et al.*[47] (*right*).

Considering the reactivity of NHCs in metal coordination this class of molecules can be compared to phosphane ligand systems. NHCs have a very strong σ-donor character and react in the same way like other two electron donors like phosphanes, amines and ethers. The σ-donor capabilities are stronger than for phosphane ligands, with minor π-interaction.[35] As a result, NHCs form stronger bonds towards the central metal atom, unfortunately this makes a dissociation in a catalytic pathway rather improbable and in reaction pathways which require a dissociation of a ligand the corresponding phosphane ligands are much more favored. Especially the salts of most carbenes are stable and show no signs of decomposition towards air whilst phosphanes tend to oxidize.
The electronic and steric features of NHCs are, as well as in phosphanes, highly tuneable e.g. substituents at the positions N1 and N3 are preferred for changing the steric properties of the ligand system and at C4 and C5 an influence on the electronic situation can be achieved (see Figure 1.5.3 for numbering scheme). [38,51]

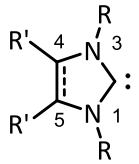

Figure 1.5.3: Substitution pattern of a generic imidazole derived NHC.

The bond properties of NHCs are comparable to those of phosphanes and their ylid like binding with the exception that NHCs tend to be much more electron rich and possess higher σ- donor properties. This σ- donor strength can be determined with different indirect techniques. A routinely used process by HUYNH *et al*.[52] is to determine the σ-donor strength by measuring the chemical shift in a ^{13}C NMR of a carbene carbon atom of a Pd(II)-benzimidazolylidene-complex which coordinates to the probing NHC.
Another often used technique is the determination of the "Tolman-Electronic-Parameters" (TEP). In here one determines the *trans*-standing CO-stretching vibration in regard to the NHC ligand in a $[Ni(CO)_3(NHC)]$ complex. The strong σ-donor properties of the NHC ligand leads to a stronger population of the antibonding π*-orbital of the CO ligand in trans position (*trans-effect*) and therefore

leads to a reduction of the stretching vibration because of the weakening of the bond.[53] Further examples of less toxic NHC complexes which are used for the TEP determination consists of $[IrCl(CO)_2(NHC)]$ and cis-$[RhCl(CO)_2(NHC)]$. This technique can be adapted for different ligand systems and was originally used to classify the electron donating or withdrawing properties of phosphane ligands as well as their steric properties described by the Tolman cone angle.[53]

Lastly a third technique to determine the electronic properties of a NHC ligand can be done via cyclic voltammetry. It is possible to measure the "Lever-Electronic-Parameter" (LEP). Herein the electro chemical potential E_0 of a Ru(II)/R(III) complex with the corresponding NHC ligand is determined.[54,55]

Since NHCs have a very high σ-donor character and because of the strong covalent bonding between a metal and the carbon these ligand systems are a very good choice to form main group and d-block metal complexes giving access to organocatalysts and other complexes which need stable but reactive intermediates during a reaction pathway. [56] One, if not the most prominent, example for the versatility and usefulness of NHCs are the catalyst by GRUBBS used in olefin metathesis and cross coupling reactions which was awarded the Nobel prize in 2005.[57,58] The catalyst is shown in Figure 1.5.4.

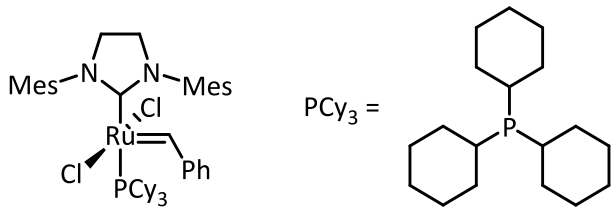

Figure 1.5.4: GRUBBS-Type(II)-Catalyst used in olefin metathesis.

Synthesis of NHCs can be considered a little bit more convenient in comparison with corresponding phosphane ligands since phosphane systems tend to oxidize easily and overtime. One can see the development of catalysts with less to none phosphorus atoms with the GRUBBS catalysts which moved away from PCy_3 – ligands in newer generations. Furthermore, NHCs can be found with a high structural versatility, there are multitudes of chelating, chiral, or highly functionalized carbenes making this class of compounds very interesting for different uses in the laboratory.

1.6 Abnormal and Mesoionic Carbenes (MICs)

As already described in the previous chapter NHCs utilize an already strong σ-donor character, one of the reasons these compounds tend to replace the phosphane systems. Therefore, an

interesting topic in NHC development is to even further increase the σ-donor capacity. Unfortunately the widely used nitrogen atoms in close proximity to the carbene atom help to stabilize the carbene with its "push-pull-mechanism" while simultaneously decreasing the σ-donor strength.[59] To counter this effect it is possible to reduce the amount of nitrogen atoms or to move them one or two positions further away from the carbene carbon atom at the cost of the stability of the free carbene.[60,61] Another option is to move the carbene carbon atom to a different position giving rise to new classes of NHCs like remote-NHC (rNHC) and abnormal NHC (aNHC).[59] In remote NHCs the carbene atom is not located right next to a nitrogen atom while in abnormal NHCs the metal-carbon bond occurs not at the C2 position between the nitrogen atoms but still on a carbene atom in close proximity to one nitrogen. The different classes are depicted in Figure 1.6.1.

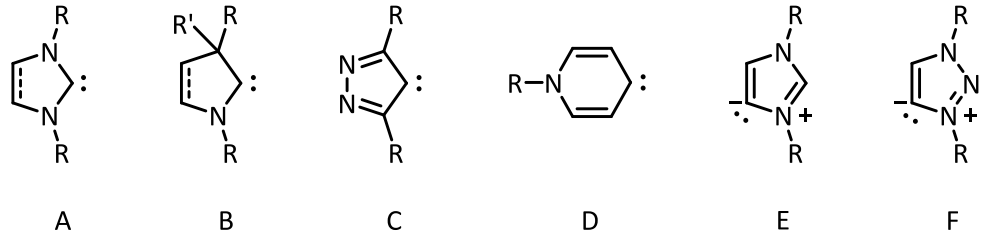

Figure 1.6.1: Different classes of NHCs (A,B), rNHCs (C,D) and aNHCs (E,F).

The abnormal NHCs have been first described by CRABTREE *et al*. while connecting a NHC ligand to an iridium complex which is shown in Scheme 1.6.1.[62,63]

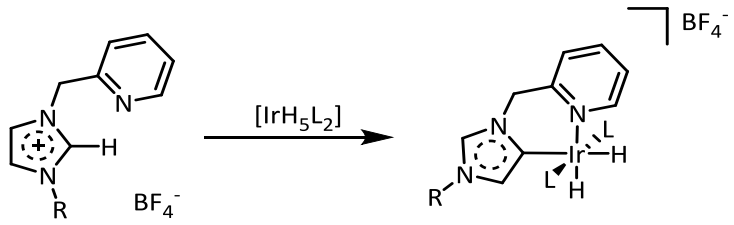

Scheme 1.6.1: Abnormal carbene (aNHC) by CRABTREE *et al*..[62,63]

This interesting behavior was rather unexpected at first since the C2 atom is considered to be more acidic hence the normal metalation often occurs here.[64,65] Because of this, these types of bonding at the C4 and C5 position led to the term of "abnormal" carbenes.[59,66] To better reflect the electronic properties of the abnormal carbenes it is necessary to introduce two opposite charges when drawing structures on paper to better account for the different resonance form. According to the IUPAC golden books[37] this fulfils the criteria for mesoionic compounds and henceforth these compounds are referenced as mesoionic carbenes (MICs).

MICs show not only an increased σ-donor strength but also a slightly altered reactivity in comparison with the other types of NHCs e.g. NOLAN *et al*. showed in 2004 a MIC-palladium-complex which was able to catalyze HECK reactions while the corresponding NHC-complex did not show any catalytic activity.[67]

While NHC complexes are primarily synthesized in a reaction between the metal and the free carbene the same reaction pathway is slightly hindered when using MICs because of the higher basicity of the protonated MIC therefore the free MIC is not that easily accessible. BERTRAND *et al*. were one of the first groups who showed a path for isolation of a free MIC in 2009.[68] The reaction is shown in Scheme 1.6.2.

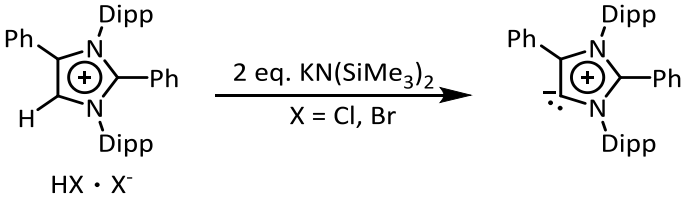

Scheme 1.6.2: First free mesoionic carbene by BERTRAND *et al.*.[68]

It was also shown, that the free MICs do not tend to dimerize easily and therefore the steric shielding can be further reduced in comparison with NHCs. Further research on this topic lead to new reaction pathways towards metalation that do not need the isolation of the free carbene species e.g. via transmetalation or C-H bond activation.[69]

1.6.1 Mesoionic Carbenes Derived from 1,2,3-Triazolylidenes

While the bulk of studies regarding MICs concentrate on the imidazole-4-ylidene some groups could show that the 1,2,3-triazole-4-ylidene MICs also provide interesting properties. For the first time ALBRECHT *et al*. reported in 2008 about triazolic MICs[9] and two years later BERTRAND *et al*. isolated the first free triazolic MIC.[70] The complex is drawn in Scheme 1.6.3.

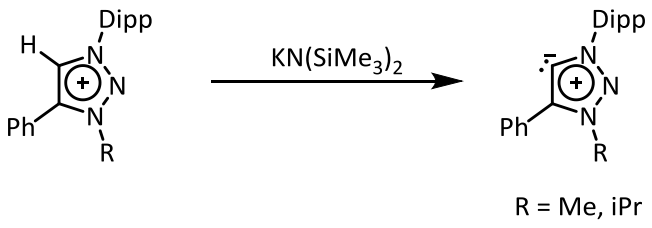

Scheme 1.6.3: First free triazolic carbene by BERTRAND *et al.*.[70]

In a cooperation between BERTRAND and GRUBBS in 2011 these types of MICs were tested towards stability and catalytic activity especially in combination with the GRUBBS type catalysts. Therefore different ligands on the catalysts were exchanged for the MICs and a NHC-MIC-hybrid could be formed which showed a higher catalytic activity than the normal catalysts in that range.[71] Apart from the well-known GRUBBS catalyst, CROWLEY *et al*. and ALBRECHT *et al*. reported in 2013 about different gold complexes with triazolic MIC ligands where the active species is formed by a cationic complex formed by two MIC ligands and a central metal atom. These compounds were also able to catalyze different organic reactions with good stereo selectivity.[72,73] An example of such a gold-MIC complex is shown in Scheme 1.6.4.

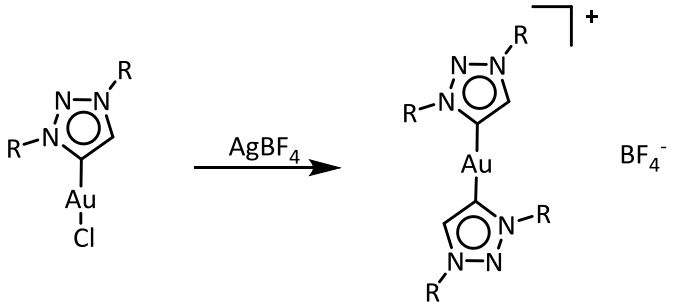

Scheme 1.6.4: Formation of the reactive species in gold-MIC-complexes by CROWLEY *et al*. and ALBRECHT *et al*..[72,73]

Additionally, these coordinative properties of the 1,2,3-triazole-4-ylidene MICs can further be enhanced when employed as coordination sites in a tripodal ligand system to form multidentate carbene ligands. Apart from the previously described dimeric coordination patterns di- and trinuclear complexes are also feasible. SARKAR *et al.* reported on the formation of such complexes with Iridium and a poly-mesoionic carbene as ligand system.[74] The reaction pathway is shown in Figure 1.6.2.

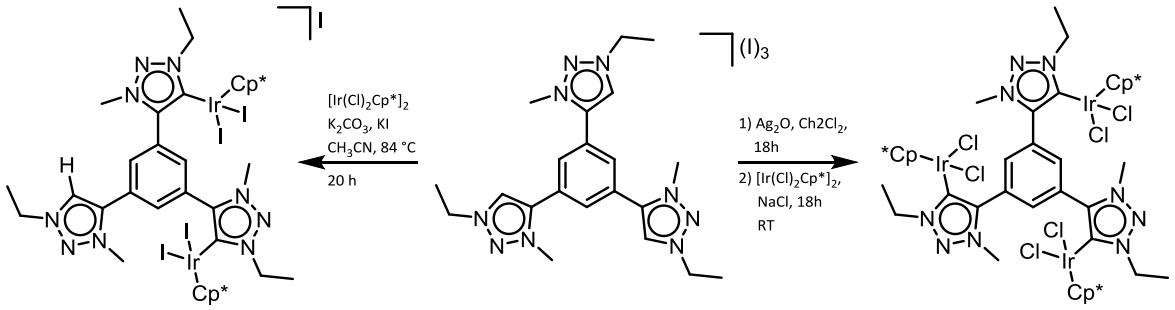

Figure 1.6.2: Synthetic pathway to the formation of di- (*left*) and trinuclear (*right*) Iridium metal complexes by SARKAR *et al.*

These findings show that one of the classic approaches to form MIC metal complexes from the triazolic precursor seems to be a promising way to also generate muli-nuclear metal complexes.[75] These steps include at first a methylation reaction with the ligand system in order to improve the reactivity of these compounds followed by a metal coordination with silver by addition of Ag_2O to the reaction and subsequent transmetallation reaction with the desired target metal.

This work aims to further build upon the, in this section, described features of the iminophosphorane and 1,2,3-triacolylidene ligand systems and subsequently enhance the understanding of their reactivity and coordinative behavior. Especially the selective formation of mono- or dimeric coordination patterns as well as mono- or multinuclear complexes is of key interest.

RESULTS AND DISCUSSION

2.1 Iminophosphorane Ligand Systems

As introduced in chapter 1.3 iminophosphorane functions can be employed in new ligand systems which are derived from the TREN-Ligand. Not only do they provide metal coordination sites in the form of the nitrogen atoms but with the presence of phosphane substituents at the nitrogen atom there is a strong σ-donor effect further improving the coordinative behavior. This leads to a ylid like bonding situation between the nitrogen and the phosphorus atom where a negative charge can be attributed to the nitrogen and a positive one to the phosphor. Leveraging on this effect, it is expected that the nitrogen atoms form stronger metal-nitrogen bonds which in return should make the general metal coordination easier.[28] The ligand system can also be further adjusted by the introduction of more or less steric demanding substituents at the phosphor atoms. This is an interesting feature in regard to the overall metal coordination since a steric demanding substituent would filter out large metal atoms as well as stabilize transition states later on during catalytic reactions with the metal complex.

Additionally, by selecting a C_3 symmetric starting material it is also possible to transfer this symmetry during the synthesis to create the tripodal ligand system. It might also be able to keep the C_3 symmetry after a metal coordination creating a complex which provides the advantages of this symmetry described in chapter 1.2.1.

Cumulating these aspects leads to two ligand systems **2** and **3** shown in Figure 2.1.1 reminisced to those that have been reported by BEAUFORT *et al.*.[76]

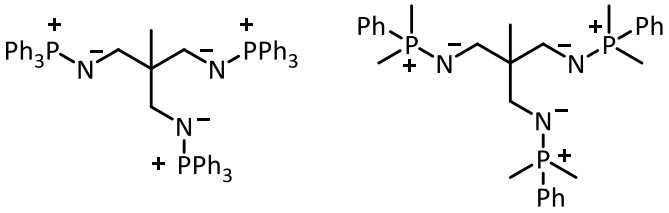

Figure 2.1.1: Iminophosphorane ligand systems 2 (*left*) reported by BEAUFORT *et al.*[76] and 3 (*right*) examined in this work.

The first ligand system **2** bears a bulky triphenylphosphane (PPh_3) substituent on each of the side arms. The bulky substituents tailor the coordination pocket between the three nitrogen atoms towards smaller metals in relation to the ligand system **3**. Also, this ligand system can only provide a tridentate binding motif. Additionally, the presence of other smaller ligands like halides at the metal atoms may be avoided due to the steric bulk of the aforementioned substituents. In **3** the steric demand of the ligand system has been greatly reduced with the introduction of $PPhMe_2$ substituents at the end of the ligand arms. This modification should allow the coordination of bigger metal atoms and also give more space in the coordination pocket resulting in a broader selection of possible metal coordination partners.

First preliminary results on the synthesis and coordination of these iminophosphorane ligand systems have been carried out by KRATZERT in the STALKE group.[77,78] This work intends to build upon these findings and gain further and a more complete insight into the reactivity of these systems. The synthesis of the iminophosphoranes **2** and **3** was initially embarked on by the synthesis of a C_3 symmetric compound which could be used as the backbone of the system. The organoazide, 1,1,1-tris(azidomethyl)ethane **1** was selected as starting material for the subsequent functionalization reactions. It could be used in the synthesis of the iminophosphoranes described in here by well know routes like the STAUDINGER[79] and KIRSANOV[80] reactions. Favorably, it can also be used without adaptations in the [3+2]-cycloaddition also known as click-chemistry reactions which demand an azide to form the resulting 1,2,3-triazolylidenes. More insight into this topic can be found in chapter 2.2. The synthetic route towards the organoazide **1** was described by BEAUFORT *et al*. in 2007 and is shown in Scheme 2.1.1.[76]

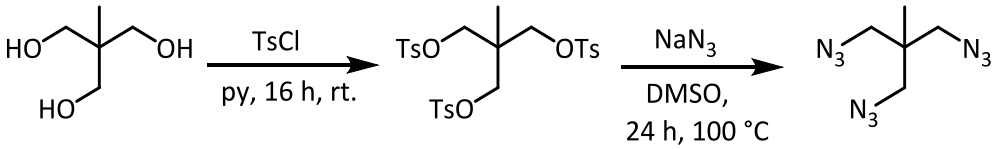

Scheme 2.1.1: Synthesis of 1,1,1-tris(azidomethyl)ethane 1 **by BEAUFORT *et al*..**[76]

The starting material 1,1,1-tris(hydroxymethyl)ethane needed to undergo a tosylation step prior to the generation of the organoazide **1.** This synthetic step is necessary since the tosylat group is a better leaving group than the hydroxyl group. While the overall reaction has been improved by this synthetic step, the general reaction time to form the organoazide **1** from the tosylated precursor 1,1,1-tris[(4-tolylsulfonyl)methyl]ethane is still quite long. BEAUFORT *et al*. reported reaction times of 4 h at 90 °C but the overall yield of **1** could be improved up to 93% by raising the reaction time to 24 h with a slight increase in reaction temperature to 100 °C. Workup was done by pouring the

reaction mixture into cold water, followed by an extraction with diethyl ether. The workup continued with a washing step with water to remove unreacted starting material and DMSO. The water phase was then extracted with diethyl ether. The organic phases were dried over $MgSO_4$ and the solvent was removed *in vacuo* to give the organoazide 1,1,1-tris(azidomethyl)ethane **1** as a yellow oil. Special caution and safety equipment was required when handling the azides **1** and NaN_3, since this class of compounds are potentially explosive substances which might undergo violent decomposition when exposed to energy from an external source. Sodium azide reacts violently with common laboratory chemicals like halides, BRØNSTED acids and heavy metals as well as chlorinated solvents like DCM and chloroform. The formation of toxic and highly instable compounds like hydrazoic acids and methyl azides can occur when attempting new reactions and should be strongly avoided. The organoazide **1** was generally used directly in subsequent reactions after the initial synthesis or stored at -6 °C under exclusion of light. If **1** was stored for a prolonged time, solutions with diethyl ether in concentrations of 1 M to 3 M were prepared. Limited experiments have shown that the pure organoazide **1** appears to be stable for prolonged storage and also shock resistant. While decomposition reactions can only be observed above of 250 °C with the generation of colorless smoke and a color change of the substrate. Nevertheless, utmost care and suitable safety equipment should be employed when handling these types of compounds.

After successful synthesis of the starting material, organoazide **1**, it was then converted to the corresponding iminophosphorane, by a reaction with PPh_3 or $PPhMe_2$ to form the respective ligand system. The product formation can be approached by two different routes, the STAUDINGER reaction[79] and the KIRSANOV reaction[80]. The KIRSANOV reaction is commonly used to synthesize Iminophosphoranes starting from alkyl amines and therefore do not need hazardous organoazides as starting materials at the expense of harsher reaction conditions and hence much more side products formed during the reaction. The "STAUDINGER-Reaction" requires the organoazide as starting material but favors much milder reaction conditions. This reaction gives the Iminophosphorane in a nucleophilic addition of the phosphane with an azide while releasing nitrogen gas. Both reaction pathways are shown in Scheme 2.1.2.

Because of the availability of the starting material shown in Scheme 2.1.1 the mild reaction conditions and the reduced amount of side products the STAUDINGER reaction was used primarily to build the ligand systems. These products are prone to hydrolysis to form the amine and the corresponding phosphane oxide and therefore were handled under proper SCHLENK conditions in an argon atmosphere.

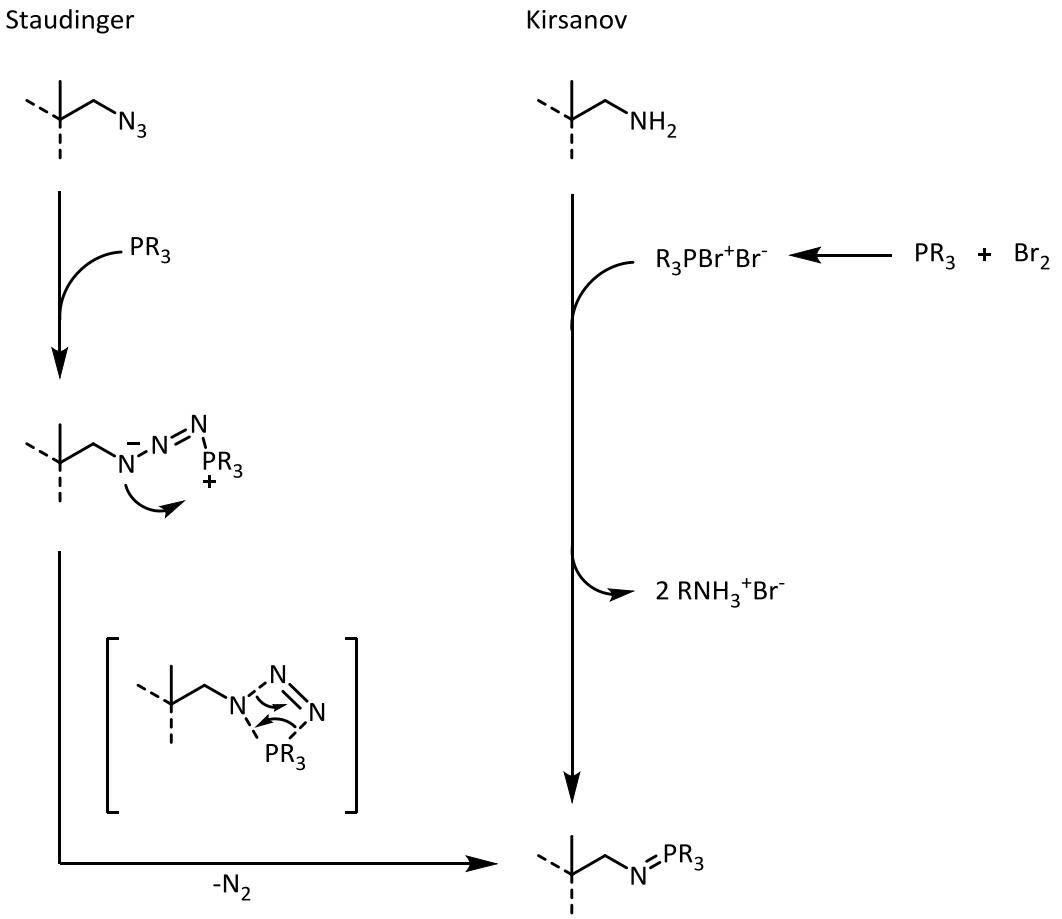

Scheme 2.1.2: STAUDINGER and KIRSANOV reaction pathways to synthesize the iminophosphorane ligand systems 2 and 3.

The metal coordination abilities of the synthesized ligand systems **2** and **3** should be examined further, based on the previous results from the STALKE group.[77] The synthesis of the ligand system **2** containing triphenylphosphane moieties was achieved according to the literature known procedure by dissolving the triphenylphosphane in toluene and slow addition of the organoazide, redissolved in toluene.[76] During the addition of the organoazide **1** a light gas emission could be observed presumable due to the nitrogen release. The reaction mixture was then heated to 60 °C for 12 h and subsequent removal of the solvent gave the desired product **2** in nearly quantitative yields. The chemical equation can be seen in Scheme 2.1.3.

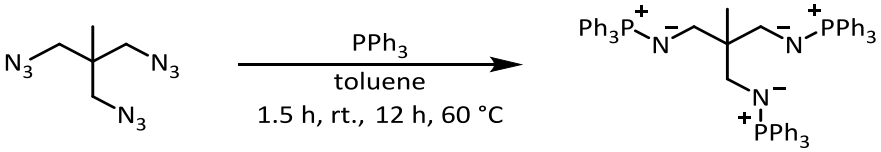

Scheme 2.1.3: Synthesis of the tripodal ligand system 2 bearing PPh_3 substituents at the ligand arms.[76]

The synthesis itself has been reported by BEAUFORT *et al*.[76] and the crystal structure was reported by KRATZERT.[78] The recrystallization from the reaction mixture at -20 °C for seven days could be repeated.[78] From the crystal structure of ligand system **2** by KRATZERT[78], shown in Figure 2.1.2, insights into the specific C_3 symmetric properties can be gained. The ligand crystalizes in the space group $R\bar{3}$ in a trigonal crystal system.

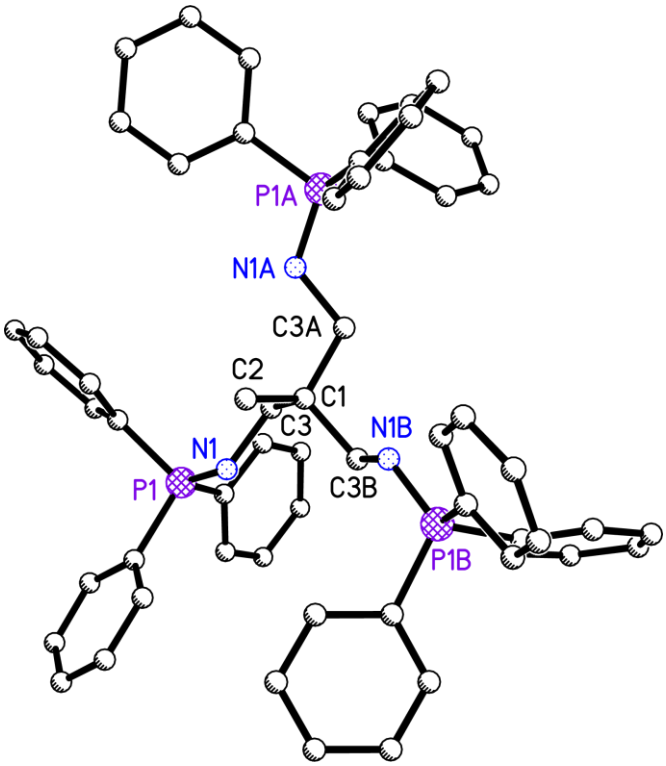

Figure 2.1.2: Crystal structure of 2 reported by KRATZERT[78]. 2 crystalizes in the space group $R\bar{3}$ in a trigonal crystal system with *α* = 90°, *β* = 90°, *γ* = 120° and *a* = 15.312(1) Å, *b* = 15.312(1) Å, *c* = 37.946(3) Å. The hydrogen atoms, disorder and solvent has been omitted for clarity.

The central bridging atom C2 and the methylene group at the C1 carbon atom are positioned along the threefold axis. Because of that only one arm of the ligand system can be found in the asymmetric unit while the remaining ones are symmetry generated by the symmetry operator. The intact C_3 symmetry can be seen in a projection along the *c* axis of the cell shown in Figure 2.1.3.

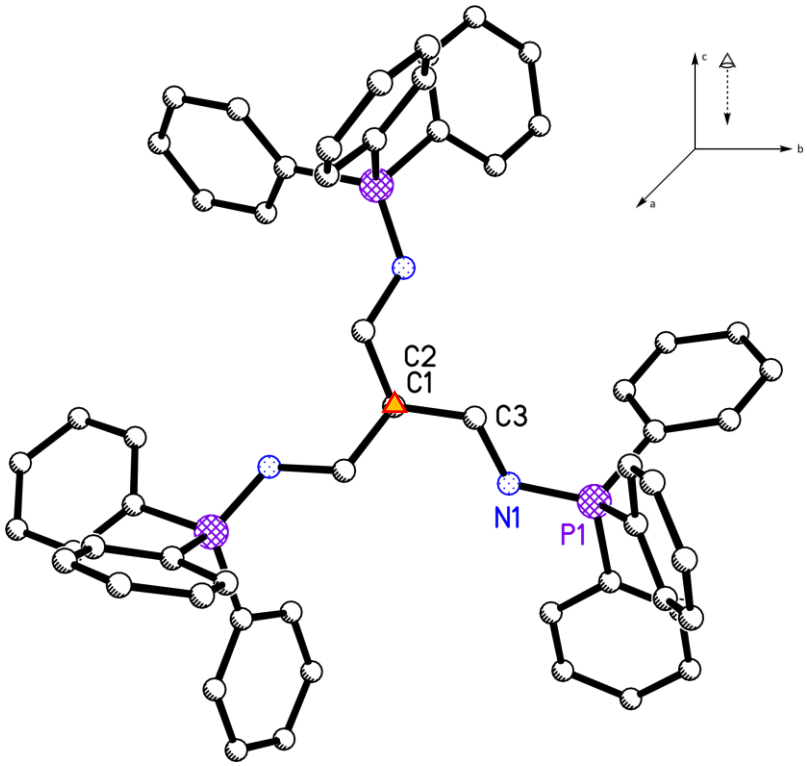

Figure 2.1.3: View along the c axis of the cell for 2. The hydrogen atoms, disorder and solvent has been omitted for clarity.

It can be concluded that the synthesis of a C_3 symmetric ligand system was successful with the chosen synthetic approach and the symmetry of the starting material **1** translates well into further functionalization attempts.

For the synthesis of the second ligand system **3** with a $PPhMe_2$ substituent at the nitrogen atom the same reaction pathway was tested but unfortunately the solubility of the starting material $PPhMe_2$ was very low in toluene. This caused not only a rather low yield but also the formation of a multitude of side products, obvious from the ^{31}P-NMR. Among the signal for the hydrolysis product O-$PPhMe_2$ there were many more unassigned signals presumably corresponding to different oxidized phosphor species and polymers. In order to cure such unsatisfactory results, the solvent was changed to diethyl ether to give a better solubility for the starting material and the reaction temperature was lowered to -10 °C to reduce the overall reactivity and accompanying formation of the unwanted side products. This change proved to be successful in synthesizing **3** as a sluggish yellow oil. The reaction pathway is depicted in Scheme 2.1.4.

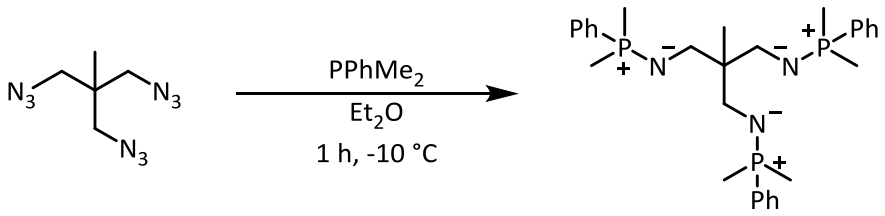

Scheme 2.1.4: Synthesis of the tripodal ligand system 3 bearing $PPhMe_2$ substituents at the ligand arms.

Both iminophosphorane ligand systems tend to oxidize over time or decompose via hydrolysis therefore these ligand systems were synthesized and worked up prior any subsequent use and not stored for a prolonged time. While trying to crystallize the iminophosphorane **3** a side product **4** could be isolated which is shown in Figure 2.1.4.

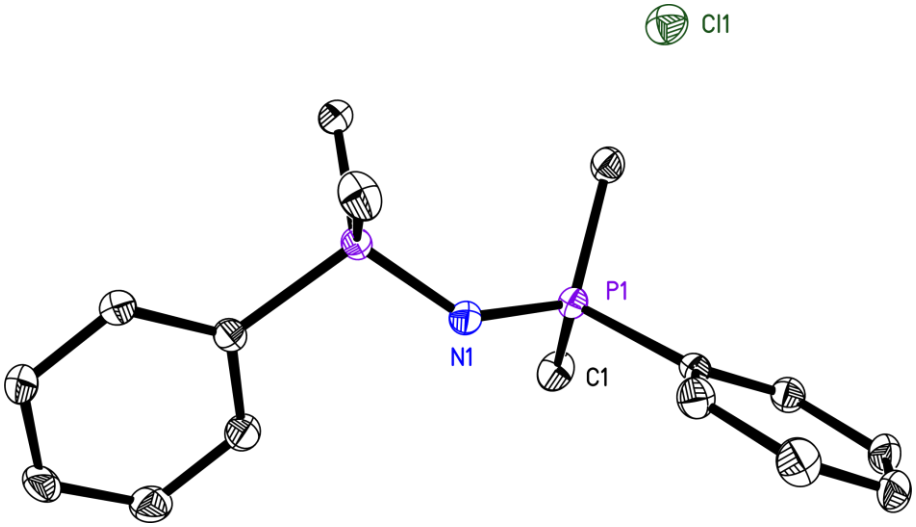

Figure 2.1.4: Crystallized side product 4 during the formation of 3. 4 crystalizes in the space group *P*ccn in an orthogonal crystal system with *α* = 90°, *β* = 90°, *γ* = 90° and *a* = 7.630 (1) Å, *b* = 10.803(1) Å, *c* = 20.437(2) Å. The anisotropic displacement parameters are depicted at the 50% probability level. The hydrogen atoms have been omitted for clarity.

The structure shows two dimethylphenylphosphane substituents bridged by a single nitrogen atom with chloride as the counter ion. These findings suggest a positive charge at each of the phosphor atoms and a negative at the nitrogen atom. The P1 – N1 bond lengths of 1.58(1) Å are at the short end of the average bond length for a P – N bond.[81] Again this can be attributed to the ylid like bonding between the two atoms. The angle of 138.9(1)° at P1 – N1 – P'1 further suggest such a bonding type with a short single bond and delocalized electrons over the whole binding motif.

A possible explanation for the formation of this side product might lay in the synthesis of the organoazide **1**. It can be assumed, that the source of the bridging nitrogen atom can be related to

some unreacted sodium azide from the first reaction step. As mentioned earlier the workup of this reaction is hindered due to the explosive nature of its components.

Some of the NMR signals in the ^{31}P-NMR of the iminophosphorane **3** can be attributed to the formation of this side product. To prevent the side reaction an additional washing step with water/diethyl ether was added to the workup of the starting material, the organoazide **1** to further reduce the amount of excess salts like NaN_3 and TsCl in the reaction. This step proved to be useful but ultimately could not prevent some impurities. Because of the instability and explosive nature of the azide **1** a distillation was not attempted while a column chromatography led to the decomposition of the compound. Therefore, small traces of the side product **4** were to be expected in subsequent reactions.

In the previous work by KRATZERT[78] he reported the crystal structure for **3** which is shown in here for comparison.[78]

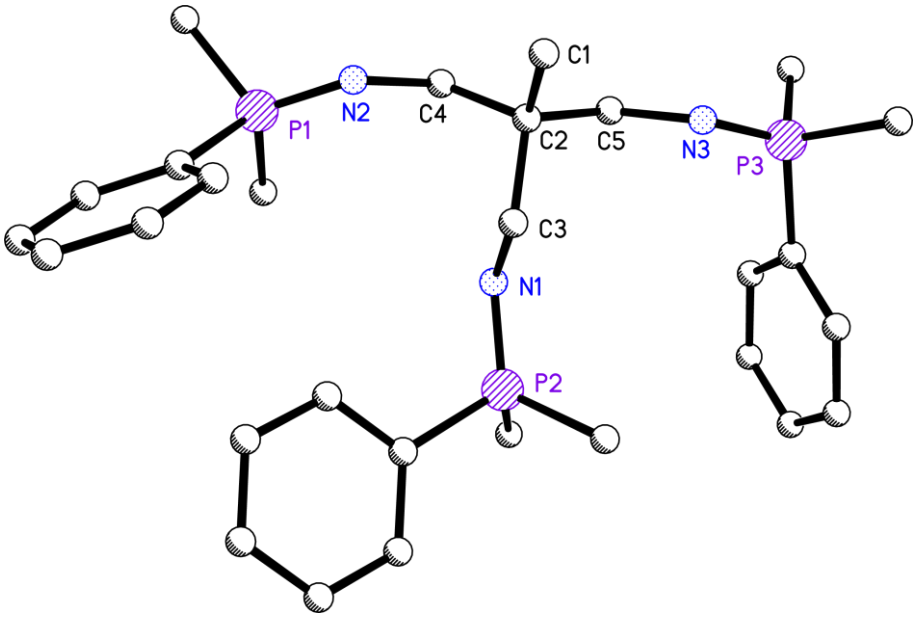

Figure 2.1.5: Crystal structure of 3 determined by KRATZERT.[78] 3 crystalizes in the space group $P\bar{1}$ in a triclinic crystal system with α = 81.41(1)°, β = 83.90(1)°, γ = 70.21(1)° and a = 8.656(1) Å, b = 9.337(1) Å, c = 19.359(3) Å. The hydrogen atoms have been omitted for clarity.

In direct comparison of the crystal structures of **2** and **3** one can see that the C_3 symmetry of the bridging alkyl backbone, which is built from the organoazide **1** is still present. Contrary to the iminophosphorane **2** the C_3 symmetry of the overall molecule has been lost. This can be attributed to intermolecular interactions in the cell lattice. The protons on the methyl groups of the ligand side arms deviate towards the negatively charged nitrogen atom of a second molecule of **3** in the crystal lattice. Also the protons on the phenyl rings align themselves towards the π-system of an adjacent phenyl ring. The packing and some selected short contacts (less than sum of VAN-DER-WAALS radii)

can be seen in Figure 2.1.6. While the C_3 symmetry of the whole molecule might be lost in the solid state the three arms can still move freely in solution by a rotation of the C – N bond or the N – P bond and adapt to the steric demands of a coordinated metal atom in subsequent coordination reactions.

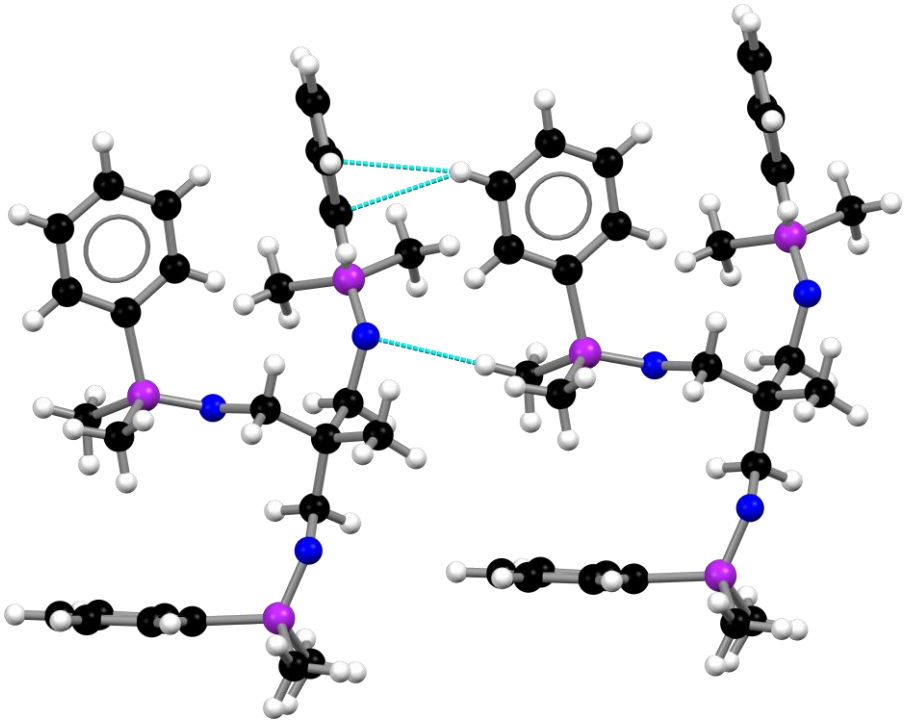

Figure 2.1.6: Selected short contacts (less than sum of vDW radii), H ⋯ N and H_{Ph} ⋯ π_{Ph}, between two molecules of 3.

With the synthesis of the iminophosphorane ligand systems **2** and **3** it was possible to gain access to two interesting ligand systems with a C_3 symmetric backbone. Both ligand systems are available in good yields with an optimized synthetic route. The systems are prone to oxidation reactions and because of the hazardous and explosive starting material not every isolation method is feasible. Nonetheless, the formed side products could be identified as oxidized species and compound **4**. The synthesized iminophosphoranes **2** and **3** differ primarily in their steric bulk at the phosphorus atom on each of the three ligand arms while their electronic structure around the coordination center at the nitrogen atoms should be close to equal to each other with its ylid like binding motif. The steric bulk is expected to be the leading factor during different coordination reactions to determine which metal atoms are feasible coordination partners. Simultaneously it is to be expected that the rigid C_3 symmetric backbone will additionally force the shape and size of the coordination pocket and will force the overall structure into a tripodal claw like appearance.

2.1.1 Iminophosphorane Ligand Systems in Metal Coordination

After the successful synthesis of the iminophosphoranes **2** and **3** bearing a triphenylphosphane substituent (PPh_3) or a dimethylphenylphosphane substituent ($PPhMe_2$) at the nitrogen atoms of the three arms these compounds were used as ligand systems and tested for their behavior in metal coordination reactions. BEAUFORT *et al*.[76] described the formation of such compounds by employing transition metal salts in the form of $NiBr_2$, CuBr and $PdCl_2$ to give metal complexes with the iminophosphorane ligand system **2**. They were not able to produce crystals suitable for X-ray structure analysis but with the help of NMR and IR spectroscopic measurements they concluded that a tridentante binding motif with the ligand is to be expected without the formation of oligomeric or polymeric aggregates. The tridentate binding motif is shown in Figure 2.1.7.

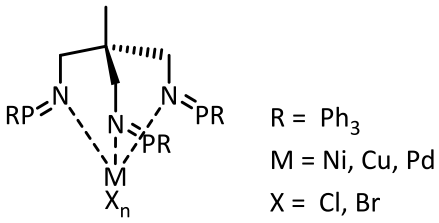

Figure 2.1.7: Proposed binding motif by BEAUFORT *et al*. for the metal complexes with ligand system 2[76].

During the work of KRATZERT[77] within the STALKE group he was able to get some initial results in reacting the triphenylphosphane ligand **2** with tin(II)-bis(trimethylsilyl)amide (SnHMDS) as well as the dimethylphenylphosphane ligand **3** with $NiCl_2$. The corresponding binding motifs determined from the respective crystal structures are shown in Figure 2.1.8.

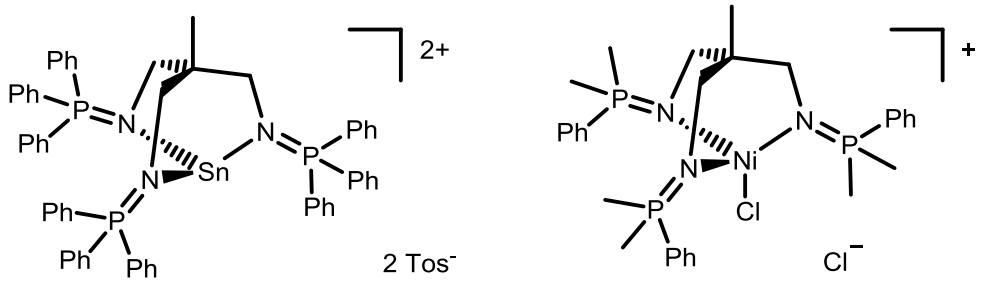

Figure 2.1.8: Metal complexes with ligand system 2 and 3 by KRATZERT.[77]

One can see that in the case of the Sn-complex the counter ion is derived from the starting material tosyl chloride which was present during the initial synthesis of the organoazide **1.** As described earlier because of the hazardous and explosive starting materials during the initial synthesis of **1** more advanced workup techniques like distillation or column chromatography are not accessible with this class of compounds and therefore utmost care during the washing step must be taken to reduce the amount of starting material which gets carried over into subsequent reactions. Nevertheless, these findings indicate that the iminophosphorane ligand systems **2** and **3** are able to provide a tridentante binding motif.

Based on these findings the scope of this work was to further expand on the synthesis of possible new metal complexes and elucidate the range of metals which can be coordinated in regard to charge, atom size and possible new binding motifs.

The synthetic pathway for the coordination between the ligand systems **2** or **3** and a suitable metal atom was to separately dissolve the ligand system and the metal salt in toluene or THF and then slowly add the solution of the ligand system to the metal salt. The reaction was carried out at room temperature under Schlenk conditions and stirred for a prolonged time. The overall reaction pathway is shown in Scheme 2.1.5.

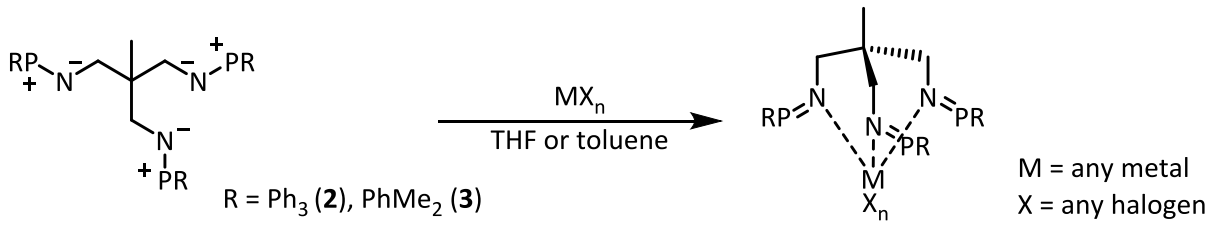

Scheme 2.1.5: General reaction pathway for the coordination reaction between the ligand system 2 or 3 and a metal salt MX_n.

Since KRATZERT succeeded in the coordination of a tin complex with a counter ion derived from the synthesis of the starting material, organoazide **1**, it was tried to reproduce his findings and selectively coordinate a main group metal to the iminophosphorane ligand **2**. For this task the lighter homologue germanium was chosen, with its approximately 2.8 % smaller VAN-DER-WAALS radius of 211 pm in comparison to tin with 217 pm[82]. Germanium is still small enough to fit into the sterically demanding coordination pocket of ligand **2**. It can also provide the same oxidation states as tin with -4, 2, 4, while 2 and 4 being the most common, and thus the same coordination pattern should be reproducible. For the synthesis $GeCl_2$·dioxane was chosen as a source of germanium. The already coordinated $GeCl_2$ with 1,4-dioxane is much more stable and easier to handle substance as opposed to the pure $GeCl_2$ or $GeCl_4$ which are prone to hydrolysis reactions. The synthetic approach for the metal complexation was to dissolve $GeCl_2$·dioxane in toluene and add a redissolved solution of the

ligand system slowly to it because there should always be an excess of the metal salt in regard to the ligand system. As expected, the overall solubility of the reactants in the unpolar solvent was scarce and therefore some DCM were added to the reaction mixture to increase the solubility. Supplementary tests have shown that the solubility of this ligand system **2** in different common lab solvents ranging from unpolar to more polar solvents (hexane, pentane, THF, DCM, Et_2O, toluene, MeCN, dioxane, DMSO, acetone, methanol, ethanol) tends to be quite low, further limiting adequate synthetic options.

During the reaction the formation of an off white precipitate could be observed. After additional two days at room temperature the reaction mixture was stored at 0 °C to fully precipitate the formed product which was then filtered off. A small fraction of the reaction solution was stored at -20 °C for 10 days to afford crystals suitable for X-ray diffraction analysis. The structure of the formed germanium metal complex **5** is depicted in Figure 2.1.9.

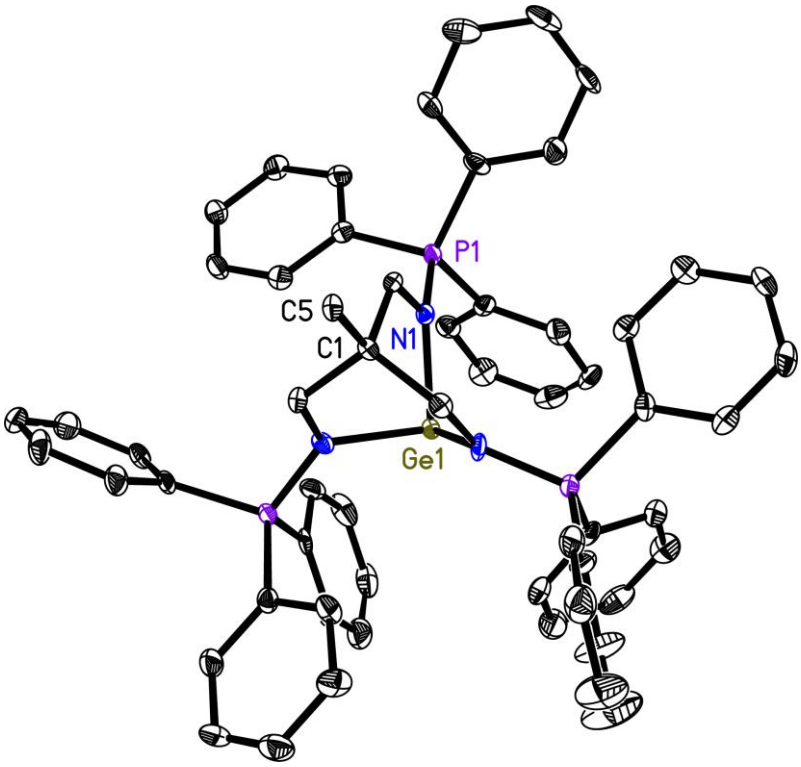

Figure 2.1.9: Crystal structure of 5. 5 crystalizes in the space group $P\bar{1}$ in a triclinic crystal system with α = 97.03(1)°, β = 96.78(1)°, γ = 114.88(1)° and a = 13.35(2) Å, b = 14.85(2) Å, c = 19.45(1) Å. The anisotropic displacement parameters are depicted at the 50% probability level. The hydrogen atoms, solvent and a $GeCl_4$ molecule have been omitted for clarity.

The structure shown in Figure 2.1.9 shows the solid state structure of [Ge{$(Ph_3PNCH_2)_3CMe$}] (**5**). The central germanium metal atom is coordinated to the ligand system in a tridentate manner. Omitted for clarity is a disordered $GeCl_4$ molecule which cocrystallizes within the crystal lattice as

well as multiple DCM solvent molecules forming a solvent channel. Refinement of these highly disordered DCM molecules could be achieved but small amounts of residual electron density presumably belonging to multiple additional DCM molecules still remains. Still a structure solution for the main molecule could be found and refined within proper crystallographic quality criteria. The complete refinement is shown in chapter 5.1.2. The structure of the main molecule shows that no additional halide atom is coordinated to the metal atom. In the course of the reaction, the formation of a disordered molecule could be observed in the form of $GeCl_4$ with a Ge – Cl bonding angle which can be averaged to 110.13° with a mean bond length of 2.27 Å. This finding indicates a neutral metal complex of **5.** Because of the high disorder and the presence of small amounts of residual electron density it can be argued that the $GeCl_4$ molecule rather consists of a $[GeCl_3]^-$ anion with an additional chloride in close proximity. This would imply that the metal complex **5** should be described as a dication. A similar bonding motif for a germanium dication has been described by REID *et al*. in 2009.[83] Additionally, the formation of a monocationic metal complex of **5** can be considered if one interprets the remaining residual density as an artifact from the multiple solvent molecules within the structure leaving only one $[GeCl_3]^-$ as counterion in the structure. STALKE *et al.* as well as BREHER *et al.* both reported metal complexes with a germanium atom coordinated to three pyrazol molecules *via* the nitrogen atoms.[84,85,86] These molecules can be described as well as monocationic with a $[GeCl_3]^-$ counterion. With the available data from the x-ray diffraction experiment no definitive answer can be obtained and additional structural information need to be gathered like IR and Raman spectra to identify the true nature of the cocrystallized molecule. In regards to the available bond lengths and angles the observation of complete $GeCl_4$ molecule with a neutral metal complex seems to be the most plausible. In the metal complex the germanium atom is positioned right in the center of the coordination pocket and coordinated with a bond length of Ge1 – N1 2.00(1) Å, Ge1 – N2 1.99(1) Å and Ge1 – N3 1.98 (1) Å to each of the three nitrogen atoms. As a result of the coordination the N – P bonds are slightly elongated from 1.550 Å in the free ligand **2** to 1.62(1) Å for the three N – P bonds in the metal complex **5**. The structure also shows, that the C_3 symmetry of the rigid carbon backbone is forced upon the coordination pocket. This can be seen in a top down view along the C5 – C1 bond onto the molecule with drawn in planes shown in Figure 2.1.10. These planes stretch out to a mean angle of 60° between each other. The nitrogen atoms are positioned right underneath the adjacent carbon atoms and only the phosphorus atoms deviate out of the plane to accommodate the steric demand of the phenyl groups.

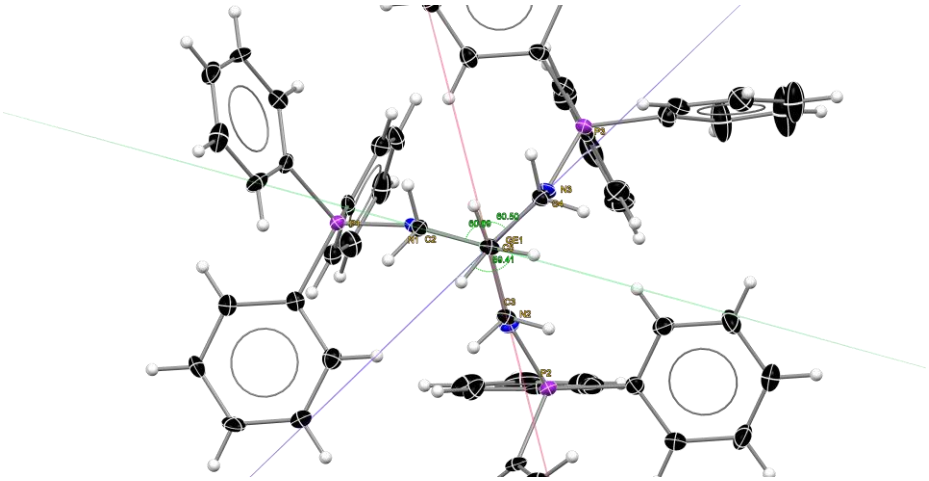

Figure 2.1.10: View along the C5 – C1 bond of 5 with drawn in planes and corresponding angles.

Because of the steric demand of the phenyl rings these orient each other towards the least steric hindrance to each other and their neighboring molecules in the cell. Subsequently the C_3 symmetry of the whole molecule is lost in the solid state , in contrast to the structure of the free ligand **2.** Still the reactivity defining coordination pocket keeps the C_3 symmetry. This behavior is to be expected when working with bulky groups on the end of the three ligand arms. It can be seen in a projection along the central threefold axis though Ge1, C1 and C5 shown in Figure 2.1.11. One can see the intact C_3 symmetry around the central coordination pocket consisting of the alkyl backbone and the nitrogen atoms. The PPh_3 substituents come close but ultimately deviate slightly resulting in a loss of the symmetry.

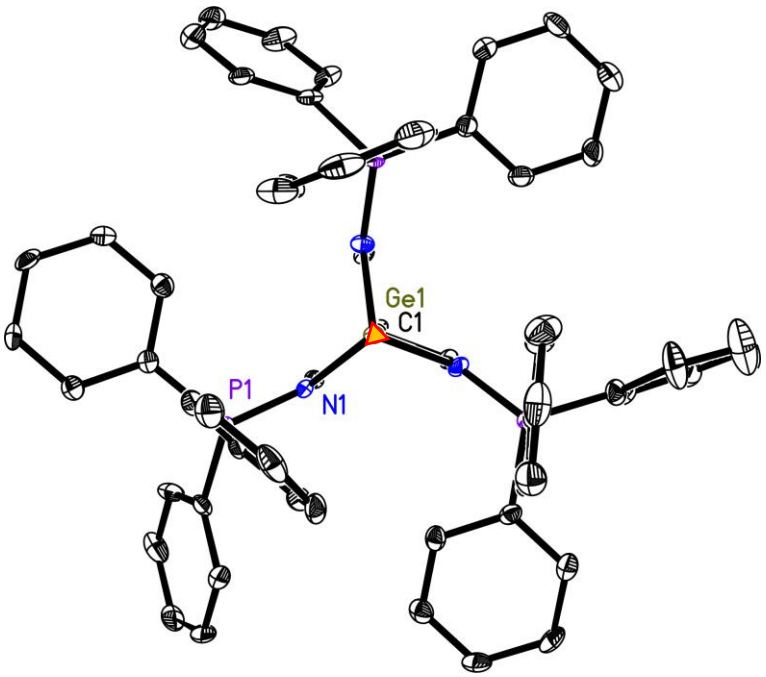

Figure 2.1.11: View along the threefold symmetry axis along Ge1, C1 and C5 of 5 with drawn in symmetry operator.

It is feasible that the three phenyl rings at the phosphorous atom of each arm provide such a steric strain, that only the free metal cation is able to coordinate and any further smaller ligand like a halide atom is left out of this sphere. A space filling model of compound **5** with an atom size depicted at their respective VAN-DER-WAALS radii can be seen in Figure 2.1.12.

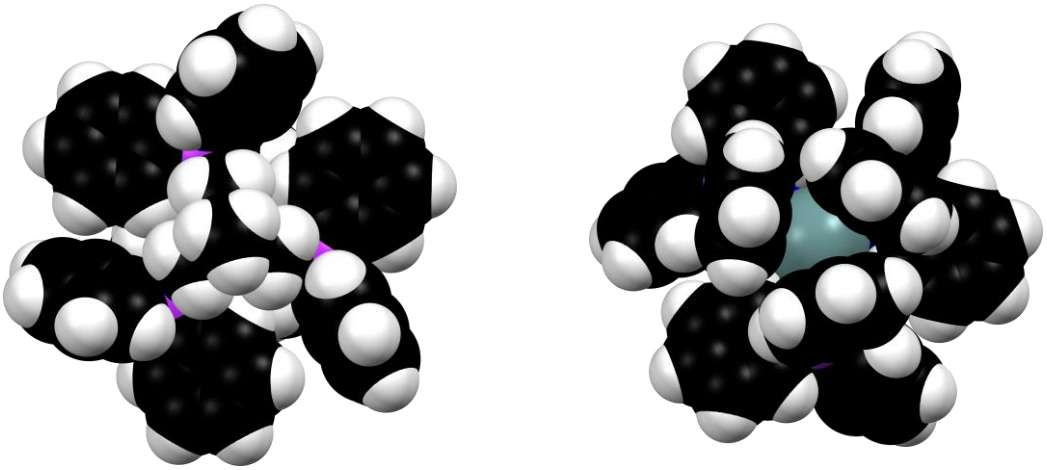

Figure 2.1.12: Space filing model of 5 with atom size depicted at their respective VAN-DER-WAALS radii. Top view (*left*) and bottom view (*right*) with central germanium atom (*turquoise*).

The findings in here show that the ligand system **5** is able to selectively bond to metal atoms with a VAN-DER-WAALS radius between 211 pm and 217 pm which can accommodate the tridentate binding motif. Unfortunately, the free ligand **2** as well as the resulting metal complex **5** are almost insoluble in many organic solvents which reduces the overall reactivity and hinders subsequent analytical methods.

The second ligand system **3** used has a dimethylphenylphosphane moiety at the three ligand arms and provides a much better solubility in these organic solvents. With the exception of hexane and pentane most solvents can be used during synthesis making it much easier to find suitable reactants where also the metal salt can be solved rather than employing a suspension. Such should lead to higher yields and a better reactivity. Initial experiments by KRATZERT[78] and BEAUFORT[76] showed that this ligand is suitable for metal coordination with a central nickel atom, shown in Figure 2.1.8, palladium and copper. Based on these findings further main-group and transition metals were to be tested towards their behavior during coordination reactions with **3**. The ligand system **3** showed already promising results in metal coordination reactions with d-block elements and from the previous experience with ligand system **2** it appears, that metal salts which are already

weakly coordinated to a ligand tend to give better results in regard to solubility, reactivity and subsequently yield. Therefore, ligand **3** was tested in a coordination reaction with $ZnCl_2$·dioxane. The synthesis was run in a solution of $ZnCl_2$·dioxane in THF to that the ligand system **3** was slowly added at room temperature according to the general reaction pathway shown in Scheme 2.1.5. Storage for three days at 0 °C afforded crystals suitable for X-ray diffraction. The resulting structure solution of the resulting complex **6** is shown in Figure 2.1.13.

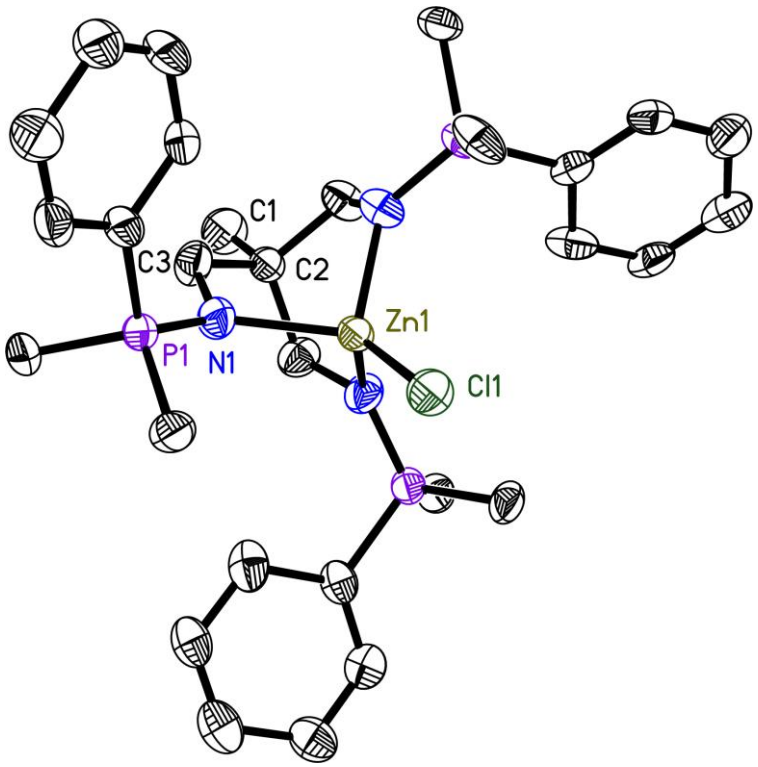

Figure 2.1.13: Crystal structure of 6. 6 crystalizes in the space group $I\bar{4}3d$ in a cubic crystal system with *α, β, γ* = 90° and *a*, *b*, *c* = 25.442(1) Å. The anisotropic displacement parameters are depicted at the 50% probability. The hydrogen atoms, solvent and chlorine anion have been omitted for clarity.

The crystal structure of $[ClZn\{(PhMe_2PNCH_2)_3CMe\}]^+[Cl]^-$ (**3**) shows the ligand system coordinated to a central zinc atom in a tridentate fashion similar to the previous coordination experiment with the triphenylphosphane bearing ligand system **2**. In here one chloride is still bonded to the metal and an additional halide can be found in close proximity countering the positive charge of the metal complex. As expected, the reduced steric congestion of the two phosphorus bound methyl groups opens up the coordination sphere around the three nitrogen atoms to accommodate such a binding motif. The reduced steric demand can also be seen in a space filling model of **6** shown in Figure 2.1.14.

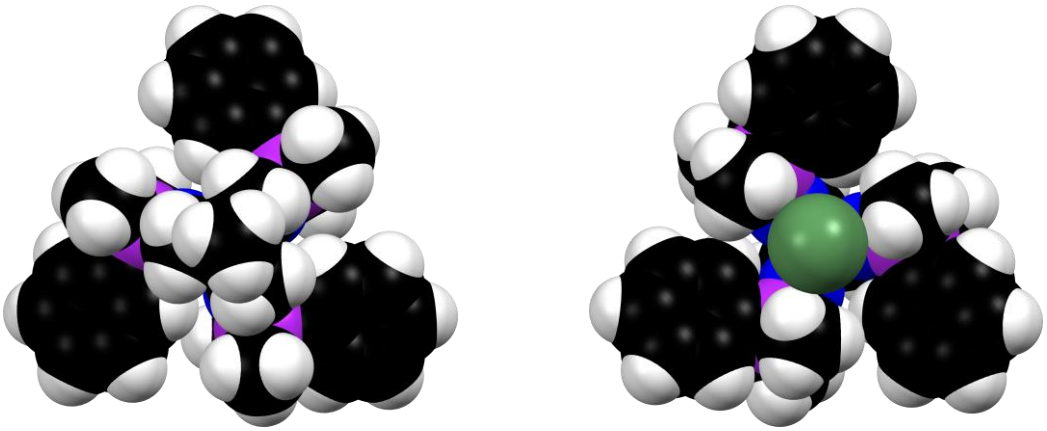

Figure 2.1.14: Space filling model of 6 with atom size depicted at their respective VAN-DER-WAALS radii. Top view (*left*) and bottom view (*right*) with central chloride atom (*green*).

A side view comparison between the two metal complexes **5** and **6** further indicates the reduced steric demand of the second ligand system and is shown in Figure 2.1.15.

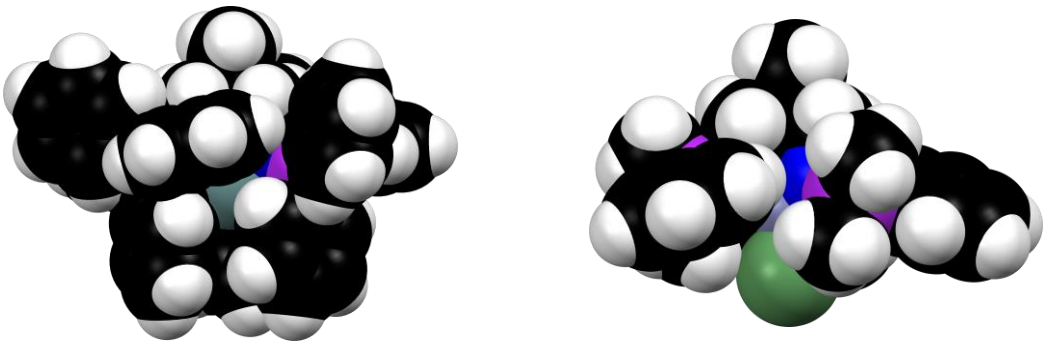

5 **6**

Figure 2.1.15: Space filling model of a side view of metal complexes 5 and 6. With atom sizes depicted at their respective VAN-DER-WAALS radii.

These findings suggest that the second ligand system **3** should be more suitable in following reactions where an access to the central metal is needed.

Another interesting finding one can see in the crystal structure of **6** is the intact C_3 symmetry for the whole molecule. This can be attributed to the rigid backbone which transfers its symmetry to the adjacent ligand arms and the lower steric demands of the $PPhMe_2$ at its end. These arms are now less steric demanding and can accommodate the symmetry without the need to shift their position because of intra- and intermolecular interactions. The complex crystalizes in the space group $I\bar{4}3d$. A threefold axis can be found in the central position through the C1, C2, Zn1, Cl1 atom positions. Through the rotation of this axis the whole molecule can be build. A view of the bottom of the molecule along the threefold axis can be seen in Figure 2.1.16.

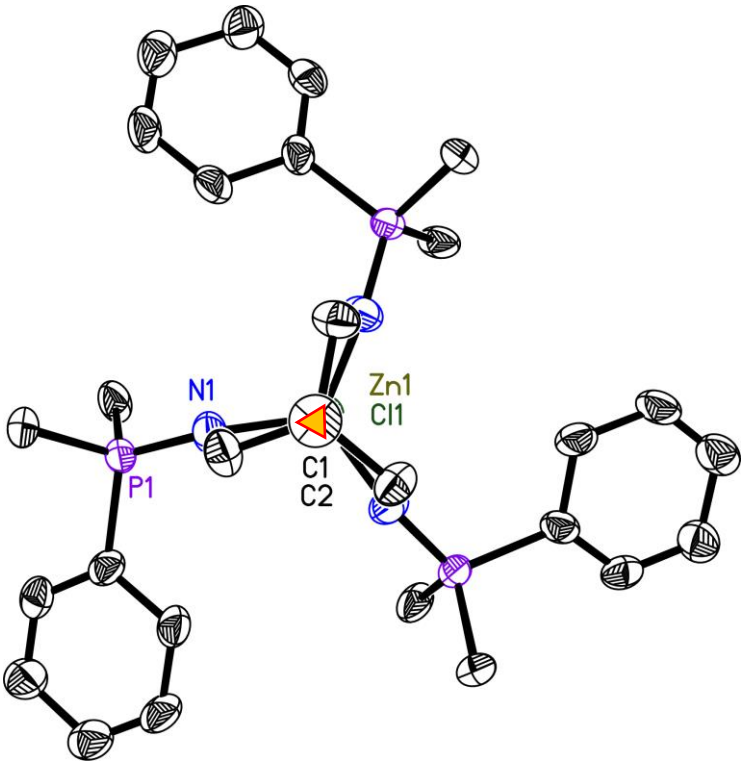

Figure 2.1.16: View along the three fold symmetry axis along C1, C2, Zn1, Cl1 of 6 with drawn in symmetry operator.

A minor result of the change in steric demand on the ligand arms allows for a slight torsion of 11.97° of the nitrogen plane against the alkyl backbone plane. This slight torsion can also be seen in Figure 2.1.16. The C3 – N1 bond lengths stay the same with 1.474 (13) Å in comparison to 1.477 (1) Å in the previously discussed metal complex **5**, the bond angle for N1 – C3 – C2 is with 112.9(9)° also unaffected in comparison to molecule **5** with 112.9(4)°. The zinc metal atom is located in the center of the coordination pocket with a bond length of 2.013(8) Å almost at the same position as germanium in **5** with a mean Ge1 – N of 1.992(5) Å. Overall the change of substituents at the phosphorus atoms allowed for the coordination of a metal atom with an additional halide atom but didn't affect the geometry of the coordination pocket.

To further build upon these findings additional main-group and transition metal atoms suitable for a coordination reaction with the ligand systems **2** and **3** were tested. For this task different main-group and transition metal salts ($MgCl_2$, $MgBr_2$, CaI_2, $SrBr_2$, $BaCl_2$, BaI_2, CdI_2, $PbCl_2$, $AlCl_3$, $GaCl_3$, $SnCl_2$, $InCl_3$), pre-coordinated derivatives ($TiCl_3(THF)_3$, $GeCl_2$·dioxane) and hexamethyldisilazane (HMDS) systems (Sn-HMDS, Ge-HMDS, Zn-HMDS) were selected. The objective was to find the limits of the ligand systems **2** and **3** in metal coordination reactions as well as to shift the scope towards main group metals and possible new interesting binding motifs. The different metals tested in here are shown in Figure 2.1.17.

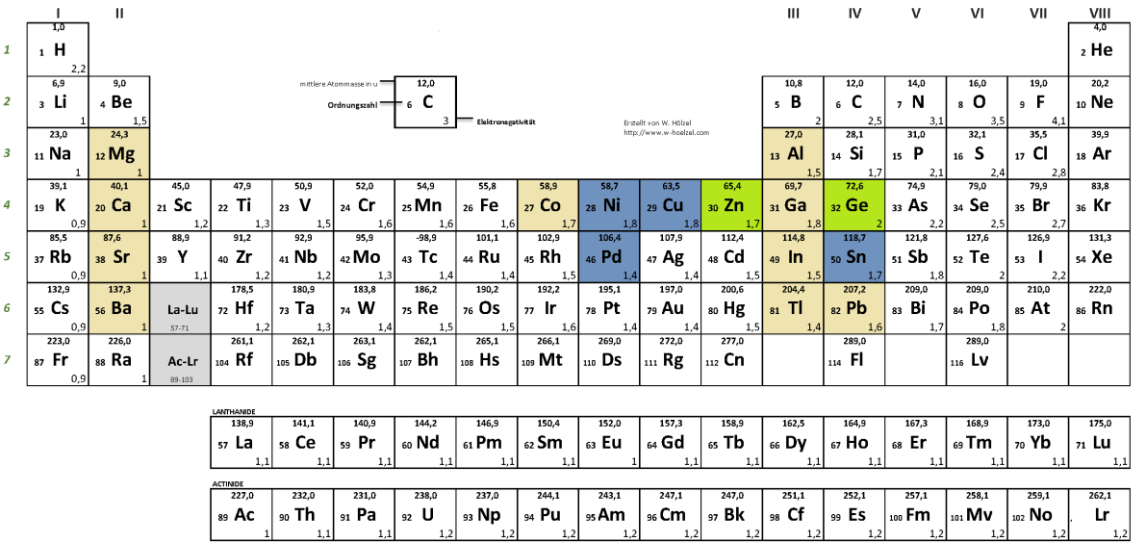

Figure 2.1.17: Metal atoms used in coordination reactions with the ligand systems 2 and 3. New successful synthesis reported in here (*green*), metal atoms used in complexes reported by KRATZERT[77] and BEAUFORT[76] (*blue*) and additionally tested metal atoms (*yellow*).

The reaction conditions were generally kept the same as outlined in Scheme 2.1.5 with THF or toluene as solvent with the occasional addition of DCM to increase the solubility of the reactants. The reaction times were varied between 1 h and up to five days at room temperature with subsequent crystallization attempts at a decreased temperature. In most cases the formation of a white powder could be observed either immediately or no later than ~12 h after the addition of the corresponding ligand system solution to the reaction mixture. The solid was then filtered off and subjected to different analytical methods in order to find an indication towards it composition. Inconveniently no solvent could be found which was able to dissolve the white powder so any solution based analytical method like NMR, recrystallization and subsequent X-ray analysis as well as some mass spectrometry experiments were not accessible. For the solid state analytics elemental analysis and mass spectrometry were chosen as well as solid state NMR experiments in cooperation with PÖPPLER at that time active within the GRIESINGER group at the Max Planck Institute for Biophysical Chemistry, Göttingen. Again, no meaningful results could be obtained to narrow down the true composition of the white powder. Mass spectrometry experiments gave a very crowded peak pattern with no distinctive syntax and only some minor carbon and proton signals could be found in the solid state NMR. In an indirect approach the composition of the remaining solution was analyzed by NMR. In the remaining solution no proton signal for the ligand systems **2** or **3** could be assigned, in fact most of the time only the proton signal for the corresponding solvent could be seen. This finding is coherent with the experimental observation, that in some cases (e.g. CaI_2 addition) the unknown white powder formed immediately upon addition of the ligand system in quantitative yields and

also a visual uptake of the metal salt could be observed in reactions where the reactants were used as a suspension.

With the lack of proper analytical data, the composition of the white powder remains unknown. From the limited results it can be speculated that the metal sources do in fact react with the ligand systems, indicated by the lack of ligand proton signals in the remaining solution, which then undergo intra- and intermolecular conversions to form some higher homologues in the form of oligomeric and polymeric compounds. Because of the limited analytical data on reactions which formed the unknown white solid as well as the remaining reactions which didn't show any sign of conversion it was concluded that the synthesis of new metal complexes with metal atoms marked in yellow in Figure 2.1.17 were not successful.

To conclude it could be shown, that the organoazide **1** is a suitable rigid backbone to build up ligand systems **2** and **3** which employ a C_3 symmetry at its center and that it is possible to keep that symmetry after a metal coordination reaction between the ligand systems and a suitable substrate. Synthesis of the iminophosphorane ligand systems **2** and **3** was possible in good yields by the STAUDINGER reaction and with the knowledge from preliminary results by KRATZERT[77,78] and BEAUFORT[76] more analytical data could be obtained on the ligand systems as well as the crystal structures of two new metal complexes **5** and **6**. The metal coordination could be achieved with two new metals (Zn, Ge) which are able to form a tridentate coordination sphere with the nitrogen atoms of the ligand systems. With the coordination reactions it could be observed that the substituents on the phosphorus atoms play a vital role in forming the coordination pocket the ligand is able to provide. With the more space demanding triphenylphosphane substituents in ligand **2**, only binding motifs where the central metal atom alone bonds to the nitrogen atoms of the ligand in a tridentate fashion are possible. With the less steric demanding dimethylphenylphosphane $PPhMe_2$ substituents in **3** the coordination pocket is large enough for the metal to keep one halide which allows the coordination of a broader selection of metal atoms. The ligand system **2** with the bulky PPh_3 moieties appears to be inferior to the other one **3** in regard to probable catalytic reactions. Because of the high steric demand of the ligand, an access to the central metal atom is hindered for a substrate which is needed in catalytic reaction pathways. Furthermore, the poor solubility in common solvents of the ligand and the metal complex makes subsequent reactions more difficult and reaction times even longer since mostly two phase systems need to be employed. The germanium center in $[Ge\{(Ph_3PNCH_2)_3CMe\}]$ (**5**) however might be employed to build a metal-metal bond to a LEWIS-acidic early transition metal fragment and show advantageous catalytic abilities.

The second examined ligand system **3** with the $PPhMe_2$ substituent seems more promising in these regards. Not only does it provide a much better solubility in commonly used solvents but the X-ray structure of the resulting metal complex **6** also shows that it is still possible to keep a substrate coordinated to the central metal. This halide can possibly be exchanged for another ligand.
It could be shown that both ligand systems **2** and **3** provide a very defined coordination pocket and are highly selective towards different main-group and transition metal atoms. Despite the known complexes with Ni, Pd, Cu, Sn two new complexes with Zn and Ge could be isolated. All other efforts to coordinate different metal atoms did not yield in the expected metal complex but ended in a white insoluble powder which is presumably an oligomeric or polymeric structure consisting of the ligand system and the metal salt. Since these findings impede further studies of this iminophosphorane ligand system and their metal complexes the topic was no longer pursued and instead and adaption of the ligand system was carried out to form mesoionic carbenes.

2.2 Tripodal Triazolic Ligand Systems with a Bridging Alkyl Backbone

From the results gathered in the previous chapter 2.1 one can see that innovative ligand design plays a key role in the development of efficient and versatile ligand systems. Changes in the periphery of a ligand and the coordinated atom can influence reaction rates, yields, and selectivity substantially. Therefore, the aim is to broaden the selection of ligand systems which can function as coordination units for a wide variety of metal fragments and also employ distinct ligand symmetry to comply with the different requirements towards suitable catalysts.

This research area focuses on the synthesis and characterizations of ligand systems and subsequent metal complexes which utilize a tripodal ligand sphere where three ligand arms are able to coordinate to a metal atom. By employing a tripodal azide as starting material and functionalizing the ligand arms with 1,2,3-triazoles, multiple classes of compounds with different coordination patterns are accessible.

One benefit of employing 1,2,3-triazoles is that these groups are easily accessible with a high variety by employing basic click-chemistry. HUISGEN described in 1961 an easy access route for the synthesis of 1,2,3-triazoles using a 1,3-dipolar-[3+2]-cycloaddition between azides and alkynes.[87] In 2002 reactivity and yield of the reaction could be improved by addition of a copper(I) catalyst which was independently reported by SHARPLESS *et al*. and MELDAL *et al*..[88,89] Furthermore, in 2005 SHARPLESS proposed a possible catalytic cycle for this reaction shown in Scheme 2.2.1.[90]

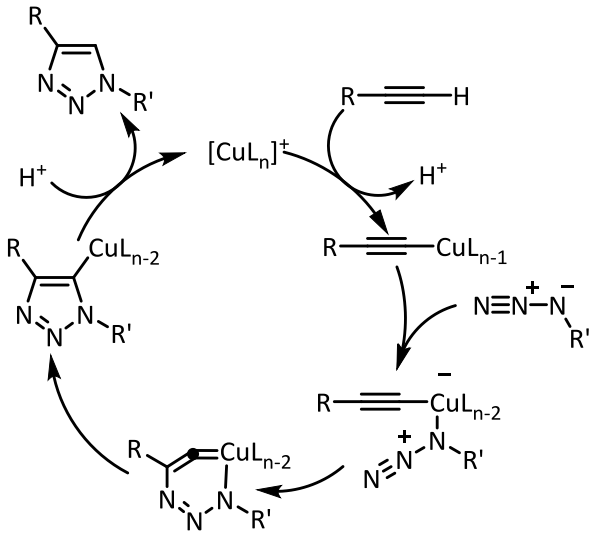

Scheme 2.2.1: Catalytic cycle of a Cu(I) catalyzed click-reaction by SHARPLESS *et al*..[90]

The catalyzed reaction offers shorter reaction times with milder conditions and an improved stereoselectivity. Most reactions can also be run at room temperature. SHARPLESS coined the term click-chemistry in 2001 describing a class of reactions where small units were clicked together to a

bigger organic compound showing high yields, mild conditions, short reaction times and an easy workup procedure.[91] Improvements to this reaction type are still in the focus of ongoing research for example in the field of ionic liquids[92], biology and drug research[93,94], and polymers[95,96].

From previous results presented in chapter 2.1 it was deemed that a rigid backbone which already employed the C_3 symmetry would be a suitable starting material to force a similar ligand design as with the iminophosphorane ligands **2** and **3**. A similar tripodal design offers better comparability between both ligand systems in regard to their coordination behavior and overall reactivity as well as the different influences of the functional groups on each arm towards metal coordination reactions. Access to the ligand system was possible in a two-step synthesis. First, a proper molecule which forms the connecting backbone needed to be identified and then functionalized to employ the azide groups. These are needed to use the click-chemistry in combination with an acetylene to build up the whole ligand with three triazolic arms.

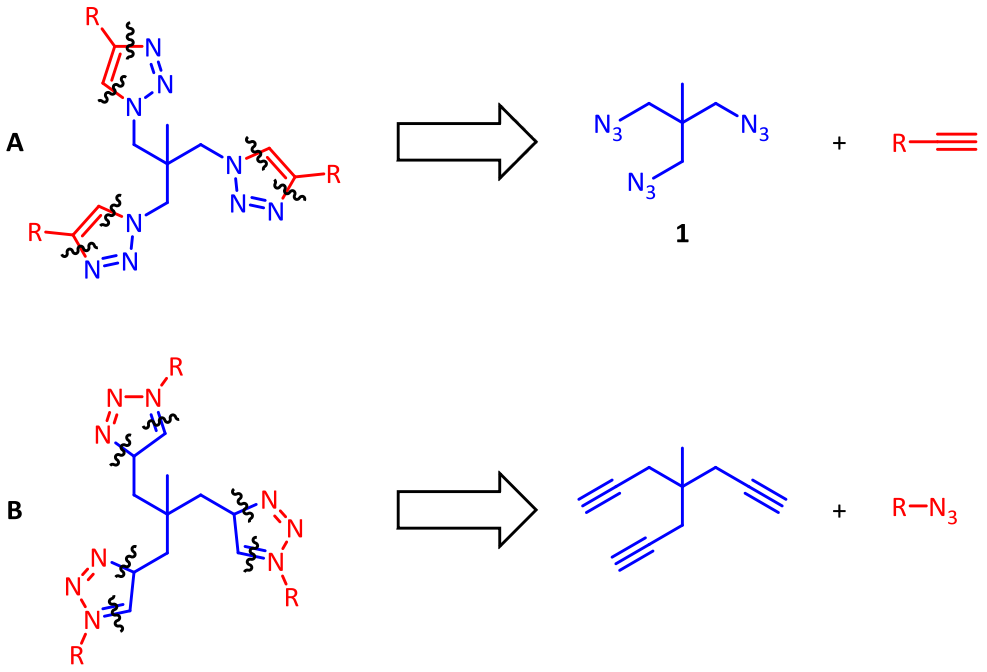

Scheme 2.2.2: Two possible starting reactions (A, B) towards a tripodal triazolic ligand with an alkyl backbone.

The reaction pathway **A** in Scheme 2.2.2 was chosen because of the availability of the organoazide **1** which was already used to build the iminophosphoranes described in chapter 2.1.. Even though organoazide **1** is still regarded as an explosive hazard with the corresponding drawbacks during synthesis and handling in the laboratory. The other possible reaction pathway **B,** which would lead to a similar ligand system by reaction of a tripodal acetylene with an azide, was discarded because the access to the acetylene was problematic. Additionally, multiple azides needed to be synthesized

to introduce the different substituents. The stability of these azides is uncertain and they could provide an even higher danger of explosive decomposition.

It is also of note, that the two proposed reaction pathways would lead to different products. In **A** the proposed product has its substituents located at one of the carbon atoms and the triazolic ring system is connected to the ligand backbone via one of its nitrogen atoms. In **B** the binding is switched with the substituents located at a nitrogen atom from the triazolic ring which is connected to the ligand backbone via a carbon atom. One could argue that the connection of the ligand backbone to one of the sp^2 hybridized carbon atoms of the ring system would lead to an overall more rigid ligand system and that the tilting of the triazolic rings against the ligand backbone would be hindered. The C – N bond in **A** on the other hand can be bent a little bit more out of their ideal bonding angles and would provide a more flexible ligand system.

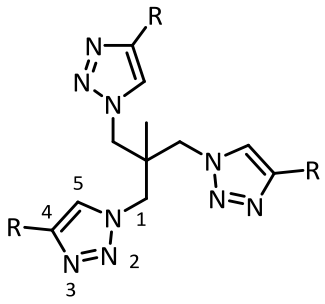

A

Figure 2.2.1: Numbering scheme for the proposed ligand systems A in Scheme 2.2.2.

The addition of a substituent R at the C4 position of the triazolic rings proves to be necessary since the unsubstituted triazolic rings would be to unreactive towards a deprotonation reaction because of the rather high *pks* value of the system.[97,98] Furthermore, preliminary results[77] indicated that these described functionalization to the triazolic rings are still not enough to sufficiently active the rings and reduce its *pks* value. Therefore, an additional methylene group at the triazolic rings is needed. With the introduction of a methylene group at the N3 position, the ligand system **A** can be sufficiently activated to act as a mesoionic carbene in subsequent reactions. In comparison, ligand system **B** would have its corresponding nitrogen atom N1 in close proximity to the ligand backbone which might shield the position hindering an alkylation reaction on that position. A deeper and more detailed insight into these methylation reactions is a topic of a later chapter in chapter 2.4.1. Because of the described characteristics, the proposed ligand system **A** in Scheme 2.2.2 is considered to be more promising in forming suitable tripodal triazolic ligand systems with an alkyl backbone. Synthesis of the starting material, namely the 1,1,1-tris(azidomethyl)ethane (**1**) can be

achieved on the same route introduced in chapter 2.1 by BEAUFORT *et al*.[76] For reference the synthetic pathway is shown again in Scheme 2.2.3.

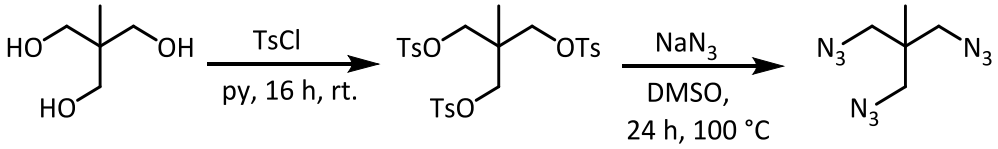

Scheme 2.2.3: Synthesis of 1,1,1-tris(azidomethyl)ethane (1) by BEAUFORT *et al.*.[76]

In the second step of the ligand synthesis the organoazide **1** is reacted with an acetylene derivative in a copper(I) catalyzed click-reaction to form the corresponding ligand systems. The general reaction pathway for the ligand synthesis can be seen in Scheme 2.2.4.

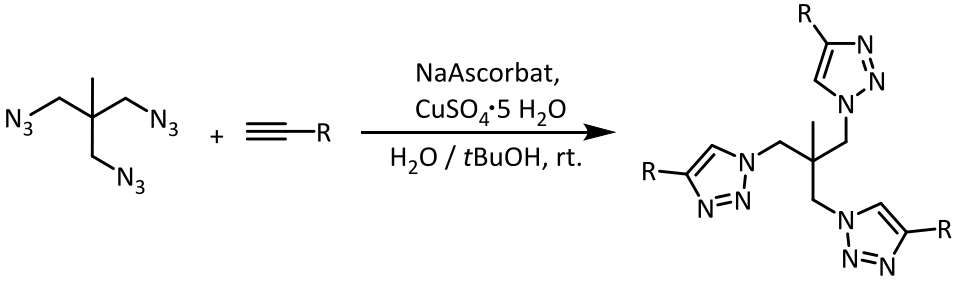

R = none (**7**), *n*Pr (**8**), *cy*Pr (**9**), *i*Pr (**10**), *t*Bu (**11**), Ph (**12**), Mes (**13**), FeCp (**14**)

Scheme 2.2.4: General reaction pathway for the formation of the triazolic ligand systems by employing click-chemistry type of reactions.

In most cases the organoazide **1** and the acetylene derivative were added to a 1:1 mixture of *t*BuOH / H_2O and subsequently the precursors to the copper(I) catalyst were added as $CuSO_4 \cdot 5\ H_2O$ and sodium ascorbate. The catalyst loading varied between sets of I) 2.0 mol% $CuSO_4 \cdot 5\ H_2O$, 10 mol% sodium ascorbate and II) 4.4 mol% $CuSO_4 \cdot 5\ H_2O$ with 20 mol% sodium ascorbate in regard to the amount of acetylene. While different catalyst loadings were tested the reported values in here lead to the best yields. Apart from that for the synthesis of **7** CuI was used as a catalyst precursor with a catalyst loading of 20 mol% with 20 mol% sodium ascorbate and the solvent was changed to a 1:2 mixture of H_2O / MeCN. For the synthesis of **14** benzoic acid was added to the reaction mixture, catalyst loading was reduced to 1.0 mol% $CuSO_4 \cdot 5\ H_2O$ with 1.0 mol % sodium ascorbate and the solvent was changed to a 2:1 mixture of *t*BuOH / H_2O. With these reaction conditions good yields of the target ligand systems could be obtained of 70+ %. In Table 2.2.1 the number of the ligand system, the alkyne derivative used during synthesis as well as the catalyst and loading and the solvent mixture can be seen in.

ligand system	alkyne	catalyst loading	solvent
7	none (CaC_2)	20 mol% CuI, 20 mol% sodium ascorbate	H_2O / MeCN (1:2)
8	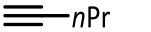	4.4 mol% $CuSO_4 \cdot 5\ H_2O$, 20 mol% sodium ascorbate	^{t}BuOH / H_2O (1:1)
9	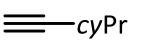	4.4 mol% $CuSO_4 \cdot 5\ H_2O$, 20 mol% sodium ascorbate	^{t}BuOH / H_2O (1:1)
10	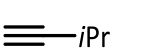	2 mol% $CuSO_4 \cdot 5\ H_2O$, 10 mol% sodium ascorbate	^{t}BuOH / H_2O (1:1)
11		4.4 mol% $CuSO_4 \cdot 5\ H_2O$, 20 mol% sodium ascorbate	^{t}BuOH / H_2O (1:1)
12		4.4 mol% $CuSO_4 \cdot 5\ H_2O$, 20 mol% sodium ascorbate	^{t}BuOH / H_2O (1:1)
13		2.0 mol% $CuSO_4 \cdot 5\ H_2O$, 10 mol% sodium ascorbate	^{t}BuOH / H_2O (1:1)
14		1.0 mol% $CuSO_4 \cdot 5\ H_2O$, 1.0 mol% sodium ascorbate, 1.0 mol% benzoic acid	^{t}BuOH / H_2O (2:1)

Table 2.2.1: Ligand system number, alkyne derivative, catalyst and catalyst loading and solvent mixture used in the synthesis of the different ligand systems.

Because of the steric hindrance of the alkyl backbone all reactions gave the pure 1,4-substituted derivative and none of the 1,5-substituted one and therefore stereo chemical considerations were not an issue.

In general, the quality of the click-chemistry reaction depends on different factors for example the employed solvent, amount of solvent, solvent ratios and the employed catalyst. In here a homogenous mixture of *t*BuOH / H_2O was used most of the time since all starting materials showed a good solubility in it and the copper(I) species could also form easily within. The amount of solvent was also kept to as low as possible to provide a high concentration of the reactants which also improved the overall yields of the reactions.

Some of the synthesis shown in here for the ligand systems **8**, **11**, and **12** could be improved on by tailoring the reaction conditions towards the desired target ligand system in regard to the solvent mixture as well as catalyst and catalyst loading. Especially by using copper(I) catalysts derived from carbenes in a DCM solution led to an increase in yield for some of these reactions. This reaction optimization was done in a cooperation with REICHMANN within the GHADWAHL and STALKE[99] group for the development of new carbene based catalysts as a part of his PhD thesis. Some of his results as well as the employed catalysts are shown in Table 2.2.2 and Figure 2.2.2.

catalyst	catalyst loading [mol%]	alkyne	yield [%]
A	1	Ph	99
B	0.5	Ph	91
B	1	Ph	79
C	1	Ph	76
A	1	*t*Bu	71
A	1	*n*Pr	87

Table 2.2.2: Alkyne-azide cycloaddition reactions with different carbene based copper(I) catalysts and corresponding yields of the tripodal triazolic ligand system reported by REICHMANN.[99]

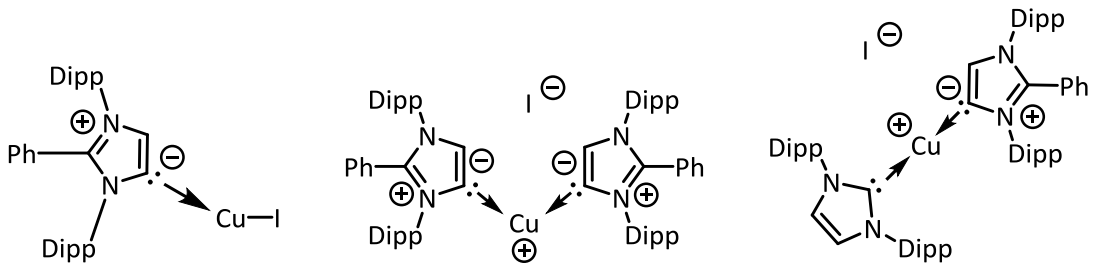

Figure 2.2.2: Carbene based copper(I) catalysts (A, B, C) synthesized by REICHMANN[99] which were used in the optimized synthesis of the ligand systems 8, 11 and 12.

Besides the increase in yield another prominent advantage of these copper(I) catalysts was a reduction in workup complexity to get the pure product out of the reaction mixture. In the classic approach described earlier, consisting of a $CuSO_4 \cdot 5\ H_2O$ and sodium ascorbate mixture to form the copper(I) catalyst in a *t*BuOH / H_2O solution, the workup was done by a washing step with aqueous

ammonia to remove all excess copper species and subsequent precipitation of the product by addition of pentane to the reaction mixture. Also the product needed to be dried and prepared accordingly if it would be used in reactions which demanded the exclusion of water. With the new catalyst the ligand synthesis could be done in dry DCM and the products could be precipitated by the addition of pentane to the reaction mixture while the catalyst stayed in the polar phase of the reaction mixture.[99]

Besides the ligand systems bearing different substituents at the triazolic rings **8** to **14** a ligand system without any substituents **7** was synthesized as an interesting benchmark system to compare to. It was therefore tried to synthesize such a compound with no substituents at the C4 and C5 position.

For the synthesis of compound **7** pure acetylene in in a reaction with a copper(I) species couldn't be used, since the highly explosive copper(I) acetylene species would form during the reaction. Thus a different approach was chosen derived from a similar reaction reported by KUANG *et al*.[100] in 2009. During this reaction acetylene is formed *in situ* from calcium carbide and readily undergoes reaction with the azide to form the triazolic rings which in turn keeps the acetylene concentration to a minimum stalling the side reaction to the copper(I) acetylene. The reaction is depicted in Scheme 2.2.5.

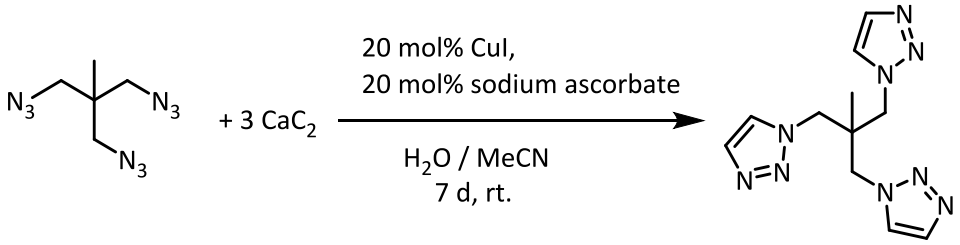

Scheme 2.2.5: Synthesis of ligand system 7 with no alkyl substituents at the triazolic rings.

In this reaction copper(I) iodide, sodium ascorbate and the organoazide **1** were dissolved in a 2:1 mixture of MeCN in H_2O and then calcium carbide was slowly added. The reaction was stirred at room temperature and brought to *pH* = 5 with conc. HCl. The reaction solution was washed with EtOAc, the organic phases were extracted, combined and washed with brine. The solution was then dried over $MgSO_4$ and pentane was added to the resulting yellow solution to precipitate the target compound. The formation of a yellowish oil is observed and all excess solvent was removed *in vacuo*. During evaporation of the solvents some crystals formed which were suitable for X-ray diffraction experiments to determine the structure of the compound which is shown in Figure 2.2.3.

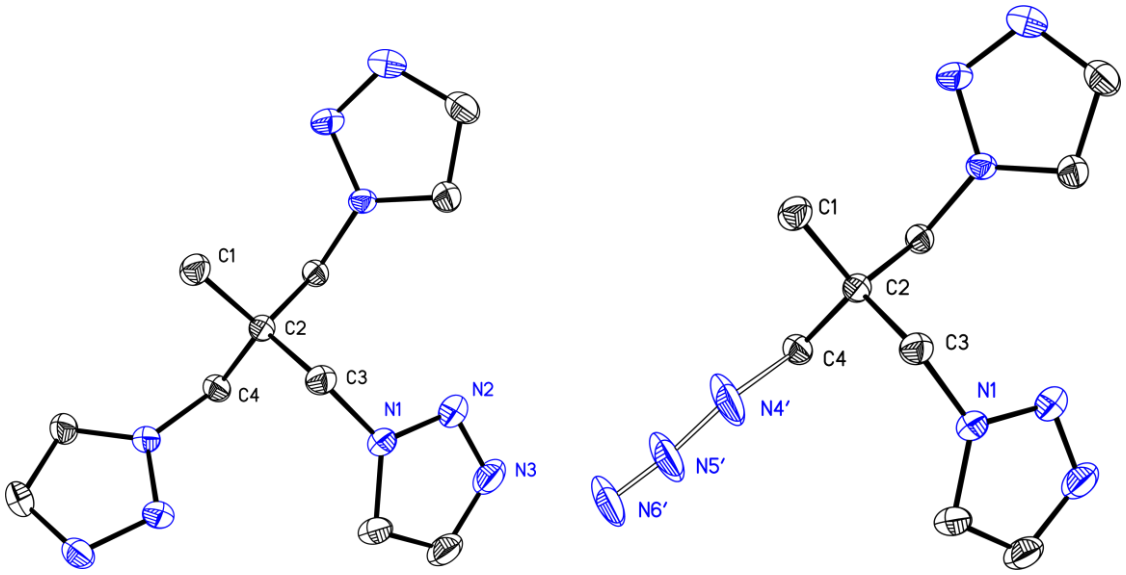

Figure 2.2.3: Crystal structure of 7 (*left*) and the second part resulting in a disorder (*right*). 7 crystalizes in the space group $P\bar{1}$ in a triclinic crystal system with α = 89.26(1)°, β = 79.02(1)°, γ = 75.29(1)° and a = 6.244(2) Å, b = 8.698(3) Å, c = 12.188(4) Å. The anisotropic displacement parameters are depicted at the 50% probability level. Hydrogen atoms have been omitted for clarity. The crystal shows 7% of a disorder which can be attributed to the second molecule (*right*) with an unreacted side arm.

The crystal structure shows the successful synthesis of the ligand system **7** where all three side arms have been converted from the azide functionality to the triazolic rings. All three rings arrange themselves in a least steric hindered fashion to each other, because of the low bulk of the ligand arms and the resulting degree of freedom. The rigid alkyl backbone is unchanged, as expected, and cannot convey its symmetry towards the ligand arms as it is seen with the iminophosphorane ligand **2** in 2.1. Because of the low steric demand of the whole ligand system all bond angles and bond lengths are within the expected ranges. The central moiety arranges in a tetrahedral fashion with bond angles of C1 – C2 – C3 with 107.78(10)°, C1 – C2 – C4 with 111.58(10)° and C1 – C2 – C5 with 110.15(10)°. The slight deviation of the C1 – C2 – C3 bond angle can be attributed to short contact interactions within the crystal lattice forcing this ligand arm in a different position.

As shown in the X-ray structure some side products have been formed during the reaction where some azide arms did not undergo the click-reaction with acetylene. In the single crystal this can be seen as a disorder which amounts to only ~7%. With the help of NMR spectroscopy and ESI mass spectrometry however it could be observed that 70% of the product mixture consists of the target compound **7** while the remaining 30% consist of side products where at least one azide side arm is not fully converted to the triazolic ring. To get a better yield of the fully functionalized product an increase of the reaction time was considered with up to seven days but ultimately provided no improvement. Another option would be an increase in reaction temperature which is not feasible

since the whole reaction is performed in a closed flask to prevent leakage of the acetylene. Therefore, a better catalyst and solvent system is needed but unfortunately, there are not many accessible alternatives in the literature regarding this specific reaction.
With the described reaction it could be shown that it is possible to form a new tripodal triazolic ligand system **7** from an organoazide **1** which employs a very low steric demand and could therefore be very useful as a benchmark system to compare with further functionalization on the ligand systems.

After the successful synthesis of the tripodal triazolic ligand **7** without any substituents on the triazolic rings it was of interest to further build up different ligand systems which slowly increase the steric demand but not change the electronic properties of the triazolic rings too much. By controlling the steric aspect of the ligand systems these could be fine-tuned towards selected metal sizes and furthermore the overall type of coordination might be controlled i.e. mono- to polymeric. Preliminary experiments with these ligand systems have been carried out by KRATZERT[77] and SCHWARZE[101] during their PhD and Master thesis in the STALKE group but. The work in here aims to build upon and unite the different findings and to comprehensively study the properties of the ligand systems in regard to synthesis optimization, reactivity, analytical data and their behavior during metal coordination.
The introduction of a *n*-propyl group (*n*Pr) and its isomeric derivatives the *i*-propyl group (*i*Pr) as well as its closely related cyclic *cy-p*ropyl group (*cy*Pr) is very well suited to modify the ligand systems and give insight in the steric demands of those. Furthermore, if one considers the later goal of functionalizing these ligand systems towards their sought of role as mesoionic carbenes, the introduction of substituents at the C4 position of the triazolic rings accomplishes two advantages. An additional substituent at the triazolic rings reduces their *pks* values[97,98] activating the ring slightly and thus making the subsequent deprotonation reactions to form the mesoionic carbenes easier to carry out with less strong bases. Also the newly introduced substituent blocks the C4 position and simultaneously the C5 position becomes the only possible coordination site in later metal coordination reactions. An additional advantage can be accomplished by the introduction of bulkier substituents which led to a stabilization of the electronic state of the mesoionic carbenes which are formed during later metal coordination reactions. More insight and discussion into the metal coordination reactions are part of later chapters 1.5 and 1.6.
Synthesis of the ligand systems with an *n*Pr (**8**), *cy*Pr (**9**) and *i*Pr (**10**) substituent at the C4 position was carried out via the general reaction pathway for this type of click-chemistry shown in Scheme 2.2.4. The azide and the corresponding acetylene starting material, 1-pentyne to form the *n*Pr system **8**, cyclopropylethyne for the *cy*Pr system **9**, and 3-methyl-1-butyne for the *i*Pr system **10**, were

dissolved in a *t*BuOH / H_2O 1:1 mixture. The copper sulfate and sodium ascorbate mixture (for catalyst loading see Table 2.2.1) was added to form *in situ* the copper(I) catalyst. The reaction was stirred for 48 h to 72 h and subsequently quenched with ice water and extracted with DCM. The copper species were removed by washing with ammonia solution to form the copper-ammonia complex and the water phase was extracted with DCM. Removal of the solvent gave the corresponding product as a pure white powder in 50 – 70 % yields. The reaction could be improved upon the previous results by KRATZERT[77] and SCHWARZE[101] changing the catalyst loading from 4.4 mol% to 2.0 mol% of the $CuSO_4 \cdot 5\ H_2O$ precursor in the case of the reactions which yielded **9** and **10**. Also increased reaction times resulted in a slight increase of yield as well as the addition of an extra washing routine which included the separation of the organic and water phase followed by multiple washing steps with ammonia in water and subsequent extraction of the organic phases. The reaction which gave ligand system **8** was improved upon by employing a carbene based copper(I) catalyst as described earlier in this chapter. To confirm the successful synthesis with the improved reaction conditions crystallization attempts have been made for ligand system **8**, **9** and **10**. Slow evaporation of a small sample of **8, 9** or **10** in MeCN was used to precipitate crystals suitable for X-ray diffraction. The resulting crystal structures can be seen in Figure 2.2.4 (**8**), Figure 2.2.5 (**9**) and Figure 2.2.6 (**10**).

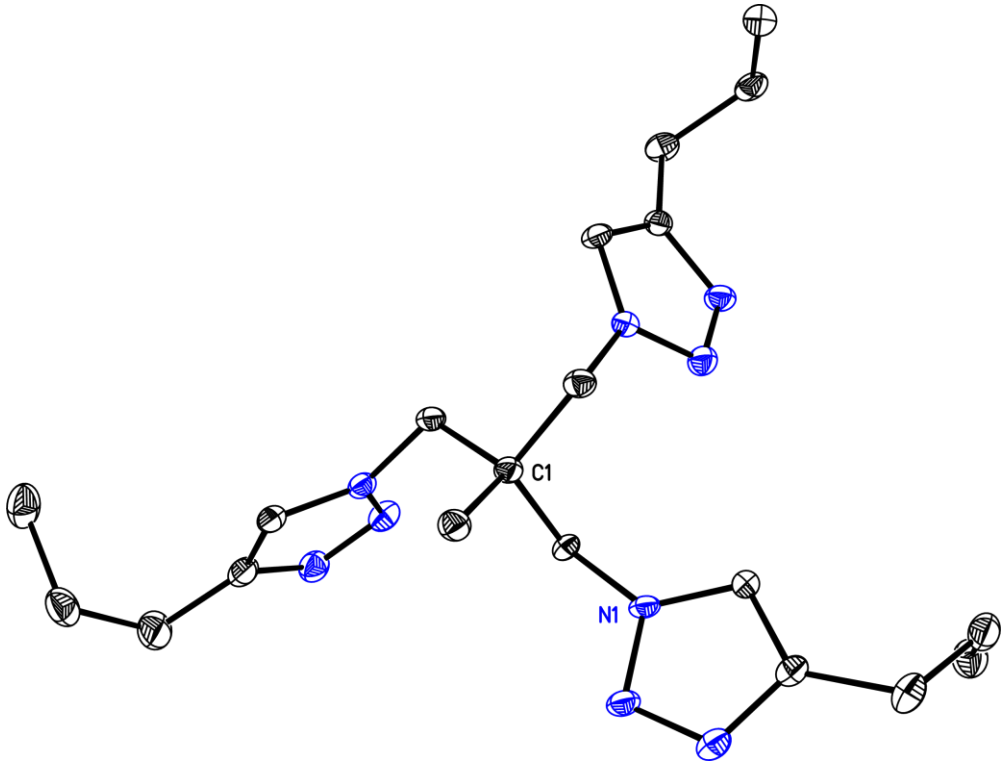

Figure 2.2.4: Crystal structure of 8. 8 crystalizes in the space group $P2_1/c$ in a monoclinic crystal system with α = 90°, β = 111.96(2)°, γ = 90° and a = 12.790(2) Å, b = 15.986(3) Å, c = 11.371(2) Å. The anisotropic displacement parameters are depicted at the 50% probability level. Hydrogen atoms have been omitted for clarity.

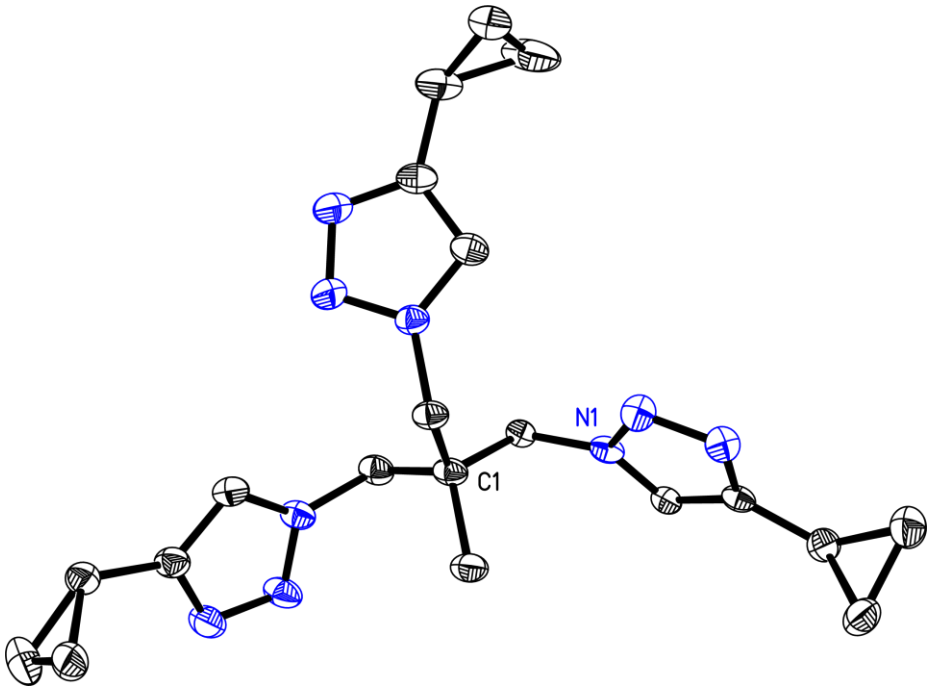

Figure 2.2.5: Crystal structure of 9. 9 crystalizes in the space group $P\bar{1}$ in a triclinic crystal system with α = 108.88(2)°, β = 96.34(2)°, γ = 108.103(3)° and a = 9.507(2) Å, b = 10.704(2) Å, c = 11.123(3) Å. The anisotropic displacement parameters are depicted at the 50% level. Hydrogen atoms have been omitted for clarity. The crystal structure shows a disordered side arm.

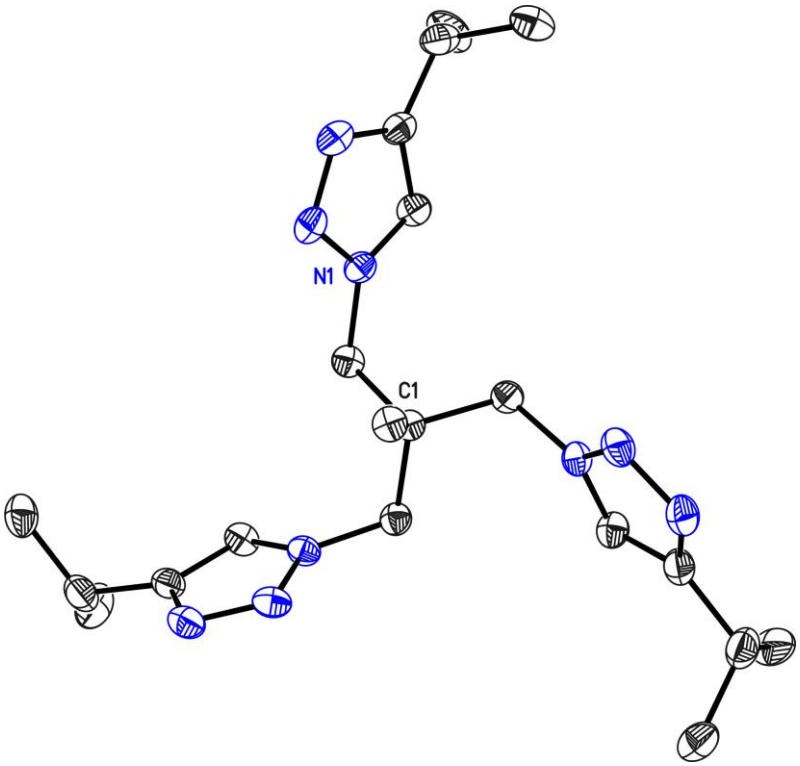

Figure 2.2.6: Crystal structure of 10. 10 crystalizes in the space group *R*3c in a trigonal crystal system with α = 90°, β = 90°, γ = 120° and a = 11.759(2) Å, b = 11.759(2) Å, c = 27.741(3) Å. The anisotropic displacement parameters are depicted at the 50% probability level. Hydrogen atoms have been omitted for clarity. The crystal structure shows three disordered *i*Pr substituents.

The structures for **8** and **9** have already been reported by KRATZERT[77] but without additional analytical data. The work done in here could fill in the missing data and provide a full crystallographic, NMR and mass spectrometry analysis of these ligand systems.
The crystal structures of **8**, **9** and **10** show the central moiety intact with its well defined rigid C_3 symmetric symmetry. All three arms are located in a least amount of steric hindrance to each other and the different rotations of the triazolic rings in regard to the backbone can be attributed to interatomic interactions in the crystal lattice. In the case of ligand system **9** and **10** a positional disorder of the substituents as well as one of the side arms can be observed. While the crystal structure of the previously discussed ligand system **7**, which had no substituents at the triazolic rings, showed a disorder in the form of an unreacted side arm this type of disorder cannot be found here. All three arms in the respective structures have been fully functionalized from an azide to the triazolic rings. NMR and mass spectrometry data also confirm the reaction of all three side arms in solution and solid state. All bond lengths and angles are well within the expected ranges for their corresponding bond type.[81]

On the basis of these results with different propyl group isomers some more functionalization of the ligand system could be achieved by synthesizing a system with a *t*Bu moiety (**11**) which completes this set of substituents with little to none electronic effects at the triazolic ring. The latter provides even more steric demand. This ligand was synthesized according to the general reaction pathway depicted in Scheme 2.2.4 with 3-methyl-1-butyne as the starting material which reacted with the organoazide **1** via click-chemistry employing a catalyst loading of 4.4 mol % of $CuSO_4 \cdot 5H_2O$ and 20 mol % of sodium ascorbate in a mixture of *t*BuOH / H_2O of 1:1 as a solvent. Workup proceeds in the way as applied to the previous examples by quenching the reaction with ice water, extraction with DCM and subsequently complexation of the copper catalyst with an ammonia in water mixture to form the ammonia-copper-complex. Extraction with DCM, drying over $MgSO_4$ and removal of the solvent gave the product as a white powder. The reaction could also be slightly improved upon with the use of the carbene based copper(I) catalyst provided by REICHMANN[99] which eliminated some steps of the reaction workup since this copper(I) catalyst was easier to remove.
Crystals for the X-ray diffraction experiment could be obtained by slow evaporation of the organic solvent. Unfortunately, these type of crystals derived from the ligand system do not diffract up to higher resolutions. Nevertheless, the refinement of the data led to a full description of the structure confirming the proper synthesis. The structure of **11** is shown in Figure 2.2.7.

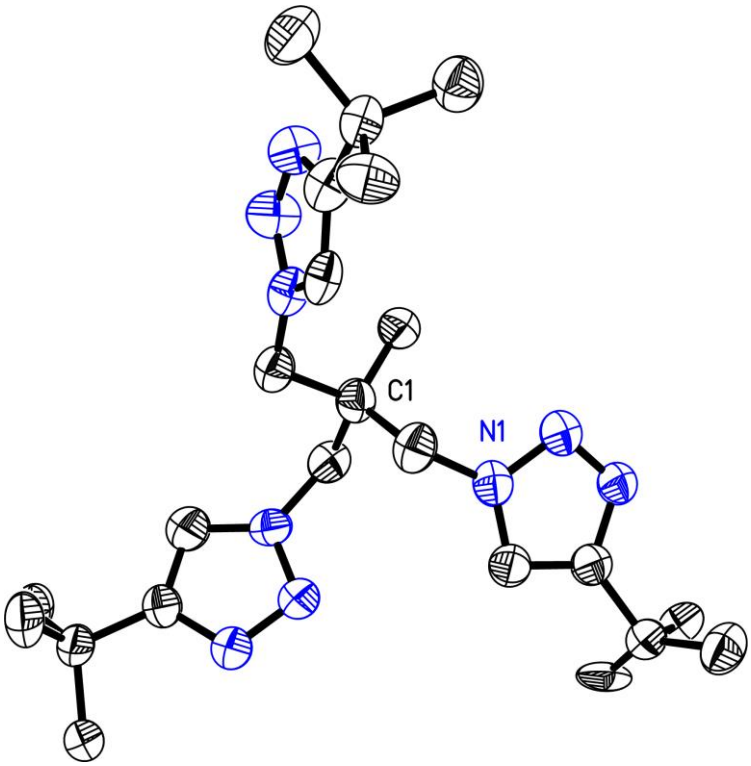

Figure 2.2.7: Crystal structure of 11. 1110 **crystalizes in the space group *C*2/c in a monoclinic crystal system with *α* = 90°, *β* = 90.97(1)°, *γ* = 90° and *a* = 31.940(8) Å, *b* = 17.739(4) Å, *c* = 9.082(2) Å. The anisotropic displacement parameters are depicted at the 50% probability level. Hydrogen atoms have been omitted for clarity. The crystal structure shows two disordered *t*Bu substituents.**

It could be shown that with the use of click-chemistry in a standard protocol of catalyst and catalyst loading the synthesis of four derivatives of a tripodal triazolic ligand system (**8**, **9**, **10**, **11**) was possible in good yields.

To further expand the library of suitable ligand systems for the metal coordination and to examine not only the kinetic but also the electronic influences a substituent imposes on the triazolic ring two more bulky substituents were introduced which are well established in carbene chemistry. A phenyl group was introduced via phenylacetylene to the triazolic rings leading to ligand system **12** and furthermore with mesitylacetylene a higher steric demanding mesitylene group could be introduced in ligand system **13**. These two groups have already shown to be very useful in asymmetric catalysis for example to enhance the diastereo- and enantioselectivity as well as being able to stabilize low oxidation states or low coordination numbers in organometallic chemistry.[102] As shown in chapter 1.5 their steric bulk can also help stabilize the carbene intermediate which is formed in later reactions.

Again they were synthesized along the established protocol shown in Scheme 2.2.4. Unfortunately, with the introduction of bulkier substituents the overall solubility of the starting materials as well as the products tends to decrease, which leads to an increased amount of solvent and a subsequent reduction in yields. As described earlier an improvement for the formation of **12** could be achieved in cooperation with REICHMANN[99] by employing his copper(I)carbene complexes. Crystallization of **12** and **13** could not be achieved, still the successful synthesis could be confirmed by NMR and mass spectrometry data.

As described in chapter 1.4 the electronic properties of the NHCs are prone to diverse changes by adjustments of the ring size, introduction of hetero atoms, aromaticity of the hetero cycles and in particular the electronic properties of the substituents in close proximity to the carbene functionality. There have been multiple developments towards switchable NHC-Ligand systems where these properties can be controlled. e.g. the switch is made possible by a reversible oxidation or reduction step in the periphery of the ligand.[54] Some examples are shown in Scheme 2.2.6 where the change in the *trans*-CO-stretching vibration can be seen before and after a successful oxidization / reduction step.

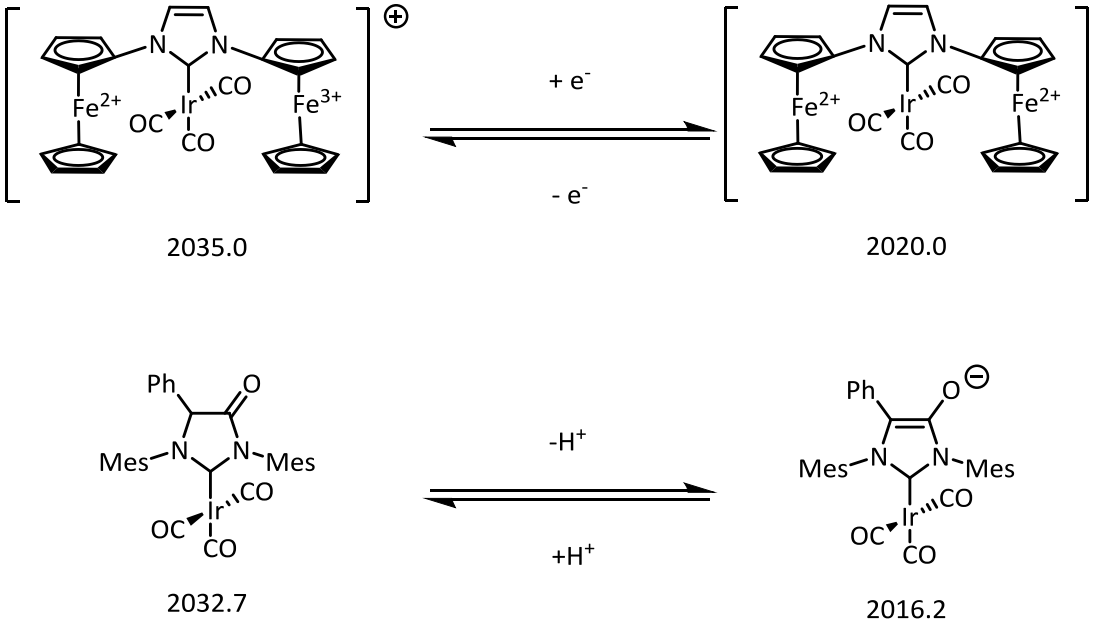

Scheme 2.2.6: Switchable NHC derived metal complexes and their corresponding *trans*-CO-stretching vibration in [cm^{-1}].

The monitoring of the CO-stretching vibration in a metal carbonyl complex is a useful tool to determine the electronic properties of the employed ligand system.[54] The metal is donating electrons into the empty π* anti-bonding orbitals of the carbonyl ligand forming a π backbonding strength-

ening the metal – carbon bond while simultaneously weakening the carbon – oxygen bond. Subsequently, the CO-stretching vibration decreases from its value of 2143 cm^{-1} in the uncoordinated CO molecule. When another non-carbonyl ligand is coordinated, the electron density at the metal atom gets either increased or decreased depending on the ligand properties resulting in a further decrease or increase of the carbon – oxygen vibration. This technique is used to determine the Tolman-electronic-parameter in which the measurement of the frequency of the C – O vibration can be correlated to the electron donating or withdrawing properties of a ligand system .[53]

With the introduction of ferrocene substituents to the ligand system the described redox switchable properties could also be made accessible. On top of that another technique to determine the electronic properties of the ligand systems can be made available by measuring the "Lever-Electronic-Parameter" (LEP) with a cyclic voltammetry experiment described in chapter 1.5.

A proper approach to functionalize the tripodal backbone with three ferrocene moieties which can be oxidized and reduced independently is to first synthesize an ethynylferrocene precursor. One way to synthesize this compound was described by DOISNEAU *et al*. in 1992[103] and is shown in Scheme 2.2.7.

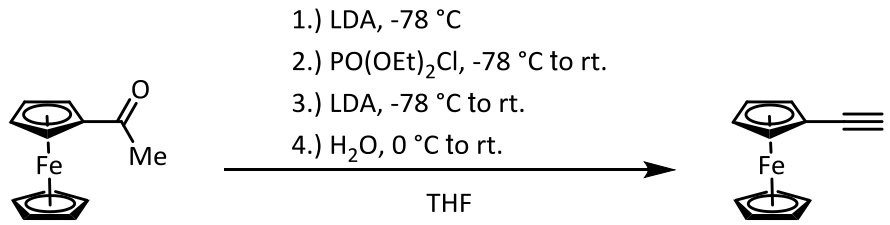

Scheme 2.2.7: Synthesis of ethynylferrocene via acetylferrocene and LDA by DOISNEAU *et al*..[103]

First acetylferrocene is reduced with LDA at -78°C and reacted with $PO(OEt)_2Cl$ to form an intermediate phosphor ether which is reduced again with LDA to form the desired target molecule. While the synthesis gives easily isolable products the yields are rather low in the range of 10 to 20 %. A different synthetic approach was tested to give the desired product in better yields which was proposed by CIAMPI *et al*. in 2013[104] and is shown in Scheme 2.2.8.

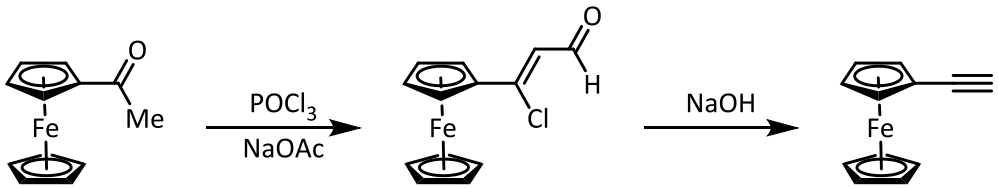

Scheme 2.2.8: Synthesis of ethynylferrocene via acetylferrocene and $POCl_3$ by CIAMPI *et al*..[104]

Unfortunately, this synthetic route did not turn out to be very useful since the resulting products and side products were difficult to separate. Even with extensive column chromatography only small yields of the pure product could be obtained.

A third approach was chosen, this time switching the starting material from acetylferrocene to formylferrocene. Formylferrocene was reacted with triphenylphosphane in the presence of CCl_4 to form a halogenated product which could then be reacted with *n*BuLi to the desired ethynylferrocene. This reaction pathway, shown in Scheme 2.2.9, was proposed by LUO *et al*. in 2000.[105]

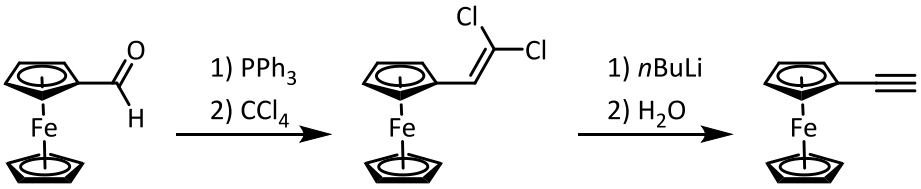

Scheme 2.2.9: Synthesis of ethynylferrocene via formylferrocene by LUO *et al*..[105]

Synthesis of the starting material, the formylferrocene, was achieved from pure ferrocene with DMF and $POCl_3$ by SU *et al.* and the reaction pathway is shown in Scheme 2.2.10.[106]

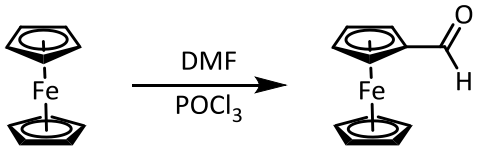

Scheme 2.2.10: Synthesis of formylferrocene by SU *et al*..[106]

This reaction pathway turned out to be much more useful since the desired product ethynylferrocene could easily be isolated in good yields.

To form the corresponding ligand system **14**, the click-chemistry route was again utilized to build up the triazolic rings. As a catalyst the same protocol consisting of $CuSO_4 \cdot 5\ H_2O$ and sodium ascorbate was used to form the copper(I) species but additionally benzoic acid was added as a promoting agent which forms an active intermediate with the copper(I) species, further improving the yield and reactivity during the catalytic cycle. Some studies on this enhancing behavior in the presence of carboxylic acids have been conducted by SHAO *et al*.[107] The chemical equation leading to the triazolic ligand system **14** is shown in Scheme 2.2.11.

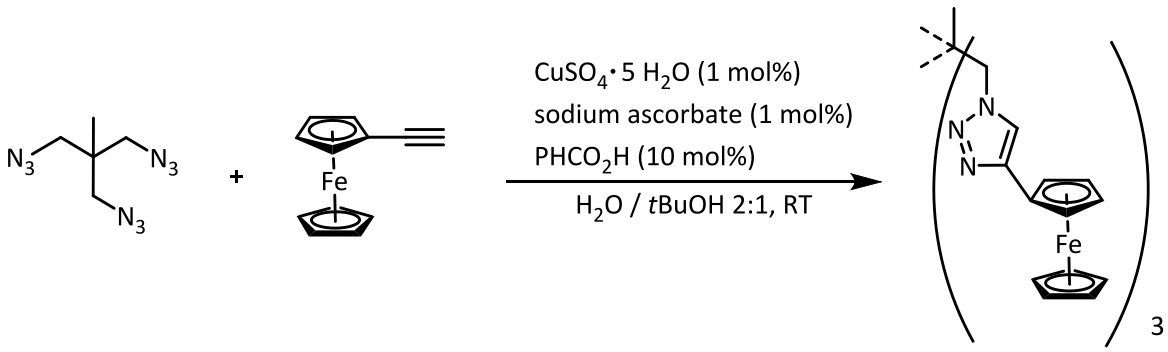

Scheme 2.2.11: Synthesis of the triazolic ligand system with ferrocene substituents 14. Only one side arm of the ligand system is drawn.

Successful synthesis of the ferrocene substituted product could be monitored by NMR measurements which clearly show the ferrocene moieties as an intense singlet at 4.02 ppm with an integral of 15 as well as two triplet signals at 4.27 and 4.70 ppm with an integral of six. Also the methylene bridge of the ligand backbone is still intact and can be found at 4.38 ppm with an integral of six. The ratios of the integrals as well as the absence of additional methylene protons show that there are no unreacted azide groups and that the reaction gives nearly quantitative yields.

By slow evaporation of a concentrated solution in $CDCl_3$ some single crystals could be obtained which were suitable for X-ray structure determination. The resulting crystal structure can be seen in Figure 2.2.8.

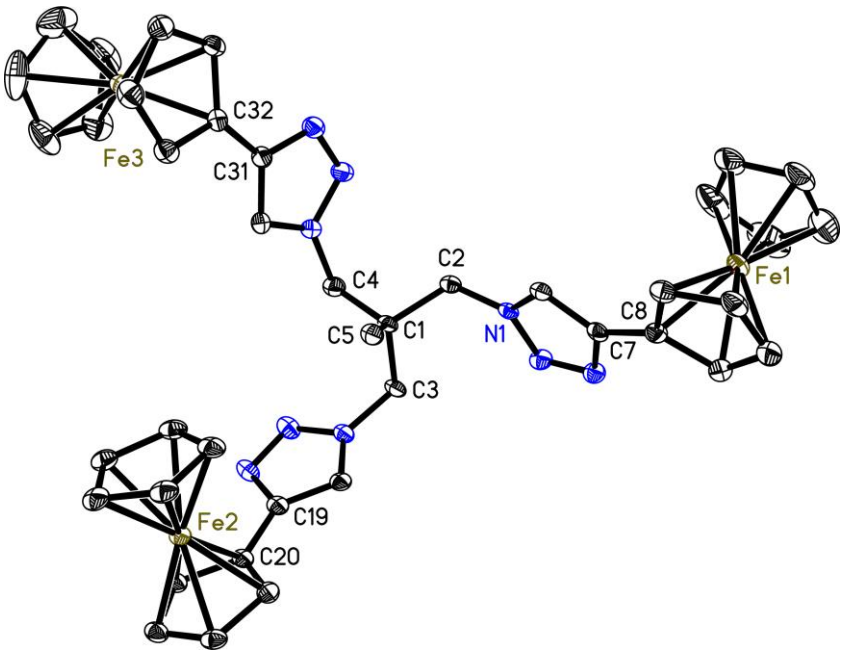

Figure 2.2.8: Crystal structure of 14. 14 crystalizes in the space group $P\bar{1}$ in a triclinic crystal system with α = 74.61(3)°, β = 74.72(2)°, γ = 60.70(2)° and a = 12.687(2) Å, b = 12.711(2) Å, c = 16.835(3) Å. The anisotropic displacement parameters are depicted at the 50% probability level. Hydrogen atoms and a disordered solvent molecules have been omitted for clarity.

The molecule crystalizes in the triclinic space group $P\bar{1}$ with two chloroform molecules in the asymmetric unit. Obviously all three triazolic rings have been formed without any disorder ruling out only partial formation of the molecule which was already indicated by NMR measurements. In line with the other discussed ligand systems all triazolic rings with the ferrocene substituents are turned to a position reducing the steric strain among each other. Interestingly, one would assume that the methyl group C5 would be on top of an overall claw like appearance of the structure like in the preceding examples but in here the claw is inverted with the methyl group C5 in the center of the structure shown in Figure 2.2.9.

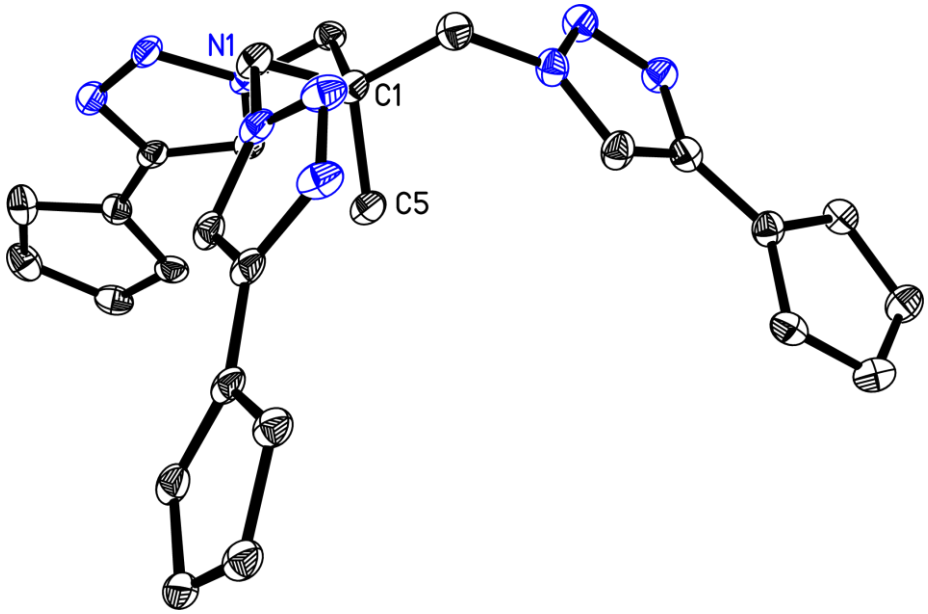

Figure 2.2.9: View of 14 showing the claw like structure with C5 in the center. The anisotropic displacement parameters are depicted at the 50% probability level. Hydrogen atoms, solvent molecules and parts of the ferrocene substituents have been omitted for clarity.

This can be credited to the substantially increased steric demand of the ferrocene substituents. These substituents also interact with neighboring molecules in the crystal lattice as in that the protons on the cp rings align themselves to the π-system of a cp ring in close proximity or the protons of the triazolic rings. These short contact interactions and intermolecular interactions in the solid state lead also to a slight rotation of the connecting bond (C7 – C8, C19 – C20, C31 – C32) between the triazolic rings and the cp ring of the ferrocene substituent. This rotation amounts to 8.29° for the C7 – C8 bond, 10.54° for the C19 – C20 bond, and 12.34° for the C31 – C32 bond. The geometry of the ferrocene substituents is also affected by these effects, in the free ferrocene the ecliptic form of the ferrocene cp rings would be the preferred orientation in here one can see a small shift from the ideal orientation. The cp rings around Fe1 have an average rotation against each other of 7.05° with a tilt of 0.16° and the cp rings of Fe2 deviate with 14.15° with a tilt of 5.09° and around Fe3

the cp rings deviate with 13.08° with a tilt of 1.28°. The different values originate in different amounts of short contact π interaction of the different substituents. A picture of the cell with some selected intermolecular short contacts can be seen in Figure 2.2.10.

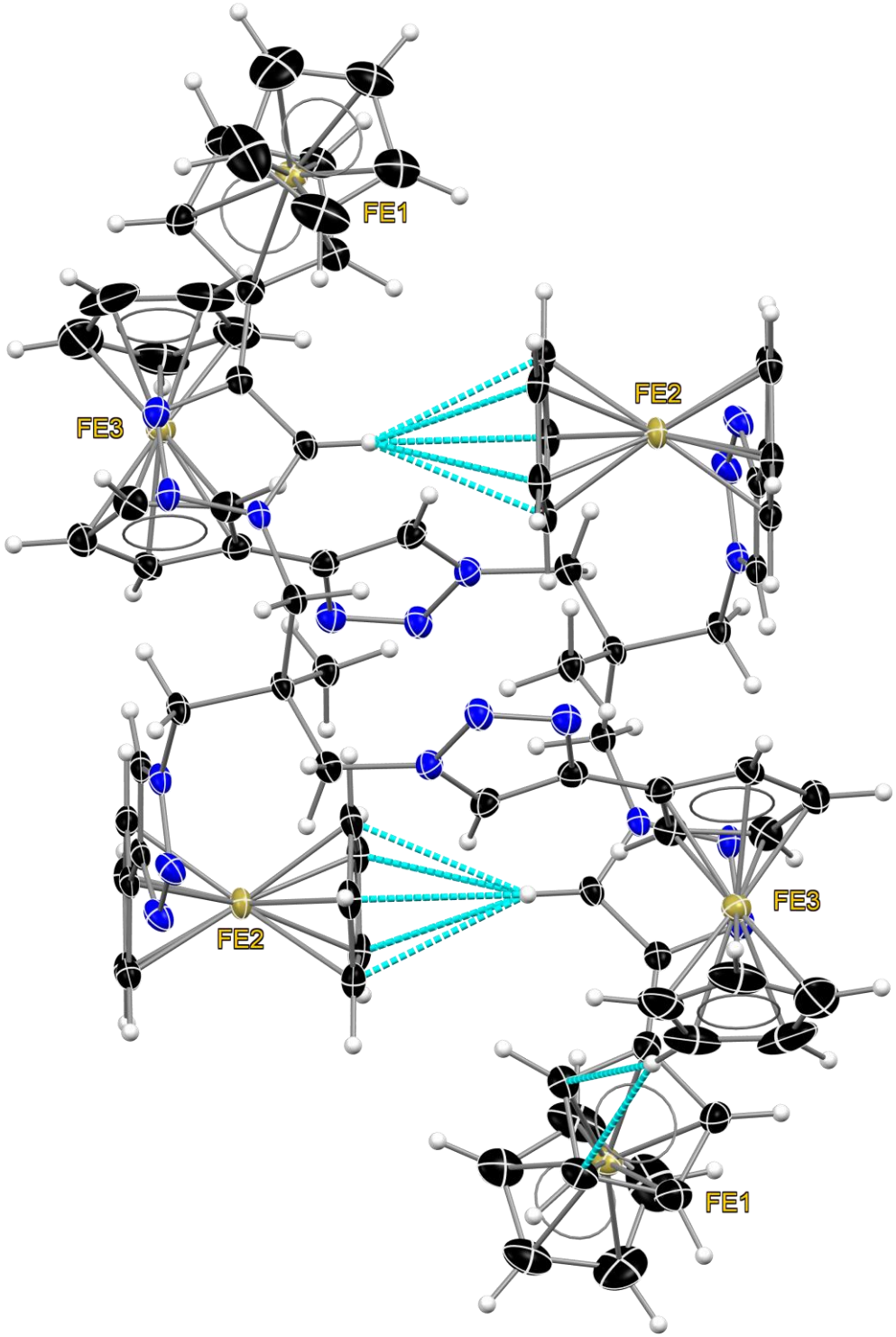

Figure 2.2.10: View of the cell of 14 with selected intermolecular short contacts (less than sum of VAN-DER-WAALS radii). Hydrogen atoms and solvent molecules have been omitted for clarity.

As proposed earlier this ligand system might be used as a precursor towards switchable NHC ligands. Therefore, the electronic properties of the free ligand **14** are of interest to determine if all three ferrocene substituents act separately and are indistinguishable from each other or if they do interact with each other. With the use of cyclic voltammetry these properties could be determined. The cyclic voltammogram is shown in Figure 2.2.11.

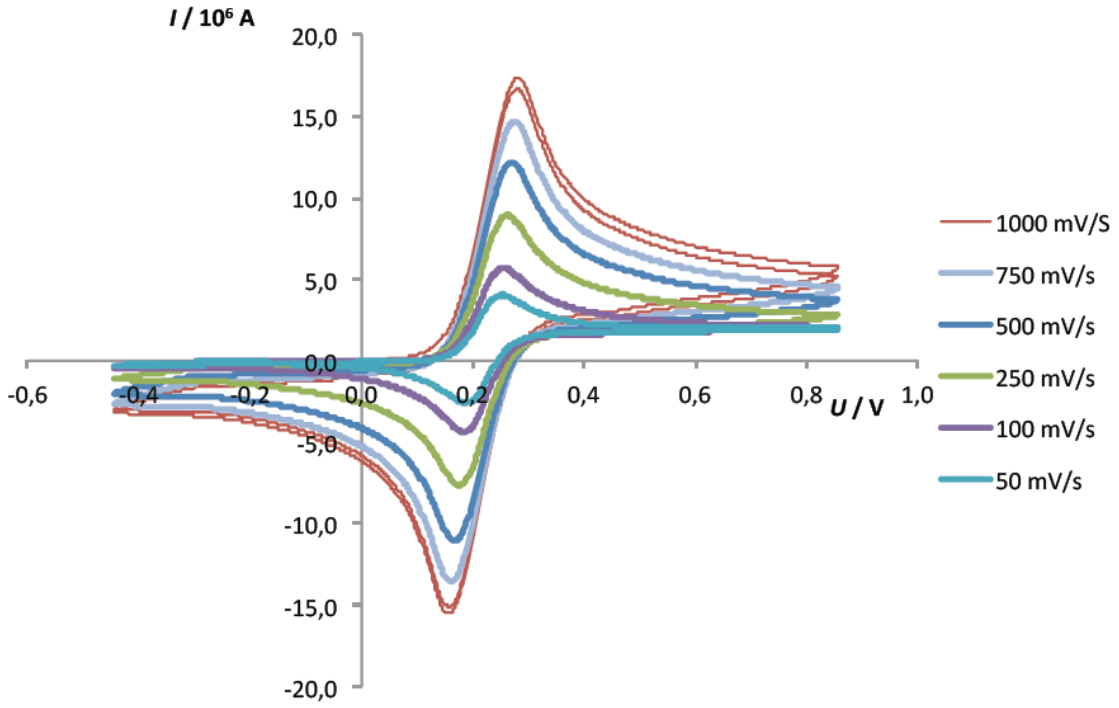

Figure 2.2.11: Cyclic voltammogram of 14 in DCM [0.1 m [N^nBu_4][PF_6], with different scan speeds.

The cyclic voltammetry measurement shown in Figure 2.2.11 reveals that the ferrocene moieties of the ligand system **14** do not couple electro chemically among each other since all three arms have the same potential of 0.22 V and are therefore equal to each other. Reduction of the scan speeds showed reversible cycles, indicating that the molecule can be oxidized and reduced reversibly.[108] In comparison with the $FeCp_2$* standard with a potential of -0.012 V[109] this determined potential for the ligand system is higher indicating an oxidation and reduction step should be harder to achieve.

With the synthesis and characterization of the eight ligand systems **7** to **14** with five of those previously unknown (**7**, **10**, **11**, **13**, **14**) it could be shown that the prior selected synthetic route is well suited to build up compounds with proposed varying steric and electronic properties in regard to their interaction with the triazolic rings in these structure. From a pure steric influence in **8**, **9**, **10** and **11** towards a combination of steric and electronic influence in **12** and **13** and towards a redox active ligand system **14**. Both of these features are of importance in later synthesis to convert

the ligand systems to act as mesoionic carbenes. The starting organoazide **1** proved to be a useful building block in creating these tripodal triazolic ligand system and with its rigid form it is well suited to expand its C_3 symmetry over the three arms in subsequent metal coordination reactions.

2.3 Tripodal Triazolic Ligand Systems with a Bridging π-System

The previously described ligand systems (iminophosphoranes **2**, **3** and triazolic ligand systems **7** - **14**) share the organoazide **1** as a building block during the synthesis which converts to a rigid C_3 symmetric backbone. This intended and promising feature allows the transfer of the symmetry of the backbone onto the three connecting ligand arms as shown in chapter 2.1.1. One of the drawbacks of this ligand design is the reduced amount of possible coordination sites. In the iminophosphoranes only the three nitrogen atoms can be used during a coordination reaction leading to a tridentate binding motif between the metal and the ligand systems as described in chapter 2.1.1. The same behavior can be expected for the triazolic ligand systems where a possible binding only occurs at the free carbon atoms of the three triazolic rings within a ligand structure after the successful conversion to a mesoionic carbene, described in a later chapters 2.4. A metal coordination might also be possible at one of the nitrogen atoms of the triazolic rings, accordingly this would still amount to three coordination sites.

To further improve the potential of the ligand system and also to gain access to new coordination motifs a fourth coordination site was introduced to form a tripodal tetradentate ligand system. This could be achieved by employing a mesitylene ring as a building block for the connecting backbone instead of the currently used organoazide **1**. As a result, this should give access to a ligand system with three coordination sites at the ligand arms and one π-coordination site on the mesitylene backbone. The change of the expected binding motif can be seen in Scheme 2.3.1.

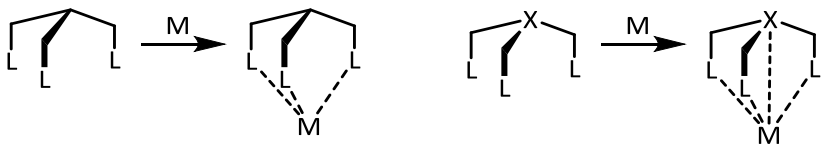

Scheme 2.3.1: Comparison of possible binding motifs between tri- and tetradentate ligand systems.

Similar ligands with a π-backbone and three carbene functionalities have been synthesized by DIAS *et al*.[23] in 1994 and in 2010 JONES *et al*.[110] reported a ligand system derived from mesitylene with three side arms consisting of triazolic rings with an additional phosphorus atom. These ligand systems are drawn in Figure 2.3.1.

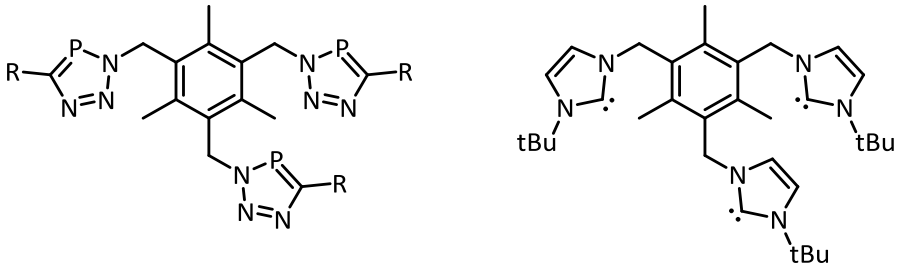

Figure 2.3.1: Ligand systems by JONES *et al*. and DIAS *et al.* with a bridging mesitylene ring.[23,110]

The general ligand design proposed in here was derived from other popular ligand systems like the tris(2-aminoethyl)amine (TREN) which is commonly used to form stable complexes with metals in the +2 and +3 oxidation state, tris(2-pyridylmethyl)amine (TPMA) which is often used to simulate the coordination environment within proteins, and Nitriloacetic acid (NTA) which is used for water softening while it bonds towards metal cations. These compounds are depicted in Figure 2.3.2.

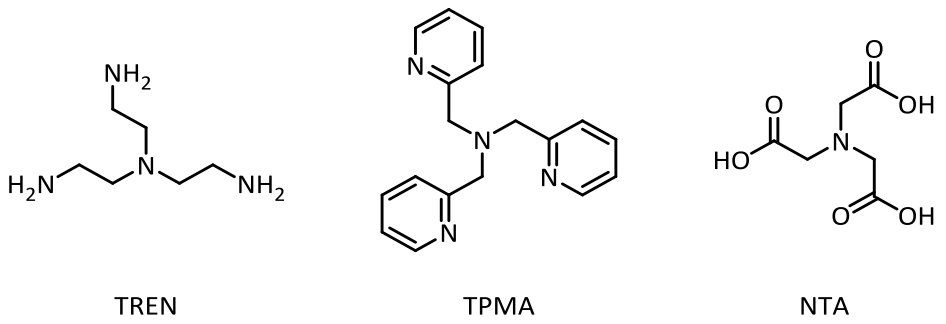

TREN TPMA NTA

Figure 2.3.2: Examples of tripodal ligand systems, tris(2-aminoethyl)amine (TREN), tris(2-pyridylmethyl)amine (TPMA), Nitriloacetic acid (NTA).

The enhancement of the previously described tripodal tridentante ligand systems towards a tripodal tetradentate ligand system improves the coordination sphere around a possible central metal atom while also supporting the desired C_3 symmetry. Different examples of this behavior can already be found regarding the TREN ligand.[25,111,112] Because of the high flexibility of the TREN ligand and the low inversion barrier of the nitrogen atom it is quite hard to synthesize chiral ligands by variation of the substituent at the nitrogen atom. Therefore systems with a different backbone or functional groups are still of high interest.[113,114]

2.3.1 Synthesis of a new Mesitylene Derived Organoazide

To introduce the π-system backbone derived from mesitylene a new synthetic approach needed to be selected. Following the previous experiences with the iminophosphoranes and triazolic ligand systems a functionalization of the mesitylene towards an organoazide which then can be used in the know click-chemistry reactions is a promising option.

First the mesitylene needed to be extended with additional sidearms to connect the three ligand arms later on. This was possible with an electrophilic substitution with paraformaldehyde and hydrobromic acid proposed by MADE *et al.* and shown in Scheme 2.3.2.[115]

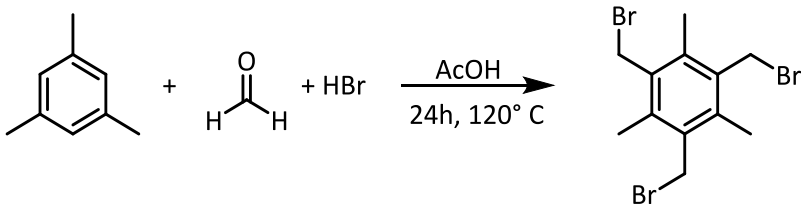

Scheme 2.3.2: Synthesis of 2,4,6-Tris(bromomethyl)mesitylene 15 by MADE *et al.*.[115]

Paraformaldehyde was dissolved in acetic acid and mesitylene was added to the reaction vessel. Additionally, 33% HBr in acetic acid was added and the reaction was stirred for 24h at room temperature. Workup contains quenching the reaction with ice water which lead to the formation of a white, slightly yellow solid. Further steps were introduced by washing the solid with diethyl ether, drying in vacuum and recrystallization from acetonitrile which gave **15** as pure product.
To prepare for the click-chemistry reaction step **15** needed to be reacted in a nucleophilic substitution to replace the bromine with azide groups shown in Scheme 2.3.3.

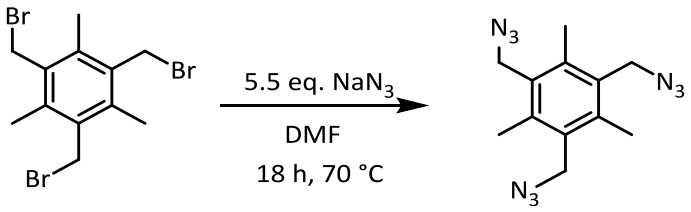

Scheme 2.3.3: Synthesis of 2,4,6-tris(azidomethyl)mesitylene 16 from 2,4,6-tris(bromomethyl)mesitylene 15.

15 was dissolved in DMF and sodiumazide was added to the reaction within 1 h. The reaction was slowly heated to 70 °C and stirred for 18 h, subsequently cooled to room temperature and DCM was added and stirred for another 2 h. The reaction solution was filtered through a pad of CELITE and stored for 24 h to precipitate the product. A slow decline of the colorless solution towards a brownish solution with a white solid forming was visible. To further augment the precipitation, the solution was reduced *in vacuo* to 50% of the reaction volume and pentane was added to reduce the solubility of the product. After 24 h most of the compound precipitated out and gave an almost clear solution with a brown sluggish containing some crystals. These crystals could be filtered off and recrystallized from DCM to give **16** as pure product. Some of the crystals were used in a X-ray diffraction experiment and the resulting crystal structure is drawn in Figure 2.3.3.

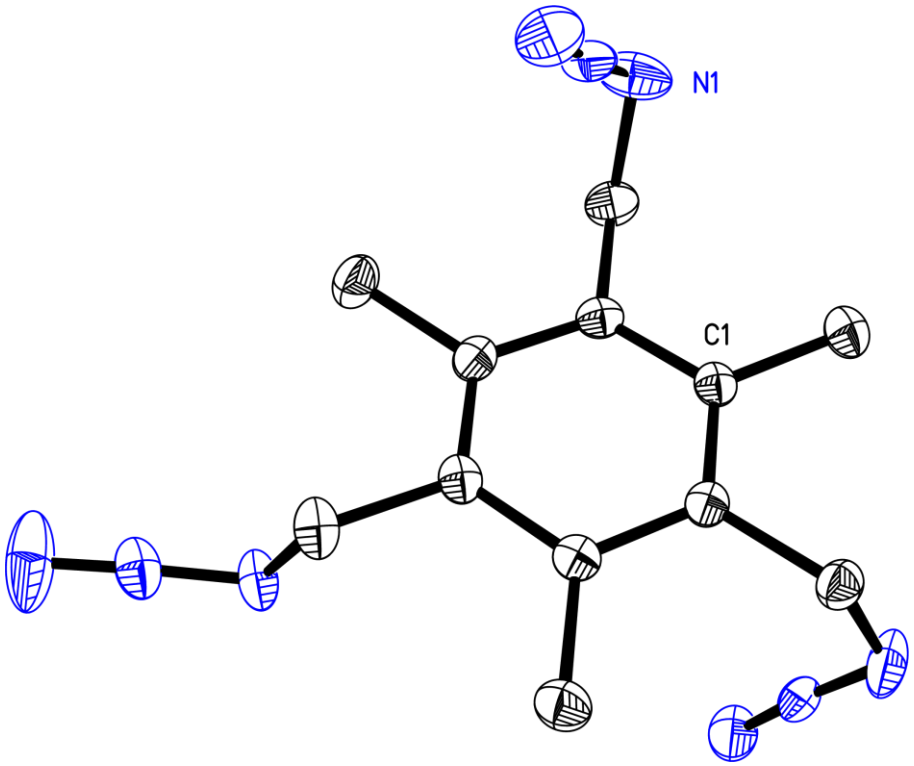

Figure 2.3.3: Crystal structure of 16. 16 crystallizes in the space group $P2_1/c$ in a monoclinic crystal system with α,γ = 90°, β = 90.77(1)°, a = 12.786(3) Å, b = 10.833(2) Å and c = 10.062(2) Å. The anisotropic displacement parameters are depicted at the 50% probability level. Hydrogen atoms have been omitted for clarity.

Unfortunately the yields of the isolated compound **16** were quite low and only the crystals could be obtained. Presumably during the isolation process most of the compound decomposed towards the unidentified brown sluggish which would form during the reaction. Attempts to prevent this unwanted side reaction were not fruitful and therefore it was decided to form the mesitylene organoazide **16** *in situ* and expose it to following reactions. With the successful synthesis of the new mesitylene derived organoazide **16** this compound could then be used in subsequent click-chemistry reactions to further build up the ligand system.

2.3.2 Tripodal Triazolic Ligand Synthesis via Click-Chemistry

To form the desired ligand system with the conversion of the three azide groups in **16** towards the triazolic rings click-chemistry was used. With the copper(I) catalyzed reaction the organoazide **16** was reacted with an acetylene derivative in a 1,3-dipolar cycloaddition reaction described by HUISGEN *et al.*[87] to form the 1,2,3-triazolic substituent out of the azide groups on each of the side arms. Since **16** was only isolated in very small yields a different approach was chosen where the precursor 2,4,6-tris(bromomethyl)mesitylene **15** was used as starting material and reacted with sodium azide to form the desired organoazide *in situ.*[116] The benefit of this reaction pathway is

that the formed organoazide can readily continue with the reaction and the equilibrium of the reaction is constantly shifted towards the formation of the organoazide so not only is the reaction workup not necessary at this step but also the overall yield should be improved.

From the previous experience in here the bulky phenyl group as well as the smaller *n*Pr group were selected to be introduced in the ligand system to gain access to ligand systems with different steric and electronic properties.

The ligand system **17** with phenyl groups as substituents at the triazolic rings has been reported by YAMADA *et al*. in 2012.[116] The synthesis was done with the use of click-chemistry and a polymeric solid state copper(I) catalyst. A similar approach to the ligand system was done by NASR-ESFAHANI *et al*. in 2014[117] and TAVASSOLI *et al*. in 2016[118] who used a silica-nanoparticle supported copper containing ionic liquid as a catalyst. Access to these solid state catalysts was not possible but because of the promising features of the ligand system and the experience with the previously described ligand systems it was tried to synthesize **17** with the known copper(I) catalyst which is formed *in situ* from copper sulfate and sodium ascorbate.

To synthesize the ligand system **17** with phenyl groups as substituents at the triazolic rings, sodium azide and phenylacetylene were dissolved in a *t*BuOH / H_2O 1:1 solution. As a catalyst the same catalyst for the click-chemistry as in chapter 2.2 was used which can be formed *in situ* from copper(II)sulfate pentahydrate and sodium ascorbate.[90] The catalyst loading needed to be increased to 12 mol% $CuSO_4 \cdot 5\ H_2O$ and 54 mol% sodium ascorbate to ensure a full conversion of all three ligand arms. The chemical equation can be seen in Scheme 2.3.4.

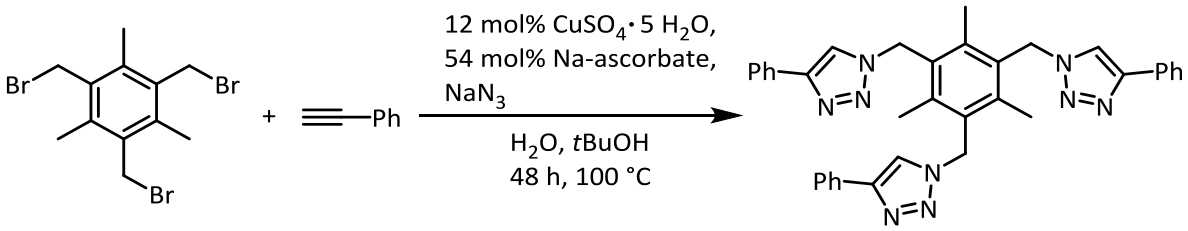

Scheme 2.3.4: Synthesis of ligand system 17 from 2,4,6-tris(azidomethyl)mesitylene 15 and phenylacetylene.

The reaction was stirred for 48 h at 100 °C during which the formation of an off white foam could be observed. After the reaction time has passed the solution was further diluted with a H_2O / EtOAc mixture and the organic phase has been separated. Unfortunately, the workup is quite extensive since the foam would mix up in the organic phase. Addition of some EtOAc proved to be beneficial in separating the organic phase. To remove the excess copper catalyst from the crude product, aqueous ammonia solution was added to form the blue copper-ammonia complex which has a very

good solubility in water and can be easily separated. Unfortunately, the blue copper-ammonia complex also mixed with the crude product and formed a blueish powder so additional workup steps needed to be introduced. This was done by washing with water, brine and some extra ammonia solution and a final washing step with an excess of EtOAc was required. Removal of the solvents gave a light blueish compound which could be identified via NMR as **17** but elemental analysis showed some major impurities.

	calculated	found	deviation [%]
C	73.03	36.37	-51.2
H	5.62	6.84	+21.7
N	21.30	11.52	-45.9

Table 2.3.1: Elemental analysis of 17 after first workup.

The cause of these impurities could not be fully determined but it is expected that it mostly consists of the copper-ammonia complex since the NMR did not show any organic impurities. Further workup was employed by dissolving the crude product in DMSO. Generally, the solubility of **17** in common solvents was rather low further impeding a proper workup. The solution was then filtered through a pad of CELITE. The colorless solution was then reduced to two thirds of the volume and methanol was added to precipitate **17** as a white powder. NMR and elemental analysis showed the successful clean-up of the desired compound.

	calculated	found	deviation [%]
C	73.03	70.90	-2.92
H	5.62	5.77	+2.67
N	21.30	20.97	-1.55

Table 2.3.2: Elemental analysis of 17 after the second workup.

Further experiments showed that the workup can be improved by first washing with an excess of water, brine and EtOAc. Subsequently removing the solvent *in vacuo* and dissolving in THF while adding the ammonia-solution to remove the copper catalyst. With this procedure the yields could be improved from 21% to 48%.

A second ligand system **18** with a *n*Pr substituents was also synthesized utilizing the same reaction pathway and catalyst loading as for **17** with a change of the starting material from phenylacetylene to the propylacetylene and is shown in Scheme 2.3.5.

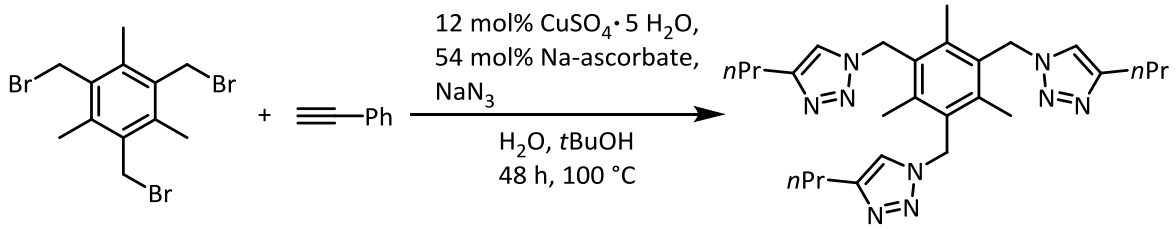

Scheme 2.3.5: Synthesis of ligand system 18 from 2,4,6-tris(azidomethyl)mesitylene 15 and propylacetylene.

Workup was carried out as previously described with a change in the last step where DCM was used to dissolve the compound and pentane was added to precipitate **18**. The product precipitated as a pure white solid with no impurities.

With the employed synthetic route two ligand systems could be synthesized with classic click-chemistry which both employ a bridging π-system as a connecting backbone giving rise to possible new higher dentate binding motifs. With the known ligand system **17** with phenyl rings as substituents a steric demanding ligand system could be synthesized with a classic approach towards the click-chemistry and a new second ligand system with far less steric demand **18** could be obtained by the same route further improving the ligand system selection for the subsequent coordination reactions.

2.4 Selected Tripodal Triazolic Ligand Systems in Metal Coordination

2.4.1 Triazolic Ring Activation via a Methylation Reaction

After the successful synthesis of a broad range of different triazolic ligand systems described in chapter 2.2 and 2.3 the triazolic rings on these ligands (**8 - 14**, **17**, **18**) needed to be further activated to form the salt of the mesoionic carbene used in later coordination reactions. The ligand systems used in the subsequent methylation reactions are shown in Figure 2.4.1.

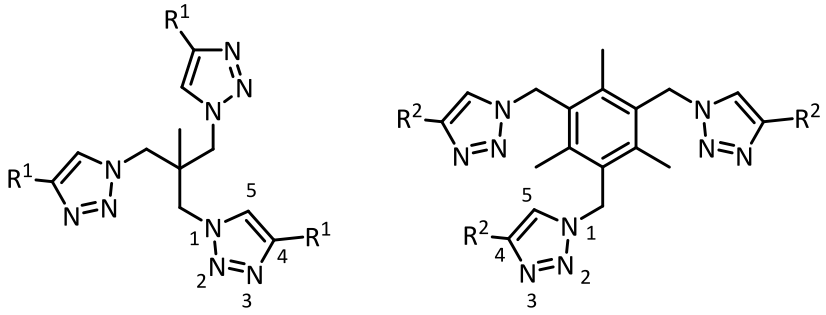

R^1 = *n*Pr (**8**), *cy*Pr (**9**), *i*Pr (**10**), *t*Bu (**11**), Ph (**12**), Mes (**13**), FeCp (**14**)
R^2 = Ph (**17**), nPr (**18**)

Figure 2.4.1: Ligand systems 8 - 14, 17, 18 used in methylation reactions to form the salt of a mesoionic carbene and numbering scheme.

The activation of the triazolic rings would allow a deprotonation reaction with a mild base to occur on the remaining unsubstituted carbon atom of the rings to form the mesoionic carbene which then undergoes a coordination reaction with a suitable metal atom. Without this additional reaction step the conversion of the ligand systems towards mesoionic carbenes would necessitate the use of a very strong base. Early results have shown that this would presumably lead to a decomposition of the whole ligand system.[101]

The transfer to the salt of a mesoionic carbene can be achieved by the introduction of a methyl group at the N3 position of the triazolic sidearms. The alkylation is necessary to activate the triazolic rings since the non-methylated derivatives are to unreactive for further synthesis. BEGTRUP *et al*.[97] compared in 1990 the *pKs* values of 1,2,3-triazole with pK_s = 9.3 and 1-methyl-1,2,3-triazole with pK_s = 1.2, while another study by ABBOUD *et al*.[98] determined the *pKs* value of the 3-*H*-1-methyl-4-phenyl-1,2,3-triazolium cation to be at *pKs* = 0.06. Figure 2.4.2 shows the comparison of the different *pks* values.

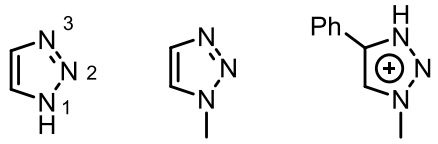

pKs = 9.3 *pKs* = 1.2 *pKs* = 0.06

Figure 2.4.2: Change of *pKs* values depending on the substitution at the N3 position by BEGTRUP *et al.*[97] and ABBOUD *et al*[98]. 1,2,3-triazole (*left*), 1-methyl-1,2,3-triazole (*middle*), 3-*H*-1-methyl-4-phenyl-1,2,3-triazolium cation (*right*).

The methylation reaction generally occurs at the most nucleophilic nitrogen atom which is the N3 in here. Because of the electronic influence towards the stability of the triazolic ring especially the resulting electron density reducing quaternary ammonium cation at the N3 position this methylation step has been a routinely applied part in the synthesis of 1,2,3-triazolic mesoionic carbenes.[35] In here the methylation step was done with the use of methyl iodide as a methylation reagent since KRATZERT[77] reported promising results with this reaction to functionalize ligand system **8** bearing *n*Pr substituents at the triazolic rings unfortunately only one crystal structure of that compound could be obtained with numerous disordered moieties. SCHWARZE[101] could show, during his master thesis, with the use of ligand system **9** with *cy*Pr substituents that the needed amount of methyl iodide is quite high with up to 30 eq. in regard to the ligand system. Furthermore, a higher steric demand of the ligand systems caused by the bulky substituents at the triazolic rings demands higher amounts of methyl iodide as well as prolonged reaction times in order to ensure a full conversion of all three ligand arms within one ligand system. The NMR shift of the proton signal at the unsubstituted C5 carbon atom of the triazolic rings can be used to quantify the methylation reaction. Because of the change in electron density at the ring the proton signal is shifted towards lower fields indicating a successful reaction on all three sidearms of a ligand system. The results by SCHWARZE[101] can be seen in Figure 2.4.3.

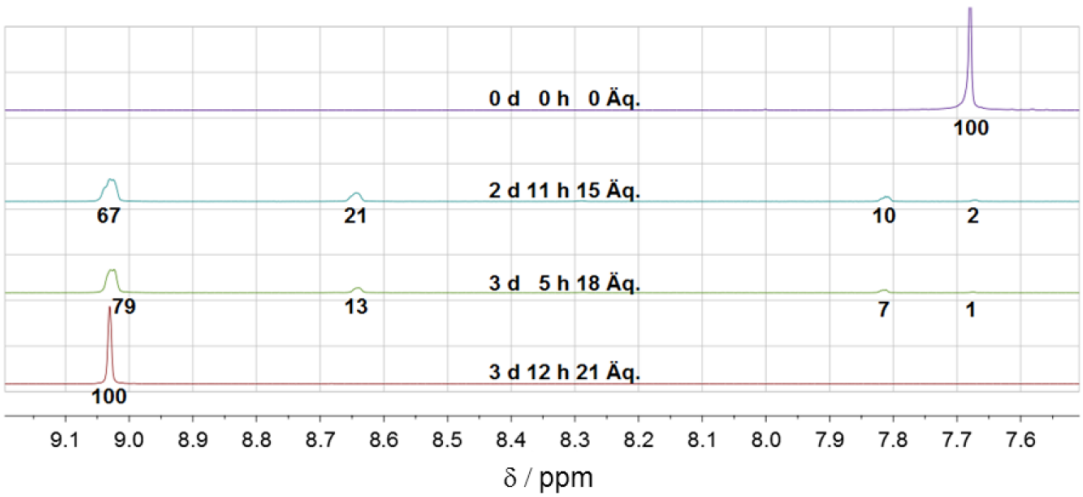

Figure 2.4.3: ^{1}H NMR spectra monitoring of the proton signal at the C5 carbon atom of the triazolic rings during the methylation reaction of ligand system 9 with *cy*Pr substituents obtained by SCHWARZE.[101] Reaction times and equivalents of methyl iodide are shown in the middle.

The methylation reaction leads to cationic ligand systems with iodide as a counter ion. Because of the three arms within a ligand a charge of +3 is achieved for the ligand and subsequently three iodide anions are present.

Based on these findings by KRATZERT[77] and SCHWARZE[101] all ligand systems with an alkyl backbone **8 - 14** were subjected to the methylation reaction with methyl iodide. The general reaction pathway is depicted in Scheme 2.4.1.

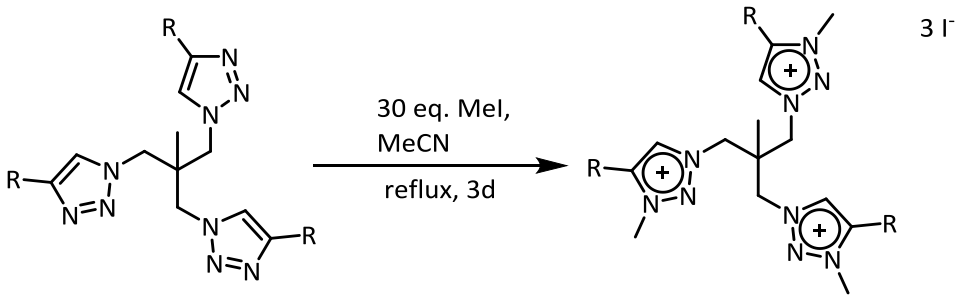

R = *n*Pr (**8**), *cy*Pr (**9**), *i*Pr (**10**), *t*Bu (**11**), Ph (**12**), Mes (**13**), $FeCp_2$ (**14**)

Scheme 2.4.1: General reaction pathway for the methylation and transfer to the salt form of a mesoionic carbene of the triazolic ligand systems 8 - 14.

In all reactions 30 eq. of methyl iodide in acetonitrile were used and the reaction was stirred under reflux for three days. NMR experiments were run along to monitor the reaction progress. When a full methylation of all three arms could be stated the reaction was stopped and the solvent and excess methyl iodide was removed *in vacuo*. Because of the high toxicity of methyl iodide special care was carried out during this process. Excess methyl iodide was quenched with 10% ammonia

solution to form the methylammonium iodide. The solid was then redissolved in DCM and washed with an excess of cold pentane to precipitate as a white to yellowish solid.

The success of the methylation reaction could be observed in the NMR spectra and in a low field shift of the proton on the C5-carbene position indicating a decline in the shielding of the proton and consequently a rise in the acidity.

With the described method in here it was possible to synthesize seven new ligand systems **20 - 25** bearing the methyl group at the N3 position. The corresponding molecules are shown in Figure 2.4.4.

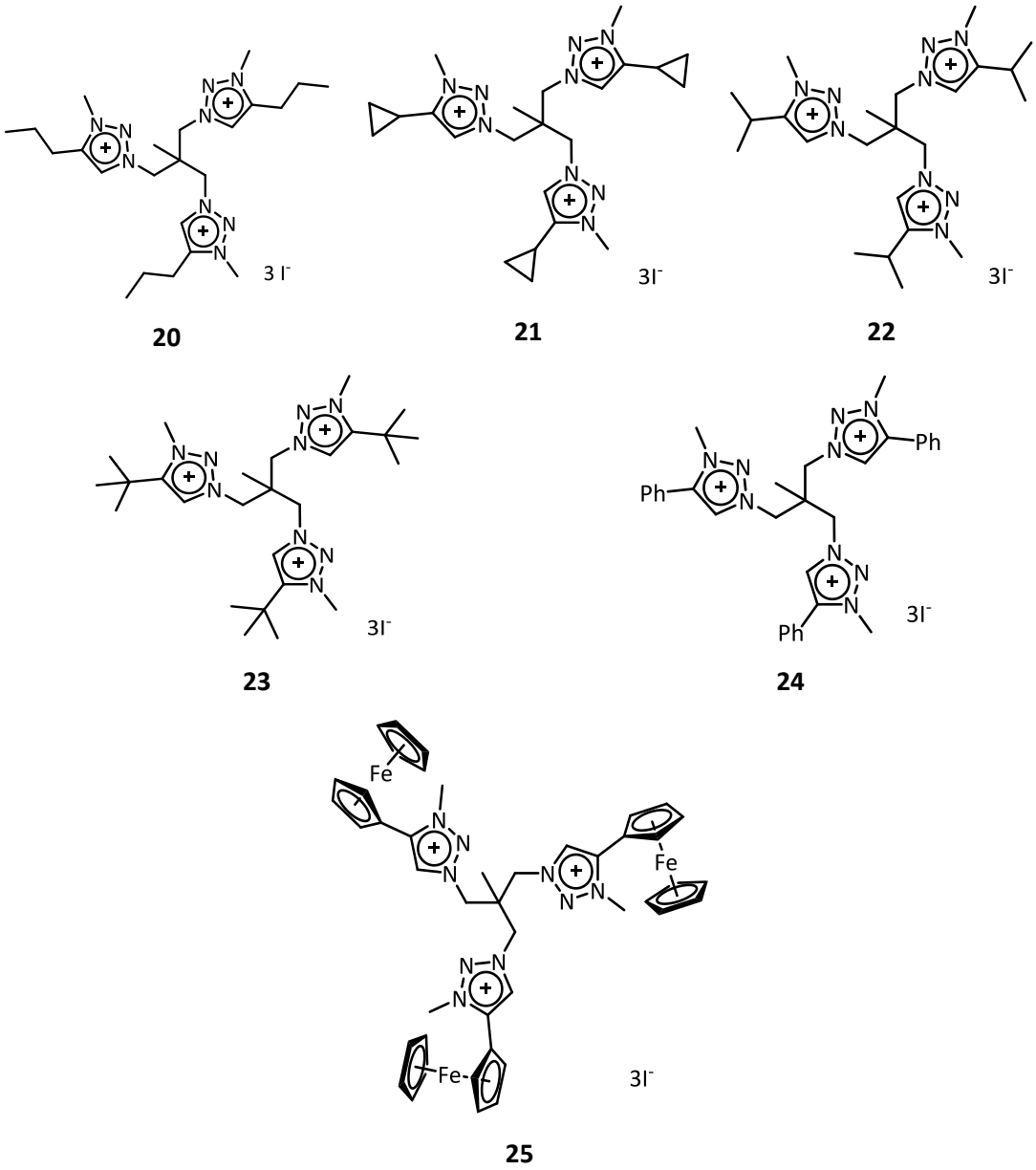

20 **21** **22** **23** **24** **25**

Figure 2.4.4: Six ligand systems 20 - 25 synthesized via methylation reaction with methyl iodide.

Despite NMR and mass spectrometry analysis further proof of the successful synthesis could be gained by X-ray diffraction experiments. Slow evaporation of a saturated solution of the ligand systems **20**, **24** and **25** in DCM yielded crystals suitable for X-ray diffraction analysis. The structures for **20** bearing a *n*Pr substituent and **21** bearing a *cy*Pr substituent have already been reported by KRATZERT[77] and SCHWARZE[101] during their initial examinations albeit missing additional analytical data. A full analytical verification of their findings could be achieved in this work including NMR, mass spectrometry, and elemental analysis as well as a recrystallization of these ligand systems. For the purpose of discussion and comparison the structure solutions by KRATZERT[77] and SCHWARZE[101] are shown in Figure 2.4.5 and Figure 2.4.6.

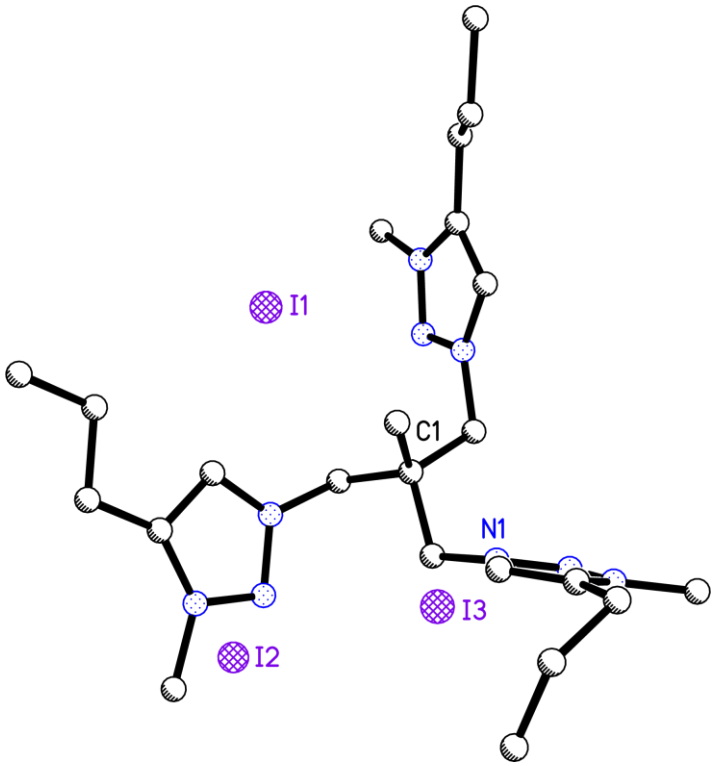

Figure 2.4.5: Crystal structure of 20 reported by KRATZERT[78]. 20 crystalizes in the space group $P2_1/c$ in a monoclinic crystal system with $\alpha, \gamma = 90°$, $\beta = 112.05(1)°$ and $a = 12.025(1)$ Å, $b = 28.413(2)$ Å, $c = 13.214(1)$ Å. The hydrogen atoms, disordered ligand arms and DCM solvent molecules have been omitted for clarity.

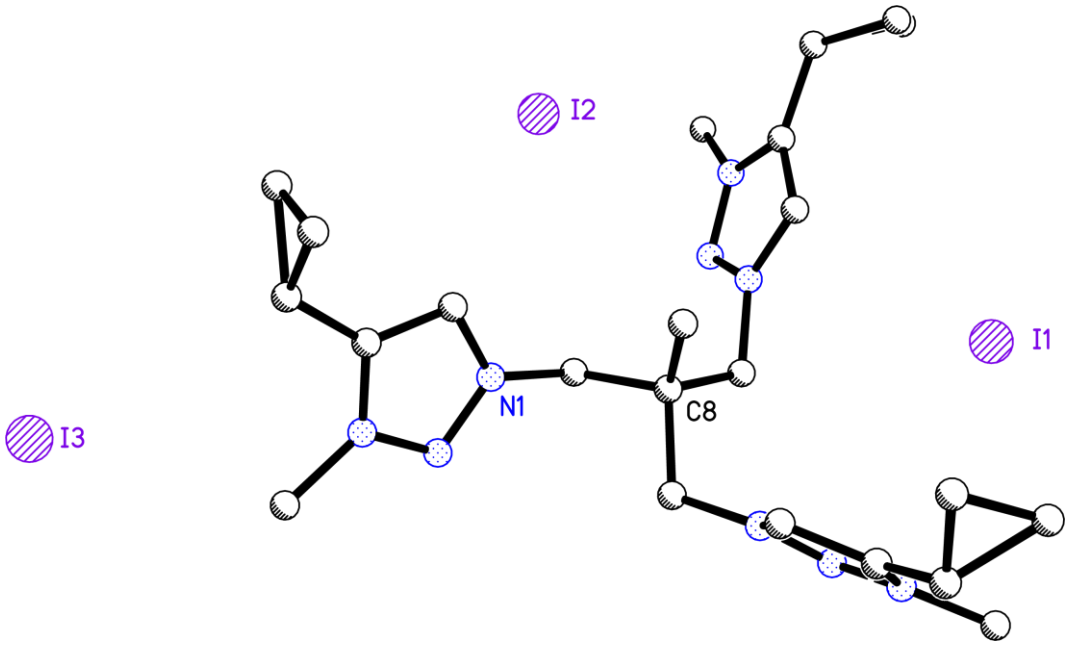

Figure 2.4.6: Crystal structure of 21 reported by SCHWARZE.[101] 21 crystalizes in the space group $P2_12_12_1$ in a orthorhombic crystal system with α, β, γ = 90° and a = 7.591(5) Å, b = 12.607(7) Å, c = 34.764(19) Å. The hydrogen atoms and solvent have been omitted for clarity.

The structure of **20** and **21** in Figure 2.4.5 and Figure 2.4.6 show the respective ligand system with an additional methyl group at the N3 position of each triazolic ring. Also three iodide anions countering the +3 charge of the ligand system are present within the crystal lattice. While the whole ligand arms show some signs of disorder no indications can be found hinting towards a partial transfer of the three azide groups to the triazolic rings. The overall structure shows the same type of orientation as their non-methylated precursor ligand system with all three arms oriented to minimize the steric hindrance as much as possible. Interestingly the structures are now inverted with the methyl group at the alkyl backbone positioned inside the claw created by the three ligand arms. A similar behavior could be seen in the case of ligand system **14** with $FeCp_2$ substituents described in chapter 2.2. It can be concluded that this orientation appears to be the favored one when increasing the steric bulk around the triazolic rings.

With a similar approach to the crystallization it was also possible to gain crystals suitable for X-ray diffraction of the methylated ligand system **24** with phenyl groups at the triazolic rings. The structure is shown in Figure 2.4.7.

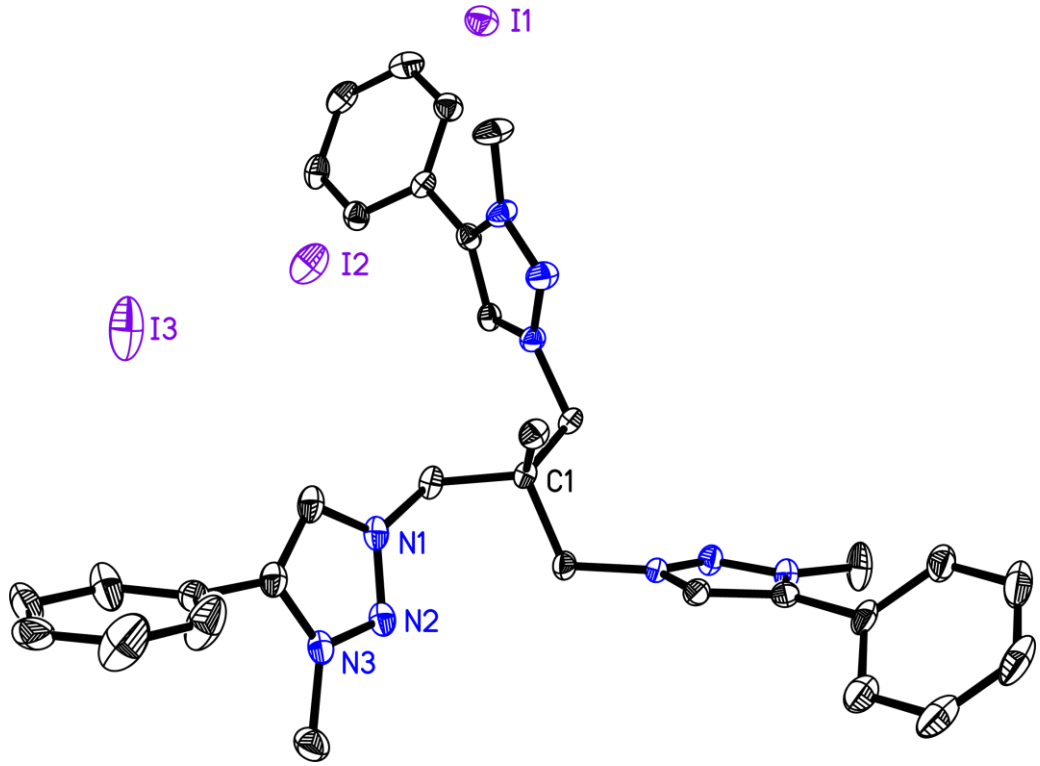

Figure 2.4.7: Crystal structure of 24. 24 crystallizes in the space group $P2_1/n$ in a monoclinic crystal system with α,γ = 90°, β = 91.70(1)°, a = 16.244(2) Å, b = 11.539(2) Å and c = 19.459(3) Å. The anisotropic displacement parameters are depicted at the 50% probability level. Hydrogen atoms have been omitted for clarity.

The ligand system **24** crystalizes in the monoclinic space group $P2_1/n$. In here the main ligand system as well as the three iodide anions crystallize without the presence of solvent molecules. Again the structure is inverted with the methyl group at the bridging alkyl backbone pointing into the center of the structure further indicating that this orientation is preferred when increasing the steric demand at the ligand system. In contrast to the previous ligand system **20** there are no DCM solvent molecules co-crystallized within the structure separating the ligand molecules from each other within a cell. Since the same orientation of the molecule can be observed it can be deduced that the influence of the solvent molecules is rather small in dictating the orientation of the ligand system further reinforcing the observation that this inverted orientation is preferred. Although an electronic influence of the newly introduced methyl group is to be expected no change in the bond lengths and angles of the triazolic rings could be observed. For example the bond length within one triazolic ring amount to N1 – N2 1.326(4) Å, N2 – N3 1.320(4) Å, N3 – C7 1.363(5) Å, C6 – C7 1.369(5) Å and N1 – C6 1.361(5) Å in comparison to the non-methylated ligand system **12** with N1 – N2 1.333(8) Å, N2 – N3 1.306(8) Å, N3 – C7 1.360(9) Å, C6 – C7 1.366(10) Å and N1 – C6 1.366(8).

As with the previous structures all arms are methylated at the N3 position with no signs of disorder proving the successful synthesis of the ligand system.

It was also possible to crystallize the ligand system **25** with $FeCp_2$ substituents after the successful methylation reaction. Due to not optimal crystal quality and measurement conditions the overall data resolution was lower than normal and some residual electron density was higher than normal but the features of the structure could still be identified unambiguously. The structure is shown in Figure 2.4.8.

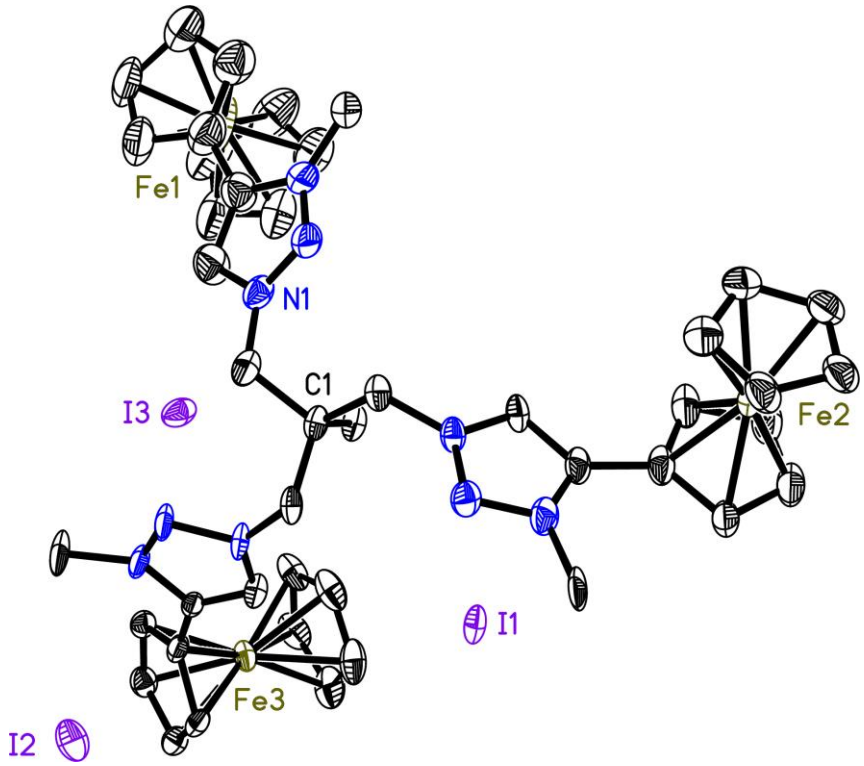

Figure 2.4.8: Crystal structure of 25. 25 crystallizes in the space group $P2_1/c$ in a monoclinic crystal system with α,γ = 90°, β = 103.65(1)°, a = 13.565(1) Å, b = 27.502(1) Å and c = 13.445(1) Å. The anisotropic displacement parameters are depicted at the 50% probability level. Hydrogen atoms have been omitted for clarity.

In here one can also see the overall combining binding motif and orientation of these ligand systems in the crystal structure. The compound crystallizes in the monoclinic space group $P2_1/c$ with three iodide anions in close proximity and DCM solvent molecules. The structure is again inverted with the methyl group at the bridging alkyl backbone pointing inwards of the coordination pocket formed by the three ligand arms. The same explanation presented earlier can be referenced here, that this orientation appears to be preferred when bulky substituents are present at the ligand arms. Again all three triazolic rings have been methylated and no signs of disorder pointing towards

insufficient transfer of the azide groups of the precursor **14** of each arm could be identified. A further proof that the presented methylation pathway works very well in combination with bulky and steric demanding substituents in close proximity albeit prolonged reaction times of multiple days at reflux are needed. One of the $FeCp_2$ substituent consisting Fe1 exhibit signs of a disorder due to the lack of short contact interactions of this substituent within the cell. Another $FeCp_2$ substituent with Fe3 is titled against the triazolic ring with a torsion angle of 55.34° because of the intermolecular interactions with a neighboring molecule within the crystal lattice. The same tilting could be observed in a smaller range with the non-methylated ligand system **14** indicating the ability of the rotation around the C – C bond connecting the substituents with the triazolic rings which is a necessity in later coordination reactions to make way for the coordination of the metal atom at the carbene functionality at C3 in close proximity.

With the three crystal structures shown in here of the ligand systems **20**, **24** and **25** as well as the NMR data from the ligand systems **21**, **22**, and **23** it could be shown that the methylation with methyl iodide is a suitable reaction to prepare the ligand systems for the coordination reactions and form the salt form of the mesoionic carbenes used later on.

From the crystal structures presented in here a deeper understanding of the ligand system and its properties in regard to its steric demand and alignment abilities could also be gained. The inverted structure with the methyl group of the bringing alkyl backbone pointing inwards of the claw like structure generated by the three arms appears to be a reoccurring orientation motif with these ligand systems. Furthermore, the NMR shift of the proton signal at the C3 atom of the triazolic rings at which the later metal coordination is expected to occur points towards a change in the electronic properties of the triazolic rings. A reduced *pKs* value for this proton is expected facilitating a deprotonation reaction to form *in situ* the mesoionic carbene prior to the metal coordination reaction.

Based on these findings, the same methylation step was deemed necessary for the ligand systems described in chapter 2.3 with a bridging π-system derived from mesitylene. The methylation was done via the same generic route described in here by dissolving **17** and **18** in acetonitrile and adding 30 eq. of methyl iodide. The reaction pathway is shown in Scheme 2.4.2.

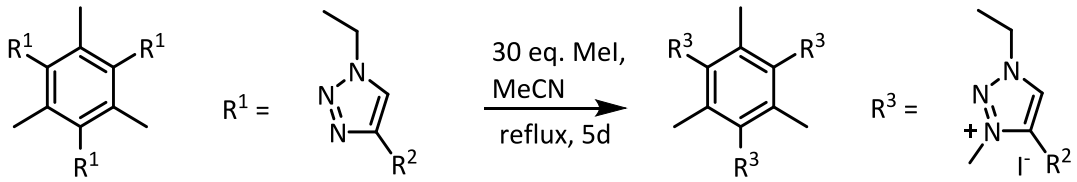

R^2 = Ph (**18**), nPr (**19**)

Scheme 2.4.2: Methylation of 17 and 18 at N3 of the triazolic arms with methyl iodide.

The reaction was stirred under reflux at 82 °C for five days and the reaction was monitored by NMR-spectroscopy. To calculate the percentage of the methylation the determined integrals were divided by the expected integrals and normalized to 100. Consequential for **17** it was obvious that only 33% of the ligand has been methylated at all three arms while 12% have been methylated on two arms and the remaining ~50% have been methylated on only one arm while the remaining 5% are non-methylated starting material. Figure 2.4.9 shows the overlay of the NMR spectra of the non-methylated starting material **17** (*red*) and the NMR spectra during the reaction. With E = starting material, E-Me = mono-methylated, E-Me_2 = di-methylated and E-Me_3 = tri-methylated compound.

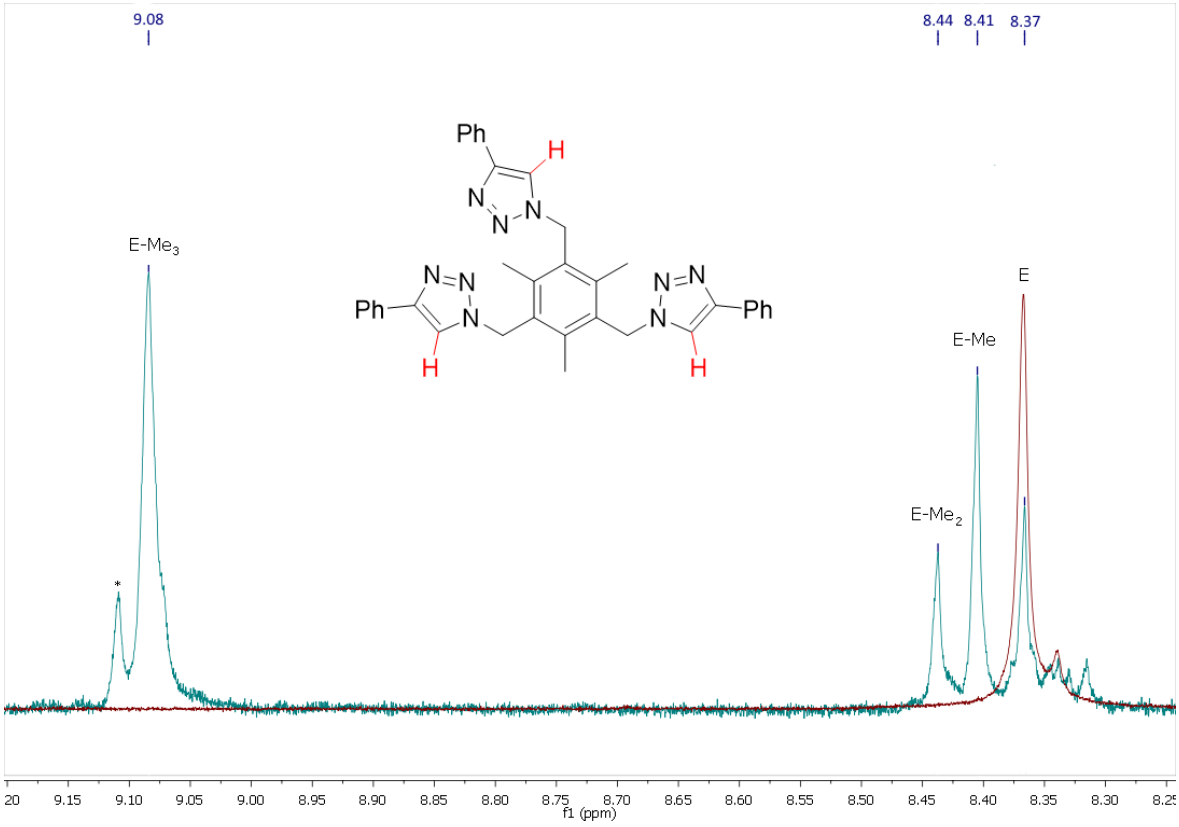

Figure 2.4.9: Reaction control of the methylation of 17 via NMR-spectroscopy (blue: during the methylation reaction; red: starting material).

The same reaction behavior could be examined for ligand system **18** with a *n*Pr substituent. Therefore, another 48 h of reaction time at 82 °C were added. Unfortunately, some decomposition could be seen in the NMR spectra and therefore the reaction was quenched, and all volatile components were removed *in vacuo*. During evaporation some crystals could be obtained belonging to a side product **19** which were suitable for X-ray diffraction analysis. The resulting structure is shown in Figure 2.4.10.

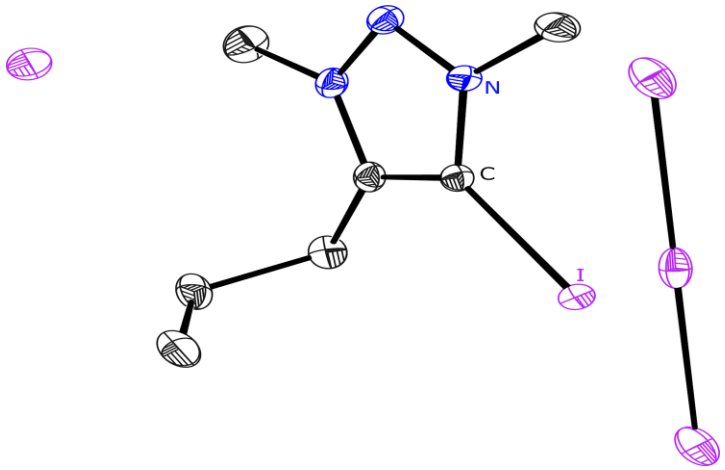

Figure 2.4.10: Crystal structure of 19 **after the methylation reaction.** 19 **crystallizes in the space group $P2_1/c$ in a monoclinic crystal system with α,γ = 90°; β = 105.90(2)°, a = 12.706(3) Å, b = 12.967(2) Å and c = 8.586(2) Å. The anions I^- and I_3^- are on a special plane with 50% occupancy combining to one negative charge. The anisotropic displacement parameters are depicted at the 50% probability level. Hydrogen atoms have been omitted for clarity.**

The determined crystal structure of **19** shows a molecule which appears to only consists of one sidearm of the ligand system which has been methylated at the N1 and N3 position and an additional substitution of the proton at C1 with an iodine atom.

The formation of this side product can be explained with the proposed reaction pathway in Scheme 2.4.3.

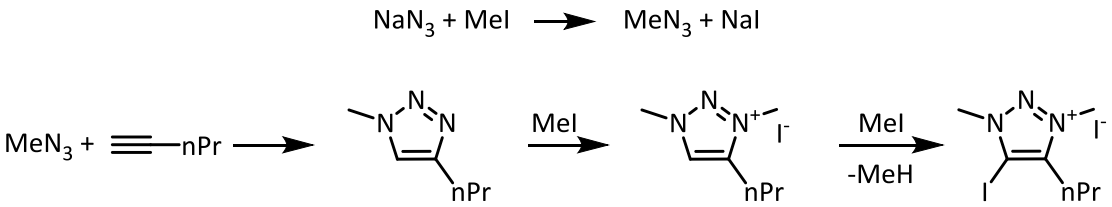

Scheme 2.4.3: Proposed reaction pathway for the formation of 19**.**

During the synthesis of the organoazide **16** the same difficulties during the reaction workup apply when handling the explosive azide components. As already described in chapter 2.1 the workup options are limited and therefore some impurities of the different starting materials still can be present in ongoing reactions. In here one could assume that unreacted sodium azide reacts to the highly explosive methyl azide in the presence of methyl iodide. Propyl acetylene which is present during the *in situ* reaction to form the ligand system from the staring material **15** can then react with methyl azide and excess methyl iodide to the side product **19**. Considering this proposed mechanism to be correct the main product, the methylated ligand systems should still be formed. Unfortunately, the NMR spectra of both compounds show the decline of the proton signal for the bridging

CH_2-group which connects the triazolic rings to the mesitylene backbone. Therefore, the formation of **19** can no longer be regarded as a side reaction and one must assume that a decomposition of the ligand system **18** also occurs during the methylation reaction in addition to the proposed reaction pathway in Scheme 2.4.2.

For the previous compound **17** with phenyl substituents at the triazolic rings no crystals could be obtained but still the corresponding NMR shows the same decline of CH_2 proton signal suggesting the same decomposition reactions.

In conclusion, during the methylation reactions indications of the formation of the desired ligand systems **17** and **18** could be seen in the NMR spectra but prolonged reaction times always lead to the decomposition of the molecules before all three side arms could be reacted. Therefore, these type of ligand systems could not be used in subsequent metal coordination reactions.

2.4.2 Ion Exchange Reactions to Weakly-Coordinating Anions

In the previously described methylation reactions iodide was introduced as a counter ion during the methylation reaction of the ligand system. Iodide is a strongly coordinating anion and it can hinder potential transmetalation reactions in planned synthesis. Furthermore, the coordinating iodide anions can tend to hamper the carbene formation and gives rise to low yields and extended reaction times. ALBRECHT *et al.*[119] showed in 2008 with imidazolium salts, that the NHC formation mostly happens under a heterolytic bond cleavage while the MIC is formed during an oxidative addition pathway. Consequently, small coordinating anions favor the formation of NHCs while weakly-coordinating anions favor the formation of MICs in compounds which are able to produce both products. With the current ligand systems with triazolic rings at the side arms it is not possible to form the NHC. NOLAN *et al.*[39] could show in 2005 that the type of counter-ion and its polarizability during the formation of a metal carbene complex can play a vital role in controlling the resulting binding motif. By employing weakly-coordinating anions, the selection of possible ligand systems in this work can be further broadened allowing a comparison of the reactivity during coordination reactions between the different types of anions in order to quantify the influence of the chosen cation.

These weakly-coordinating anions are characterized by their tendency to form only marginal interactions because of their bulkier appearance and the more delocalized electron density over the increased area. Classic weakly-coordinating anions are for example $[CF_2SO_3]^-$, $[BF_4]^-$, $[ClO_4]^-$ and $[PF_6]^-$. In contrast coordinating anions are considered to be hard on the basis of the PEARSON HSAB concept with a localized electron density and a tendency to form dative bonds. Mostly halides and

cyanide-ions react in this way, which is only desirable when the so added stability improves the stability of the final target complex. However, here the strong bond to iodide prevents additional reactions on the substrate because of the extra energy needed for the dissociation of the anion. Hence the coordination sphere of the cation can be blocked by the coordinating anion.

The borate derived anions are a suitable class of possible counter-ions to use in conjunction with the triazolic ligand systems. The steric demanding examples in this class of compounds like the tetrakis(3,5-bis(trifluoromethyl)phenyl)borate commonly abbreviated as $[BAr^{F}_{4}]^{-}$ and the tetrakis(3,5-bis(trichlor)phenyl)borate, $[BAr^{Cl}_{4}]^{-}$ are used within this work and are shown in Figure 2.4.11.

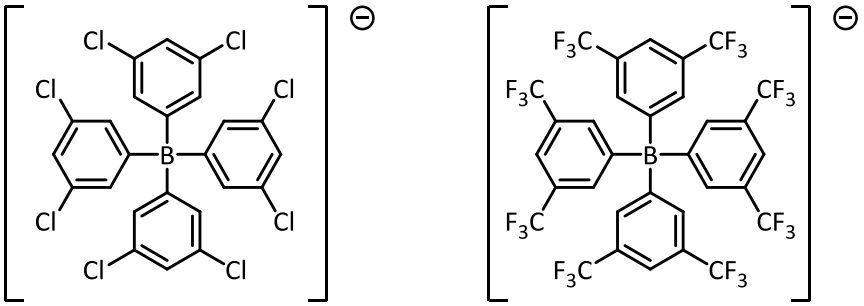

Figure 2.4.11: Anions used for the anion exchange $[BAr^{Cl}_{4}]^{-}$ (*left*) and $[BAr^{F}_{4}]^{-}$ (*right*).

While the $[BAr^{F}_{4}]^{-}$ has a higher steric demand with a bigger area to delocalize and stabilize the negative charge the $[BAr^{Cl}_{4}]^{-}$ derivative was also used since intended X-ray diffraction analysis would be much more facilitated with this anion, because it would not suffer from disordered CF_3 groups. The anions were first synthesized as their sodium salts along a literature know synthesis by YAKELIS *et al*. [120] Starting with 1,3-bis(trifluoromethyl)-5-bromobenzene or 1-bromo-3,5-dichlorobenzene respectively to which *i*PrMgCl was added at -20 °C and subsequently $NaBF_4$. The reaction mixture was finally warmed to room temperature and stirred for 48 h. Crystallization gives the pure product. The reaction scheme is depicted in Scheme 2.4.4.

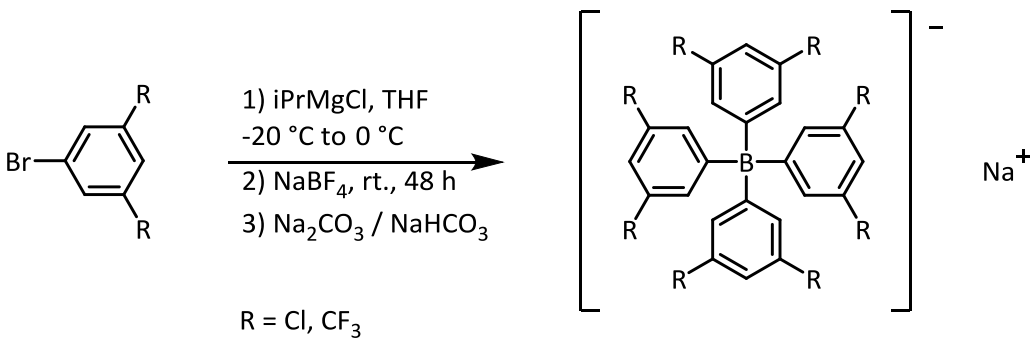

Scheme 2.4.4: General reaction pathway for the synthesis of the $[BAr^{Cl}_{4}]^{-}$ and $[BAr^{F}_{4}]^{-}$ anions.

The ion exchange reaction with the corresponding methylated ligand system was accomplished with the methylated ligand systems **20** with *i*Pr as a substituent on the triazolic rings and **24** bearing phenyl rings at the triazolic rings. These two ligand systems were chosen to test this reaction pathway because both offer the best compromise of the different classes described in chapter 2.2. The *i*Pr ligand system **20** has a very low steric demand and electronic influence in close proximity to the unsubstituted carbon atom of the triazolic ring while the phenyl bearing ligand system **24** shows a much bulkier substituent with a stronger influence on the triazolic ring. Both ligand systems were chosen as initial test substances because of their described features out of all the ligand system synthesized so far.

The ion exchange reaction was run at room temperature with the ligand systems pre-dissolved in methanol for the *i*Pr ligand **20** and acetonitrile for the phenyl ligand system **24** to which the sodium salt derivatives of the $[BAr^{Cl}{}_4]^-$ or $[BAr^{F}{}_4]^-$ anions were added. The reaction pathway is shown in Scheme 2.4.5.

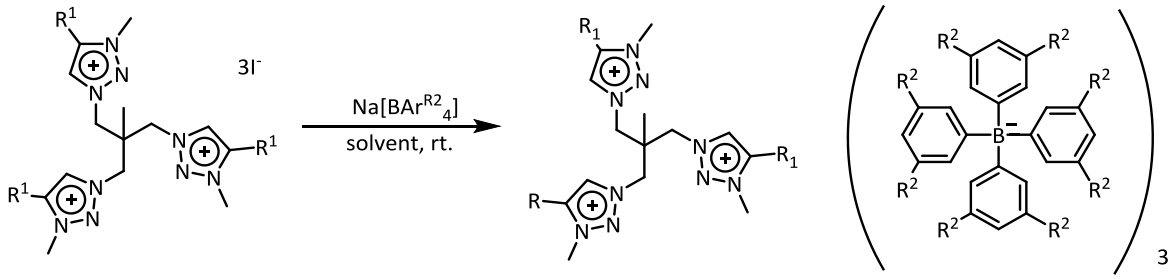

R1 = *i*Pr (**20**), Ph (**24**)
R2 = Cl, CF_3

I) R1 = *i*Pr; R2 = Cl (**27**)
II) R1 = *i*Pr; R2 = CF_3 (**28**)
III) R1 = Ph; R2 = Cl (**29**)
IV) R1 = Ph; R2 = CF_3 (**30**)

Scheme 2.4.5: Ion exchange reaction between the methylated ligand system 20 and 24 and $Na[BAr^{R2}{}_4]^-$ to form the ligand systems 26 - 29 with weakly-coordinating anions.

Upon addition a white solid started to precipitate presumably the insoluble sodium iodide which is the driving force of the reaction. Prolonged reaction times ensured a high yield of the target compound, while the reactions with the $[BAr^{F}{}_4]^-$ anion seemed to be fast and readily accessible the reactions with $[BAr^{Cl}{}_4]^-$ tended to be slower and benefited most from the prolonged reaction times as well as higher concentrations of the reaction solution. To ensure the complete reaction the white solid was filtered of and treated with nitric acid, silver nitrate and a 25% ammonia solution was added to form the citrus-yellow silver iodide. Thus the adequate course for the ion exchange could be ensured. An overview of the employed ligand system and subsequent yields is shown in Table 2.4.1.

number	substituent at the triazolic ring	counter Ion	yield [%]
26	*i*Pr	$[BAr^{Cl}_4]^-$	90
27	*i*Pr	$[BAr^{F}_4]^-$	90
28	Ph	$[BAr^{Cl}_4]^-$	70
29	Ph	$[BAr^{F}_4]^-$	98

Table 2.4.1: Yields of the ion exchange reactions with the ligand systems 20 and 24 to generate the ligand systems 26 - 29 with weakly-coordinating anions.

It could be shown, that the ion exchange reaction presented in here is a viable option to transfer the methylated ligand systems **20** and **24** with a coordinating halide anion to a system with bigger and weakly-coordinating anions **26 - 29**. The reaction can be done in good yields because of the strong driving force of the formation of the insoluble sodium iodide salt. With the four new ligand systems at hand a deeper understanding on the influence of the counter ion during the coordination reaction as well as the *in situ* formation of the mesoionic carbenes can be gained.

2.4.3 Selected Tripodal Triazolic Ligand Systems in Metal Coordination with Coinage Metals (Cu, Ag, Au)

After the successful synthesis of the salt form of the mesoionic carbenes **20** - **29** described in chapter 2.4.1 these compounds were then subjected to a deprotonation and metal coordination reaction with silver oxide to form a silver-MIC complex. An additional transmetalation reaction is then applied in order to get the target metal complex with the corresponding coinage metal.

In general, there are a multitude of different synthetic approaches to generate NHC and MIC metal complexes. These approaches can be summarized into IV different sub species I) reaction of a free carbene with a metal precursor, II) reaction of an olefin with an organometallic fragment III) reaction of an imidazolium salt with a transition metal salt and IV) transmetalation reaction with silver-carbene complexes.[121]

The latter approach was first described by WANG and LIN in 1998[122] who reported that the weak and labile silver-NHC bond could be expected to form stable metal-NHC complexes in a transmetalation reaction by using it as a carbene transfer agent. This synthetic approach is rather useful, since it overcomes the obstacles of the classical ways to generate the free NHCs where often the use of strong bases, inert reaction conditions and excessive workups is needed. While it is possible to generate the silver-NHC by a reaction of a free carbene with a silver salt the most widely used method is the reaction of an imidazolium salt which undergoes an *in situ* deprotonation with a silver base like Ag_2O, AgOAc or Ag_2CO_3 with subsequent metal coordination. Since water is formed during the

reaction the resulting silver-NHC complexes can be considered relatively air and water stable. An example of such a reaction pathway for the reaction of an imidazolium salt with silver oxide is displayed in Scheme 2.4.6.

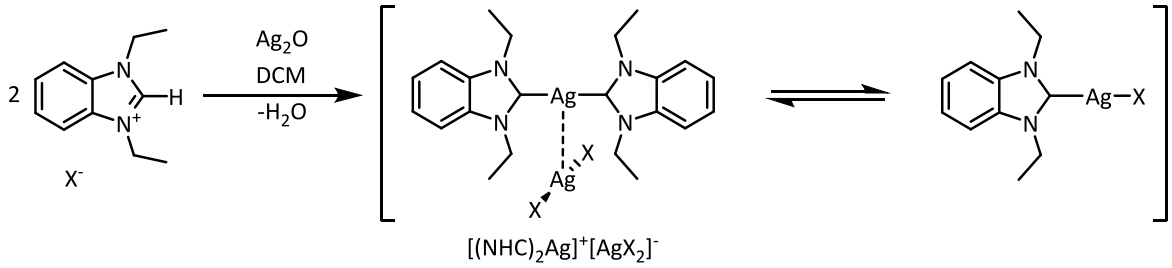

Scheme 2.4.6: Reaction of an imidazolium salt with silver oxide under water elimination.[122]

Two equivalents of the NHC salt react with one equivalent of silver oxide at room temperature. It is important to note that the formed silver-NHC complexes fluctuate in solution between the ionic and neutral complex which leads to different reaction products depending on the adjusted conditions which favor one product over the others, as to mention type of solvent, size and type of anion in the NHC salt and steric properties of the NHC.[121] This behavior is reminiscent to the well-known SCHLENK equilibrium of Grignard reagents. The equilibrium is depicted in Scheme 2.4.7 .

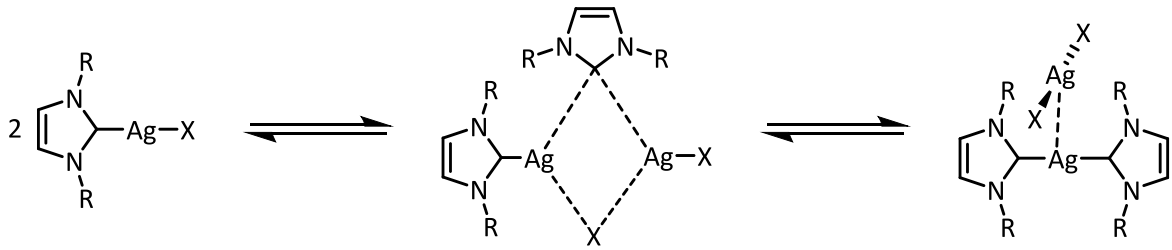

Scheme 2.4.7: Change between the neural and ionic silver-NHC complexes in solution.[121]

Provided that the right metal complex is present, the reaction can give *in situ* the product of the transmetalation. In the presence of a halide anion, either coming from the NHC salt or the metal complex, an insoluble silver halide is precipitating what drives the reaction. An example for the formation of a gold and palladium complex is shown in Scheme 2.4.8.

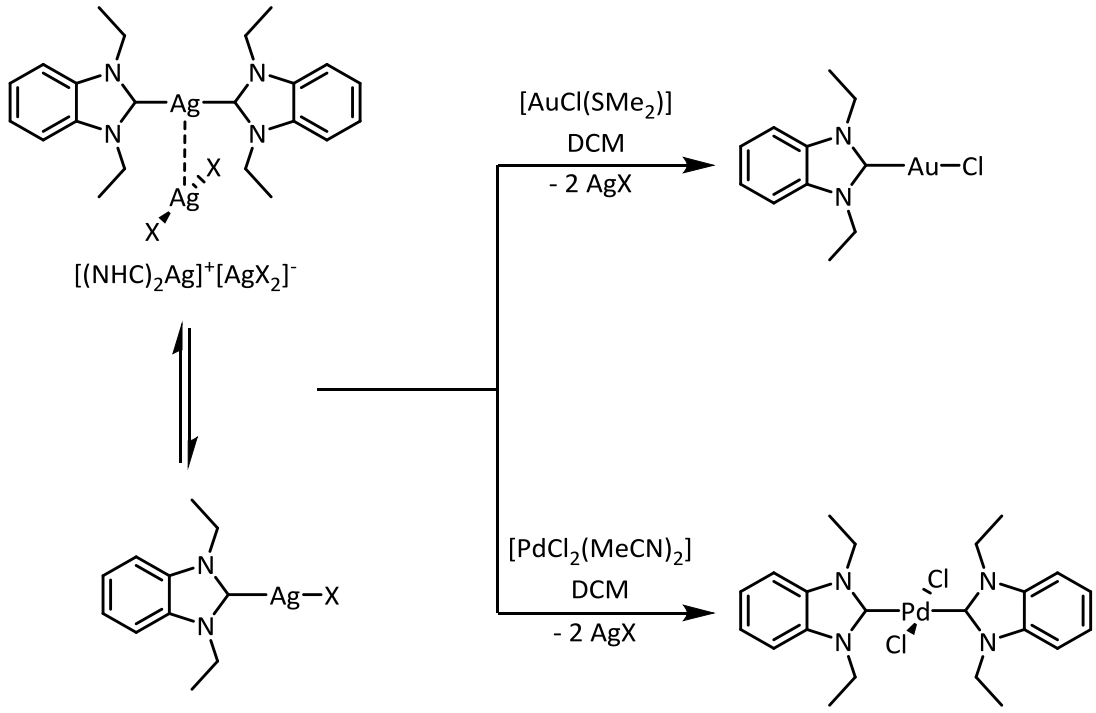

Scheme 2.4.8: Transmetalation reaction between a silver-NHC and a metal salt.[122]

Apart from the two examples in Scheme 2.4.8 more ionic and neutral structural motives in the solid state have been reported.[121,123,124,125] Some selected examples of silver-NHC complexes are shown in Figure 2.4.12 depicting different coordination motifs of the silver atom with the imidazolium salt derivative.

Depending on the reaction conditions for example the used solvent, present counter-ion and salt to metal ratio different coordination motifs are feasible. The properties of the anion present in the carbene precursor salt play a vital role in forming the structure depending on if it is a smaller coordinating anion like halides or a bigger weakly-coordinating anions like PF_6^- or $[BAr^{Cl}{}_4]^-$ and more. Non-halide containing NHC salts usually form the simpler bis-carbenes **C** while short chained imdazolium salts with chlorine or bromine as halide form structures of type **A,B** and **D**. In contrast, NHC salts with iodide favor structure type **E** among the others. Lastly the composition of the reaction solution i.e the employed solvent can also have an impact on the resulting structure especially in conjunction with halide anions. NOLAN *et al*. proposed that this might be the case due to the higher polarizability of iodide over chloride and could show in an experiment that in fact imidazolium salts with iodide as counter ions and in the presence of a polar solvent like MeCN tend to form type **B** like structures. The same reaction, done with chloride in MeCN favors a mixture of type **B** and **A** like structures.[39]

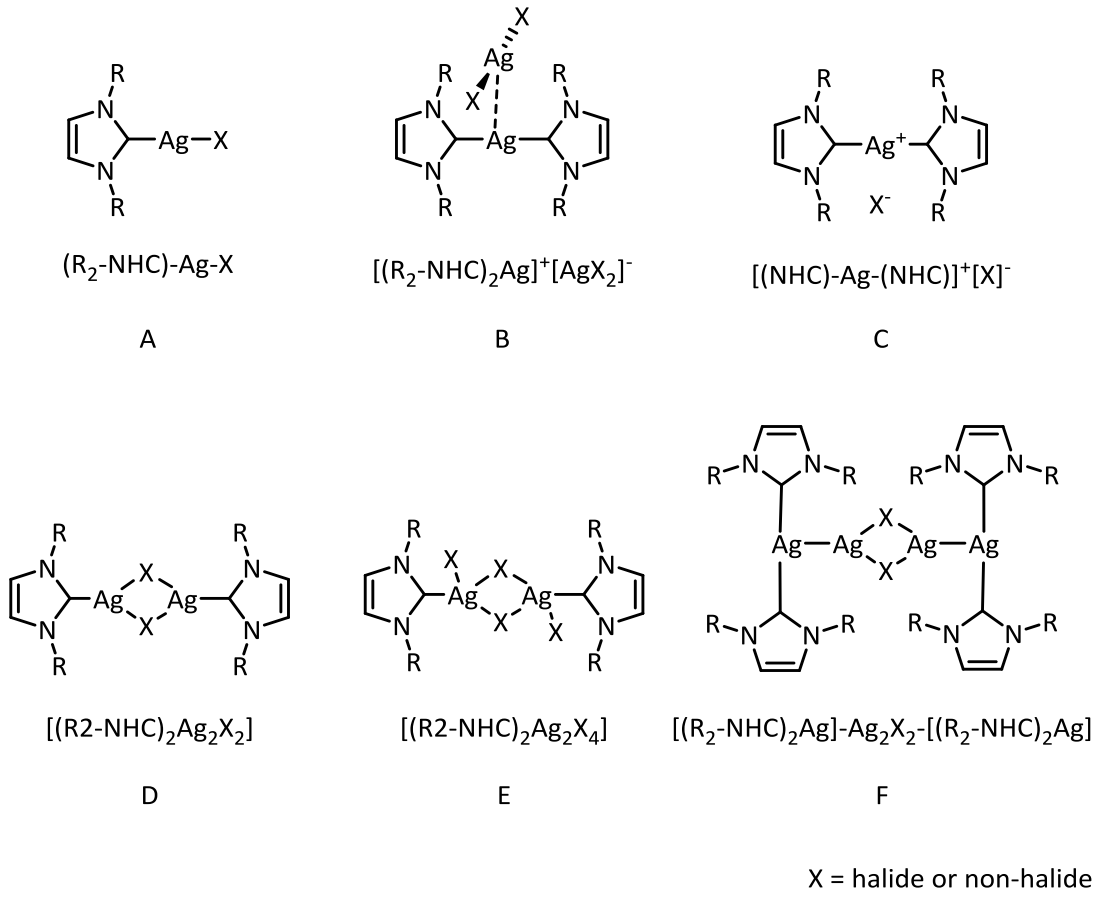

Figure 2.4.12: Examples of reported coordination motifs of Ag-NHC complexes A – F derived from imidazolium salts.[114]

Since the formations of bis-carbene complexes can be forced by proper selection of solvent and accompanying anions it is possible to connect tripodal imidazolium-salts. MEYER *et al*. designed such a ligand system and were able to prepare the silver-NHCs with the same reaction pathway which resulted in the bridging of two tripodal ligand systems via three silver atoms.[6] The reaction is depicted in Scheme 2.4.9.

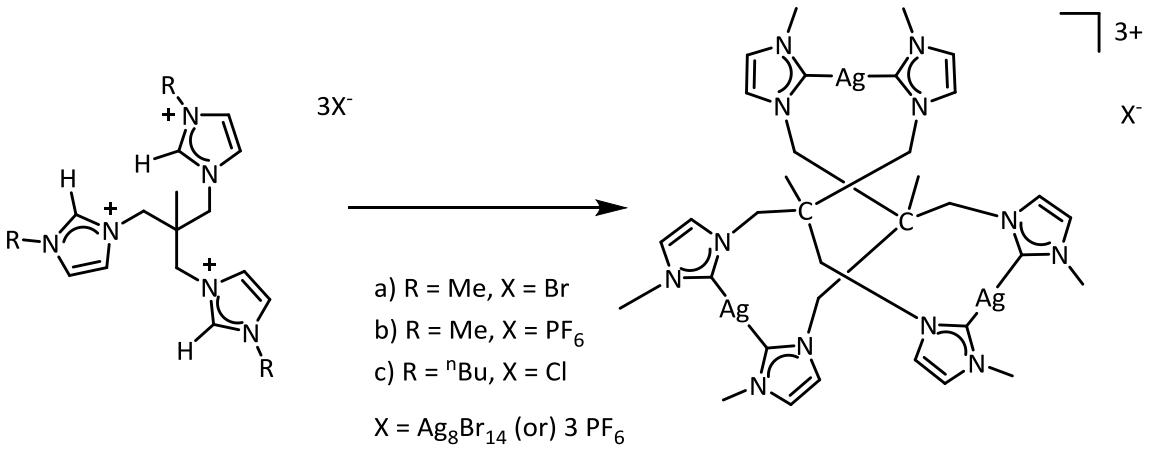

Scheme 2.4.9: Tripodal NHC ligand system connected by three silver atoms by MEYER *et al*..[6]

This initially described synthetic approach, to use silver oxide as a mild deprotonation agent, can be transferred towards the synthesis of metal-complexes with the triazolic ligand systems described in this work. This synthetic pathway can overcome the disadvantages when working with these compounds. For example it was not yet possible to isolate the free carbene and also the use of strong bases often leads to a decomposition of the ligand systems.[101] The described structural diversity of the resulting silver-MIC complexes can be helpful in selectively synthesizing mono- and bidentate coordination motifs in a subsequent transmetalation reaction.

Based upon the presented findings when working with silver-carbene complexes it is possible to control the formed products during the metal coordination reactions with silver as well as the subsequent transmetalation reaction with different metal atoms. In order to achieve this, three variables during the reaction pathway need to be controlled. These are I) the anion present in the carbene precursor salt, II) the employed solvent during the reaction and III) the type and properties of the substituent present at the triazolic rings. By controlling these factors, a specific coordination motif of a metal coordination as well as a reduction of possible side products can be achieved.

As described above, the anion present during the synthesis of the silver-MIC complex can play a vital role in the type of structure of the metal complex that is formed. The work in here features ligand systems with an iodide anion present in **20** - **25**. It is expected that there is some interaction of the anions during the metal coordination to form the silver-MIC complex and that the dimeric binding motif between two ligand systems or the bidentate binding motif within one ligand system is preferred shown in Figure 2.4.12 **B**. Still a mixture of binding type **A** and **B** might occur since in the reactions in here the slightly less polar DCM is used as solvent instead of MeCN as proposed by NOLAN *et al*.[126] which can help to force the formation of a dimeric type **B** binding motif. In contrast the synthesized ligand systems **26** - **29** bearing a bulkier weakly-coordinating $[BAr^{Cl}{}_4]^-$ or $[BAr^{F}{}_4]^-$ anion should favor the dimeric type **C** structure where there is no interaction between the anions and an additional silver metal.

Besides the described aspects of the reaction conditions, the proper ratio of silver oxide to the ligand system needs to be chosen. The triazolic ligand systems in here provides three triazolic arms while one equivalent of silver oxide is able to deprotonate two triazolic arms and form the dimeric or bidentate binding motif. This results in 2:1 ratio of triazolic arm to silver oxide. Since each ligand system consists of three side arms with a triazolic ring a ratio of 6:3 or respectively 1:1.5 ligand system to silver oxide is assumed.

Combining these aspects resulted in the following reaction pathway shown in Scheme 2.4.10. All reactions were carried out in DCM since it provided by far the best solubility for the used ligand systems and would enable the formation of monomeric as well as dimeric structures. Because of

the photosensitive properties of silver oxide all reactions have been carried out under exclusion of light and also SCHLENK technique was used in all described reactions.

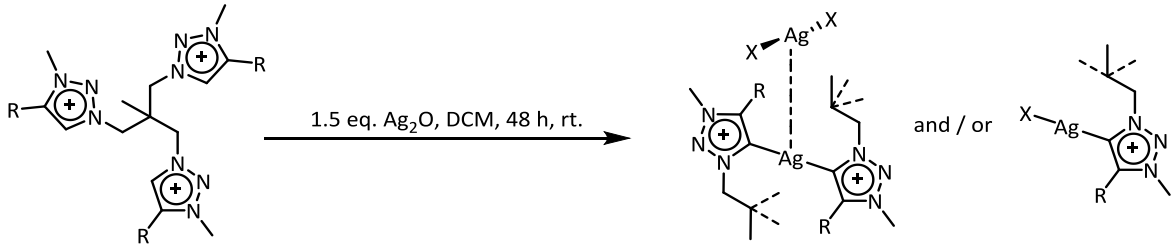

R = *n*Pr (**20**), *t*Bu (**23**), Ph (**24**), $FeCp_2$ (**25**)

Scheme 2.4.10: Proposed reaction pathway for the deprotonation and coordination reaction of the triazolic ligand system with silver oxide. Additional ligand arms have been removed for clarity and are indicated by the dotted line.

The proposed reaction pathway was tested with the ligand systems **20**, **23**, **24**, and **25**. The ligand systems were dissolved in DCM, silver oxide was added and the reaction was stirred for 24 h. During the reaction a visible uptake of the insoluble silver oxide could be observed as well as the formation of an off white solid presumably the corresponding insoluble silver-halide salt. Unfortunately, not everything of the provided silver oxide reacted. Attempts to isolate the formed silver-MIC species were not successful. In addition, NMR analysis indicated a decrease of the proton signal at the free carbon atom of the triazolic rings but also an increase of unwanted side products presumably incompletely deprotonated ligand systems or differently coordinated silver-MIC complexes. Because of the insufficient quality of NMR data multiple attempts to crystalize the products to get a better understanding of the formed silver-MIC complexes have been carried out but without success. Prolonged reaction times up to 48 h as well as heating were not suitable methods to optimize the reaction.

Since the deprotonation and coordination with silver oxide appeared incomplete it was deemed necessary to introduce the transmetalation reagent with witch the transmetalation reaction should occur from the silver-MIC complex to the target complex. By an addition of the metal salt to the reaction, the transmetalation reaction can occur during which the insoluble silver-halide complex is formed. This formation acts as a driving force of the reaction possibly ensuring a higher uptake of the silver oxide resulting in a complete deprotonation at the carbon atom of the triazolic rings of the ligand systems. Over the course of multiple reactions, it has been found that the best reaction pathway to ensure a complete deprotonation and high uptake of the silver oxide is to only add the silver oxide to the ligand system and stir for 48 h at room temperature and then add the transmetalation reagent. This would ensure a sufficient initial reaction of the ligand system with the silver

oxide. The described reaction pathway with $AuCl{\cdot}SMe_2$ and the ligand system **20** leading to a gold-MIC complex **30** is depicted in Scheme 2.4.11.

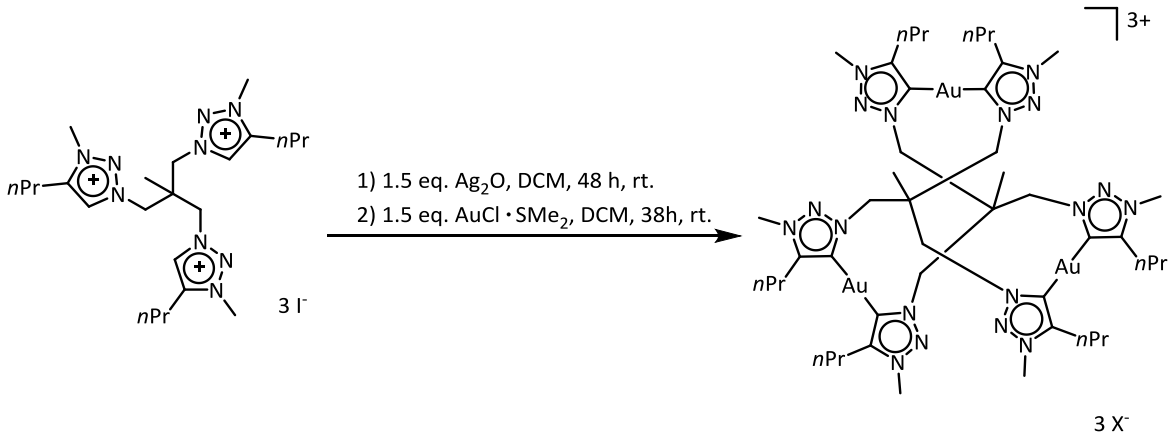

Scheme 2.4.11: Reaction pathway for the synthesis of a dimeric gold-MIC complex 30 from ligand system 20.

$AuCl{\cdot}SMe_2$ has been chosen as a source for the metal because of the interesting properties of the resulting gold complexes. These gold(I) complexes can be used, among other examples[127], to facilitate carbon – carbon bond formation[128] as well as cycloisomerization reactions.[129] Also their coordinative properties to form linear gold(I) complexes are useful for the complex formation in this work because it allows to replace the silver atoms while keeping the monomeric and dimeric coordination motifs described earlier.

The synthesis was set up at room temperature where the ligand system **20** was dissolved in DCM and silver oxide was added and stirred for 48 h. The slow formation of an off white solid could be examined indicating the coordination of silver under silver iodide precipitation. $AuCl{\cdot}SMe_2$ was added to the reaction and stirred for 38 h. The reaction solution was then filtered through a pad of CELITE and washed with DCM, excess solvent was then removed *in vacuo*. The precipitate was dissolved in a small amount of DCM and pentane was added to grow crystals suitable for X-ray diffraction analysis after 12 h at room temperature. Unfortunately, it was not possible to get a coherent refinement because of insufficient quality of the obtained data sets and the presence of severe disorder in the crystal structure. The asymmetric unit shows the dimeric structure of the gold-MIC complex as well as multiple solvent channels and the presence of heavy atoms in the vicinity presumably belonging to halide and silver clusters. Each *n*Pr substituent of the ligand arms is disordered with multiple supplementary disordered DCM molecules in close proximity. Additionally, in the crystal structure one can see the formation of accompanying clusters of anions probably consisting of silver and chloride. In here there are also signs of a positional disorder between the chloride and iodide anions. While no complete refinement of the obtained data could be achieved the

overall dimeric coordination between two ligand systems **20** where each arm is bridged in a linear fashion by a gold atom could be determined unambiguously. Figure 2.4.13 shows an isotopic representation for the gold-MIC complex **30** obtained from the X-ray diffraction experiment.

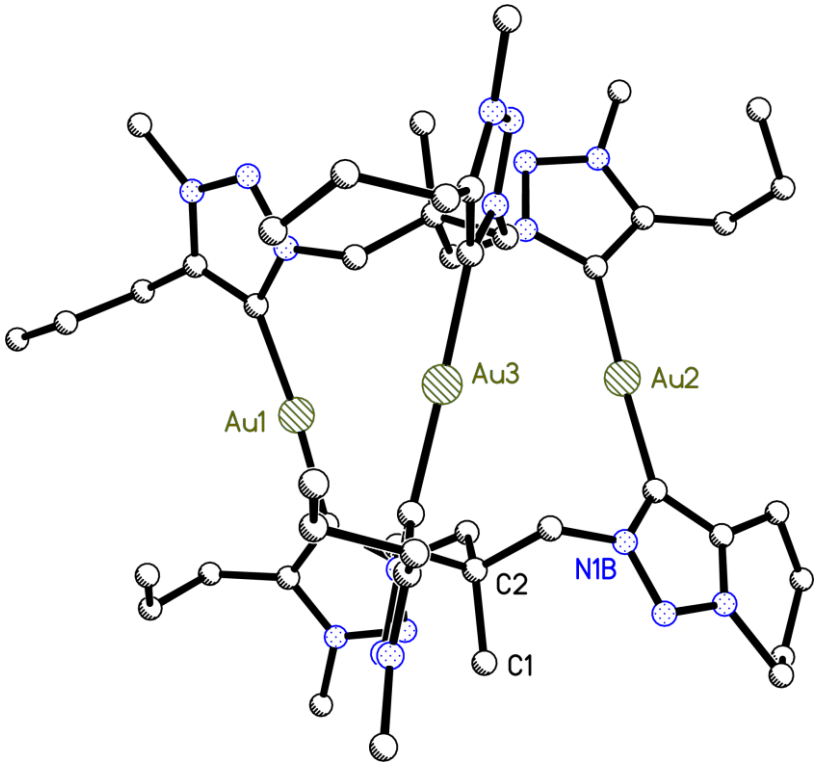

Figure 2.4.13: Isotropic representation of the gold-MIC complex 30. Disordered DCM solvent molecules, silver-halide clusters and disordered parts of the *n*Pr substituents have been omitted for clarity.

A wide range of different crystallization techniques have then been tried in order to find suitable conditions in which the metal complex **30** crystalizes without the presence of solvent or solvent which is less prone to disorder. The metal complex **30** showed only very low solubility in solvents apart from DCM and only acetone could be used as an alternative. Regrettably, these experiments were unsuccessful in producing suitable crystals for the structure determination.

To circumvent these drawbacks, it was then tried to force the monomeric binding motif as a main product which results in a neutral metal complex. This improvement should lead to the absence of potentially disordered anionic structures and an overall smaller metal complex which might be easier to crystallize. As described earlier NOLAN *et al.*[39] proposed that the polarity of the solvent in combination with the present anion has an influence in directing the reaction towards the monomeric or dimeric product. In this work, the previous experiments have shown that DCM is the only solvent in which a reasonable solubility of the ligand system can be achieved ruling out alternatives.

In order to still force the formation of the monomeric complex it was tried to increase the equivalents of metal salt used for the transmetalation reaction to 3 eq. in regard to the ligand system. With an excess of metal salt each arm of the ligand system can be reacted after a successful deprotonation and coordination with the silver oxide. The reaction pathway is show in Scheme 2.4.12.

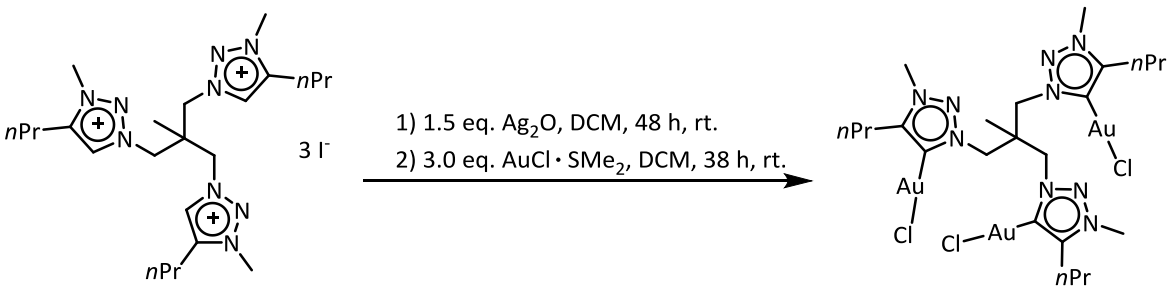

Scheme 2.4.12: Reaction pathway for the synthesis of a monomeric gold-MIC complex.

The reaction was carried out similar to the previously described one with the only change in used equivalents of $AuCl{\cdot}SMe_2$ from previously 1.5 eq. to 3.0 eq. Unfortunately, the proposed product could neither be isolated nor crystallized. NMR data indicate the proper deprotonation reaction on the triazolic rings and the formation of unknown side products. Additional mass spectrometry measurements were also not suitable to identify the product and because of the lack of sufficient analytical data this reaction was deemed unsuccessful.

To deepen the understanding of the formation of metal complexes the same reaction pathway was then tried with $CuBr{\cdot}SMe_2$. This precoordinated copper metal salt was chosen as a copper(I) source because it is also able to adopt a linear coordination motif and should be well suited to accommodate a monomeric or dimeric binding motif proposed for the ligand systems under these reaction conditions.

A first reaction was done in DCM with 1.5 eq. silver oxide and subsequent addition of 1.5 eq. of $CuBr{\cdot}SMe_2$ under SCHLENK conditions. The reaction leading to the copper-MIC complex **31** is depicted in Scheme 2.4.13 and interestingly only the monomeric complex is formed.

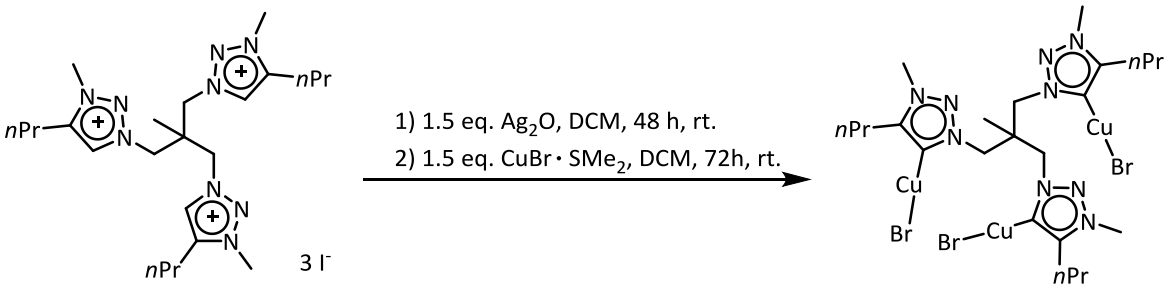

Scheme 2.4.13: Reaction pathway for the synthesis of a monomeric copper-MIC complex 31.

With prolonged reaction times the solution turned bright yellow and after 72 h the reaction was stopped. The precipitate consisting of unreacted silver oxide and the insoluble silver halide was filtered off and the volume of the solution was reduced *in vacuo*. Storage of the reaction vessel at -20 °C for 12 h resulted in the formation of crystals suitable for X-ray diffraction. The resulting structure is shown in Figure 2.4.14.

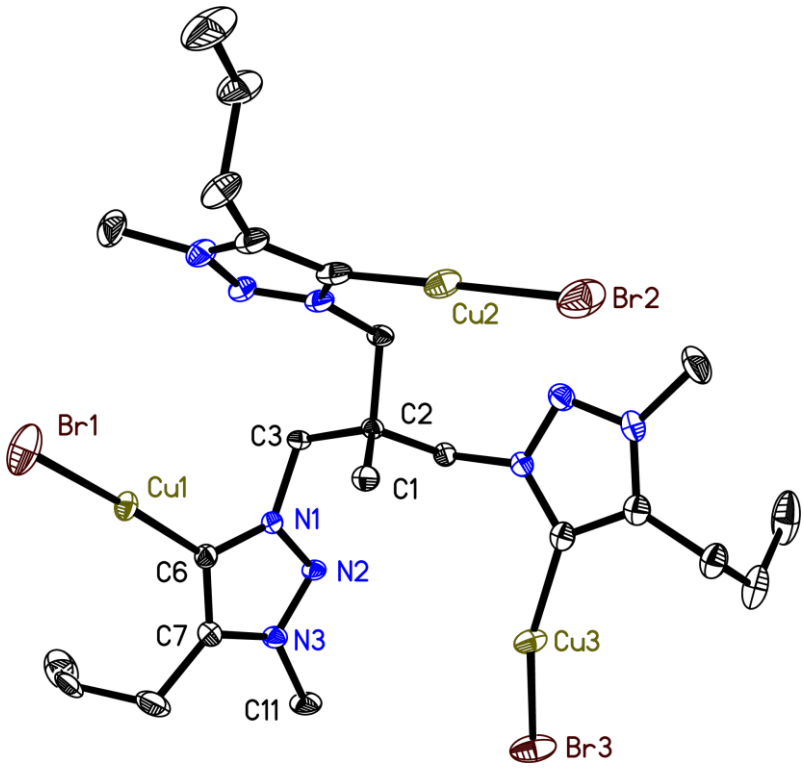

Figure 2.4.14: Asymmetric unit of 31. 31 crystallizes in the space group $P\bar{1}$ in a triclinic crystal system with α = 90.60(1)°, β = 97.20(1)°, γ = 95.31(1) Å and a = 10.309(1) Å, b = 10.616(1) Å and c = 15.703(1) Å. The anisotropic displacement parameters are depicted at the 50% probability level. Hydrogen atoms, a disordered *n*Pr substituent and solvent molecules have been omitted for clarity.

The asymmetric unit shown in Figure 2.4.14 consist of the ligand system **20** where each of the three ligand arms is coordinated to a CuBr moiety in a linear fashion. The structure shows a monomeric coordination motif even though 1.5 eq. of metal salt were used. In comparison with the same reaction done previously with AuCl·SMe_2 a dimeric structure should be expected. It is of note that only the monomeric structure crystallized and that the dimeric structure might be still present in solution. In a view along the central methyl group C1 – C2 one can see the C_3 symmetry of the alkyl backbone can almost be transferred to the whole molecule with the exception of the *n*Pr groups and the Cu3 - Br3 moiety. While this is an interesting behavior of the ligand system the symmetry

considerations for catalytic reactions described in chapter 1.2.1 can only be applied to metal complexes who can provide a C_3 symmetric tridentate coordination with the central metal atom. A view along the C1 – C2 bond is shown in Figure 2.4.15.

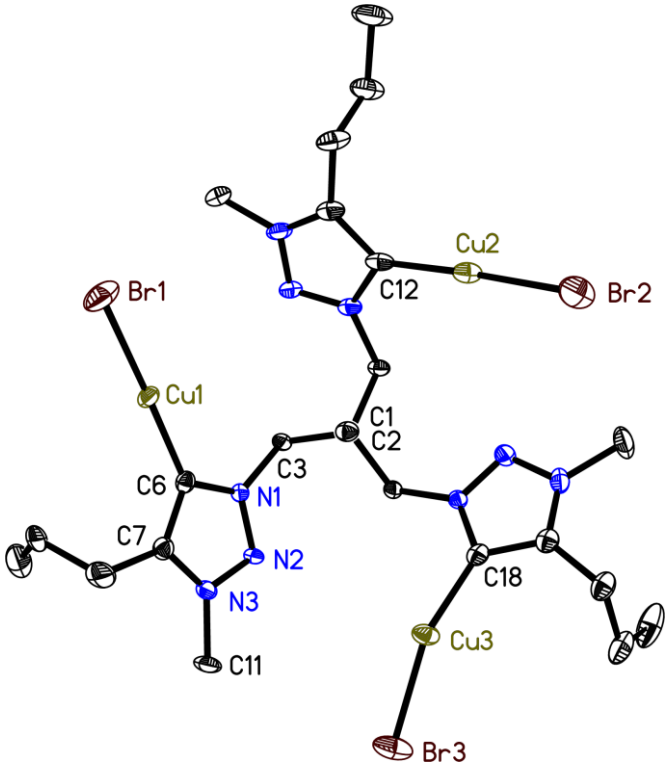

Figure 2.4.15: View along the C1 – C2 bond in the asymmetric unit of 31. The anisotropic displacement parameters are depicted at the 50% probability level. Hydrogen atoms, a disordered *n*Pr substituent and solvent molecules have been omitted for clarity.

The coordination of a copper(I) metal to each of the triazolic rings did not change the overall connectivity within the ligand arms. For example, the bond lengths within one ligand arm amount to C3 – N1 1.466(4) Å, N1 – N2 1.336(4) Å, N2 – N3 1.328(4) Å, N3 – C7 1.358(5) Å, C7 – C6 1.386(5) Å, C6 – N1 1.364(4) Å. These are similar to the other two ligand arms within the same ligand system. In comparison with the free ligand system **8** the corresponding bond lengths amount to C3 – N1 1.460(2) Å, N1 – N2 1.349(2) Å, N2 – N3 1.320(2) Å, N3 – C7 1.364(2) Å, C7 – C6 1.369(2) Å, C6 – N1 1.353(2) Å and show no considerable changes. The bond angles in one of the triazolic rings of the copper-MIC complex **31** amount to C7 – C6 – N1 101.8(3)°, N1 – N2 – N3 102.3(3)°, C6 – N1 – N2 115.8(3)° and N3 – C7 – C6 107.5(3)° and are also similar to the other two rings. The corresponding bond angles in the free ligand system **8** are at C7 – C6 – N1 105.25(15)°, N1 – N2 – N3 106.72(13)°, C6 – N1 – N2 110.76(13)° and N3 – C7 – C6 107.78(15)°. One can see, that the coordination of the copper led to a slight distortion of the triazolic rings.

The copper coordination shows bond lengths of C6 – Cu1 1.887(3) Å, C12 – Cu2 1.887(4) Å and C18 – Cu3 1.902(4) Å and also Cu1 – Br1 2.222(1) Å, Cu2 – Br2 2.228(1) Å and Cu3 – Br3 2.277(1) Å. The bond angles around the copper atoms amount to C6 – Cu1 – Br1 176.87(11)°, C12 – Cu2 – Br2 176.03(11)° and C18 – Cu3 – Br3 156.15(10)°. An interesting observation can be made when looking around the periphery of the Cu3 atom. In here a lengthening of 0.055 Å of the Cu3 – Br3 bond with 2.277(1) Å can be seen as well as a small lengthening of 0.015 Å of the C18 – Cu3 bond with 1.902(4) Å in comparison to the corresponding bonds within the ligand. The changes are accompanied by a major change of around 20° in the C18 – Cu3 – Br3 bond angle with 156.15(10)° in comparison to the almost linear angles of 176.87(11)° around Cu1 and 176.03(11)° around Cu2. These findings can be explained when looking at the asymmetric unit and a second symmetry generated molecule of **31** due to an inversion center. The resulting structure is shown in Figure 2.4.16.

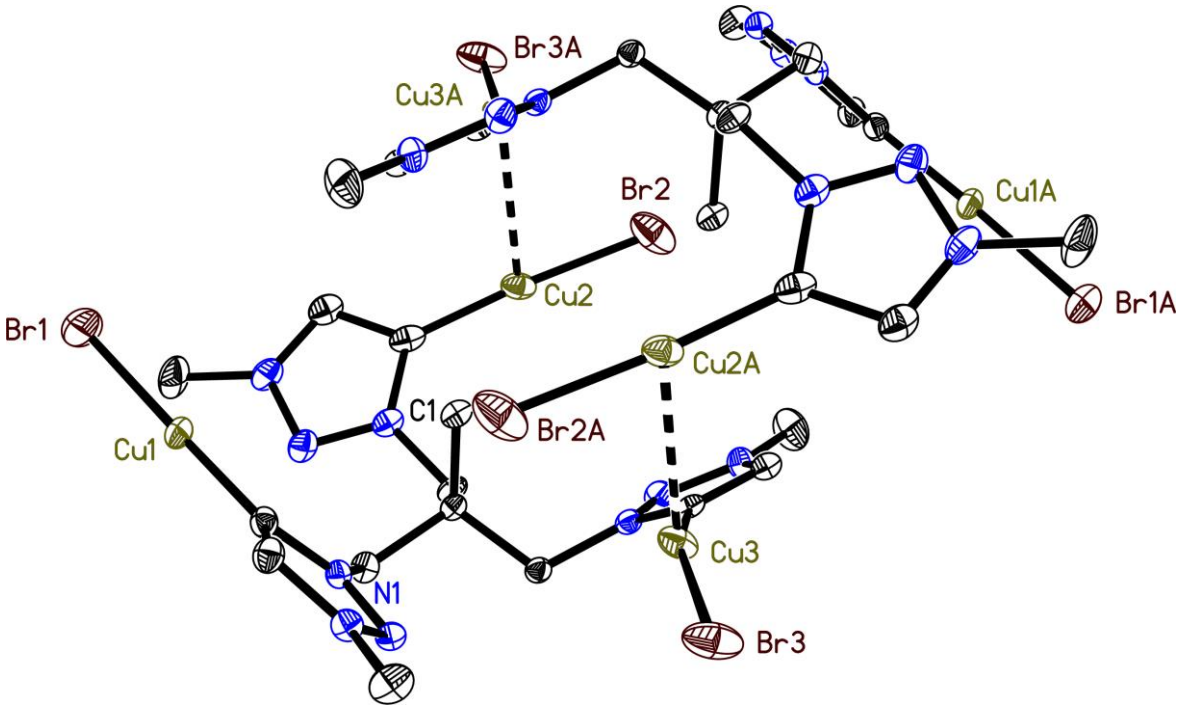

Figure 2.4.16: Crystal structure of 33 with symmetry generated second molecule. The anisotropic displacement parameters are depicted at the 50% probability level. Hydrogen atoms, *n*Pr substituents and solvent molecules have been omitted for clarity.

By the generation of a second molecule in the crystal lattice due to the symmetry operator one can see the formation of a dimeric structure connected by a Cu3 – Cu2A bond and a Cu2 – Cu3A bond respectively. In general, the copper atoms should repel each other because of their formal charge of +I. In this structure one can find a length for the metal to metal interatomic distance which amounts to Cu2 – Cu3A 2.807(1) Å. Such a metal to metal interaction between two atoms with a

closed-shell electronic configuration can be described by the term *metallophilicity*. These interactions are mostly observed within the group 11 coinage metals and most prominently the aurophilicity with a strength of about 7 – 12 kcal/mol is considered the strongest interaction comparable to a hydrogen bond.[130] In contrast, the cuprophilic interaction is considered to be weaker and their presence is still a matter of controversy.[131,132,133,134,135] SCHMIDBAUR[130] initialy coined the term of aurophilicity and PYYKKÖ[136,137] was able to identify the relativistic and correlation effects leading to their formation. A simplified explanation of these interactions can be made in that these interactions can be considered VAN-DER WAALS interactions which gets enhanced by the presence of lanthanide contraction and relativistic effects. The contraction of the orbitals in conjunction with the relativistic effects leads to an opening of the d10 configuration allowing the formation of covalent metal-metal bonds.

The bond lengths found in the structure for **31** with Cu2 – Cu3A 2.807(1) Å is well within the range of similar bond types for ligand supported and unsupported Cu – Cu bonds.[138,139,140] In order to fully characterize the bond type found in here additional spectral and theoretical investigations need to be made. From the crystal structure of **31** one can see a Cu – Cu interaction as well as short contact interactions between the Br3 halide and halogen atom of a neighboring molecule in the crystal lattice. It can be assumed, that these interactions lead to the change in the C18 – Cu3 – Br3 bond angle described previously.

With these findings the same reaction pathway was applied to the ligand systems **23**, **24**, and **25**. Unfortunately, it was not possible to isolate neither the silver-MIC complex nor the resulting metal complexes after successful transmetalation with these ligand systems. Again signs of a successful deprotonation reaction could be observed by a visible uptake of the silver oxide as well as in the NMR data in the form of a decline of the proton signal at the unsubstituted carbon atom of the triazolic rings but also the formation of multiple unknown side products.

One possible explanation could be that the increased steric demand of the substituents limits the degree of freedom in which the ligand system can adapt to the demands of a monomeric or dimeric binding motif which occurs during the reaction with silver oxide and also after the transmetalation reaction with the gold and copper salts. In some cases, the formation of a silver mirror upon addition of the gold or copper metal salt could be observed indicating a possible side reaction leading to the reduction of the silver atoms.

Even if a dimeric structure with silver oxide can be formed the substituents can shield the access to the silver metal and therefore hinder the following transmetalation reaction. Additionally, a common side reaction that can occur within triazolic MICS is a rearrangement reaction in which the

methyl group at the N3 position migrates to the free carbon atom upon deprotonation. The increase of signals found in the NMR data suggest such a behavior. Furthermore, water is formed during the deprotonation reaction with silver oxide, it can be assumed that there are unwanted oxidation reactions with the formed metal complexes. As described earlier it was tried to isolate the silver-MIC complex which led to only lackluster results and that the one-pot synthetic approach seemed more feasible. Removal of the formed water is possible but since it is expected that additional deprotonation reactions occur upon addition of the metal salt new water molecules would then be formed. Lastly the low solubility of the employed ligand systems is a major drawback with this type of compounds. This leads to a multitude of disadvantages e.g. guaranteeing proper reactant ratios, formation of homogeneous reaction conditions and also the use of solvent based analytical methods is limited.

The results presented so far show that under these conditions both, monomeric and dimeric, binding motifs are possible to achieve. As shown in Scheme 2.4.7 the silver-MIC complex is able to fluctuate between a monomeric and dimeric binding motif and depending on the reaction conditions either a mixture or only one of these options is formed in the subsequent transmetalation reaction. In here, the reaction conditions have been kept the same with only a change to the employed metal salt. From these findings it appears that a gold complexation forces the dimeric binding motif while with copper a monomeric binding motif can be achieved.
To further extend the possible binding motifs with these ligand system additional metal coordination reactions have been carried out with group 10 transition metals. The findings are present in the following chapter 2.4.4.

2.4.4 Selected Tripodal Triazolic Ligand System in Metal Coordination with Group 10 Transition Metals (Ni, Pd)

With the reaction pathway described in chapter 2.4.3 it was possible to successfully synthesize two unprecedented metal complexes **30** and **31**. Also with the use of silver oxide a suitable reaction pathway to form *in situ* the mesoionic carbene while simultaneously coordinating silver to the carbon atom of the triazolic rings could be established. This reaction pathway gave access to subsequent transmetalation reactions with different metal atoms.
Besides the coinage metals (Ag, Cu, Au) used previously in chapter 2.4.3, nickel[141,142] and palladium[143,144] play also a vital role in modern catalytic reactions.[145] Complexes employing these met-

als are predominantly used in modern cross-coupling reactions like the KUMADA[30], HECK[146], SUZUKI[29] and SONOGASHIRA[31] couplings. Bevor the rise of the NHC derived catalysts the palladium phosphane catalysts dominated the catalytic chemistry. With the access to stable NHCs more palladium carbene complexes were reported gaining interest in their catalytic properties in comparison to their phosphane counterparts.[147] Interestingly, the combination of both worlds by combination of a phosphane and carbene ligand system within one catalyst is gaining traction in recent studies.[148] Besides their NHC derivatives some variations in the form of MIC palladium complexes have been reported by CROWLEY *et al*. which possess useful properties in catalyzing different reactions like the cycloisomerization and etherification of allylic alcohols.[73] Also MIC complexes with a central nickel atom coordinated by a triazolic ligand system, shown in Figure 2.4.17, have been reported by ALBRECHT *et al.*. These complexes can be used to catalyze the SUZUKI-MIYAURA cross coupling reaction.[149]

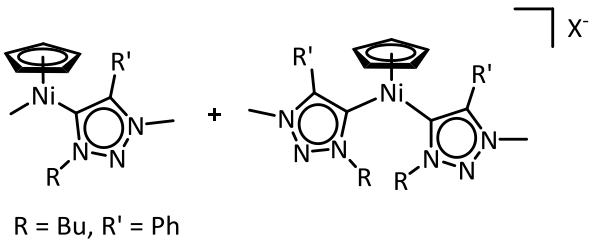

Figure 2.4.17: Ni-MIC-complexes by ALBRECHT *et al.*.[149]

Because of their described importance in modern cross coupling reactions, nickel and palladium have been selected to be tested in coordination reactions with the different ligand systems presented in this work. Initial synthesis of the metal complexes with nickel and palladium was done with the methylated ligand system **24** bearing a phenyl substituent at the triazolic rings and iodide anions as counter-ions. The ligand system was selected since it showed a very good solubility in common polar solvents which is needed to accommodate the different metal salts during the complex formation. Furthermore, the phenyl group provides a large steric demand which is helpful during asymmetric catalysis to boost stereoselectivity as well as stabilize low oxidation states of the metal atom during later possible catalytic reactions. Additionally, in the previous chapter 2.4.3 a coordination with this ligand system could not be achieved. The experiments in here were carried out in order to figure out if a metal coordination is hindered due to the steric bulk of the phenyl groups or if the properties of the metal dictate a possible coordination. The proposed reaction pathway is shown in Scheme 2.4.14.

In an argon atmosphere **24** was dissolved in DCM and under exclusion of light silver oxide was added in a 1:3 molar ratio which corresponds to a 1:1 ratio in regard to one triazolic ring to the silver

species. As described in chapter 2.4.3 the formed silver-MIC complexes can vary by the amount of silver metal present within a complex. By providing an excess it could be ensured, that all possible coordination motifs can be achieved.

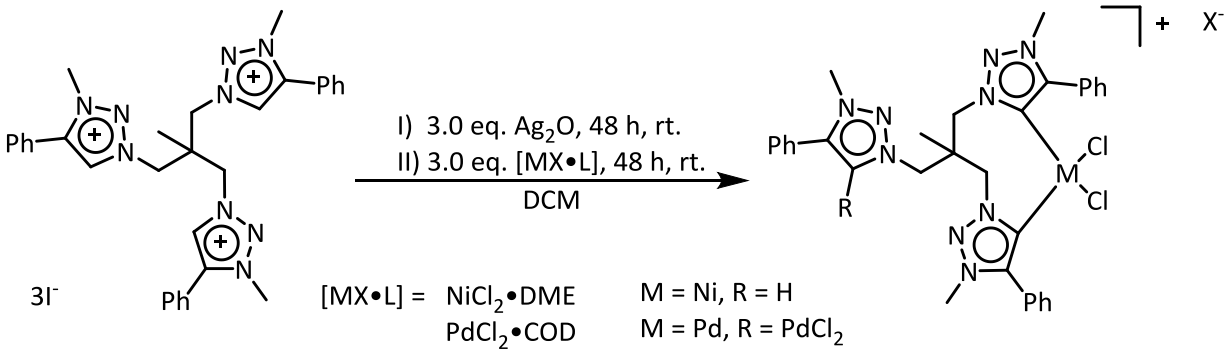

Scheme 2.4.14: Possible synthesis of palladium 32 and nickel 33 complexes from ligand system 24.

After 48 h either $PdCl_2$·COD or $NiCl_2$·DME was added to the reaction solution at room temperature. In here the pre-coordinated metal salts were used since experiments with the pure salt didn't show any promising results and the pre-coordination not only helps with solubility of the salt in organic solvents but also with the coordination since the coordination sphere is already well established. The reaction mixture was worked up and filtered through a pad of CELITE and excess solvent of the filtrate was removed *in vacuo* to give the products as dark yellow powder for the palladium species **32** and green-yellow powder for the nickel species **33**.

Analysis of the synthesized compounds was not possible with X-ray diffraction since all obtained crystals were not suitable for measurement. For the palladium complex **32** mass spectrometry was used instead as a suitable technique to gain more insight in the composition and structure of the molecule. From initial ESI spectrometry measurements it could be anticipated that at least two and possibly all three arms of the ligand system were engaged in the coordination of a metal atom either in a mono- or bidentate fashion. Further investigations with the help of NMR spectroscopy showed a distinct signal between 3.7 ppm and 4.3 ppm while the signal for the bridging CH_2 groups, connecting the triazolic rings to the alkyl backbone are missing. This indicates a change in the periphery of these carbon atoms. The NMR data is shown in Figure 2.4.18.

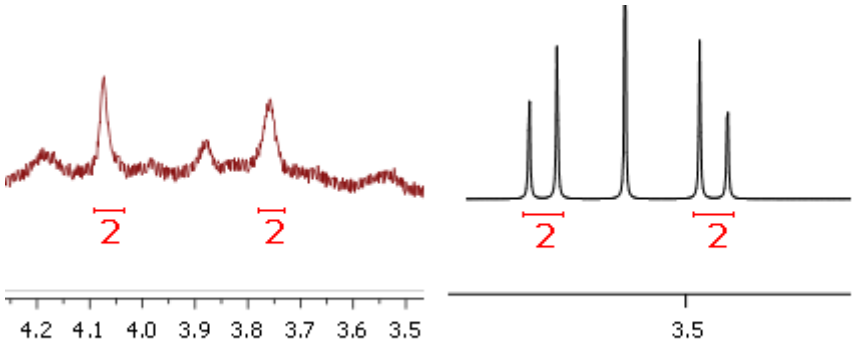

Figure 2.4.18: Excerpt from the ^{1}H NMR spectra showing diastereotopic protons for the palladium complex 32 (*left*) and simulated spectra (*right*).

This signal distribution and a comparison with a simulated spectrum suggests a group of diastereotopic protons at the position of the bridging CH_2 groups from the ligand backbone. This would be an expected result if the structure consists of at least one bidentate bonding motif. The proposed structure is depicted in Figure 2.4.19.

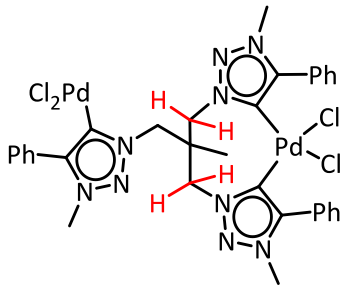

Figure 2.4.19: Proposed structure for the palladium complex 32 with diastereotopic protons marked in red.

To get further insight in the coordination sphere of the metals the palladium complex **32** and nickel complex **33** have been subjected to high resolution time of flight (TOF) and tandem mass spectrometry. The measurements were performed in cooperation with SCHNEGELSBERG within the KOSZINOWSKI group at the INSTITUTE OF ORGANIC AND BIOMOLECULAR CHEMISTRY, Göttingen. The results of these measurements for the palladium complex **32** are shown in Figure 2.4.20.

The source spectra in Figure 2.4.20 shows three peaks of the palladium-complex which, after taking into account the previously described NMR spectroscopic measurement, can be assigned to two different structures **A** and **B**. The peak **A** with *m/z* 500.914 shows a substituent of the ligand system where one side arm has been truncated due to fragmentation while still maintaining the chelating motif to the metal atom. The peak **B** with *m/z* 961.996 could be assigned to the proposed structure shown in Figure 2.4.19 with a bridging palladium dichloride center and with one arm of the ligand system coordinated in a linear fashion to another palladium chloride moiety. The peak at **C** with

m/z 1149.934 can be assigned to a possible intermediate during the metal coordination where the $PdCl_2$·COD starting material is still present at one of the ligand arms.

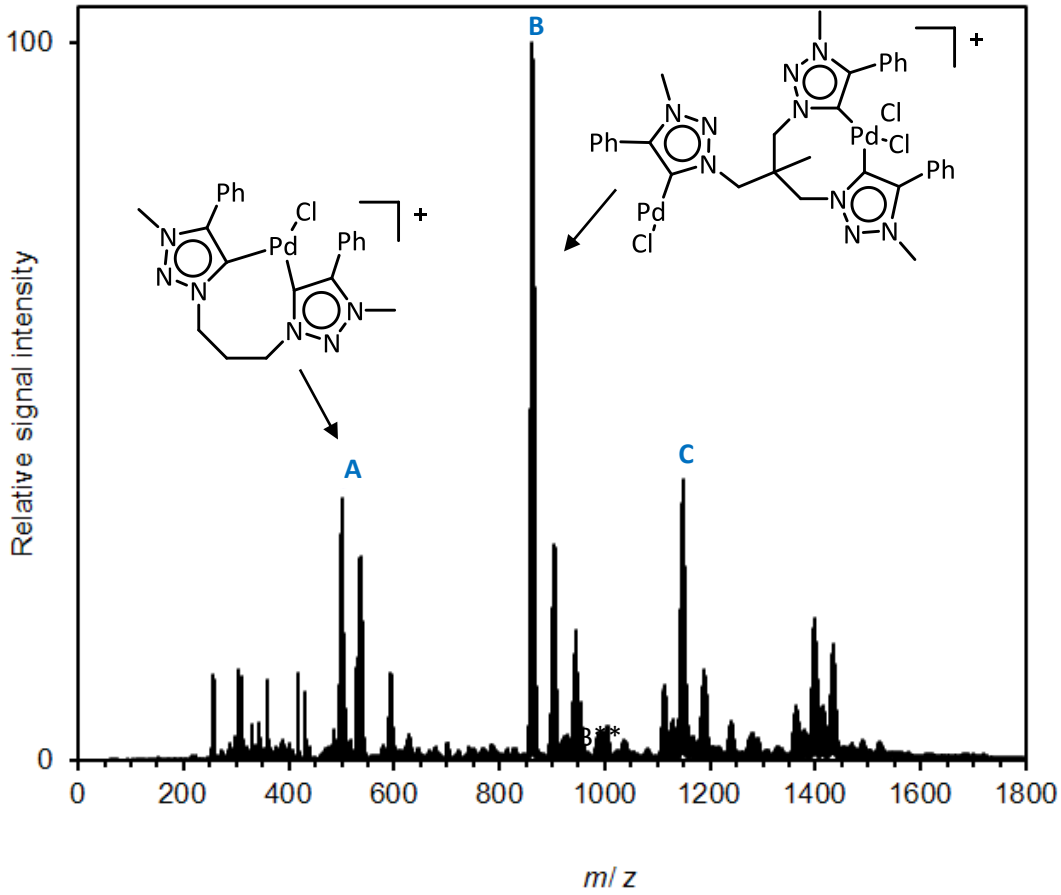

Figure 2.4.20: Positive-ion mode ESI mass spectrum of a solution of palladium complex 32 with proposed structures of the complexes with *m/z* 500.914 (A, $C_{21}H_{22}ClN_6Pd^+$), *m/z* 861.996 (B, $C_{32}H_{33}Cl_3N_9Pd_2^+$) and *m/z* 1146.934 (C, $C_{40}H_{45}Cl_5N_9Pd_3^+$).

To further confirm the proposed structures and the presence of palladium, the isotopic pattern of the main peak **B** with *m/z* 861.996 was compared to a simulated pattern for the sum formula of $C_{32}H_{33}Cl_3N_9Pd_2^+$ resulting in a perfect match. The simulation was done by the COMPASS ISOTOPE PATTERN package within the COMPASS SOFTWARE PACKAGE and the experimental and the calculated pattern can be seen in Figure 2.4.21.

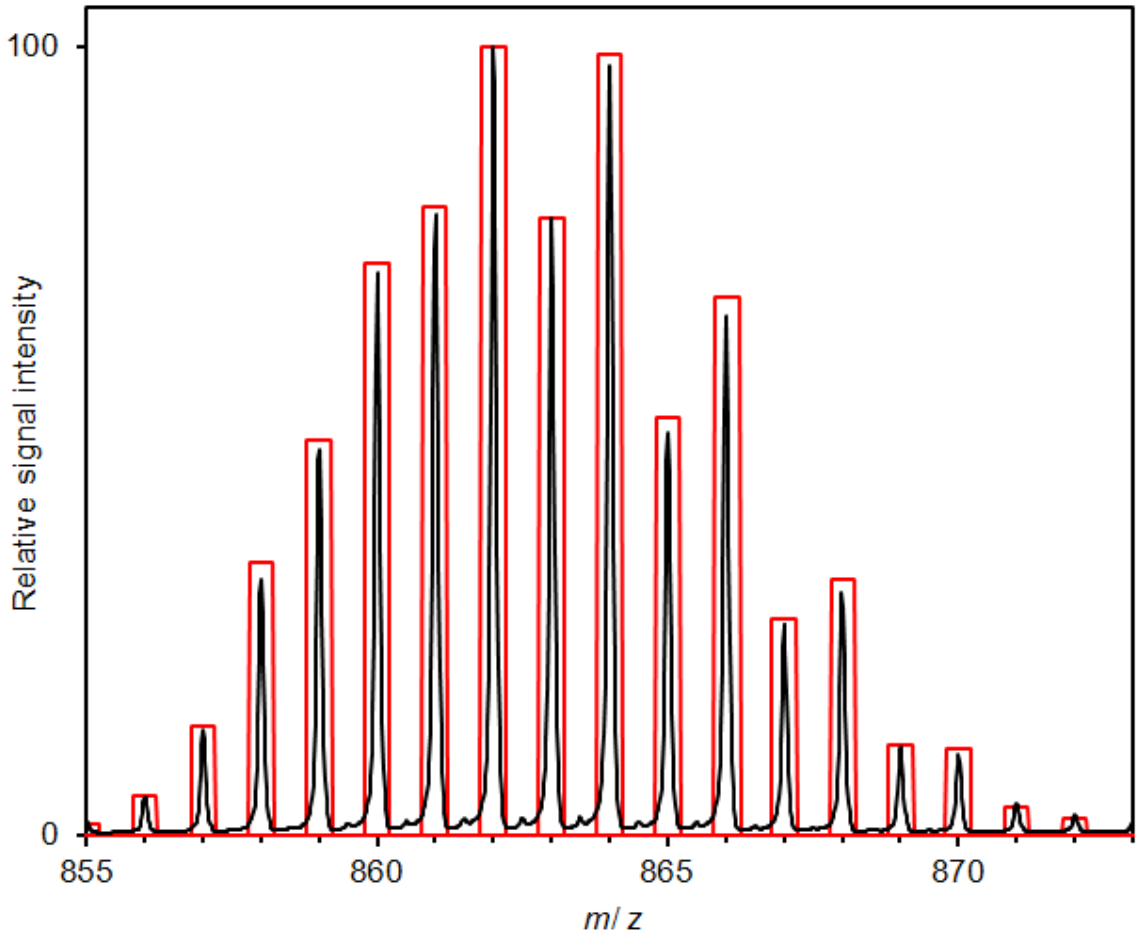

Figure 2.4.21: Enlargement of the positive-ion-mode ESI mass spectrum peak B of palladium complex 32 with *m/z* 861.996 (*black*) and the simulated isotopic pattern (*red*).

More evidence for the proposed structure for the palladium compound could also be gained by subjecting the fragment at **B** to a tandem mass spectrometry experiment. With this method it is possible to isolate single fragments and by the simultaneous use of collision induced dissociation (CID) get data on smaller fragments of the original peak. The spectrum is shown in Figure 2.4.22.

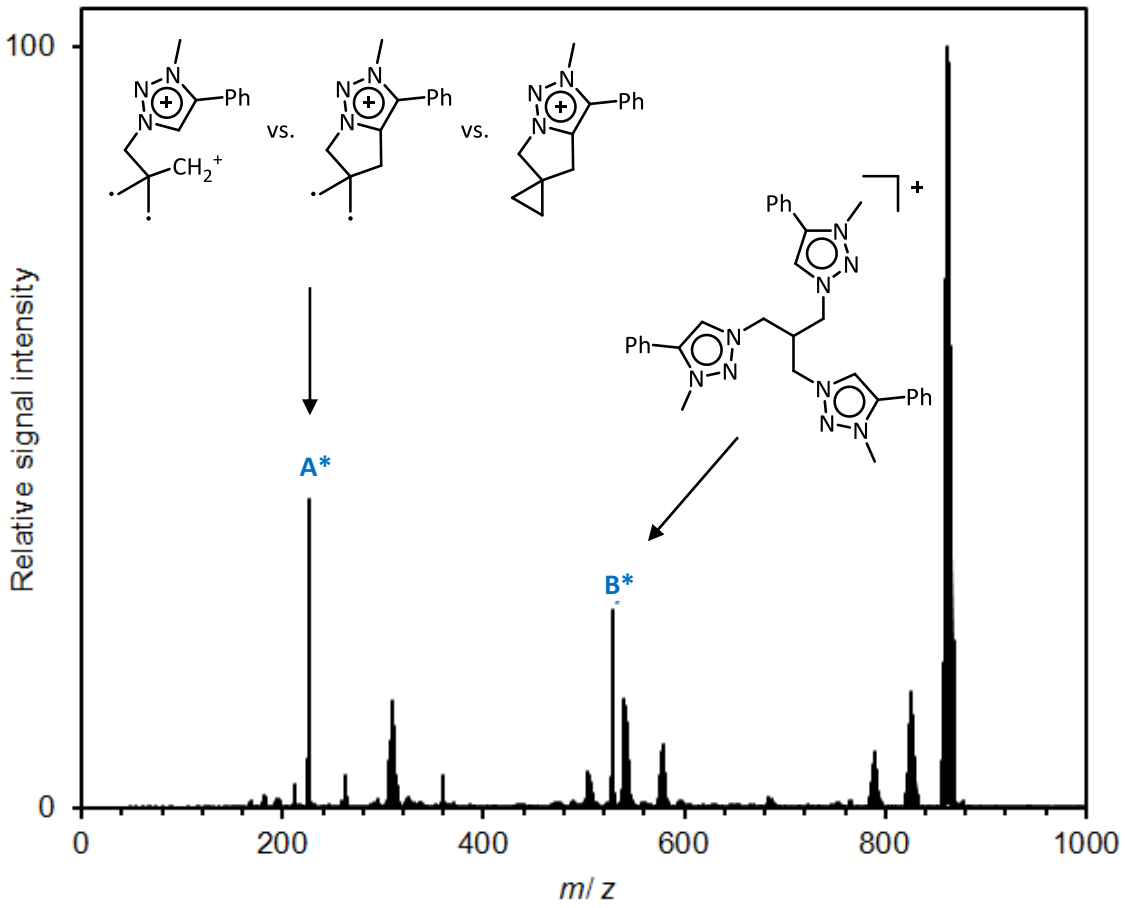

Figure 2.4.22: Mass spectrum of mass-selected peak B (*m/z* 861.996, $C_{32}H_{33}Cl_3N_9Pd_2^+$) in Figure 2.4.20 of the palladium complex 32 and its fragment ions produced upon collision-induced dissociation with E_{LAB} = 40 eV. Including proposed structures for A* (*m/z* 226.143, $C_{14}H_{16}N_3^+$) and B* (*m/z* 528.510, $C_{31}H_{30}N_9^+$).

Figure 2.4.22 shows two peaks **A*** and **B*** originating from the motherion peak **B** with *m/z* 861.996. These could be assigned to fragments from the ligand systems side arms for **A*** and the complete ligand system for **B*.**

Together with the NMR data showing diastereotopic protons, the high resolution TOF mass spectrum confirms the presence of palladium, and with a tandem mass spectrometry experiment with CID it could be shown that the ligand system is still intact with two arms chelating to a palladium dichloride moiety as well as one pendant arm bonding to a palladium monochloride moiety. This supports strongly the proposed structure for the palladium species shown in Figure 2.4.23.

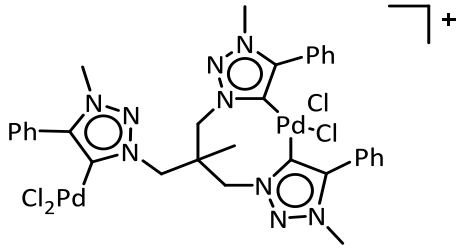

Figure 2.4.23: Proposed palladium complex 32 formed during synthesis.

The same analytical approach was also chosen for the synthesized nickel complex **33** since it was not possible to grow single crystals suitable for X-ray crystallography. Again TOF tandem mass spectrometry with CID was performed as an appropriate analytical tool. The spectrum of the initial measurement is shown in Figure 2.4.24.

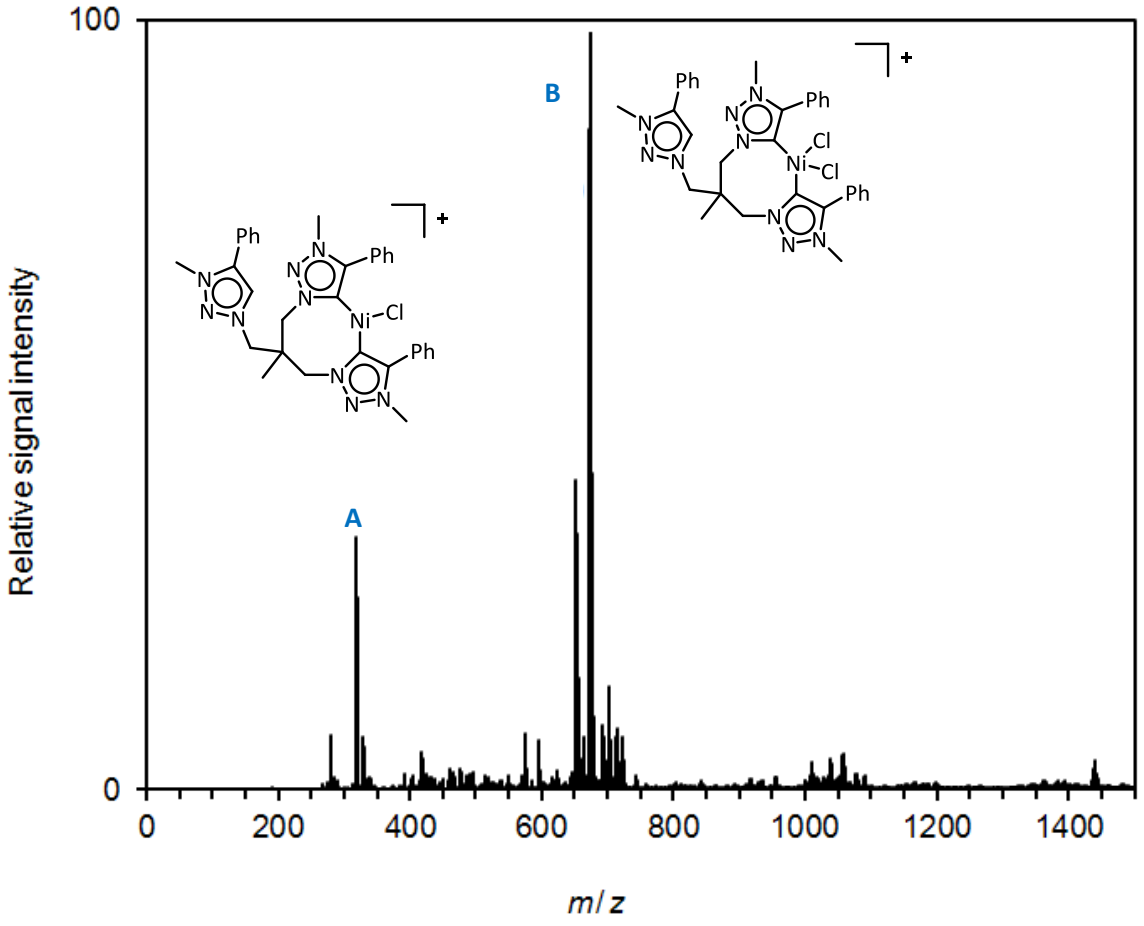

Figure 2.4.24: Positive-ion mode ESI mass spectrum of a solution of nickel complex 33 with proposed structures of the complexes with *m/z* 318.602 (A, $C_{32}H_{34}ClN_9Ni^+$) and *m/z* 674.170 (B, $C_{32}H_{34}Cl_2N_9Ni^+$).

The source spectrum of the nickel complex shows two prominent peaks which could be assigned to two proposed structures **A** and **B**. The previous experiences with the palladium complex **32** were

taken as a guideline. Again, it was anticipated that at least two arms would chelate the nickel atom while the third arm is either pendant or coordinated to another metal atom. By comparison of the high resolution peak patterns of **A** and **B** with simulated spectrums the sum formula of the proposed structures can be verified as $C_{32}H_{34}ClN_9Ni^+$ for **A** shown in Figure 2.4.25, and $C_{32}H_{34}Cl_2N_9Ni^+$ for **B** shown in Figure 2.4.26.

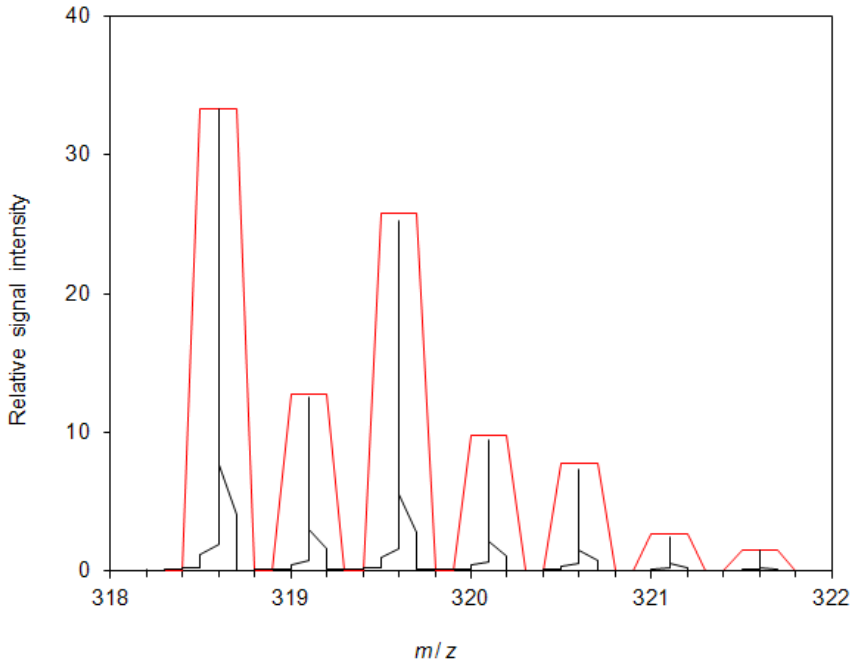

Figure 2.4.25: Enlargement of the positive-ion-mode ESI mass spectrum peak A of the nickel complex 33 with *m/z* 318.602 (*black*) and the simulated isotopic pattern (*red*).

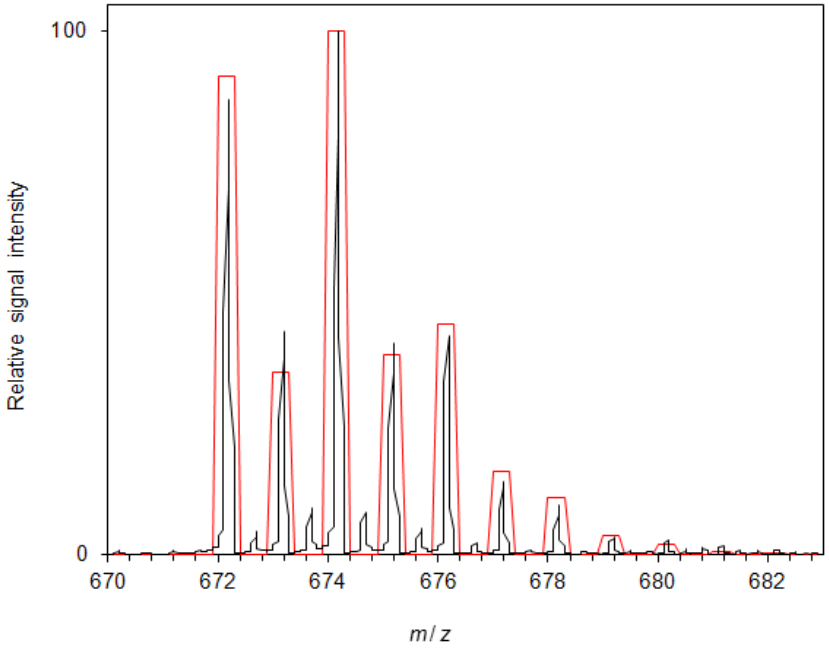

Figure 2.4.26: Enlargement of the positive-ion-mode ESI mass spectrum peak B of the nickel complex 33 with *m/z* 674.170 (*black*) and the simulated isotopic pattern (*red*).

Obviously the simulated isotope pattern is in good accordance to the measured one confirming the composition of the proposed structure for peak **A** in Figure 2.4.24.

The same match could be found for peak **B** further confirming the general sum formula of the proposed compound as well as confirming the presence of the metal atom in this structure. To gather proof for the general coordination pattern and the structure of the ligand system a CID experiment was conducted with the fragment of the motherion peak **B** in Figure 2.4.24. The results are shown in Figure 2.4.27.

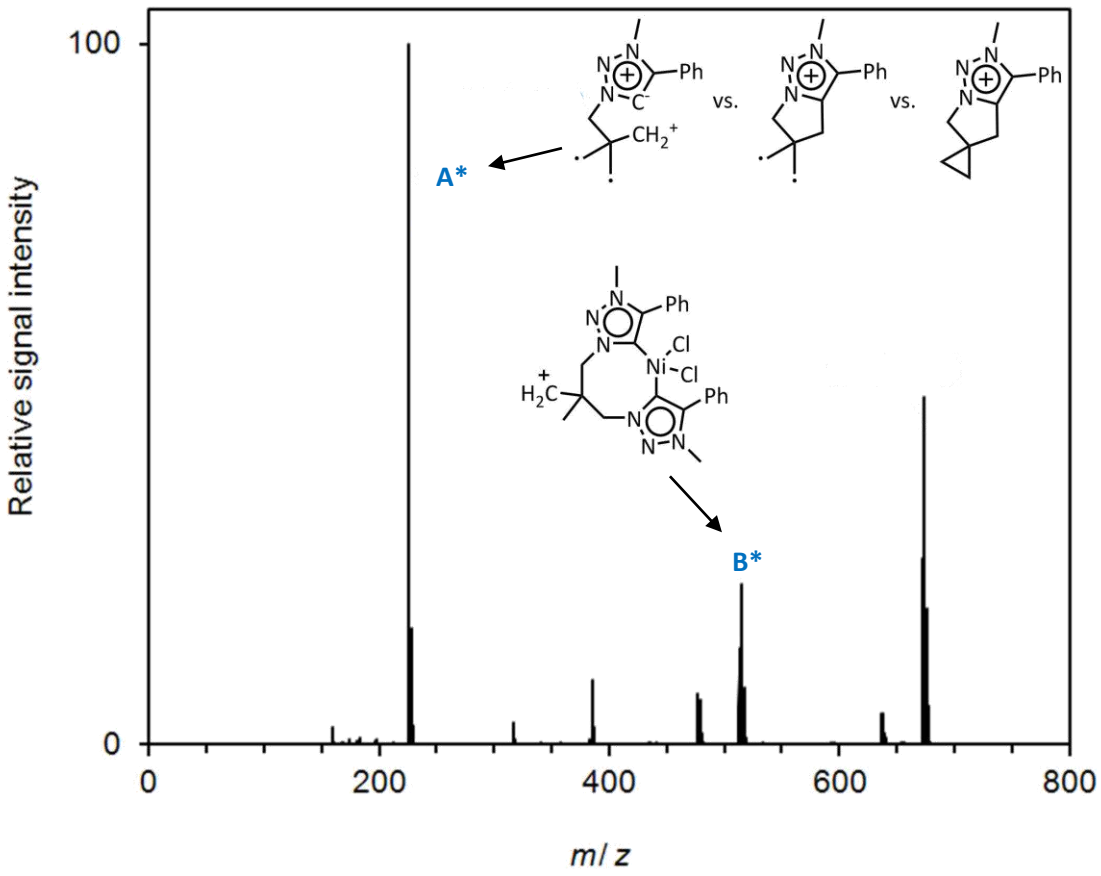

Figure 2.4.27: Mass spectrum of mass-selected peak B (*m/z* 674.170, $C_{32}H_{34}Cl_2N_9Ni^+$) in Figure 2.4.24 of the nickel complex 33 and its fragment ions produced upon collision-induced dissociation with E_{LAB} = 20 eV. Including proposed structures for A* (*m/z* 226.143, $C_{14}H_{16}N_3^+$) and B* (*m/z* 515.075, $C_{23}H_{25}Cl_2N_6Ni^+$).

The CID spectrum in Figure 2.4.27 shows two fragments resulting from the motherion peak at *m/z* 674.170 in Figure 2.4.24. Peak **A*** at *m/z* 226.143 corresponds to the same ligand fragments which were already presented in the spectrum for the palladium species shown in Figure 2.4.22. This further proves the presence of the ligand system which fragmentizes to small increments of the side arms for the nickel as well as the palladium species. The peak **B*** in Figure 2.4.27 with *m/z* 515.075 corresponds to parts of the ligand system which is still connected to the metal atom. With the help of peak pattern simulation, the sum formula for this peak and therefore the presence of the metal could be confirmed. With the data gained by the TOF mass spectrometry and CID experiment there is strong evidence for the proposed structure for the nickel compound shown in Figure 2.4.28.

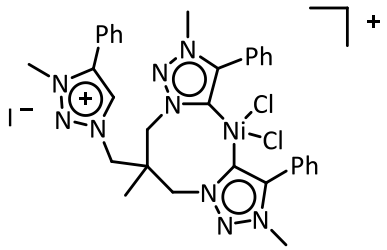

Figure 2.4.28: Monometallic nickel complex 33 formed during synthesis with a bidentante coordination pattern and one free side arm.

With the help of TOF mass spectrometry in combination with CID experiments it was possible to determine two new unprecedented complexes **32** and **33** with novel binding motifs for the triazolic ligand system **24**. Both complexes bind to their metal atoms in a bidentate fashion leaving the third ligand arm either unsubstituted or coordinated to a second metal atom. These findings show the versatility of the employed ligand system to accommodate different metal atoms and their coordinative demands.

In the case of the palladium complex **32** two ligand arms bind to the $PdCl_2$ substrate in a bidentate fashion. Interestingly with the third arm still coordinated to a second metal this opens up the possibility to generate bimetallic complexes where one metal atom is coordinated in a bidentante fashion and a different second metal can be coordinated to the third ligand arm by a transmetalation reaction. Furthermore, the coordination showed that the phenyl rings in close proximity are not hindering the metal coordination reaction presumably by rotation around the connecting C - C bond to a least steric hindered orientation.

The second ligand system with a nickel atom **33** shows the same coordination fashion but in here the third ligand arm did not react with the metal salt even though a similar coordination with the $NiCl_2$ substrate is deemed possible. One could assume that the deprotonation reaction with silver oxide did not occur on all three triazolic rings of the ligand system. However, the results in the previous chapter 2.4.3 showed that this reaction pathway with the ligand system is in fact able to convert all three ligand arms to the mesoionic carbene while coordination of silver takes place. Therefore, it is presumed that a protonation reaction takes place during or after the successful transmetalation reaction with the nickel substrate. To fully understand the coordination behavior shown in here additional experiments are deemed necessary and with the help of TOF mass spectrometry an identification of the formed intermediates might be possible to gain a deeper understanding of the reaction pathway.

SUMMARY AND OUTLOOK

A wide range of new and different classes of tripodal ligand systems were synthesized and characterized during this work. Their distinct behavior during metal coordination reactions could be examined with various metals with different properties leading to multiple new and interesting binding motifs.

3.1 Iminophosphorane Ligand Systems in Metal Coordination

Starting with the class of iminophosphoranes it was possible to synthesize two systems from the staring material, the organoazide **1,** via the STAUDINGER reaction. The resulting iminophosphoranes **2** and **3** differ by their employed substituents at the nitrogen atoms of the three ligand arms. With the iminophosphorane **2** bearing PPh_3 substituents a more steric demanding system could be synthesized while iminophosphorane **3** employs $PPhMe_2$ substituents leading to a lower steric demand of the whole ligand system. Both compounds have been subjected to metal coordination reactions with multiple main- and transition metals in order to pinpoint the influence of the employed substituents as well as to get a deeper understanding of the coordinative properties of these ligand systems. During this examination it was possible to isolate a new metal complex for each of the employed iminophosphoranes, one with a central germanium atom (**5**) and additionally a metal complex with a central zinc atom (**6**). With these complexes and in combination with the previous work done in the STALKE[77,101] group it was possible to determine the limits of the ligand systems in which a metal coordination can occur as well as the influence of the substituents towards the resulting binding motif with a metal atom. A higher steric demand of the substituents leads to the coordination of a single metal atom in a tridentate fashion while a reduction of steric demand leads to the formation of metal complexes where a central metal atom which is also able to coordinate to an additional substrate. Symmetry observations could also be made with the solid state structures of these complexes leading to the discovery that these iminophosphorane ligand system are well suited to transfer their own C_3 symmetry of the alkyl backbone to the formed metal complexes. This can lead to an improved behavior of the metal complexes within subsequent catalytic reactions. The ligand systems and structures of the synthesized metal complexes are shown in

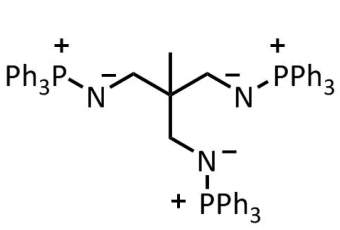

2

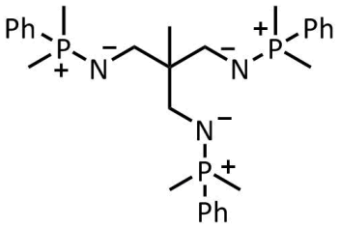

3

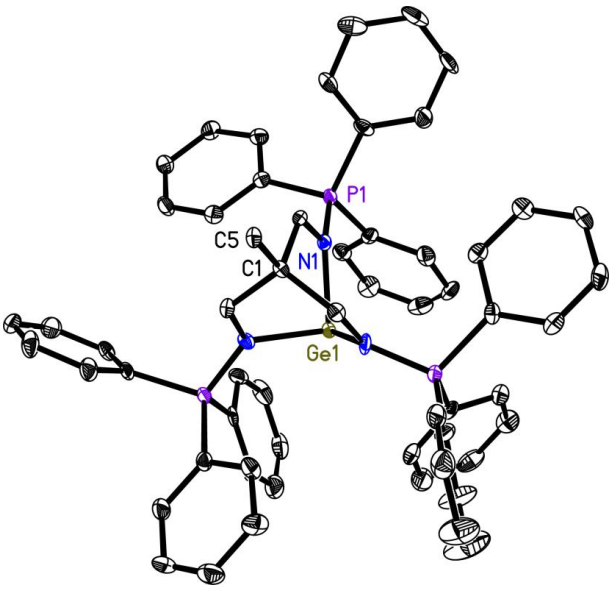

5

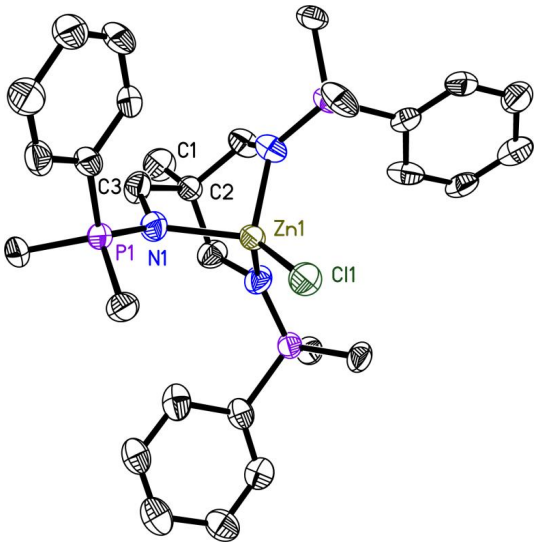

6

Figure 3.1.1: Iminophosphorane ligand systems 2 and 3 as well as the resulting metal complexes 5 and 6 discussed in chapter 2.1.

For the iminophosphorane ligand systems and complexes future work should be focused around the catalytic properties of the resulting metal complexes. The metal complex **5** is of special interest in here since it employs a metal atom which can readily interact with a proper substrate and also the overall structure shows C_3 symmetric properties. It would be of great interest to determine the influence of the symmetry in catalytic reaction pathways. In addition, most of the reactions with these ligand systems ended in the formation of a white insoluble powder it would be of advantage to optimize the reaction pathway or improve the ligand systems in order to prevent this behavior and broaden the scope of such kind of ligands.

3.2 Triazolic Ligand Systems - Synthesis, Functionalization and Metal Coordination

On the basis of the experiences with the iminophosphorane ligand systems further functionalization to the alkyl backbone was performed. The tripodal alkyl backbone derived from the organoazide **1** proved to be a valuable structural building block to synthesize tripodal triazolic ligand systems. With the introduction of 1,2,3-triazole rings to each arm of the organoazide **1** by employing classic click-chemistry it was possible to synthesize and characterize eight triazolic ligand systems **7** to **14** with five of those system previously unknown (**7**, **10**, **11**, **13**, **14**). These ligand systems are shown in Figure 3.2.1.

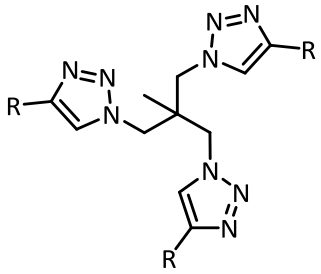

R = none (**7**), *n*Pr (**8**), *cy*Pr (**9**), *i*Pr (**10**), *t*Bu (**11**), Ph (**12**), Mes (**13**), FeCp (**14**)

Figure 3.2.1: Tripodal triazolic ligand systems discussed in chapter 2.2.

The used catalyzed click-chemistry reaction could be improved upon by changes in catalyst loadings, reaction times and conditions. Furthermore, in a cooperation with REICHMANN[99] a new carbene based copper catalyst could be identified which lead to a further optimization of the reaction and the resulting yields of the target compounds. It was also possible to crystalize some of these ligand systems and determine their solid state structure with an X-ray diffraction experiment giving further insight into the structure of these compounds. All ligand systems differ in their respective substituent at the triazolic rings varying from small less steric demanding substituents to bulkier substituents. With this selection of different ligand systems subsequent metal coordination reactions were made possible in order to get a further understanding of the influence of these substituents during coordination reactions.

Additionally, it was deemed necessary to try and further functionalize the triazolic ligand systems with an additional coordination site at the ligand backbone. The previously mentioned ligand systems **7** - **14** offer three possible coordination sites with one at each of the ligand arms. With the change of the alkyl backbone to a mesitylene ring a fourth possible coordination site could be

gained by the introduction of a π-system. To accomplish this a new organoazide **16** could be synthesized as a starting material for the buildup of the ligands. The compounds could then be synthesized by the mentioned click-chemistry approach to give rise to ligand system **17** and a second new ligand system **18** which are shown in Figure 3.2.2.

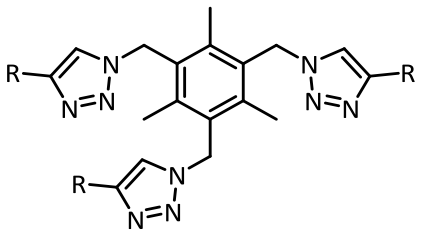

R = Ph (**17**), *n*Pr (**18**)

Figure 3.2.2: Ligand systems 17 and 18 with a bridging π-system discussed in chapter 2.3.

Unfortunately, the employed copper catalyst made the workup of these reactions very difficult lowering the yields substantially. Some side reactions could also be identified during the reaction further hindering the initial synthesis. These unexpected difficulties and the low solubility of the target compounds in common solvents lead to a termination of this part of the work and no further reactions have been carried out on these two ligand systems.

In order to prepare possible metal coordination reactions with the ligand systems **8** - **14** bearing an alkyl backbone these compounds have been subjected to a methylation reaction with methyl iodide to generate the salt form of a mesoionic carbene. By doing this a methyl group could be introduced at the N3 position of the triazolic rings leading to a decrease of the *pks* value. This opened up new reaction pathways where milder bases could be used in order to deprotonate the triazolic rings and form *in situ* the mesoionic carbene. The resulting compounds **20** - **25** are shown in Figure 3.2.3.

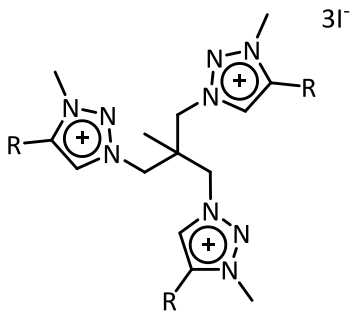

R = *n*Pr (**20**), *cy*Pr (**21**), *i*Pr (**22**), *t*Bu (**23**), Ph (**24**), $FeCp_2$ (**25**)

Figure 3.2.3: Salts of mesoionic carbenes 20 - 25 discussed in chapter 2.4.1.

The iodide anions present in the salts can influence the reactivity of the ligand systems because of their coordinating properties and their tendency to form bigger anionic clusters during later coordination reactions. Therefore two of these ligand systems **20** and **24** were subjected to an ion exchange reaction with bulky weakly-coordinating anions in order to eliminate the possible influence of the iodide anions. As weakly-coordinating anions $[BAr^{Cl}_4]^-$ and $[BAr^{F}_4]^-$ have been chosen. This lead to four new compounds **26** - **29** shown in Figure 3.2.4.

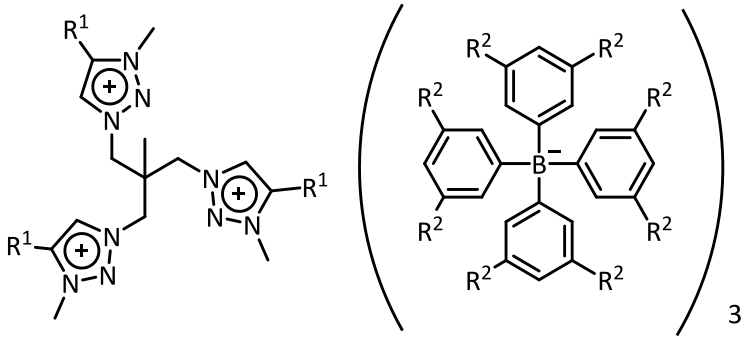

R^1 = *n*Pr; R^2 = Cl (**26**) R^1 = Ph; R^2 = Cl (**28**)
R^1 = *n*Pr; R^2 = CF_3 (**27**) R^1 = Ph; R^2 = CF_3 (**29**)

Figure 3.2.4: Salts of ligand systems (26 - 29) with weakly-coordinating anions discussed in chapter 2.4.2.

After the successful synthesis of a wide range of ligand systems with varying properties it was then tried to get an understanding of their behavior in metal coordination reactions. A proper synthetic route could be identified to transfer the previously synthesized salt forms of a mesoionic carbene with the help of silver oxide to a metal complex. Initially, by addition of silver oxide to the ligand system, a deprotonation reaction occurs forming the mesoionic carbene which then undergoes a coordination reaction with the provided silver atom. This silver-MIC complex can then react in a transmetalation reaction with an additional metal salt to form the target metal complex. With this reaction pathway two new unprecedented structures could be synthesized. One metal complex **30** with a dimeric binding motif where two ligand systems are bridged by gold atoms on each of the ligand arms and also another complex **31** with a monomeric binding motif consisting of a ligand system where each arm is coordinated to a CuBr moiety. Additionally the copper complex **31** possesses interesting structural properties. The reaction pathway leading to the formation of these complexes could be optimized and a better understanding of the variables involved to selectively form either a monomeric or dimeric complex could be gained. These complexes are shown in Figure 3.2.5.

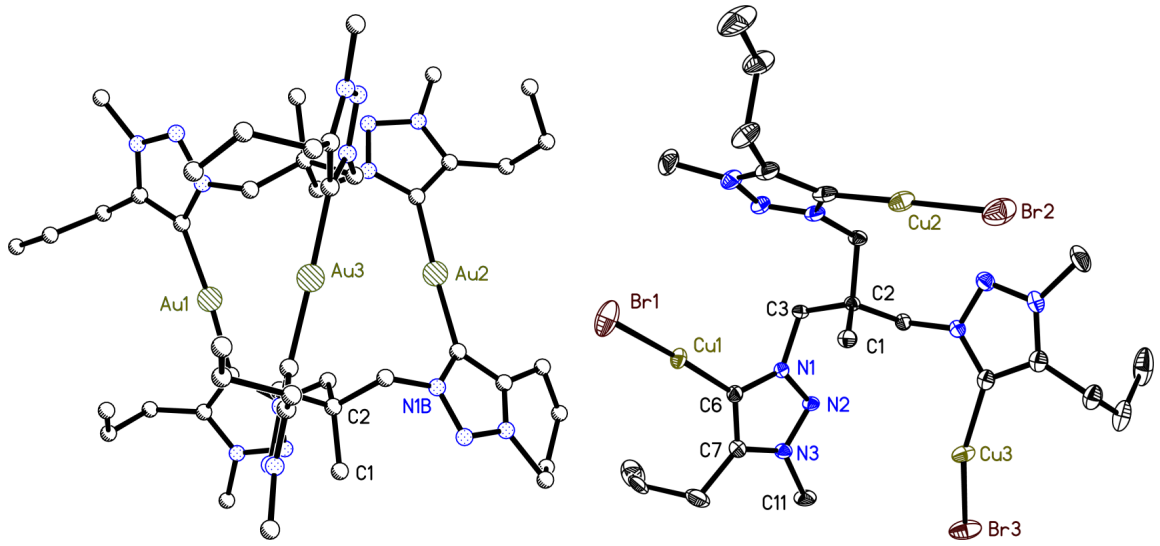

30 **31**

Figure 3.2.5: Metal complex 30 with a dimeric binding motif and bridging gold atoms and copper complex 31 discussed in chapter 2.4.3.

Additional metal coordination reactions were carried out with the catalytic relevant metal atoms palladium and nickel. Following the same reaction pathway consisting of a deprotonation/metal coordination step with silver oxide and subsequent transmetalation with a metal salt lead to two new complexes with novel binding motifs. The palladium complex 32 shows a bidentante binding motif with two of the ligand arms while the third arm bears an additional palladium metal. A comparable binding motif could be found for the nickel complex 33 where two ligand arms bind to the metal in a bidentate fashion while the third remaining arm stayed unreacted. The proposed structures are shown in Figure 3.2.6.

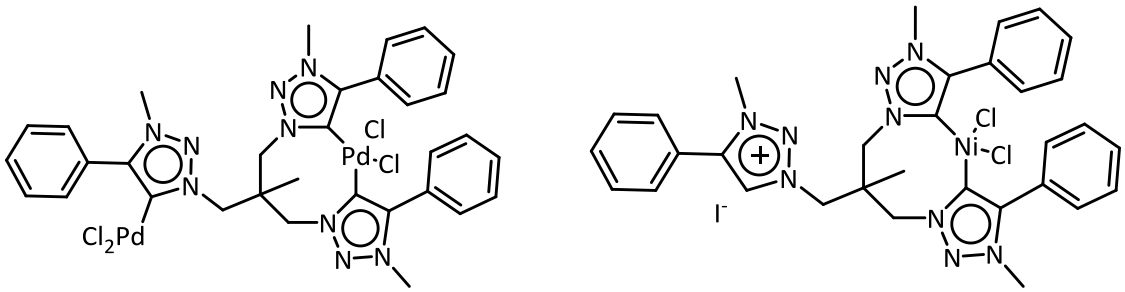

32 **33**

Figure 3.2.6: Synthesized metal complexes 32 and 33 with coordinated palladium or nickel atoms discussed in chapter 2.4.4.

With the two metal complexes **32** and **33** it was not possible to get crystals suitable for X-ray diffraction experiments and instead the structure was determined with the help of high resolution TOF mass spectrometry coupled with CID experiments.

Additional work on the topic of the tripodal triazolic ligand systems should focus around further functionalization of the employed ligand systems. One of the draw backs of the bulkier ligand systems and resulting metal complexes is their low solubility in common solvents making it more difficult to properly analyze these compounds therefore it is deemed necessary to introduce more polar groups to parts of the ligand system in order to help with the solubility in polar solvents. An increase of solubility would also lead to a better reactivity in subsequent reactions. The introduction of an additional coordination site at the connecting backbone of the ligand system is expected to lead to new binding motifs opening up the possibilities to coordinate additional main-group and transition metal atoms for example in a true tripodal binding motif after metal coordination. Further work might also center around the deprotonation and metal coordination reaction when transferring the salts to their mesoionic counterparts. Studies on the formation and type of silver complex which is formed during this synthetic step could lead to a better understanding of the properties of the ligand system in metal coordination. With this in mind a better projection into the type and binding motif of the complexes formed in subsequent transmetalation reactions can be made. The copper-MIC complex **31** is also of special interest. Additional spectroscopic experiments and theoretical considerations are needed to truly classify the nature of the Cu – Cu bond which is formed between the complex and a symmetry generated counterpart in the structure.
These proposed adaptations should lead to a further improvement of the ligand systems whereas the results presented in this work already show the huge potential for C_3 symmetric tripodal ligand systems and their metal complexes.

EXPERIMENTAL SECTION

4.1 General Procedures

All reactions with hydrolyze – or air-sensitive compounds were carried out under strict exclusion of air and moisture using modified SCHLENK-techniques in a dry and purified nitrogen or argon atmosphere, or in an argon dry box. All employed glass ware has been dried and heated in an oven at 142 °C for at least 12 h prior to use and have been put together under vacuum while still being hot. The used solvents were dried using standard laboratory procedures and were freshly distilled and stored over 3 Å molecular sieves prior to use (Et_2O, *n*-pentane from sodium/potassium alloy; THF from potassium; *n*-hexane, toluene from sodium; DCM from phosphorous pentoxide). All commercially available reactants were used as is or have been synthesized according to the given literature procedures.

4.2 Analytical Methods

4.2.1 Mass Spectrometry

M Mass spectrometry has been carried out either by the work group of PROF. DR. KOSZINOWSKI[150] or by the *Central Analytical Unit of the Institute of Organic and Biomolecular chemistry* at the Georg-August-University, Göttingen. EI spectrum were recorded using a MAT 95 device with electron ionization (EI-MS: 70 eV). High resolution ESI spectrum were recorded either with a BRUKER DALTRONICS micrOTOF-Q II or a maXis ESI-QTOF-MS. The peaks are given as a mass to charge ratio *m/z* of the fragment ions, based on the molecular mass of the isotopes with the highest natural abundance. (^{1}H, ^{12}C, ^{14}N, ^{28}Si, ^{35}Cl, $^{79/81}Br$, ^{127}I).

High resolution time of flight (TOF) mass spectrometry was carried out by SCHNEGELSBERG in the work group of PROF. DR. KOSZINOWSK. A solution of the sample was transferred into a gas-tight syringe and into the ESI source of a BRUKER microTOF-Q II mass spectrometer. The ESI source was operated at 3500 V with nitrogen dry gas and nebulizer gas. The Ions were passed through two ion funnels, a quadrupole mass filter and a quadrupole collision cell before entering the time of flight (TOF) mass analyzer of the instrument. For the detection of the ions of the recorded *m/z* range, a radio frequency of a peak-to-peak amplitude of 650 V was applied to the quadrupole collision cell. In gas-phase fragmentation

experiments performed with the HCT instrument, the mass-selected ions were accelerated by subjecting them to excitation voltages with amplitudes of V_{exc} before they were allowed to collide with the helium gas in the ion trap. Calculations of the theoretical *m/z* ratios and simulations of the isotope patterns were carried out with the COMPASS SOFTWARE PACKAGE by BRUKER DALTONIK.

4.2.2 NMR Spectroscopy

NMR spectrums were recorded at room temperature on either a BRUKER Avance III 300, Avance III 400, or a Avance 500 NMR spectrometer. Measurements were carried out at room temperature with 5-10% solutions of deuterated solvents. The chemical shifts δ are given in ppm, relative to the residual proton signal of the deuterated solvent. The coupling constant ***J*** is reported in Hz and abbreviations for multiplicity are used as follows: s = singlet, d = doublet, t = triplet, m = multiplet, br =broad and their combinations dd = doublet of doublets .[151] Tetramethylsilane was used as an external standard for ^{1}H and ^{13}C spectrums, while the residual proton signal of the deuterated solvent was used as internal standard. Corresponding shift assignment were audited by 2D correlation spectrums (HSQC, HMBC, COSY).

4.2.3 Elemental Analysis

Elemental analysis has been measured by a VARIO EL III device with combustion analysis by the *Analytical Laboratory of Institute of Inorganic Chemistry* at the Georg-August-University, Göttingen.

4.3 Synthesis and Characterization

4.3.1 Synthesis of 1,1,1-tris(azidomethyl)ethane (1)

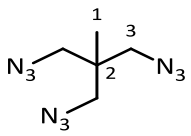

Sodium azide (15.0 g, 231 mmol, 9.00 eq.) was added to a solution of 1,1,1-tris[(4-tolysulfonyl)methyl]ethane (15.0 g, 25.7 mmol, 1.00 eq.) in DMSO (250 mL) at room temperature. The solution was stirred for 24 h at 120 °C. It was cooled to room temperature and the reaction mixture was poured in cold water. The aqueous solution was extracted with diethyl ether (3 x 200 mL) and the combined organic phases were washed with water (2 x 100 mL), dried over $MgSO_4$ and concentrated under reduced pressure.

sum formulae: $C_5H_9N_9$
molecular weight: 195.19 g/mol
Yield: 4.81 g (24.6 mmol, 96%)

^{1}H NMR (300 MHz, $CDCl_3$): δ [ppm] = 3.25 (s, 6H, CH_2), 0.97 (s, 3H, CH_3).

^{13}C NMR (75 MHz, $CDCl_3$): δ [ppm] = 55.58 (C3), 40.64 (C2), 18.90 (C1).

4.3.2 Synthesis of $MeC(Ph_3PNCH_2)_3$ (2)

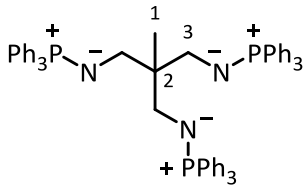

Synthesis was done by an adopted pathway published by BEAUFORT *et al*.[76] and KRATZERT[78].

To triphenylphosphane (26.3 g, 100 mmol, 3.20 eq.) dissolved in toluene (150 ml) a solution of 1,1,1-tris(azidomethyl)ethane **1** (6.13 g, 31.4 mmol, 1.00 eq.) dissolved in cold toluene (50 mL) was added over a time span of 45 min. Upon addition of the organoazide a gas emission occurred and was released through a cannula and an overpressure valve. The reaction solution was stirred for 1.5 h at room temperature and additionally for 12 h at 60 °C. The solvent was removed *in vacuo* and the colorless substituent was washed with pentane and filtered (P4). The target compound could be isolated as a white solid.

sum formulae: $C_{59}H_{54}N_3P_3$
molecular weight: 898.02 g/mol
Yield: 35.8 g, (36.8 mmol, quant.)

^{1}H-NMR (300 MHz, D_8-toluene): δ [ppm] = 1.59 (s, 3H, CH_3), 3.77 (d, J = 11.0 Hz, 6H, CH_2), 6.75-7.30 (m, 10H, Ph-*H*), 7.53-8.10 (m, 5H, Ph-*H*).

^{13}C-NMR (75 MHz, D_8-toluene): δ [ppm] = 120.14-132.50 (Ph), 45.86 (C3), 40.70 (C2), 15.45 (C1).

^{31}P-NMR (121 MHz, D_8-toluene) δ [ppm] = -0.44.

4.3.3 Synthesis of $MeC(PhMe_2PNCH_2)_3$ (3)

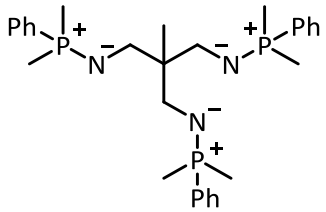

Dimethylphenylphosphane (12.6 g, 91.4 mmol, 3.10 eq.) was dissolved in Et_2O (100 mL) and cooled down to -10 °C. Over a period of 30 min 1,1,1-tris(azidomethyl)ethane (**1**) (5.75 g, 29.5 mmol, 1.00 eq.) has been added. The reaction was stirred for 1 h and the solvent was then removed *in vacuo* to give a pale yellow oil. Because of the rapid decomposition during isolation the target compound was used directly after synthesis.

Empirical formula: $C_{29}H_{42}N_3P_3$
Molecular weight: 525.60 g/mol
Yield: 15.4 g (29.4 mmol, 99%)

^{1}H-NMR (300 MHz, $CDCl_3$): δ [ppm] = 0.76 (s, 3H, *CH_3*), 1.57 (m, 24H, P-CH_3, CH_2), 7.43-7.80 (m, 15H, *Ph*).

4.3.4 Synthesis of [Ge{(Ph$_3$PNCH$_2$)$_3$CMe}] (5)

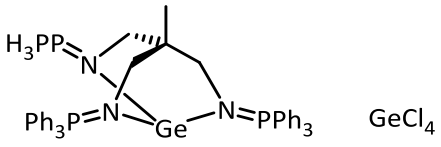

$GeCl_2$·Dioxan (44.0 mg, 1.90 mmol, 1.00 eq.) has been treated with a solution of **2** (18.8 mL, 152 µM in toluene, 1.90 mmol, 1.00 eq.) the suspension was stirred for one day at room temperature and DCM (20.0 mL) was added and the reaction mixture was stirred for additional one day. Storage at 0 °C for seven days afforded crystals suitable for X-ray diffraction. Because of the low solubility in organic solvents no further analytical data could be determined.

4.3.5 Synthesis of [ZnCl{(PhMe$_2$PNCH$_2$)$_3$CMe}]Cl (6)

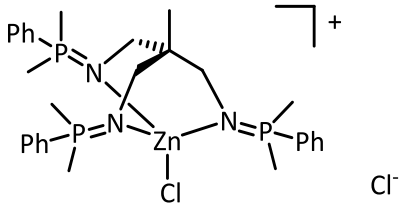

To a solution of $ZnCl_2$·Dioxane (430 µg, 1.90 mmol, 1.00 eq.) in THF (11.0 mL) was added the ligand system **3** dissolved in THF (11.0 mL, 172 µM in THF, 1.90 mmol, 1.00 eq.). The reaction was stirred for two days at room temperature. Storage at 0 °C for three days afforded crystals suitable for X-ray diffraction. Because of the low solubility in organic solvents no further analytical data could be determined.

Empirical formula: $C_{29}H_{42}N_3P_3$
Molecular weight: 525.60 g/mol

4.3.6 Synthesis of $MeC\{CH_2(N_3C_2H_2)\}_3$ (7)

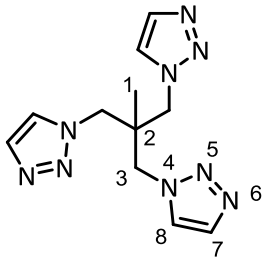

To a solution of 1,1,1-tris(azidomethyl)ethane (**1**) (1.50 g, 7.69 mmol, 1.00 eq.) in acetonitrile (60.0 mL) was added calcium carbide (1.72 g, 26.9 mmol, 3.50 eq.), copper(I)iodide (300 mg, 1.54 mmol, 0.20 eq.), sodium ascorbate (300 mg, 1.54 mmol, 0.20 eq.) and H_2O (30.0 mL). The mixture was stirred for seven days at room temperature and brought to *pH* = 5 with conc. HCl (2.00 mL). The reaction mixture was washed with EtOAc (3 x 30.0 mL) and the combined organic phases were washed with saturated NaCl solution (3 x 30.0 mL) and dried over $MgSO_4$. The resulting yellow solution was recrystallized from Pentane (300 mL) and excess solvent was removed *in vacuo* to give a yellow oil.

Empirical formula: $C_{11}H_{15}N_9$
Molecular weight: 273.30 g/mol
Yield: 1.50 g (5.48 mmol, 71%)

^{1}H-NMR (300 MHz, CD_3CN): δ [ppm] = 7.70 (d, *J* = 0.8 Hz, 3H), 4.31 (s, 6H), 3.04 (hept, 3H), 1.26 (d, *J* = 61.5, 38.6, 37.8, 13.6, 10.7, 6.9 Hz, 18H), 0.73 (s, 3H).

^{13}C-NMR (75 MHz, CD_3CN): δ [ppm] = 134.1 (C8), 127.8 (C7), 56.6 (C3), 19.4 (C1), 19.1 (C2).

ESI-MS: *m/z* = 296.3 $[M+Na]^+$**.**

4.3.7 Synthesis of $MeC\{CH_2(N_3C_2H\text{-}n\text{Pr})\}_3$ (8)

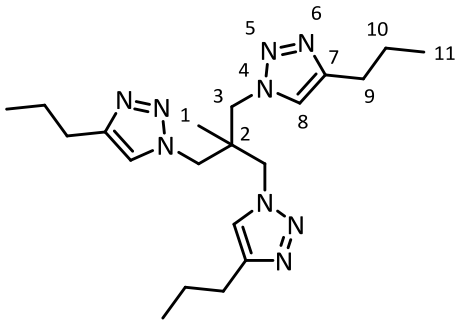

1,1,1-tris(azidomethyl)ethane (**1**) (3.00 g, 15.4 mmol, 1.00 eq.) and 1-pentin (3.14 g, 46.1 mmol, 3.00 eq.) were added to a 1:1 mixture of *t*BuOH/H_2O. Subsequently $CuSO_4 \cdot H_2O$ (510 mg, 2.03 mmol, 4.40 mol% of 1-pentin) and sodium ascorbate (1.83 g, 9.22 mmol, 20.0 mol% of 1-pentin) were added. The reaction mixture was stirred for 48 h and poured in ice water (90.0 mL) and washed with dichloromethane (3 x 30.0 mL). The organic phases were combined and excess solvent was removed *in vacuo* the crude substituent was redissolved in dichloromethane (25.0 mL) an extracted with 25% ammonia in H_2O (3 x 30.0 mL), washed with water (3 x 30.0 mL) and dried over $MgSO_4$. Excess solvent was removed *in vacuo* and the substituent was redissolved in a small amount of THF (10.0 mL) and cold pentane was added until a pure white precipitate was formed which was filtered off and dried *in vacuo*.

Empirical formula: $C_{20}H_{33}N_9$
molecular weight: 399.5 g/mol
Yield: 4.30 g (10.7 mmol, 70%)

^{1}H NMR (300 MHz, $CDCl_3$): δ [ppm] = 7.67 (d, *J* = 0.7 Hz, 3H), 4.28 (s, 6H), 2.65 (t, *J* = 7.6 Hz, 6H), 1.65 (h, 6H), 0.91 (t, *J* = 7.3 Hz, 9H), 0.72 (s, 3H).

^{13}C NMR (75 MHz, $CDCl_3$): δ [ppm] = 148.04 (C7), 123.77 (C8), 53.15 (C3), 41.60 (C9), 27.54 (C10), 22.58 (C2), 19.12 (C1), 13.75 (C11).

4.3.8 Synthesis of MeC{$CH_2(N_3C_2H$-*cy*Pr)}$_3$ (9)

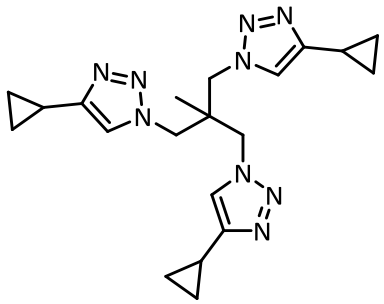

The compound was previously synthesized and completely analyzed by SCHWARZE[101] and was used as is for crystallization.

1,1,1-Tris(azidomethyl)ethane (**1**) (3.00 g, 15.4 mmol, 1.00 eq.) and cyclopropylacetylene (3.05 g, 46.11 mmol, 3.00 eq.) were added to a 1:1 mixture of *t*BuOH/H_2O (75.0 mL). Subsequently $CuSO_4 \cdot H_2O$ (190 mg, 0.77 mmol, 4.40 mol% of cyclopropylacetylene) and sodium ascorbate (610 mg, 3.08 mmol, 20.0 mol% of cyclopropylacetylene) were added. The reaction mixture was stirred for 18 h and poured in ice water (50.0 mL) and washed with dichloromethane (3 x 30.0 mL). The precipitate was washed with 25% ammonia in H_2O (3 x 50.0 mL). The water phase was extracted with DCM (4 x 50.0 mL) and the organic phases were combined washed with H_2O (100 mL) and extracted with DCM (5 x 50.0 mL). Removal of the solvent gave the product as slight yellow solid.

Empirical formula: $C_{20}H_{33}N_9$
molecular weight: 399.5 g/mol
Yield: 5.20 g (13.2 mmol, 86%)

4.3.9 Synthesis of $MeC\{CH_2(N_3C_2H\text{-}iPr)\}_3$ (10)

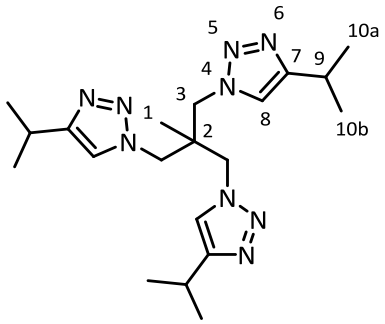

To a solution of 1,1,1-tris(azidomethyl)ethane (**1**) (2.39 g, 12.2 mmol, 1.00 eq) and 3-methyl-1-butin (3.75 mL, 36.7 mmol, 3.00 eq) in a 1:1 mixture of *t*BuOH/H_2O (64.0 mL) was added $CuSO_4 \cdot H_2O$ (180 mg, 730 µmol, 2.00 mol% of 3-methyl-1-butin) and sodium ascorbate (730 mg, 3.67 mmol, 10.0 mol% of 3-methyl-1-butin). The reaction mixture was stirred for 72 h excess solvent was removed *in vacuo* and ice water (100 mL) was added to the crude product. The solution was extracted with dichloromethane (3 x 100 mL), the organic phases were combined and extracted with 25% ammonia solution in H_2O (4 x 150 mL) and the ammonia/water phase was extracted with dichloromethane (2 x 100 mL). The organic phases were combined and washed with water (2 x 100 mL) and brine (100 mL) and dried over $MgSO_4$. Excess solvent was removed *in vacuo* and the substituent was redissolved in a small amount of dichloromethane. An excess of cold pentane was added until a white precipitate was formed. The precipitate was filtered of to give the pure white product.

Empirical formula: $C_{20}H_{33}N_9$
Molecular weight: 399.29 g/mol
Yield: 2.68 g (6.70 mmol, 55%)

^{1}H-NMR (300 MHz, $CDCl_3$): δ [ppm] = 7.73 (s, 3H, H8), 4.34 (s, 6H, H3), 3.06 (hpt, *J* = 6.9 Hz, 3H, H9), 1.29 (d, *J* = 6.9 Hz, 18 H, H10a, H10b), 0.76 (s, 3 H, 1-H).

^{13}C-NMR (300 MHz, $CDCl_3$): δ [ppm] = 154.5 (C7), 122.6 (C8), 53.2 (C3), 41.8 (C9), 26.0 (C2), 22.2 (C10a, C10b), 19.3 (C1).

EI-MS: *m/z* = 400.4 $[M+H]^+$, 422.4 $[M+Na]^+$, 99.8 $[2M+H]^+$, 1199.1 $[3M+H]^+$.

elemental analysis (*calc*): C: 59.28 (60.12), H: 8.54 (8.33), N: 30.78 (31.55).

4.3.10 Synthesis of MeC{$CH_2(N_3C_2H$-*t*Bu)}$_3$ (11)

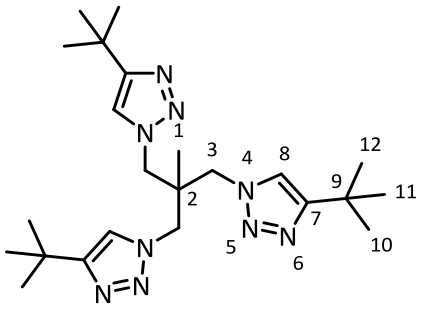

3,3-Dimethyl-1-butyne (2.00 g, 24.5 mmol, 3.00 eq.) was added to a solution of 1,1,1-tris(azidomethyl)ethane (**1**) (1.58 g, 8.12 mmol, 1.00 eq.) in a 1:1 mixture of *t*BuOH/H_2O. $CuSO_4 \cdot 5H_2O$ (260 mg, 1.07 mmol, 4.4 mol%) and sodium ascorbate (960 mg, 4.87 mmol, 20.0 mol%) were then added to the reaction mixture and stirred for 2 h at room temperature. The reaction was poured onto ice water (100 mL) and extracted with DCM (3 x 100 mL). The organic phase was washed with ammonia (25% in H_2O, 4 x 150 mL), brine was added and the water phase was re-extracted with DCM (2 x 100 mL). The organic phases have been combined and dried over $MgSO_4$. The solvent was removed to small amount and cold pentane was added (150 mL) to precipitate the white product.

Empirical formula: $C_{23}H_{39}N_9$
Molecular weight: 441.63 g/mol
Yield: 2.53 g (5.70 mmol, 70%)

^{1}H-NMR (3000 MHz, CD_2Cl_2): δ [ppm] = 7.62 (s, 3H, H8), 4.27 (s, 6H, H3), 1.27 (s, 18H, H10, H11, H12), 0.70 (s, 3 H, H1).

^{13}C-NMR (75 MHz, $CDCl_3$): δ [ppm] = 157.6 (C7), 121.9 (C8), 53.2 (C3), 41.7 (C9) 30.5 (C10, C11, C12), 31.0 (C2), 22.2 (C10a, C10b), 19.4 (C1).

4.3.11 Synthesis of $MeC\{CH_2(N_3C_2H\text{-}Ph)\}_3$ (12)

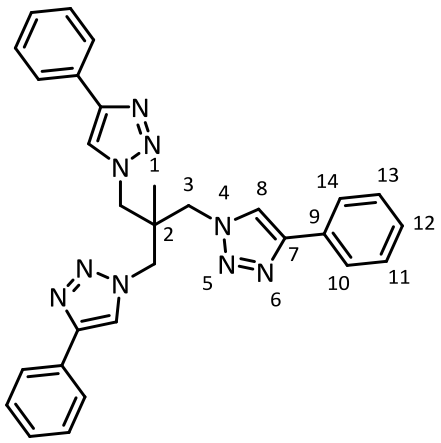

1,1,1-Tris(azidomethyl)ethane (**1**) (1.51 g, 7.72 mmol, 1.00 eq.) was dissolved with phenylacetylene (2.60 mL, 23.7 mmol, 3.00 eq.) and sodium ascorbate (912 mg, 4.60 mmol, 20.0 mol%) in a 1:1 mixture of *t*BuOH/H_2O (80.0 mL). $CuSO_4 \cdot 5\ H_2O$ (250 mg, 1.00 mmol, 4.40 mol%) was added and the reaction was stirred for six days at room temperature. The solvent was removed *in vacuo* and the substituent was dissolved in DCM (40.0 mL) und washed with ammonia (25% in H_2O, 6 x 100 mL). The water phases have been combined and were extracted with DCM (2 x 100 mL), washed with water (2 x 100 mL) and brine. The organic solvent was reduced and cold pentane was added to precipitate the product which was filtered of as a yellow solid.

Empirical formula: $C_{29}H_{27}N_9$
Molecular weight: 501.60 g/mol
Yield: 3.69 g (7.30 mmol, 95%)

^{1}H-NMR (300.13 MHz, $CDCl_3$): δ [ppm] = 8.38 (s, 3 H, H8), 7.88 (d, 6 H, Phenyl-H), 7.42 (m, 9 H, Phenyl-H), 4.56 (s, 6 H, H3), 0.98 (s, 3 H, H1).

^{13}C-NMR (75 MHz, $CDCl_3$): δ [ppm] = 147.9 (C7), 130.1 (C-Ph), 129.1 (C-Ph), 128.7 (C-Ph), 125.9 (C-Ph), 122.8 (C8), 53.48 (C3), 42.03 (C2), 19.39 (C1).

4.3.12 Synthesis of $MeC\{CH_2(N_3C_2H\text{-}MES)\}_3$ (13)

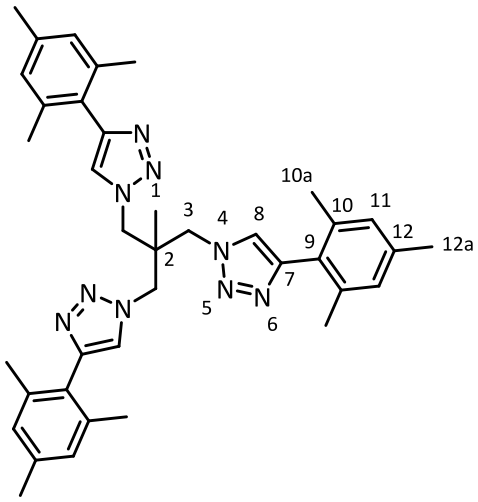

Mesitylacetylene (1.00 g, 6.93 mmol, 3.00 eq.) and 1,1,1-tris(azidomethyl)ethane (**1**) (450 mg, 2.31 mmol, 1.00 eq.) were dissolved in a 1:1 mixture of *t*BuOH/H_2O (32.0 mL) and sodium ascorbate was added (14 mg, 69 µmol, 10.0 mol %). Afterwards $CuSO_4 \cdot 5H_2O$ (4.00 mg, 140 µmol, 2.00 mol %) was added and the reaction solution was stirred for 72 h at room temperature. The reaction was poured onto ice water and extracted with DCM (3 x 30.0 mL). The organic phase was washed with ammonia (25% in H_2O, 3 x 30.0 mL, 1 x 20.0 mL), brine was added and the water phase was extracted with DCM (2 x 20 mL). The organic phases have been combined and dried over $MgSO_4$, removal of the solvent gave the target compound as slightly yellow solid.

Empirical formula: $C_{38}H_{45}N_9$
Molecular weight: 627.38 g/mol

^{1}H-NMR (300 MHz, $CDCl_3$): δ [ppm] = 8.00 (s, 3 H, H8), 6.95 (s, 6 H, H11), 4.60 (s, 6 H, H3), 2.32 (s, 9 H, H12a), 2.12 (s, 18 H, H10a, H14a), 0.90 (s, 9 H, H1).

^{13}C-NMR (75 MHz, $CDCl_3$): δ [ppm] = 154.5 (C7), 122.6 (C8), 53.2 (C3), 41.8 (C2), 26.0 (C9), 22.2 (C10a, C10b), 19.3 (C1).

ESI-MS: *m/z* = 628.4 $[M+H]^+$.

4.3.13 Synthesis of $MeC\{CH_2(N_3C_2H\text{-}FeCp_2)\}_3$ (14)

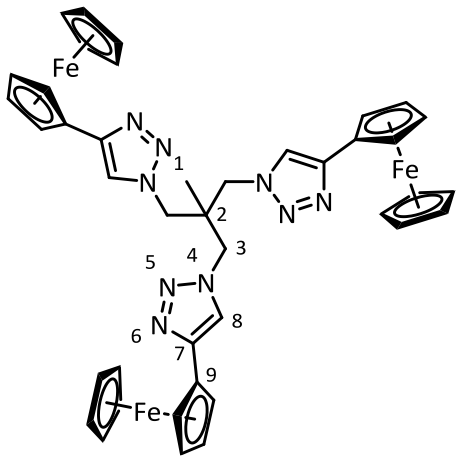

Ethinylferrocene (2.00 g, 9.50 mmol, 3.00 eq.), $CuSO_4 \cdot 5H_2O$ (25.0 mg, 950 µmol, 0.01 eq.), sodium ascorbate (18.8 mg, 950 µmol, 0.01 eq.) and benzoic acid (116 mg, 950 µmol, 0.10 eq.) were suspended in H_2O/*t*BuOH (15.0 mL, 2:1) and 1,1,1-tris(azidomethyl)ethane (**1**) (619 mg, 3.17 mmol, 1.00 eq.) was added. The reaction was stirred for 20 min at room temperature and the water phase was decanted off and extracted with DCM (50.0 mL). The substituent was suspended in DCM (150 mL) and all organic phases have been combined, washed with water (2 x 50.0 mL) and re-extracted with DCM (150 mL). Excess solvent was removed *in vacuo* to give the desired product as an orange solid. Crystallization was achieved by slow evaporation of a saturated solution in $CDCl_3$.

Empirical formula: $C_{41}H_{39}Fe_3N_9$
Molecular weight: 825.36 g/mol
Yield: 2.56 g (3.10 mmol, 98%)

^{1}H-NMR (300 MHz, $CDCl_3$): δ [ppm] = 7.93 (s, 3H, H8), 4.70 (t, *J* = 1.85 Hz, 6H, R-CpH_2), 4.38 (s, 6H, H3), 4.27 (t, *J* = 1.85 Hz, 6H, R-CpH_2), 4.02 (s, 15H, Cp*H*), 0.81 (s, 3H, H1).

MS(MALDi): *m/z* **=** 825.1 (100) $[M]^+$, 848.1 (8.62) $[NaM]^+$.
elemental analysis (*calc*): C: 58.91 (59.66), H: 4.92 (4.76), N: 14.62 (15.27).

Cyclic voltammetry was performed in an argon-atmosphere with 1.2 mg of (X) in a 0.1 M solution of $[N^nBu_4][PF_6]$. A glassy-carbon-electrode was used as counter electrode and a Pt-electrode as the working electrode. The resulting spectra were referenced against an Ag/Ag^+-electrode. Standard measurement was done with $FeCp_2$* and the resulting potential has been set to -0.012 V.[109]

4.3.14 Synthesis of $(CH_3)_3C_6(CH_2Br)_3$ (15)

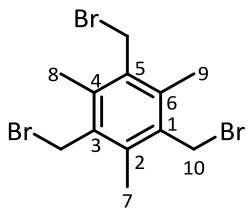

Mesitylene (3.49 mL, 3.00 g, 25.0 mmol, 1.00 eq.) was added to a solution of paraformaldehyde (3.60 g, 120 mmol, 4.80 eq.) in acetic acid. Subsequently HBr in acetic acid (33%, 20.0 mL, 110 mmol, 4.40 eq.) was added and the reaction was heated up to 120 °C and stirred for 24 h. The reaction solution was then added to 100 mL ice water and a white – yellow solid precipitated. The solid was filtered off and washed with diethyl ether (3 x 30.0 mL) and dried *in vacuo*. Recrystallization from Acetonitrile gave the product as a white-yellow solid.

Empirical formula: $C_{12}H_{15}Br_3$
Molecular weight: 398.96 g/mol
Yield: 9.37 g (23.4 mmol, 94%)

^{1}H-NMR (300 MHz, $CDCl_3$): δ [ppm] = 4.58 (s, 6H, H10), 2.47 (s, 9H,H7, H8, H9).

^{13}C-NMR (75 MHz, $CDCl_3$,: δ [ppm] = 137.89 (C2, C4, C6), 133.27 (C1, C3, C5), 29.88 (C10), 15.40 (C7, C8, C9).

EI-MS: *m/z* = 399.8 $[M+H]^+$, 318.9 $[M-Br]^+$, 238.0 $[M-2Br]^+$, 159.1 $[M-3Br]^+$.

elemental analysis (calc.): C: 35.90 (36.13), H: 3.82 (3.79).

4.3.15 Synthesis of $(CH_3)_3C_6(CH_2N_3)_3$ (16)

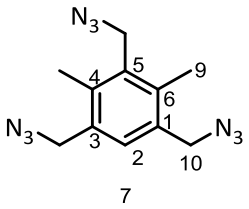

1,3,5-Tris(bromomethyl)-2,4,6-trimethylbenzene (**15**) (4.72 g, 11.8 mmol, 1.00 eq.) was added to a solution of sodium azide (4.05 g, 62.2 mmol, 5.50 eq.) in DMF (20.0 mL). The solution was stirred at 70 °C for 18 h subsequently DCM was added and stirred for another 2 h. Subsequently the solution was filtered through a pad of CELITE and left to cool to room temperature overnight. An off white solid precipitated out and half of the solvent was removed *in vacuo*. Pentane (50.0 mL) was added and the solution was stirred for 24 h, filtered, excess solvent was removed and the solid was recrystallized from DCM in the cold.

Empirical formula: $C_{12}H_{15}N_9$
Molecular weight: 285.32 g/mol
Yield: 80.0 mg (280 µmol, 3%)

^{1}H-NMR (300 MHz, CD_2Cl_2): δ [ppm] = 4.52 (s, 6H, H10), 2.46 (s, 9H, H7, H8, H9).

^{13}C-NMR (75 MHz, $CDCl_3$): δ [ppm] = 138.61 (C2, C4, C6), 131.31 (C1, C3, C5), 49.33 (C10), 16.65 (C7, C8, C9).

EI-MS: *m/z* = 285.1 $[M]^+$, 243.1 $[M\text{-}N_3]^+$, 200.1 $[M\text{-}N_3\text{-}HN_3]^+$.

elemental analysis (calc.): C: 50.71 (50.52), H: 5.38 (5.30), N: 42.26 (44.18).

4.3.16 Synthesis of $(CH_3)_3C_6(CH_2N_3C_2H\text{-}Ph)_3$ (17)

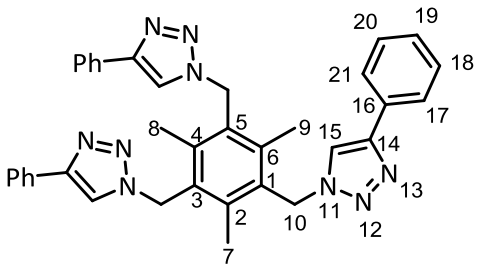

1,3,5-Tris(bromomethyl)-2,4,6-trimethylbenzene (**16**) (4.50 g, 11.3 mmol, 1.00 eq.), phenylacetylene (3.57 g, 35.0 mmol, 3.84 mL, 3.10 eq.), sodium azide (6.63 g, 102 mmol, 9.00 eq.), $CuSO_4 \cdot 5H_2O$ (1.12 g, 4.50 mmol, 0.40 eq.) and sodium ascorbate (4.04 g, 20.4 mmol, 1.80 eq.) were added to a solution of H_2O/*t*BuOH (1:1, 100 mL) and refluxed at 100 °C for 48 h. The reaction solution was diluted with H_2O/EtOAc (1:1, 100 mL) and subsequently EtOAc (100 mL) were added and the organic phase was separated from the water phase. The water phase was washed with EtOAc (3 x 30.0 mL) and the combined organic phases were washed with brine (3 x 30.0 mL), ammonia (33% in H_2O, 3 x 60.0 mL) and EtOAc (100 mL). Excess solvent was removed *in vacuo* and the resulting solid was redissolved in DMSO (300 mL) and filtered through a pad of CELITE and methanol (300 mL was added) an off white solid precipitated and was filtered off.

Empirical formula: $C_{36}H_{33}N_9$
Molecular weight: 591.72 g/mol
Yield: 3.01 g (5.09 mmol, 49%)

^{1}**H-NMR (300 MHz, DMSO-d$_6$,):** δ [ppm] = 8.32 (s, 3H, H15), 7.78 (d, *J* = 8.1 Hz, 6H, H17, H21), 7.36 (t, *J* = 14.4 Hz, 6H, H18, H20), 7.29 (t, *J* = 14.4 Hz, 3H, H19), 5.74 (s, 6H, H10) 2.46 (s, 9H, H7, H8, H9).

ESI-MS: *m/z* = 591.3 $[M]^+$, 461.2 $[M\text{-}C_8H_6N_2]^+$.

elemental analysis (calc.): C: 73.07 (70.90), H: 5.77 (5.62), N: 20.97 (21.03).

4.3.17 Synthesis of $(CH_3)_3C_6(CH_2N_3C_2H\text{-}n\text{Pr})_3$) (18)

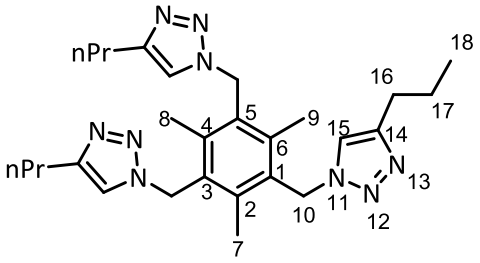

1,3,5-Tris(bromomethyl)-2,4,6-trimethylbenzene (**16**) (4.50 g, 11.3 mmol, 1.00 eq.), propylacetylene (2.38 g, 35.0 mmol, 3.46 mL, 3.10 eq.), sodium azide (6.63 g, 102 mmol, 9.00 eq.), $CuSO_4 \cdot 5H_2O$ (1.12 g, 4.50 mmol, 0.40 eq.) and sodium ascorbate (4.04 g, 20.4 mmol, 1.80 eq.) were dissolved in H_2O/DCM (1:1, 100 mL) and refluxed for 48 h at 55 °C. Excess DCM was removed *in vacuo* and EtOAC (50.0 mL) was added. The organic phase was separated from the water phase and the water phase was extracted with DCM (3 x 30.0 mL). The combined organic phases were washed with brine (50.0 mL) and ammonia (33% in H_2O, 3 x 30.0 mL). The clear organic phase was dried over $MgSO_4$, filtered and excess solvent was removed *in vacuo*. The resulting substituent was soaked up with a small amount of DCM and pentane (250 mL) was added. A white solid precipitated out which was filtered of.

Empirical formulae $C_{27}H_{39}N_9$
Molecular weight: 489.67 g/mol
Yield: 2.64 g (5.39 mmol, 48%)

^{1}H-NMR (300 MHz, CD_3CN,): δ [ppm]= 7.15 (s, 3H, H15), 5.53 (s, 6H, H10), 2.48 (t, J = 7.5 Hz, 6H, H16), 2.31 (s, 9H, H7, H9, H9), 1.51 (m, 6H, H17),0.80 (t, J = 7.4 Hz, 9H, H18).

^{13}C-NMR (75 MHz, $CDCl_3$): δ [ppm] = 148.49 (C1, C3, C5), 139.69 (C2, C4, C6), 132.02 (C14), 121.70 (C15), 46.62 (C10), 28.22 (C16), 23.44 (C17), 16.71 (C7, C8, C9), 13.93 (C18).

ESI-MS: m/z = 489.3 $[M]^+$.

4.3.18 Synthesis of $[MeC\{CH_2(N_3C_3H_4\text{-}n\text{Pr})\}_3]I_3$ (20)

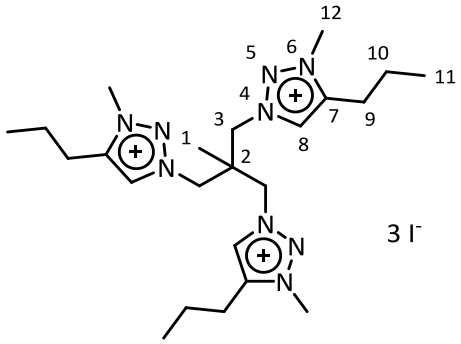

To a suspension of **8** (3.00 g, 7.51 mmol, 1.00 eq.) in acetonitrile (150 mL) methyl iodide (14.0 mL, 225 mmol, 30.0 eq.) was added under constant stirring. The mixture was heated up until reflux and stirred for 24 h at 82 °C. Excess solvent and methyl iodide was removed *in vacuo* and transferred to a washing flask with a conc. ammonia solution. The yellow substituent was redissolved in DCM, precipitated with an excess of cold pentane and filtered off. The target compound could be obtained as a yellow solid.

Empirical formula: $C_{23}H_{42}I_3N_9$
Molecular weight: 825.37 g/mol
Yield: 5.13 g (6.22 mmol, 83%)

^{1}H-NMR (300 MHz, CD_3CN): δ [ppm] = 9.12 (s, 3H, H8), 5.08 (s, 6H, H3), 4.16 (s, 9H, H12), 2.75 (t, J = 7.6 Hz , 6H, H9), 1.70 (m, 6 H, H10), 0.97 (t, J = 7.3 Hz, H11).

^{13}C-NMR (75 MHz, CD_3CN): δ [ppm] = 144.69 (C7), 130.43 (C8), 54.68 (C3), 40.83 (C9), 38.16 (C12), 24.67 (C10), 19.66 (C2), 17.24 (C1), 12.44 (C11).

4.3.19 Synthesis of $[MeC\{CH_2(N_3C_3H_4\text{-}iPr)\}_3]I_3$ (22)

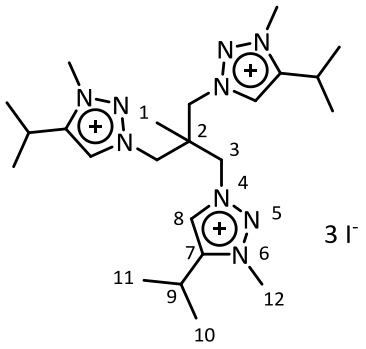

To a suspension of **10** (580 mg, 1.45 mmol, 1.00 eq.) in acetonitrile (80.0 mL) methyliodide (2.80 mL, 45.0 mmol, 31.0 eq.) was added under constant stirring. The mixture was heated up until reflux and stirred for 24 h at 82 °C. Excess solvent and methyl iodide was removed *in vacuo* and transferred to a washing flask with a conc. ammonia solution. The yellow substituent was redissolved in DCM and precipitated with an excess of cold pentane and filtered off. The target compound could be obtained as a yellow solid.

Empirical formula: $C_{23}H_{42}I_3N_9$
Molecular weight: 825.37 g/mol
Yield: 700 mg (850 µmol, 59%)

^{1}H-NMR (300 MHz, $CDCl_3$): *δ* [ppm] = 9.95 (s, 3H, H8), 7.26 (s, 3H, H9), 5.39 (s, 6H, H3), 4.39 (s, 9H, H6a), 3.20 (p, 3H, *i*Pr-*H*), 1.70 (s, 3H, H10a, H10b), 1.47 (d, 15H, H10, H11).

^{13}C-NMR (75 MHz, $CDCl_3$): *δ* [ppm] = 149.37 (C7), 129.48 (C8), 55.00 (C3), 38.38 (C12), 23.57 (C9), 20.89 (C11, C12), 17.4 (C1).

ESI-MS: *m/z* = 848.1 $[M+3I^+Na]^+$, 698.2 $[M+2I]^+$, 570.2 $[M+I]^{2+}$.

4.3.20 Synthesis of $[MeC\{CH_2(N_3C_3H_4\text{-}tBu)\}_3]I_3$ (23)

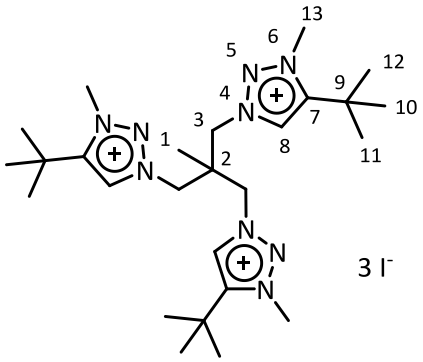

To a suspension of **11** (1.00 g, 2.27 mmol, 1.00 eq.) in acetonitrile (100 mL) methyliodide (4.23 mL, 68.0 mmol, 30.0 eq.) was added under constant stirring. The mixture was heated up until reflux and stirred for 48 h at 82 °C. Excess solvent and methyl iodide was removed *in vacuo* and transferred to a washing flask with a conc. ammonia solution. The dark yellow substituent was redissolved in DCM, precipitated with an excess of cold pentane and filtered off. The target compound could be obtained as a yellow solid.

Empirical formula: $C_{26}H_{48}I_3N_9$
Molecular weight: 867.45 g/mol

^{1}H-NMR (300 MHz, CD_3CN): δ [ppm] = 9.29 (s, 3H, H8), 5.11 (s, 3 H, H13), 4.33 (s, 6 H, H3), 1.43 (s, 18H, H10, H11, H12), 1.26 (s, 3H, H1).

^{13}C-NMR (75 MHz, CD_3CN): δ [ppm] = 151.20 (C7), 116.92 (C8), 54.58 (C3), 41.09 (C9), 30.09 (C2), 29.27 (13), 27.79 (C10, C11, C12), 17.19 (C1).

ESI-MS: *m/z* = 890.2 $[M+Na]^+$, 740.3 $[M+2I]^+$.

4.3.21 Synthesis of $[MeC\{CH_2(N_3C_3H_4\text{-}Ph)\}_3]I_3$ (24)

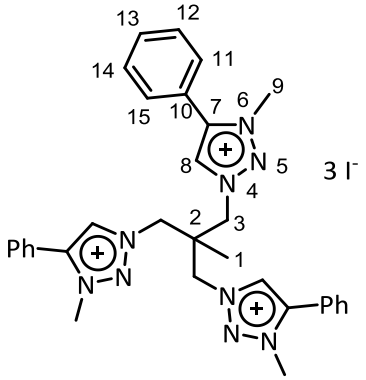

12 (2.80 g, 5.60 mmol, 1.00 eq.) was dissolved in acetonitrile (70.0 mL) and methyliodide (10.0 mL, 22.7 g, 160 mmol, 30.0 eq.) were added and the solution was refluxed at 85 °C for one week. The yellow solid was filtered of and washed with EtOAc (3 x 30.0 mL) and diethylether (3 x 30.0 mL).

Empirical formula: $C_{32}H_{36}I_3N_9$

Molecular weight: 927.42 g/mol

Yield: 3.90 g (4.20 mmol, 75%)

^{1}H-NMR (300 MHz, MeCN-d_3): δ [ppm] = 9.54 (s, 3H, H8), 7.82 (dd, 6H, H11, H15), 7.64 (m, 9H, 12H, H13, H14), 5.38 (s, 6H, H3), 4.33 (s, 9H, H9), 1.65 (s, 3H, H1).

^{13}C-NMR (75 MHz, $CDCl_3$): δ [ppm] = 143.95 (C7), 132.21 (C-Ph), 131.57 (C-Ph), 130.37 (C-Ph), 129.76 (C-Ph), 121.76 (C8), 55.89 (C3), 42.11 (C2), 18.39 (C1).

ESI-MS: *m/z* = 800.3 $[M\text{-}I^-]^+$, 336.7 $[M\text{-}I_2]^{2+}$.

elemental analysis (calc.): 39.74 (41.44), H: 4.12 (3.91), N: 13.17 (13.59).

4.3.22 Synthesis of $[MeC\{CH_2(N_3C_3H_4\text{-}FeCp_2)\}_3]I_3$ (25)

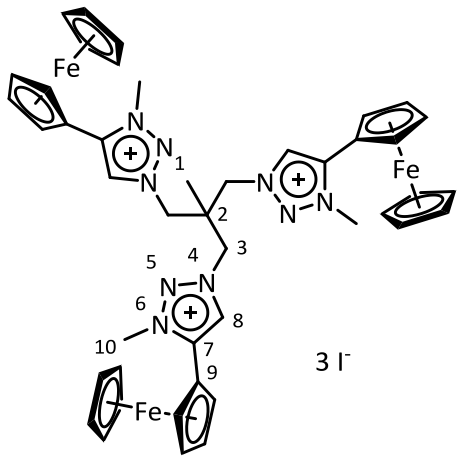

14 (2.00 g, 2.41 mmol, 1.00 eq.) was dissolved in acetonitrile (120 mL) and methyliodide (10.3 g, 4.55 mL, 72.7 mmol, 30.0 eq.) was added. The solution was stirred for four days at 85 °C. The formed yellow precipitate was filtered off and the substituent was washed with MeCN and dried *in vacuo*.

Empirical formula: $C_{44}H_{48}Fe_3I_3N_9$
Molecular weight: 1251.18 g/mol
Yield: 2.41 g (1.93 mmol, 80%)

^{1}H-NMR (300 MHz, $CDCl_3$): δ [ppm] = 10.12 (s, 3H, H8), 5.53 (s, 6H, H3), 4.86 (t, *J* = 2.01 Hz, 6H, R-CpH_2), 4.51 (t, *J* = 2.01 Hz, 6H, R-CpH_2), 4.40 (s (b), 15H, Cp*H*, 9H, H10), 1.92 (s, 3H, H1).

MS(MALDi): *m/z* = 290.1 (100) $[M - 3\ I^-]^{3+}$, 498.6 (39.5) $[M - 2\ I^-]^{2+}$.

elemental analysis (calc.): C: 36.84 (42.24), H: 3.61 (3.87), N: 9.20 (10.08).

4.3.23 Synthesis of $[MeC\{CH_2(N_3C_3H_4\text{-}iPr)\}_3][BAr^{Cl}_4]_3$ (26)

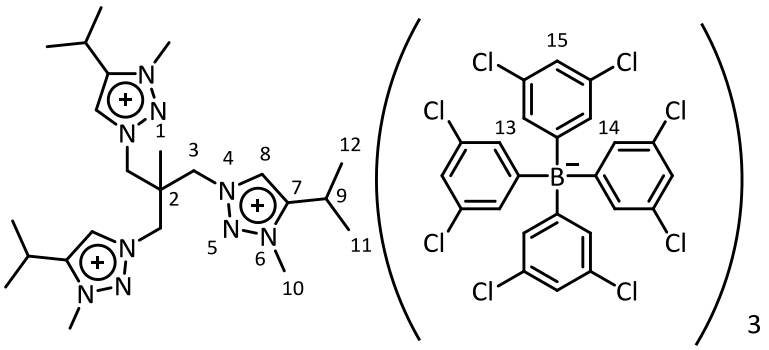

To a suspension of **22** (94.0 mg, 100 µmol, 1.00 eq.) in DCM (4.00 mL) was added a solution of with $Na[BAr^{Cl}_4]$ (284 mg, 320 µmol, 3.00 eq.) in DCM (4.00 mL). The resulting suspension was diluted with DCM (4.00 mL) and stirred for three days at room temperature. The solution was reduced *in vacuo* until a white solid precipitated. The solid was filtered off and the target compound could be obtained as a yellow solid.

Empirical formula: $C_{95}H_{78}N_9B_3Cl_{24}$
Molecular weight: 2216.92 g/mol
Yield: 481 mg (90.0 µmol, 90%)

^{1}H-NMR (300 MHz, CD_3CN): δ [ppm] = 8.24 (s, 3H, H8), 7.10 - 7.06 (m, 12H, H15), 7.03 - 6.98 (m, 24H, H13, H14), 4.64 (s, 6H, H3), 4.22 (s, 9H, H10), 3.25 (sep, *J* = 6.9 Hz, 3H, H9), 1.37 (d, *J* = 6.9 Hz, 18 H, H11, H12), 1.07 (s, 3H, H1).

^{11}B-NMR (96 MHz, CD_3CN): δ [ppm] = -7.02 (s).

ESI-MS: *m/z* = 519.6 ($C_{47}H_{54}N_9BCl_8$) $[M\text{-}(C_{24}H_{12}BCl_8)_2]^{2+}$

HR-ESI-MS *m/z* **=** 148.1185 ($C_{23}H_{42}N_9$) $[M\text{-}(C_{24}H_{12}BCl_8)_3]^{3}$; 594.8489 ($C_{24}H_{12}BCl_8$) $[M\text{-}(C_{71}H_{66}B_2Cl_{16}N_9)]^{-}$

elemental analysis (calc.): C: 49.19 (51.19), H: 3.64 (3.53), N: 5.14 (5.66).

4.3.24 Synthesis of $[MeC\{CH_2(N_3C_3H_4\text{-}iPr)\}_3][BAr^F{}_4]_3$ (27)

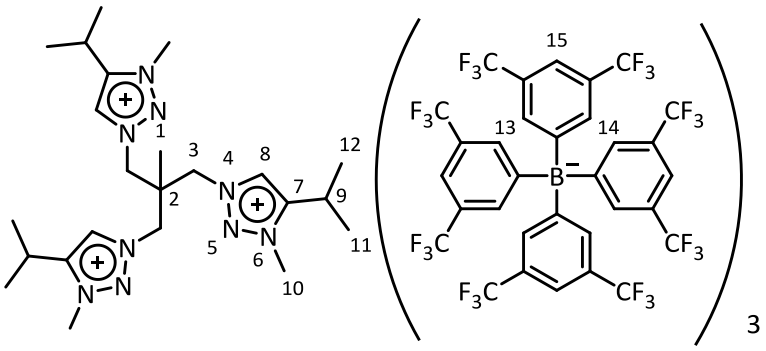

To a suspension of **22** (94.0 mg, 100 µmol, 1.00 eq.) in DCM (4.00 mL) was added a solution of with $Na[BAr^F{}_4]$ (284 mg, 320 µmol, 3.00 eq.) in DCM (4.00 mL). The resulting suspension was diluted with DCM (4.00 mL) and stirred for 3 d at room temperature. The solution was reduced in vacuo until a white solid precipitated. The solid was filtered off and the target compound could be obtained as a yellow solid.

Empirical formula: $C_{119}H_{78}N_9B_3F_{72}$
Molecular weight: 3033.55 g/mol
Yield: 289 mg (90.0 µmol, 90%)

^{1}H-NMR (300 MHz, C_3D_6O): δ [ppm] = 8.90 (s, 3 H, H8), 7.78 (m, 24 H, H13, H14), 7.67 (s, 12 H, H15), 5.35 (s, 6 H, H3), 4.70 (s, 9 H, H10), 1.57 (s, 18 H, H11, H12) 1.32 (s, 3 H, H1).

^{11}B-NMR (96 MHz, C_3D_6O): δ [ppm] = -6.566.

^{19}F-NMR (282 MHz, C_3D_6O): δ [ppm] = -63.265.

ESI-MS: *m/z* = 863.1$[B(Ph(o\text{-}CF_3)_2)_4]^+$, 143.4 $[C_2H_3(C_4H_6N_3(iPr))_3 - 5\ H]^{3+}$, 299.7 $[C_2H_3(C_4H_6N_3(iPr))_3 + C_8H_{16}N_3]^{2+}$, $[[C_2H_3(C_4H_6N_3(iPr))_3][B(Ph(o\text{-}CF_3)_2)_4] + C_3H_6]^{2+}$.

elemental analysis (calc.): C: 45.52 (47.10), H: 3.36 (2.59), N: 3.64 (4.15).

4.3.25 Synthesis of $[MeC\{CH_2(N_3C_3H_4\text{-}Ph)\}_3][BAr^{Cl}{}_4]_3$ (28)

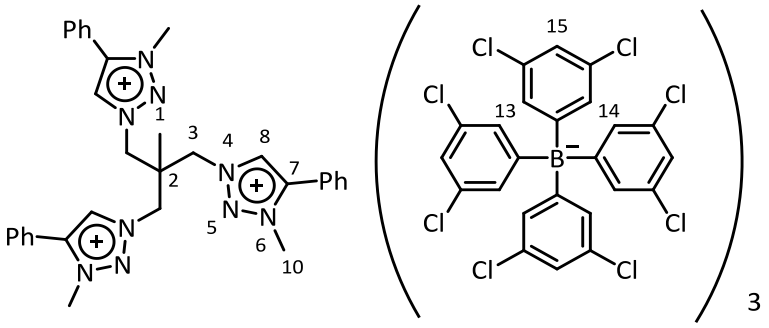

To a suspension of **24** (200 mg, 216 µmol, 1.00 eq.) in MeCN (4.00 mL) was added a solution of $Na[BAr^{Cl}{}_4]$ (400 mg, 648 µmol, 3.00 eq.) in MeCN (4.00 mL) and stirred for 48 h at room temperature. The solvent was removed *in vacuo* and DCM (8.00 mL) was added and the reaction mixture was stirred for additional 3 d. A white solid precipitated out which was filtered off, excess solvent from the solution was removed *in vacuo* to give the target compound as yellow solid.

Empirical formula: $C_{104}H_{72}B_3Cl_{24}N_9$
Molecular weight: 2331.05 g/mol
Yield: 311 mg (13 µmol, 60%)

^{1}H-NMR (300 MHz, CD_3CN): δ [ppm] = 8.76 (s, 3H, H8), 7.69 (s, 15H, Ph-H), 7.09 - 7.06 (m, 12H, H15), 7.03 - 6.98 (m, 24H, H14, H15), 4.95 (s, 6H, H3), 4.30 (s, 9H, H10), 1.36 (s, 3H, H1).

^{11}B-NMR (96 MHz, CD_2Cl_2): δ [ppm] = -6.96 (s).

HR-ESI-MS: *m/z* = 182.1029 $[M\text{-}(C_{24}H_{12}BCl_8)_3]^{3+}$, 594.8482 $[M\text{-}(C_{80}H_{60}B_2Cl_{16}N_9)]^-$, 570.5792 $[M\text{-}(C_{24}H_{12}BCl_8)_2]^{2+}$.

elemental analysis (calc.): C: 50.60 (53.59), H: 3.34 (3.11), N: 5.35 (5.41).

4.3.26 Synthesis of $[MeC\{CH_2(N_3C_3H_4\text{-}Ph)\}_3][BAr^F{}_4]_3$ (29)

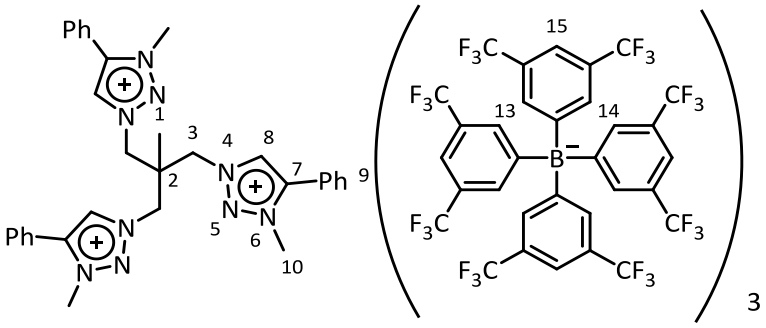

The ligand system **24** (105 mg, 113 µmol, 1.0 eq) and $NaBArF_{24}$ (300 mg, 339 µmol, 3.00 eq.) were dissolved in DCM and stirred for 3 d at room temperature. The precipitate was filtered of and excess solvent from the solution was removed *in vacuo* to give the desired product as yellow solid.

Empirical formula: $C_{128}H_{72}B_3F_{72}N_9$
Molecular weight: 3135.50 g/mol
Yield: 337 mg (110 µmol, 98%)

^{1}H-NMR (300 MHz, CD_3CN): δ [ppm] = 8.45 (s, 3H, H8), 7.78 (t, *J* = 7.2 Hz, 3H, Ph-H), 7.70 (sbr, 24H, H13, H14), 7.67 - 7.62 (m, 6H, Ph-H), 7.53 (sbr, 12H, H15), 7.42 (d, *J* = 7.2 Hz, 6H, Ph-H), 4.96 (s, 6H, H3), 4.33 (s, 9H, H10), 2.11 (s, 3H, H1).

^{11}B-NMR (96 MHz, CD2Cl2): δ [ppm] = -6.63 (s).

^{19}F-NMR (282 MHz, CD2Cl2): δ [ppm] = -62.336 (s).

HR-ESI-MS: m/z **=** 182.1030 $[M\text{-}(C_{32}H_{12}F_{24}B)_3]^{3+}$, 863.0694 $[M\text{-}(C_{96}H_{60}B_2F_{48}N_9)]^-$.

elemental analysis (calc.): C: 48.43 (49.02), H: 2.74 (2.31), N: 3.71 (4.02).

4.3.27 Synthesis of $[[MeC\{CH_2(N_3C_3H_3\text{-}n\text{Pr})\}_3]_2Au_3]X_3$ (30)

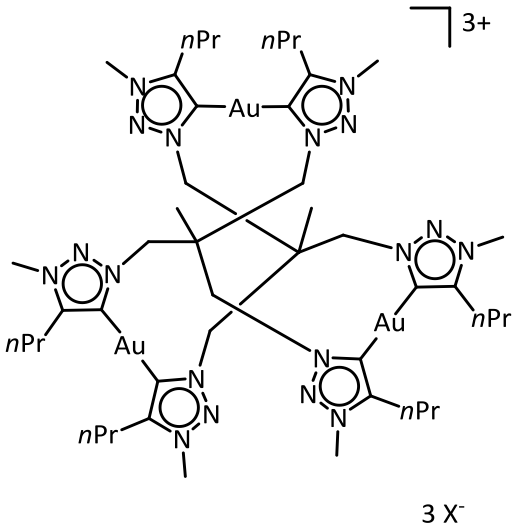

The methylated ligand system **20** was dissolved in DCM (10.0 mL) and Ag_2O (84.0 mg, 363 µmol, 1.50 eq.) was added under exclusion of light. The suspension was stirred for 24 h and $AuCl{\cdot}SMe_2$ (107 mg, 363 µmol, 1.50 eq.) was added and the reaction mixture was stirred at room temperature for additional 48 h. The suspension was filtered through a pad of CELITE and washed with DCM (3 x 20.0 mL). The solvent was reduced to a small amount *in vacuo* and an excess of pentane (10.0 mL) was added to precipitate the target compound as a white solid. The solvent was decanted of and the substituent dried *in vacuo* to give the pure product.

The metal complex could not be synthesized in higher quantities to allow for additional analysis besides X-ray diffraction experiments.

Empirical formula: $C_{49}H_{86}Au_3N_{18}X_3$

4.3.28 Synthesis of $MeC\{CH_2(N_3C_3H_3\text{-}n\text{PrCuBr})\}_3$ (31)

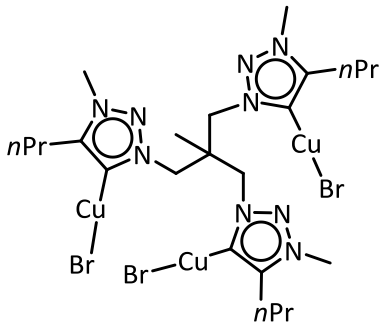

The methylated ligand system **20** (1.34 g, 1.62 mmol, 1.00 eq.) was dissolved in DCM (50.0 mL) and Ag_2O (421 mg, 1.82 mmol, 1.50 eq.) was added under exclusion of light. The suspension was stirred for 24h and $CuBr{\cdot}SMe_2$ (373 mg, 1.82 mmol, 1.50 eq.) was added and the reaction mixture was stirred at room temperature for additional 48 h. The suspension was filtered (P4) and washed with DCM (3 x 20.0 mL). The solvent was reduced to a small amount *in vacuo* and the yellow solution was stored at -20 °C to precipitate crystals suitable for X-ray diffraction.

Upon opening of the SCHLENK-flask the yellow solution turned dark green. Experiments run in an argon glove box showed the same behavior within minutes after initial synthesis. Because of the high sensitivity towards air and moisture no additional analytical data could be gained.

Empirical formula: $C_{23}H_{39}Br_3Cu_3N_9$

4.3.29 Synthesis of [MeC{$CH_2(N_3C_3H_4$-Ph)}$_3$](μ^2-$PdCl_2$)($PdCl_2$) (32)

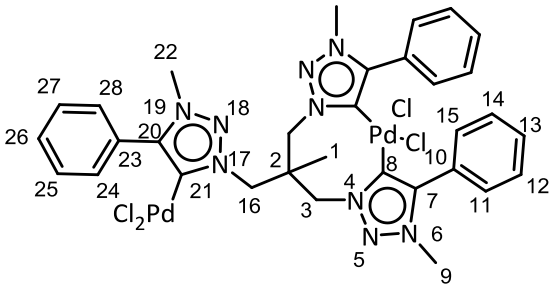

Ag_2O (430 mg, 870 µmol, 3.00 eq.) has been added to a solution of **24** (270 mg, 290 µmol, 1.00 eq.) in DCM (25.0 mL). After 24 h $PdCl_2$·COD (250 mg, 870 µmol, 3.00 eq.) was added and the reaction was stirred for another 24 h. The solution was filtered through a pad of celite and excess solvent was removed *in vacuo*. The product was washed with hexane (2 x 20.0 mL) and could be obtained as a dark yellow solid.

Empirical formula: $C_{32}H_{33}Cl_4N_9Pd_3$
Molecular weight: 898.32 g/mol

^{1}H-NMR (300 MHz, $CDCl_3$): δ [ppm] = 7.94-7.10 (m, 15H, H11, H12, H13, H14, H15, H23, H24, H25, H26, H27, H28), 4.18-3.75 (m, 6H, H3, H16), 2.77 (s, 9H, 6-H3, H22), 1.61 (s, 3H, H3).

EI-MS: *m/z* = 862.0 $[M\text{-}Cl^-]^+$.

4.3.30 Synthesis of [MeC{$CH_2(N_3C_3H_4$-Ph)}$_3$](μ^2-$NiCl_2$)I (33)

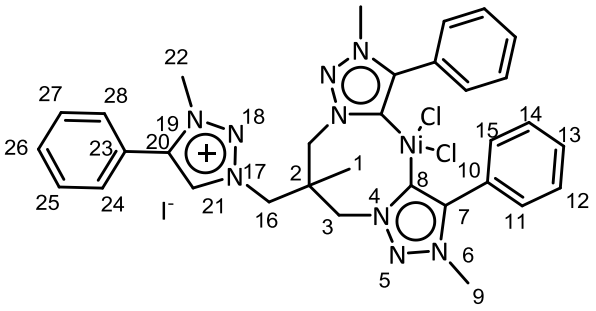

Ag_2O (330 mg, 1.40 mmol, 3.00 eq.) has been added to a solution of **24** (430 mg, 0.47 mmol, 1.0 eq.) in DCM (25.0 mL). After 24 h $NiCl_2$·DME (250 mg, 1.40 mmol, 3.00 eq.) was added and the reaction was stirred for another 24 h. The solution was filtered through a pad of celite and excess solvent was removed *in vacuo*. The product could be obtained as a green-yellowish solid.

Empirical formula: $C_{32}H_{33}Cl_2IN_9Ni_3$
Molecular weight: 932.46 g/mol

^{1}H-NMR (300 MHz, CDCl3): δ [ppm] = 7.60 (m, 6H, H11, H15, H24, H28), 7.18 (m, 9H, H12, H13, H14, H25, H26, H27), 4.31 (m, 4H, H3), 4.10 (s, 2H, H16), 3.72 (s, 9H, H6, H22), 1.82 (s, 3H, H3).

EI-MS: *m/z* = 674.2 $[M\text{-}I]^+$, 318.6 $[M\text{-}I\text{-}Cl]^{2+}$

CRYSTALLOGRAPHIC SECTION

4.4 Crystal Selection and Handling

Suitable crystals for single crystal X-ray diffraction analysis of the presented compounds were selected under an argon atmosphere and transferred into perfluorated oil on a microscope slide, which was cooled with a nitrogen gas flow by the X-Temp2 device[152,153]. Crystals were mounted to the tip of a MiTeGen©MicroMount using a polarizer microscope, fixed to a goniometer head and shock cooled to 100(2) K by the crystal cooling device.[154]

4.5 Data Collection and Processing

Data collection was performed either on a BRUKER SMART APEX diffractometer with an INCOATEC IμS-Mo-Microsource (λ = 0.71073 Å), a BRUKER TXS rotating-Mo-anode (λ = 0.71073 Å) or a BRUKER SMART APEX with an INCOATEC IμS-Ag-Microsource (λ = 0.56086 Å).[155] All diffractometer were equipped with an OXFORD CRYOSYSTEMS crystal cooling device, an *APEX II CCD* detector and either INCOATEC *Quazar* or *Helios* mirror optics, mounted on a D8- goniometer.

The diffractometers were controlled by the *APEX2*[156] program suite. Prior to each experiment a test run (*matrix-scan*) was recorded to check the crystal quality, cell parameters and to determine the exposure time. Measurements were conducted in a ω-scan mode with a step width of 0.5°. Determination and refinement of the unit cell was done with the *APEX2* program suite. All data were integrated with *SAINT*[157] and a semi-empirical absorption correction with *SADABS*[158] was applied. Additional 3λ correction of the data was carried out if necessary.[159] Data statistics and preliminary space group determination as well as file setup for structure solution and refinement was carried out with *XPREP*.[160]

4.6 Structure Solution and Refinement

All structures have been solved by direct methods using *SHELXT* within *SHELXTL*.[161] Structure solution was performed on F_0^2, which are directly proportional to the measured integrities, via *SHELXL* within *SHELXTL* using the *ShelXle GUI*.[162] If not stated otherwise all C-bonded hydrogen atoms were refined isotropically on calculated positions using a riding model. The positions were geometrically optimized and the U_{iso} were constrained to 1.2 U_{eq} of the pivot atom or 1.5 U_{eg} of the methyl carbon

atom. All refinements were carried out to minimize the function $M(p_i, k)$ shown in Eq. 4.6.1. using the weights w_H defined in Eq. 4.6.2.

Eq. 4.6.1. $$M(p_i, k) = \sum_H w_h[k|F_{obs}(H)|^2 - |F_{calc}(H)|^2]^2 = min$$

Eq. 4.6.2. $$w_H^{-1} = \sigma_H^2 F_{obs}^2 + (g1 \cdot P)^2 + g2 \cdot P \; with \; P = \frac{F_{obs}^2 + 2F_{calc}^2}{3}$$

The results of the refinements were verified by comparison of the calculated and the observed structure factors. Commonly used criteria are the residuals *R1* shown in Eq. 4.6.3. and *wR2* shown in eq. 4.6.4.) with *wR2* being more significant since the model is refined against F^2.

Eq. 4.6.3. $$R1 = \frac{\sum_H w_H(|F_{obs}| - |F_{calc}|)}{\sum_H w_H |F_{obs}|}$$

Eq. 4.6.4. $$wR2 = \frac{\sum_H w_H(|F_{obs}|^2 - |F_{calc}|^2)^2}{\sum_H w_H |F_{obs}|^4}$$

Furthermore, the goodness of fit (GoF, S). a figure of merit showing the relation between deviation of F_{calc} from F_{obs} and the over-determination of refined parameters is calculated with eq. 4.6.5.

Eq. 4.6.5. $$S = \sqrt{\frac{\sum(w_H(F_{obs}^2 - F_{calc}^2)^2)}{(n-p)}}$$

Residual densities from the difference Fourier analysis should be small. These residuals are normally found in the bonding regions due to the model restrictions. Higher residuals for heavy scatterers are acceptable as they arise mainly from absorption effects and FOURIER truncation errors due to the limited recorded resolution range. The highest peak and deepest hole from difference FOURIER analysis are listed in the crystallographic tables. The quality of the model is depicted by the size, ellipticity and orientation of the ADPs. These ADPs should be equal in size with little ellipticity and oriented perpendicular to the bonds. All graphics were generated and plotted with the XP[163] program with the anisotropic displacement parameters at the 50 % probability level unless stated otherwise.

4.7 Treatment of Disorder

Structure solutions with signs of disordered moietys were refined using constraints and restraints. Common distance restraints like *SADI* and *SAME* were employed and additionally anisotropic displacement parameter restraints like *SIMU*, *DELU* and *RIGU*. These restraints are treated as additional experimental observations, increasing the data to refine against. Thus the minimization function changes to Eq. 4.7.1.

Eq. 4.7.1. $$M = \sum w(F_{obs}^2 - F_{calc}^2)^2 + \sum w_r(R_{target} - R_{calc)}{}^2$$

Constraints such as the site occupation factor and AFIX instruction have been used during refinement of the disorder

DETERMINED STRUCTURES

5.1 Structures of Self - Synthesized Compounds

5.1.1 Crystal structure of $[N(P(CH_3)_2(C_6H_5))_2]Cl$ (4)

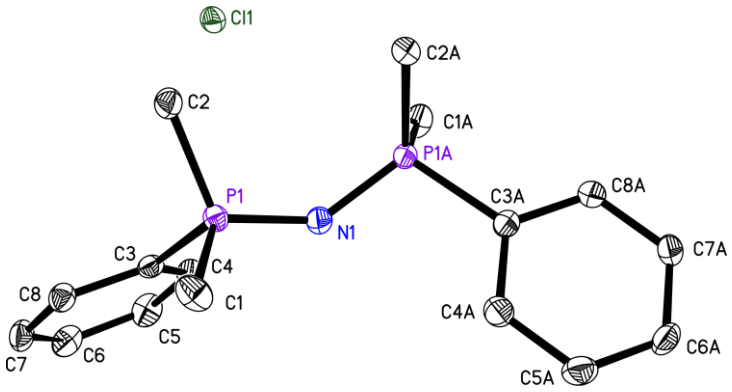

Figure 5.1.1: Crystal structure of 4. The anisotropic displacement parameters are depicted at the 50 % probability level. The hydrogen atoms are omitted for clarity.

structure code	PSK_007b	Z	4
Empirical formula	$C_{16}H_{22}Cl_1N_1P_2$	ρ_{calc} [Mg·m^{-3}]	1.284
Formula weight [g/mol]	325.73	μ [mm^{-1}]	0.213
Temperature [K]	100(2)	F(000)	688
Wavelength [Å]	0.56087	θ range [°]	2.165 to 20.262
Crystal system	Orthorhombic	Reflections collected	15262
space group	*P*ccn	Independent reflections	1664
a [Å]	7.630(1)	R(int)	0.0392
b [Å]	10.803(1)	Max. / min transmission	0.745 / 0.5889
c [Å]	20.437(2)	Restraints / parameter	0 / 94
α [°]	90	GooF	1.083
β [°]	90	R1 /*w*R2 (I > 2σ(I))	0.0287 / 0.0780
γ [°]	90	R1/ *w*R2 (all data)	0.0352 / 0.0818
Volume [Å³]	1684.6(3)	max. diff peak / hole [e·Å-^{3}]	0.379 / -0.352

Table 5.1.1: Crystal data of 4.

5.1.2 Crystal structure of [Ge{(Ph$_3$PNCH$_2$)$_3$CMe}] (5)

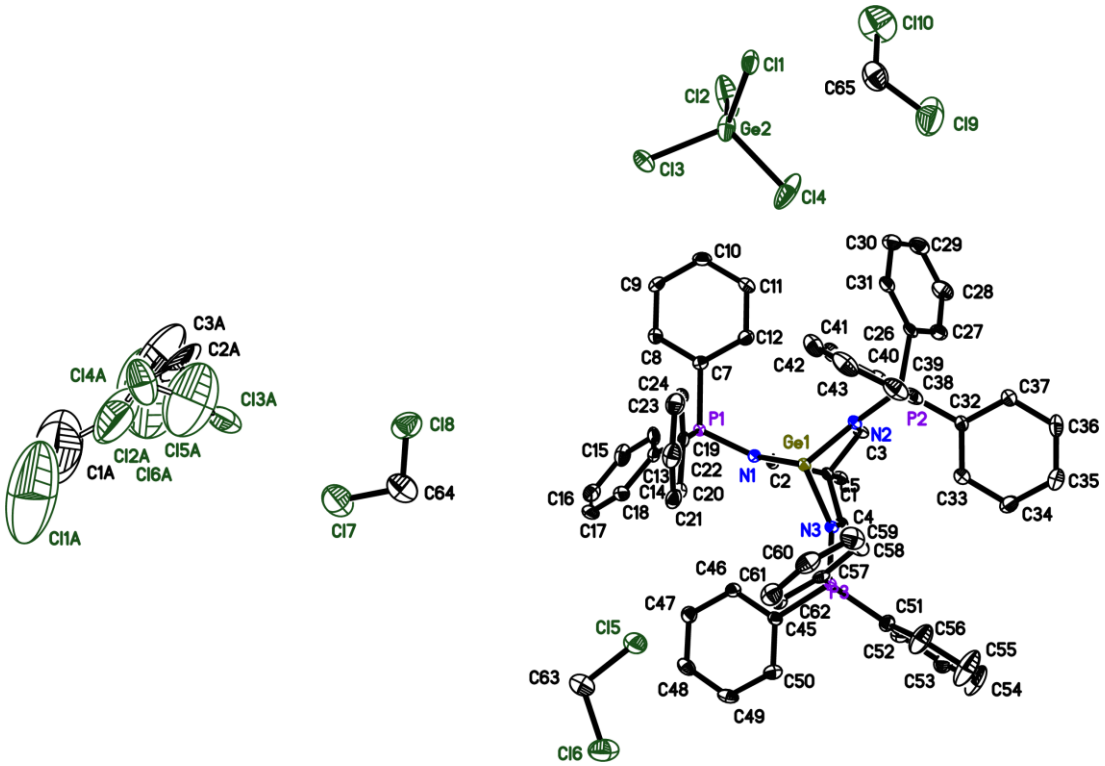

Figure 5.1.2: Asymmetric unit of 5. The anisotropic displacement parameters are depicted at the 50 % probability level. The hydrogen atoms are omitted for clarity.

structure code	PSK_007b	Z	1
Empirical formula	$C_{127}H_{120}Cl_{25.68}Ge_{3.92}N_6P_6$	ρ_{calc} [Mg·m^{-3}]	1.515
Formula weight [g/mol]	1555.45	μ [mm^{-1}]	0.770
Temperature [K]	100(2)	F(000)	1576
Wavelength [Å]	0.56087	θ range [°]	0.847 to 19.900
Crystal system	Triclinic	Reflections collected	77505
space group	$P\bar{1}$	Independent reflections	12709
a [Å]	13.348(2)	R(int)	0.0442
b [Å]	14.852(2)	Restraints / parameter	1277 / 807
c [Å]	19.452(2)	GooF	1.128
α [°]	97.03(1)	R1 /*w*R2 (I > 2σ(I))	0.0758 / 0.1842
β [°]	96.78(1)	R1/ *w*R2 (all data)	0.0891 / 0.1919
γ [°]	114.88(1)	max. diff peak / hole [e·Å^{-3}]	2.906 / -1.809
Volume [Å³]	3409.8(8)		

Table 5.1.2: Crystal data of 5.

Diffuse concentrated residual electron density could be observed in the crystal lattice presumably due to solvent channels consisting of heavily disordered DCM molecules. The refinement of the solvent molecules was incomplete. Changes in the residual electron density with and without modeled solvent molecules are depicted in Figure 5.1.3 and Figure 5.1.4. The structure of the main molecule could be determined unambiguously.

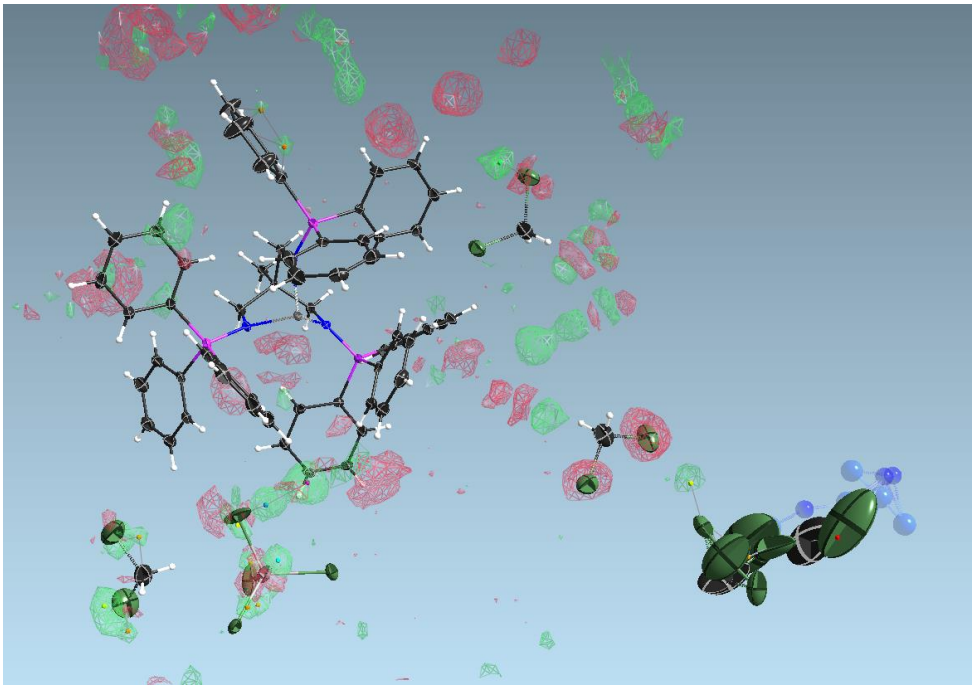

Figure 5.1.3: Residual electron density with modelled DCM solvent molecules.

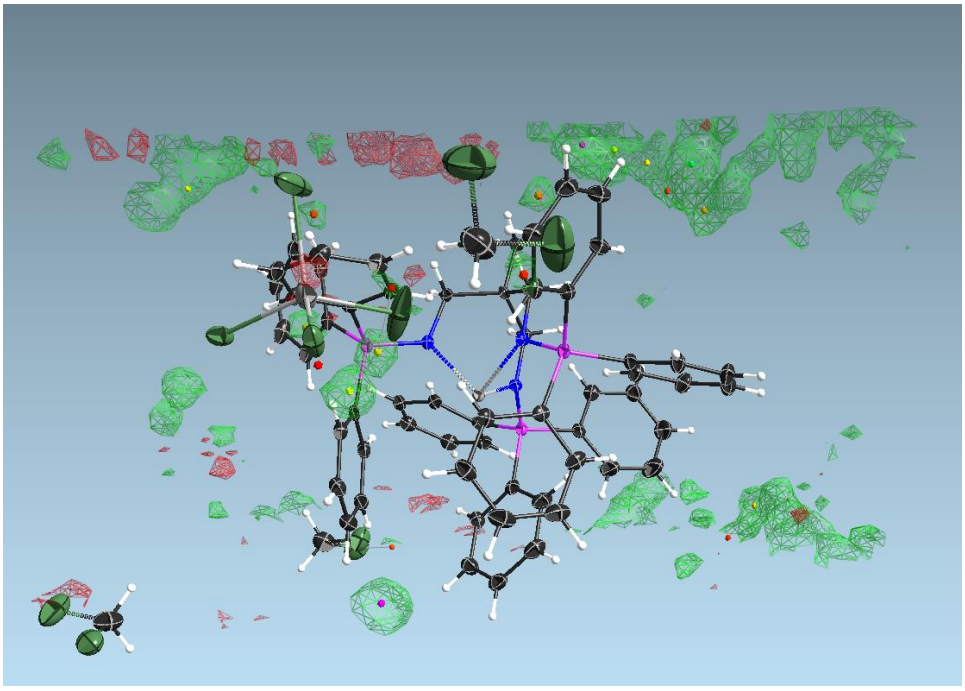

Figure 5.1.4: Residual electron density without modelled sDCM solvent molecules.

5.1.3 Crystal structure of [ZnCl{(PhMe$_2$PNCH$_2$)$_3$CMe}]Cl (6)

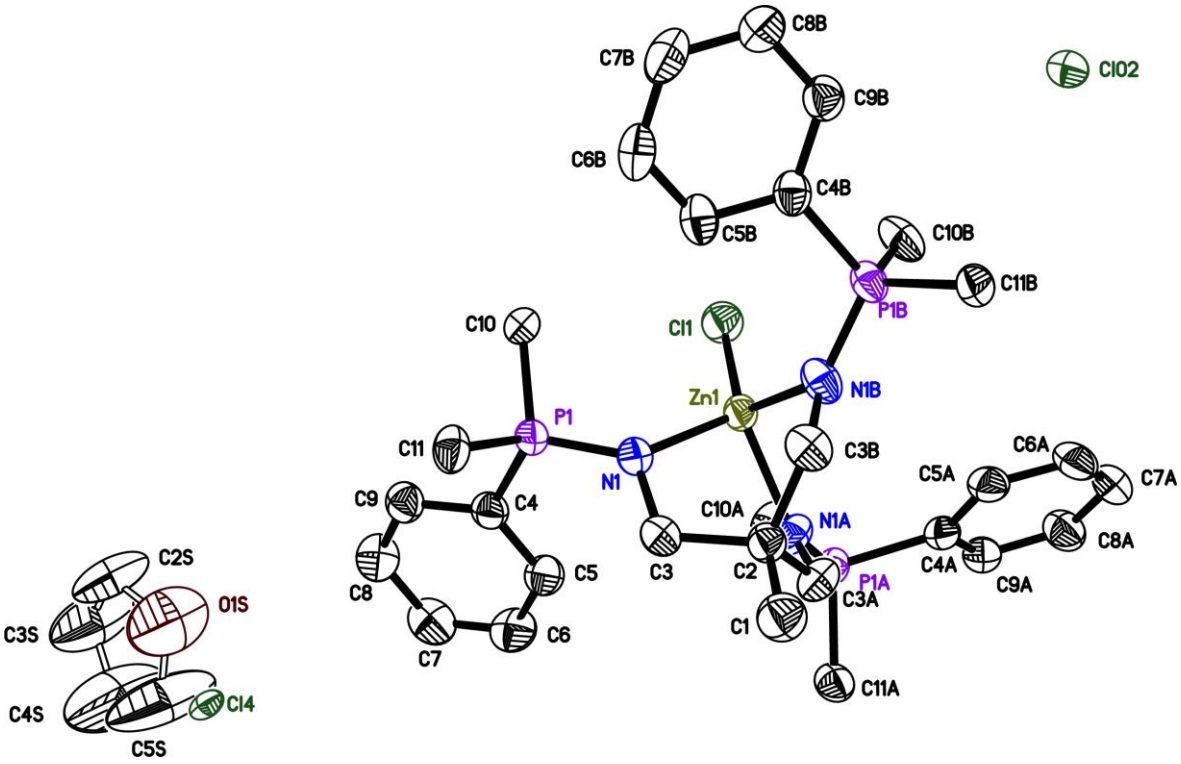

Figure 5.1.5: Crystal structure of 6. The anisotropic displacement parameters are depicted at the 50 % probability level. The hydrogen atoms are omitted for clarity.

structure code	PSK012_RA	Z	8
Empirical formula	$C_{70}H_{108}Cl_4N_6O_3P_6Zn_2$	ρ_{calc} [Mg·m^{-3}]	1.242
Formula weight [g/mol]	1539.97	μ [mm^{-1}]	0.873
Temperature [K]	100(2)	F(000)	6496
Wavelength [Å]	0.71073	θ range [°]	1.961 to 26.014
Crystal system	Cubic	Reflections collected	179925
space group	$I\bar{4}3d$	Independent reflections	2723
a [Å]	25.442(1)	R(int)	0.0404
b [Å]	25.442(1)	Restraints / parameter	34 /171
c [Å]	25.442(1)	GooF	1.143
α [°]	90	R1 /*w*R2 (I > 2σ(I))	0.029 / 0.0761
β [°]	90	R1/ *w*R2 (all data)	0.0332 / 0.0795
γ [°]	90	max. diff peak / hole [e·Å^{-3}]	0.432 / -0.156
Volume [Å^3]	16468.5(19)		

Table 5.1.3: Crystal data of 6.

5.1.4 Crystal structure of $MeC\{CH_2(N_3C_2H_2)\}_3$ (7)

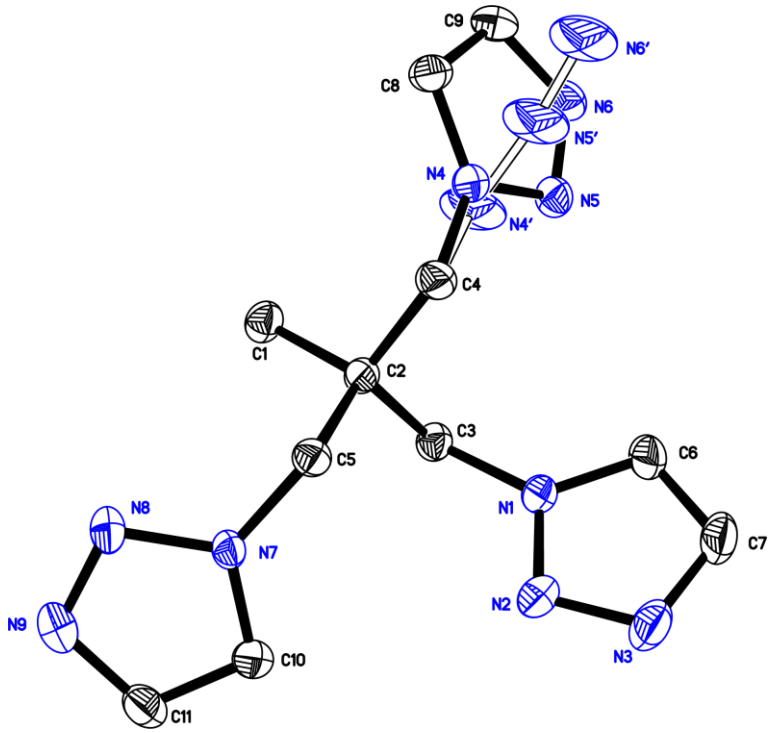

Figure 5.1.6: Asymmetric unit of 7. The anisotropic displacement parameters are depicted at the 50 % probability level. The hydrogen atoms are omitted for clarity.

structure code	PSN_014_TXS	Z	2
Empirical formula	$C_{10.84}H_{14.84}N_9$	ρ_{calc} [Mg·m^{-3}]	1.391
Formula weight [g/mol]	271.17	μ [mm^{-1}]	0.096
Temperature [K]	100(2)	F(000)	286
Wavelength [Å]	0.71073	θ range [°]	1.703 to 25.373
Crystal system	Triclinic	Reflections collected	7604
space group	$P\bar{1}$	Independent reflections	2380
a [Å]	6.244(2)	R(int)	0.0258
b [Å]	8.968(3)	Max. / min transmission	0.8620 / 0.7852
c [Å]	12.188(4)	Restraints / parameter	22 / 204
α [°]	89.262(9)	GooF	1.049
β [°]	79.017(8)	R1 /*w*R2 (I > 2σ(I))	0.0352 / 0.0896
γ [°]	75.285(8)	R1/ *w*R2 (all data)	0.0395 / 0.0929
Volume [Å³]	647.6(4)	max. diff peak / hole [e·Å^{-3}]	0.288 / -0.258

Table 5.1.4: Crystal data of 7.

5.1.5 Crystal structure of MeC{$CH_2(N_3C_2H$-*n*Pr)}$_3$ (8)

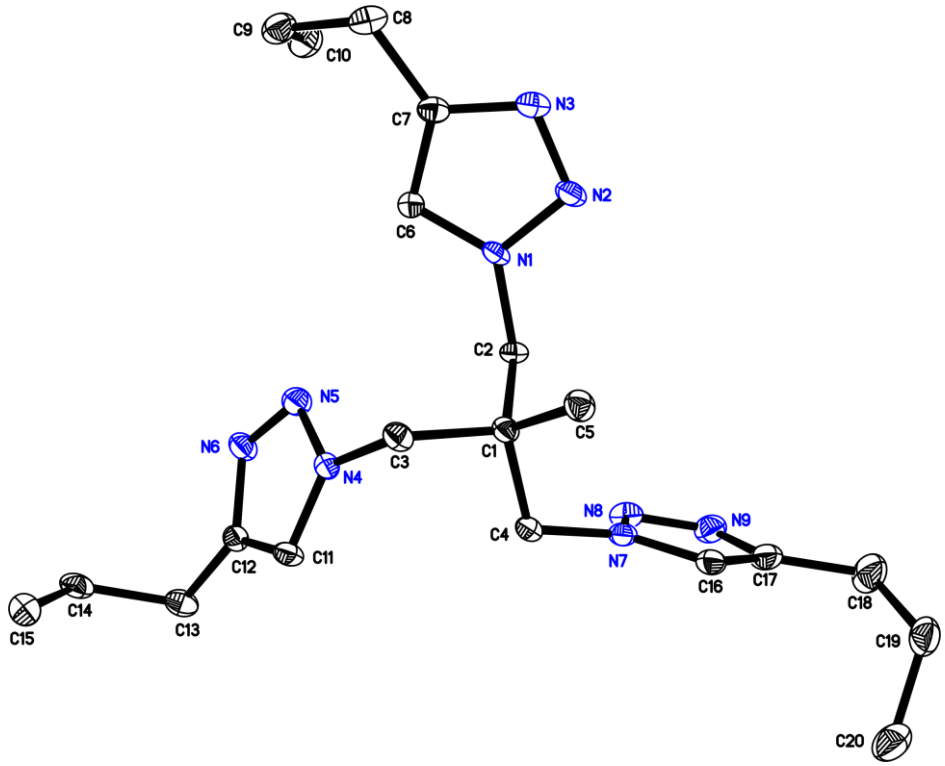

Figure 5.1.7: Asymmetric unit of 8. The anisotropic displacement parameters are depicted at the 50 % probability level. The hydrogen atoms are omitted for clarity.

structure code	PST_114	Z	4
Empirical formula	$C_{20}H_{33}N_9$	ρ_{calc} [Mg·m^{-3}]	1.231
Formula weight [g/mol]	399.55	μ [mm^{-1}]	0.079
Temperature [K]	100(2)	F(000)	864
Wavelength [Å]	0.71073	θ range [°]	1.717 to 25.387
Crystal system	Monoclinic	Reflections collected	22450
space group	$P2_1/c$	Independent reflections	3960
a [Å]	12.790(2)	R(int)	0.0442
b [Å]	15.986(3)	Max. / min transmission	0.9705 / 0.8729
c [Å]	11.371(2)	Restraints / parameter	0 / 267
α [°]	90	GooF	1.033
β [°]	111.96(2)	R1 /*w*R2 (I > 2σ(I))	0.0409 / 0.0976
γ [°]	90	R1/ *w*R2 (all data)	0.0562 / 0.1062
Volume [Å^3]	2156.2(7)	max. diff peak / hole [e·Å^{-3}]	0.248 / -0.224

Table 5.1.5: Crystal data of 8.

5.1.6 Crystal structure of $MeC\{CH_2(N_3C_2H\text{-}cyPr)\}_3$ (9)

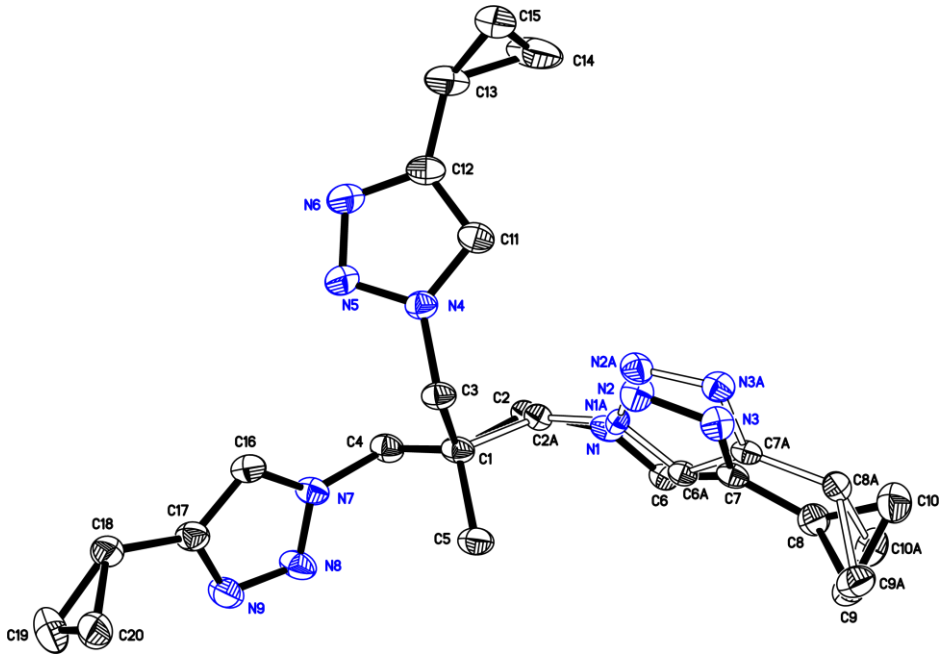

Figure 5.1.8: Asymmetric unit of 8. The anisotropic displacement parameters are depicted at the 50 % probability level. The hydrogen atoms are omitted for clarity.

structure code	PST_113_CyPr2	Z	2
Empirical formula	$C_{20}H_{27}N_9$	ρ_{calc} [Mg·m^{-3}]	1.321
Formula weight [g/mol]	393.50	μ [mm^{-1}]	0.086
Temperature [K]	99(2)	F(000)	420
Wavelength [Å]	0.71073	θ range [°]	1.991 to 25.353
Crystal system	Triclinic	Reflections collected	14041
space group	$P\bar{1}$	Independent reflections	3608
a [Å]	9.507(2)	R(int)	0.0234
b [Å]	10.704(2)	Max. / min transmission	0.9705 / 0.8729
c [Å]	11.123(3)	Restraints / parameter	348 / 339
α [°]	108.88(2)	GooF	1.009
β [°]	96.34(2)	R1 /*w*R2 (I > 2σ(I))	0.0454 / 0.1068
γ [°]	108.10(3)	R1/ *w*R2 (all data)	0.0555 / 0.1130
Volume [Å³]	989.6(4)	max. diff peak / hole [e·Å-^{3}]	0.309 / -0.287

Table 5.1.6: Crystal data of 8.

5.1.7 Crystal structure of $MeC\{CH_2(N_3C_2H\text{-}iPr)\}_3$ (10)

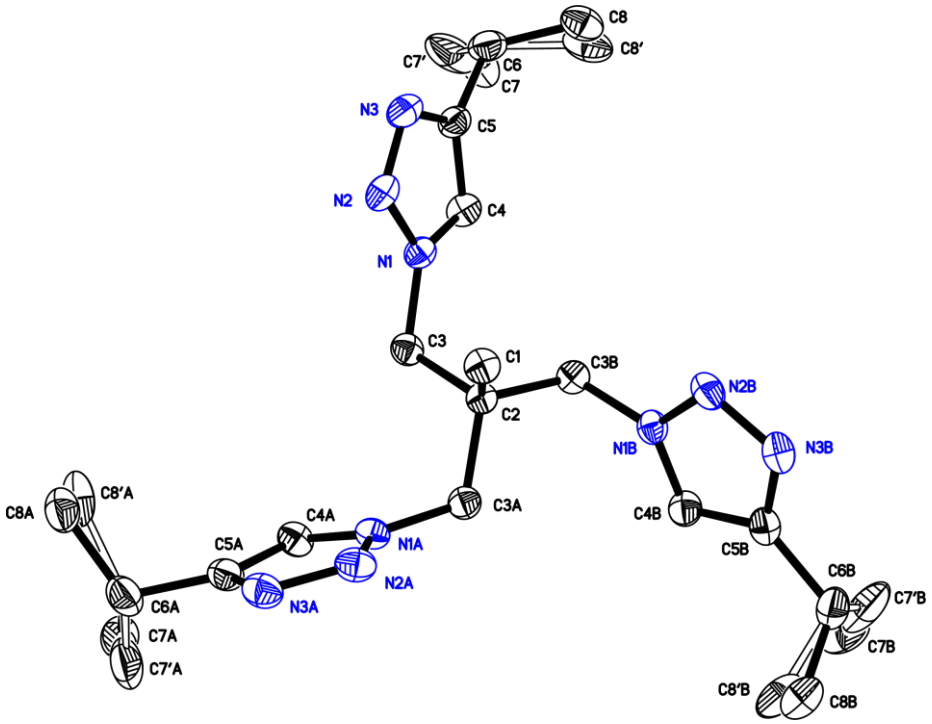

Figure 5.1.9: Crystal structure of 10. The anisotropic displacement parameters are depicted at the 50 % probability level. The hydrogen atoms are omitted for clarity.

structure code	PSJ_001	Z	6
Empirical formula	$C_{20}H_{33}N_9$	ρ_{calc} [Mg·m^{-3}]	1.198
Formula weight [g/mol]	399.55	μ [mm^{-1}]	0.077
Temperature [K]	100(2)	F(000)	1296
Wavelength [Å]	0.71073	θ range [°]	2.481 to 25.425
Crystal system	Trigonal	Reflections collected	12901
space group	*R*3c	Independent reflections	1364
a [Å]	11.759(2)	R(int)	0.0248
b [Å]	11.759(2)	Max. / min transmission	0.7452 / 0.6875
c [Å]	27.741(3)	Restraints / parameter	39 / 118
α [°]	90	GooF	1.049
β [°]	90	R1 /*w*R2 (I > 2σ(I))	0.0242 / 0.0640
γ [°]	120	R1/ *w*R2 (all data)	0.0250 / 0.0648
Volume [Å³]	3322.0(12)	max. diff peak / hole [e·Å^{-3}]	0.140 / -0.130

Table 5.1.7: Crystal data of 10.

5.1.8 Crystal structure of $MeC\{CH_2(N_3C_2H\text{-}tBu)\}_3$ (11)

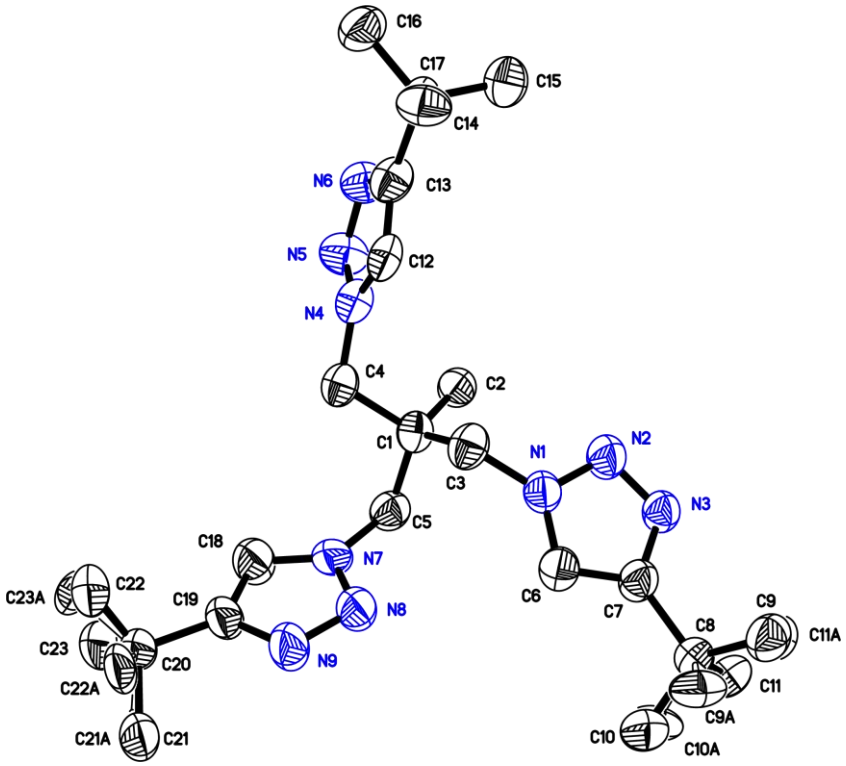

Figure 5.1.10: Asymmetric unit of 11. The anisotropic displacement parameters are depicted at the 50 % probability level. The hydrogen atoms are omitted for clarity.

structure code	PST_Triaz_R_tBu	Z	8
Empirical formula	$C_{23}H_{39}N_9$	ρ_{calc} [Mg·m^{-3}]	1.140
Formula weight [g/mol]	441.63	μ [mm^{-1}]	0.072
Temperature [K]	100(2)	F(000)	1920
Wavelength [Å]	0.71073	θ range [°]	1.275 to 24.215
Crystal system	Monoclinic	Reflections collected	18793
space group	*C*2c	Independent reflections	4100
a [Å]	31.940(1)	R(int)	0.0850
b [Å]	17.739(1)	Restraints / parameter	946 / 362
c [Å]	9.082(2)	GooF	2.625
α [°]	90	R1 /*w*R2 (I > 2σ(I))	0.2865 / 0.5671
β [°]	90.98(1)	R1/ *w*R2 (all data)	0.2940 / 0.5725
γ [°]	90	max. diff peak / hole [e·Å^{-3}]	2.426 / -1.377
Volume [Å³]	5145.0(12)		

Table 5.1.8: Crystal data of 11. Crystals of 11 only diffract to low resolutions leading to poor data quality of the refinement.

5.1.9 Crystal structure of $MeC\{CH_2(N_3C_2H\text{-}FeCp_2)\}_3$ (14)

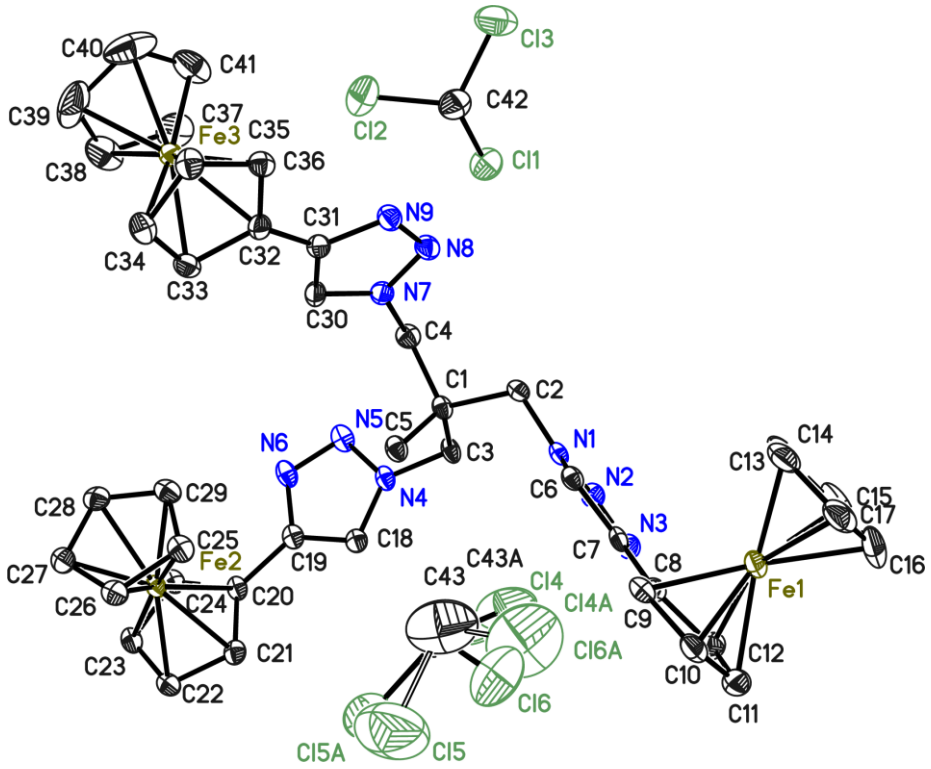

Figure 5.1.11: Asymmetric unit of 14. The anisotropic displacement parameters are depicted at the 50 % probability level. The hydrogen atoms are omitted for clarity.

structure code	PST_FeCp	Z	2
Empirical formula	$C_{43}H_{41}Cl_6Fe_3N_9$	ρ_{calc} [Mg·m^{-3}]	1.568
Formula weight [g/mol]	1064.10	μ [mm^{-1}]	1.352
Temperature [K]	100(2)	F(000)	1084
Wavelength [Å]	0.71073	θ range [°]	1.271 to 25.385
Crystal system	Triclinic	Reflections collected	47739
space group	$P\bar{1}$	Independent reflections	8262
a [Å]	12.687(2)	R(int)	0.0391
b [Å]	12.711(2)	Max. / min transmission	0.6887 / 0.5937
c [Å]	16.835(3)	Restraints / parameter	504 / 589
α [°]	74.61(3)	GooF	1.048
β [°]	74.72(2)	R1 /*w*R2 (I > 2σ(I))	0.0439 / 0.1121
γ [°]	60.70(2)	R1/ *w*R2 (all data)	0.0548 / 0.1181
Volume [Å³]	2253.6(8)	max. diff peak / hole [e·Å^{-3}]	1.430 / -0.567

Table 5.1.9: Crystal data of 14.

5.1.10 Crystal structure of $(CH_3)_3C_6(CH_2N_3)_3$ (16)

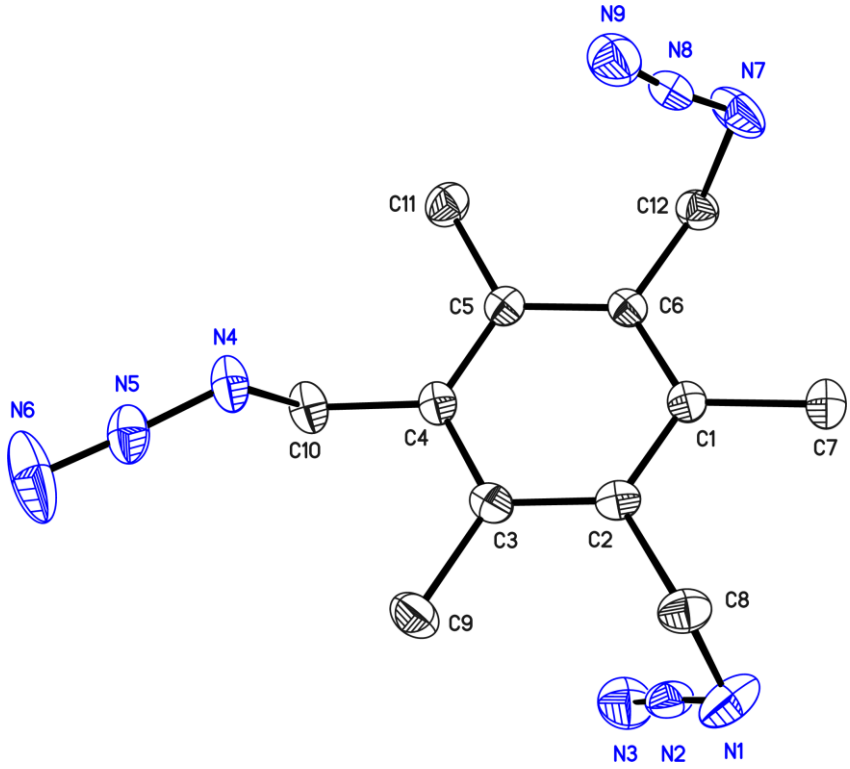

Figure 5.1.12: Asymmetric unit of 16. The anisotropic displacement parameters are depicted at the 50 % probability level. The hydrogen atoms are omitted for clarity.

structure code	PSN003	Z	4
Empirical formula	$C_{12}H_{15}N_9$	ρ_{calc} [Mg·m^{-3}]	1.360
Formula weight [g/mol]	285.33	μ [mm^{-1}]	0.093
Temperature [K]	112(2)	F(000)	600
Wavelength [Å]	0.71073	θ range [°]	1.593 to 25.429
Crystal system	Monoclinic	Reflections collected	20518
space group	$P2_1/c$	Independent reflections	2560
a [Å]	12.786(3)	R(int)	0.0389
b [Å]	10.833(2)	Max. / min transmission	0.7452 / 0.6682
c [Å]	10.062(2)	Restraints / parameter	0 / 194
α [°]	90	GooF	1.073
β [°]	90.770	R1 /*w*R2 (I > 2σ(I))	0.0364 / 0.0904
γ [°]	90	R1/ *w*R2 (all data)	0.0506 / 0.0980
Volume [Å³]	1393.6(5)	max. diff peak / hole [e·Å^{-3}]	0.245 / -0.195

Table 5.1.10: Crystal data of 16.

5.1.11 Crystal structure of $[C_7H_{13}N_3I]I$ (19)

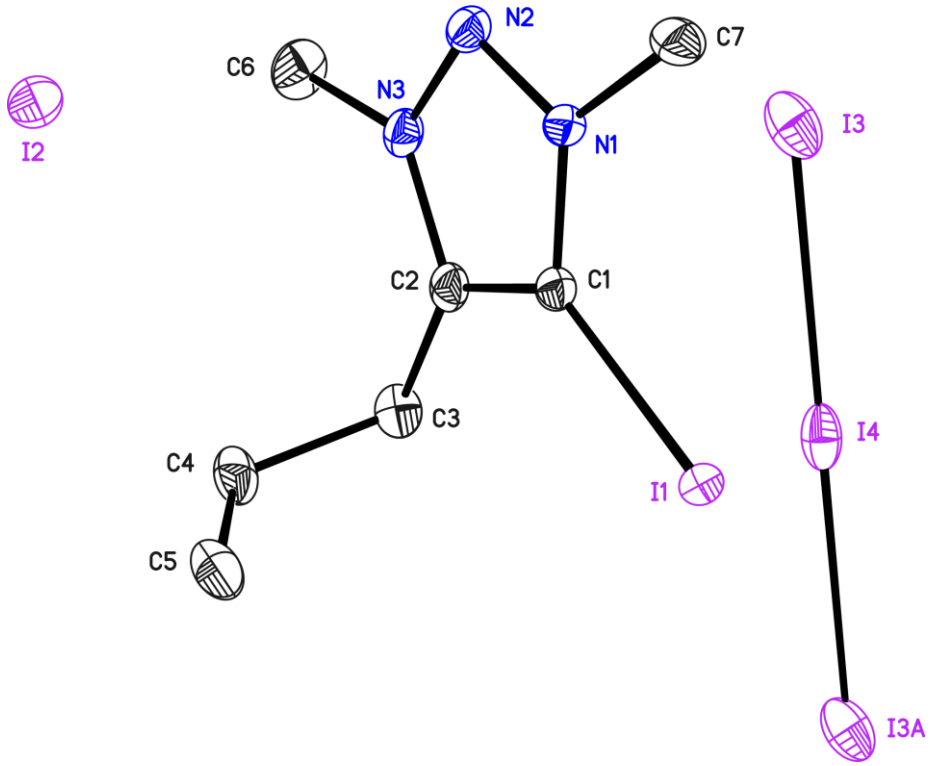

Figure 5.1.13: Asymmetric unit of 19. The anisotropic displacement parameters are depicted at the 50 % probability level. The hydrogen atoms are omitted for clarity.

structure code	PSN006	Z	4
Empirical formula	$C_{14}H_{26}I_6N_6$	ρ_{calc} [Mg·m^{-3}]	2.538
Formula weight [g/mol]	1039.81	μ [mm^{-1}]	6.861
Temperature [K]	100(2)	F(000)	940
Wavelength [Å]	0.71073	θ range [°]	1.666 to 26.044
Crystal system	Monoclinic	Reflections collected	16780
space group	$P2_1/c$	Independent reflections	2689
a [Å]	12.706(3)	R(int)	0.0297
b [Å]	12.967(2)	Max. / min transmission	0.7453 / 0.5932
c [Å]	8.586(2)	Restraints / parameter	0 / 124
α [°]	90	GooF	1.044
β [°]	105.8980(16)	R1 /*w*R2 (I > 2σ(I))	0.0141 / 0.0332
γ [°]	90	R1/ *w*R2 (all data)	0.0151 / 0.0337
Volume [Å³]	1360.5(5)	max. diff peak / hole [e·Å^{-3}]	0.557 / -0.351

Table 5.1.11: Crystal data of 19**.**

5.1.12 Crystal structure of $[MeC\{CH_2(N_3C_3H_4\text{-}Ph)\}_3]I_3$ (24)

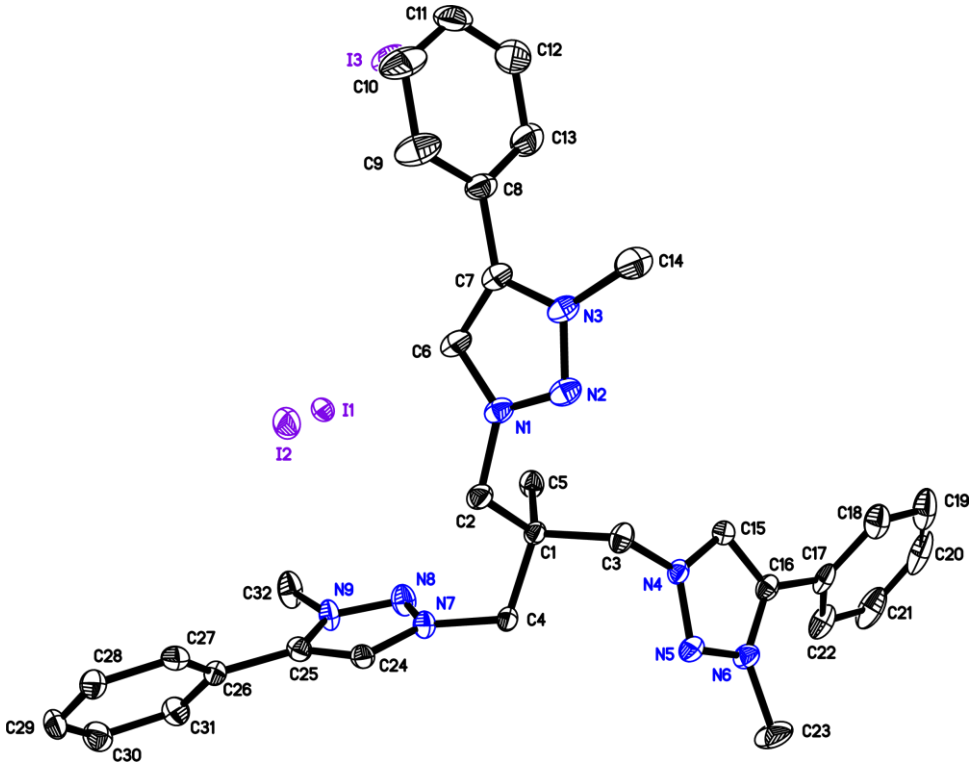

Figure 5.1.14: Asymmetric unit of 24. The anisotropic displacement parameters are depicted at the 50 % probability level. The hydrogen atoms are omitted for clarity.

structure code	PST_PSA007	Z	4
Empirical formula	$C_{32}H_{36}I_3N_9$	ρ_{calc} [Mg·m^{-3}]	1.690
Formula weight [g/mol]	927.40	μ [mm^{-1}]	2.607
Temperature [K]	100(2)	F(000)	1800
Wavelength [Å]	0.71073	θ range [°]	1.610 to 25.355
Crystal system	Monoclinic	Reflections collected	66404
space group	$P2_1/n$	Independent reflections	6662
a [Å]	16.244(2)	R(int)	0.0383
b [Å]	11.539(2)	Restraints / parameter	144 / 401
c [Å]	19.459(3)	GooF	1.045
α [°]	90	R1 /*w*R2 (I > 2σ(I))	0.0291 / 0.0674
β [°]	91.70(1)	R1/ *w*R2 (all data)	0.0359 / 0.0707
γ [°]	90	max. diff peak / hole [e·Å^{-3}]	2.233 / -1.910
Volume [Å³]	3645.8(10)		

Table 5.1.12: Crystal data of 24.

5.1.13 Crystal structure of $[MeC\{CH_2(N_3C_3H_4\text{-}FeCp_2)\}_3]I_3$ (25)

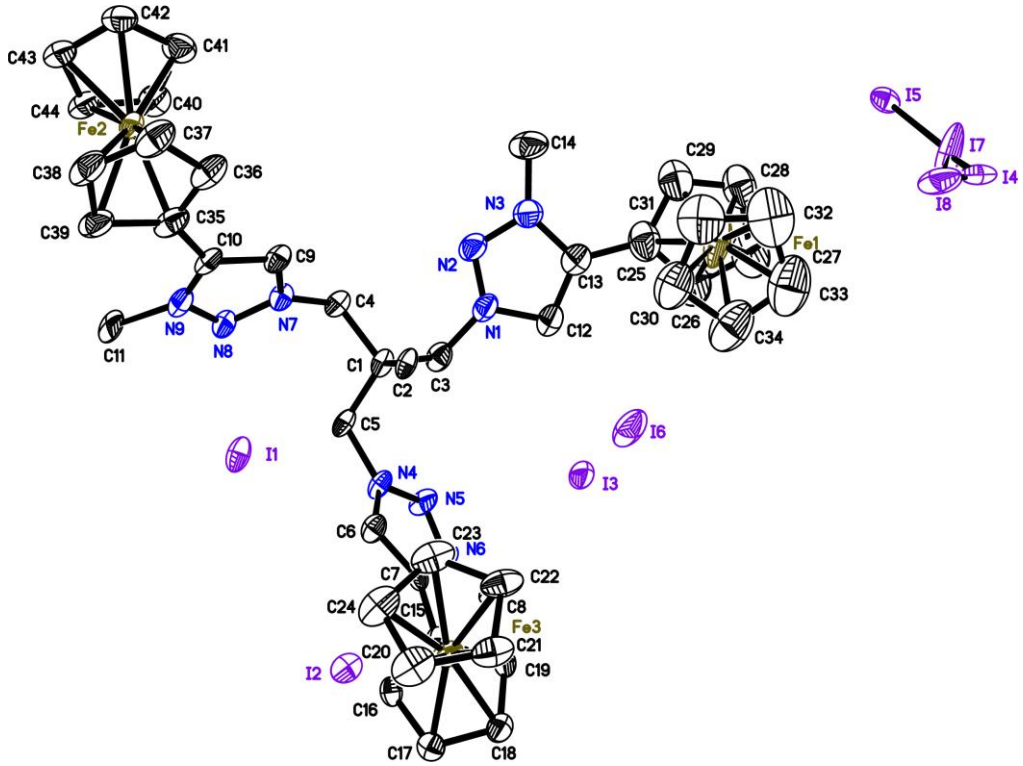

Figure 5.1.15: Asymmetric unit of 24. The anisotropic displacement parameters are depicted at the 50 % probability level. The hydrogen atoms are omitted for clarity. The occupancy of the iodide anions amount to three iodine anions.

structure code	PST135	Z	4
Empirical formula	$C_{44}H_{48}Fe_3I_3N_9$	ρ_{calc} [Mg·m^{-3}]	1.705
Formula weight [g/mol]	1251.16	μ [mm^{-1}]	2.821
Temperature [K]	100(2)	F(000)	2448
Wavelength [Å]	0.71073	θ range [°]	1.481 to 25.368
Crystal system	Monoclinic	Reflections collected	78875
space group	$P2_1/c$	Independent reflections	9030
a [Å]	13.565(1)	R(int)	0.0667
b [Å]	27.502(1)	Restraints / parameter	1121 / 590
c [Å]	13.445(1)	GooF	1.198
α [°]	90	R1 /*w*R2 (I > 2σ(I))	0.1261 / 0.2823
β [°]	103.65(1)	R1/ *w*R2 (all data)	0.1487 / 0.2941
γ [°]	90	max. diff peak / hole [e·Å^{-3}]	2.369 / -3.016
Volume [Å³]	4874.2(6)		

Table 5.1.13: Crystal data of 24.

5.1.14 Crystal structure of MeC{$CH_2(N_3C_3H_3$-*n*PrCuBr)}$_3$ (31)

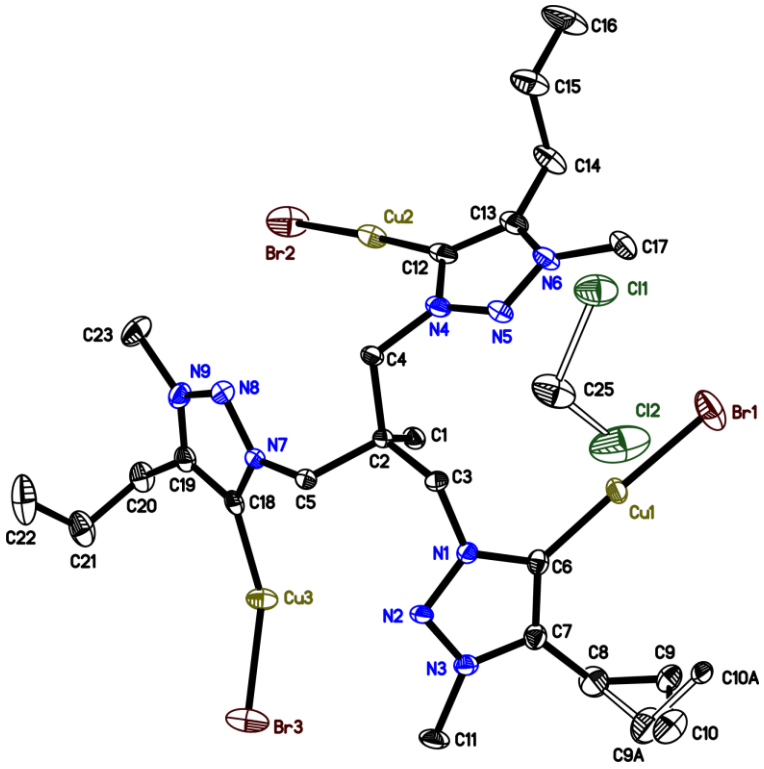

Figure 5.1.16: Asymmetric unit of 31. The anisotropic displacement parameters are depicted at the 50 % probability level. The hydrogen atoms are omitted for clarity.

structure code	PST_CuTriaz	Z	1
Empirical formula	$C_{47}H_{80}Br_6Cl_2Cu_6N_{18}$	ρ_{calc} [Mg·m^{-3}]	1.789
Formula weight [g/mol]	1828.89	μ [mm^{-1}]	5.502
Temperature [K]	99(2)	F(000)	906
Wavelength [Å]	0.71073	θ range [°]	1.307 to 25.350
Crystal system	Triclinic	Reflections collected	32810
space group	$P\bar{1}$	Independent reflections	6185
a [Å]	10.309(1)	R(int)	0.0271
b [Å]	10.616(1)	Restraints / parameter	22 / 397
c [Å]	15.703(1)	GooF	1.040
α [°]	90.60(1)	R1 /*w*R2 (I > 2σ(I))	0.0325 / 0.0828
β [°]	97.20(1)	R1/ *w*R2 (all data)	0.0384 / 0.0861
γ [°]	95.31(1)	max. diff peak / hole [e·Å^{-3}]	1.988 / -1.330
Volume [Å³]	1697.2(3)		

Table 5.1.14: Crystal data of 31.

5.2 Crystallographic Cooperation

Represented in this chapter are all crystallographic measurements from cooperation with different research groups.

5.2.1 Structures determined with Dr. Sudipta Roy within the group of Prof. Dr. H. W. Roesky

CCDC number	Reference
1035413 1035414 1035415 1035416	Roy, S.; Stollberg, P.; Herbst-Irmer, R.; Stalke, D.; Andrada, D. M.; Frenking, G.; Roesky, H. W., *Journal of the American Chemical Society* **2015,** *137* (1), 150-153.

Table 5.2.1: Published structures in cooperation with Dr. Sudipta Roy.

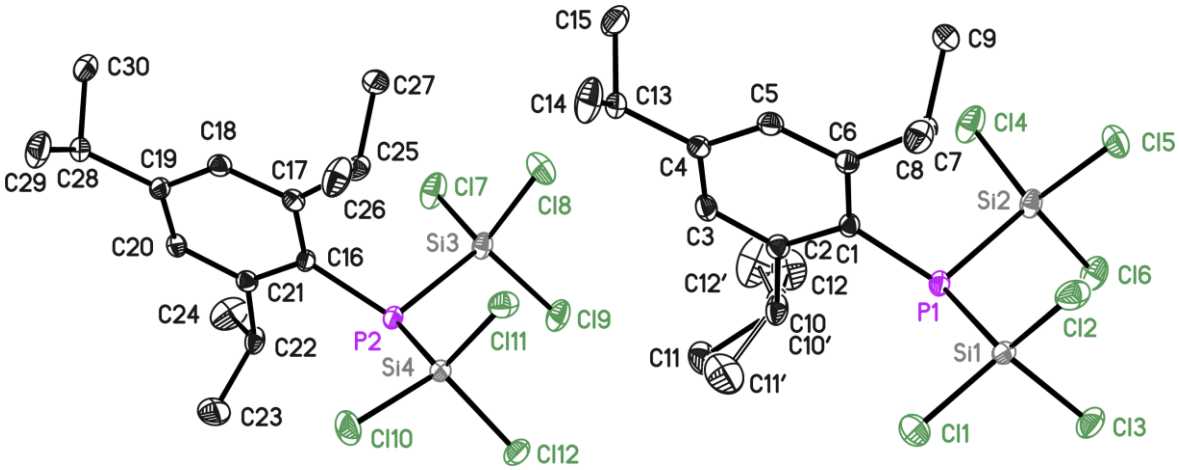

Figure 5.2.1: Asymmetric unit of CCDC no. 1035413. The anisotropic displacement parameters are depicted at the 50 % probability level. The hydrogen atoms are omitted for clarity.

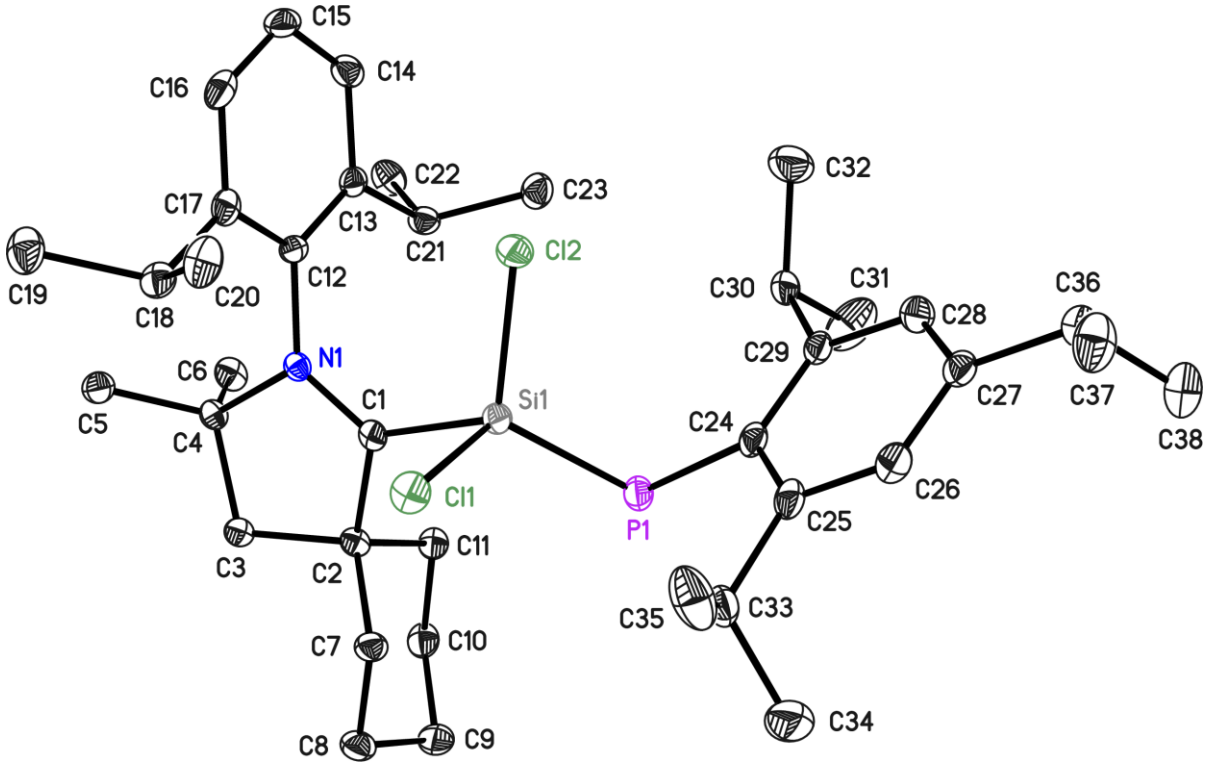

Figure 5.2.2: Asymmetric unit of CCDC no. 1035414. The anisotropic displacement parameters are depicted at the 50 % probability level. The hydrogen atoms are omitted for clarity.

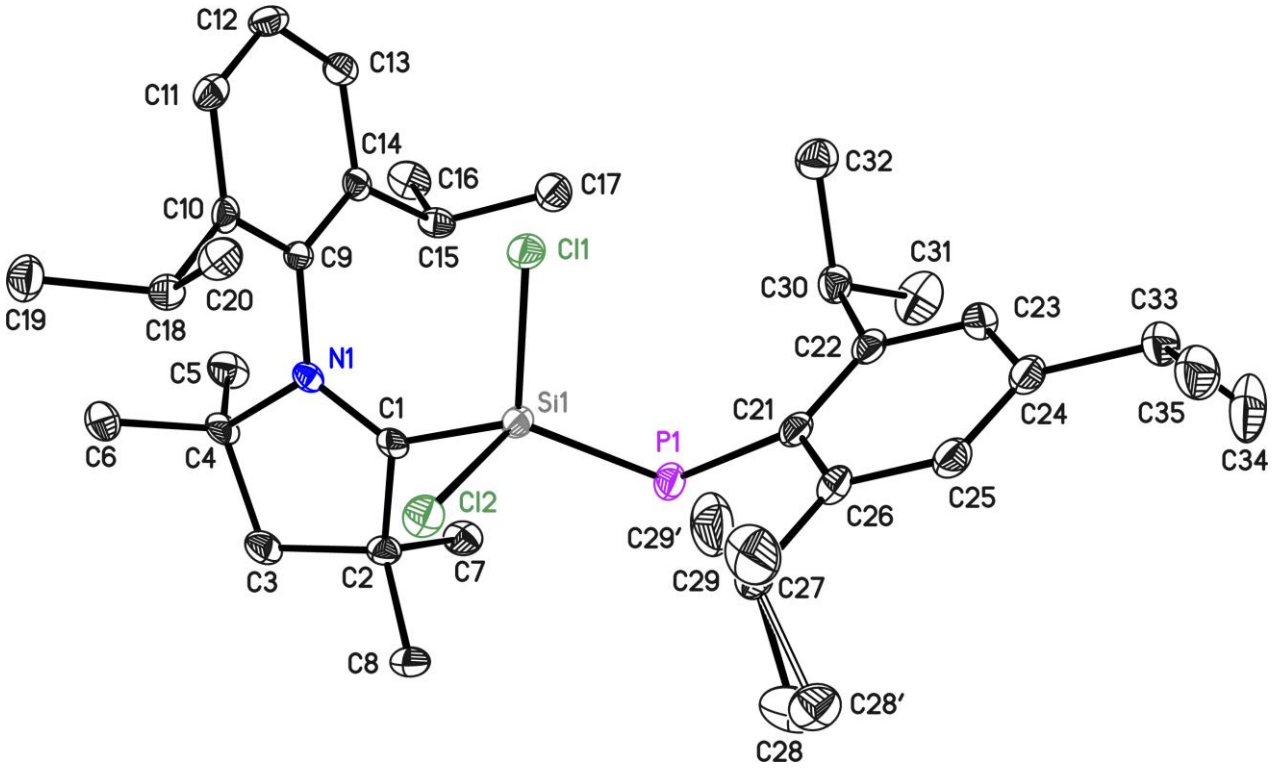

Figure 5.2.3: Asymmetric unit of CCDC no. 1035415. The anisotropic displacement parameters are depicted at the 50 % probability level. The hydrogen atoms are omitted for clarity.

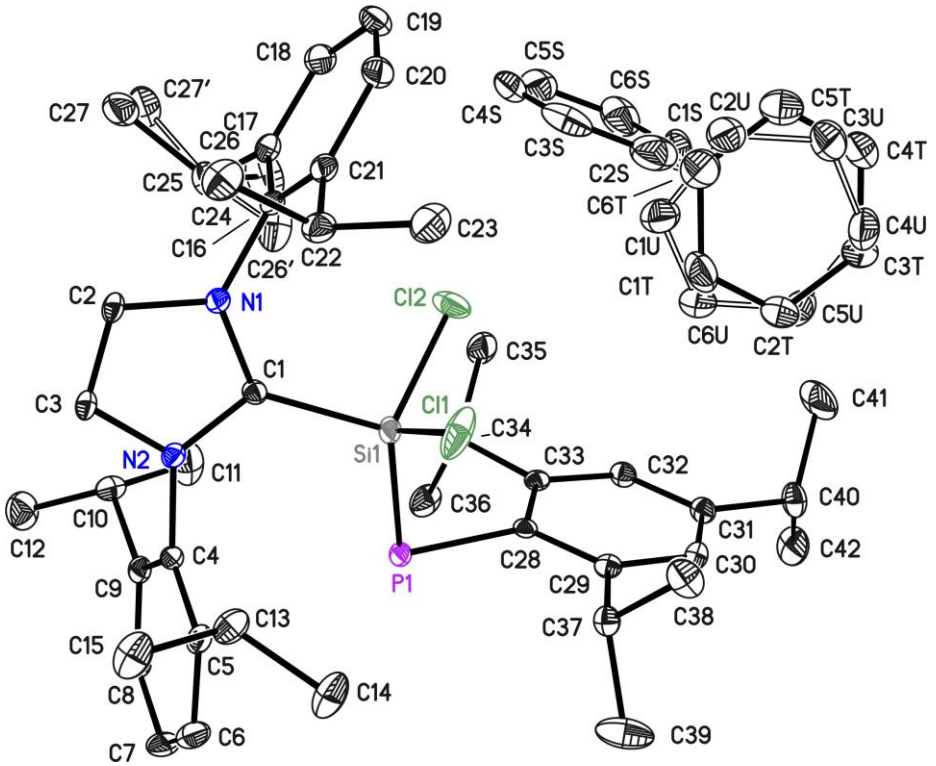

Figure 5.2.4: Asymmetric unit of CCDC no. 1035416. The anisotropic displacement parameters are depicted at the 50 % probability level. The hydrogen atoms are omitted for clarity.

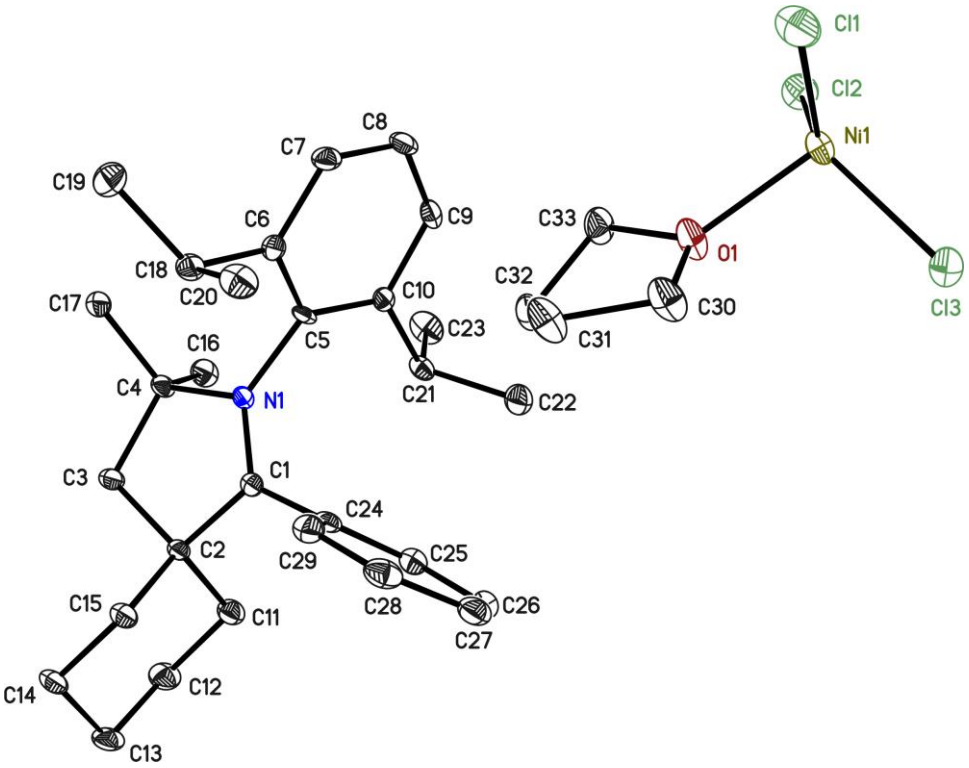

Figure 5.2.5: Asymmetric unit of [$C_{33}H_{48}Cl_3NNiO$]. The anisotropic displacement parameters are depicted at the 50 % probability level. The hydrogen atoms are omitted for clarity.

structure code	PST_KCM_001	Z	4
Empirical formula	$C_{33}H_{48}Cl_3NNiO$	ρ_{calc} [Mg·m^{-3}]	1.303
Formula weight [g/mol]	639.78	μ [mm^{-1}]	0.455
Temperature [K]	100(2)	F(000)	1360
Wavelength [Å]	0.56086	θ range [°]	1.222 to 19.650
Crystal system	Monoclinic	Reflections collected	41615
space group	$P2_1/n$	Independent reflections	5846
a [Å]	9.418(2)	R(int)	0.0522
b [Å]	18.932(2)	Max. / min transmission	0.744 / 0.6931
c [Å]	18.514(3)	Restraints / parameter	0 / 358
α [°]	90	GooF	1.021
β [°]	98.94(2)	R1 /*w*R2 (I > 2σ(I))	0.0297 / 0.0662
γ [°]	90	R1/ *w*R2 (all data)	0.0394 / 0.0708
Volume [Å³]	3261.0(10)	max. diff peak / hole [e·Å-^{3}]	0.437 / -0.316

Table 5.2.2: Crystal data of [$C_{33}H_{48}Cl_3NNiO$].

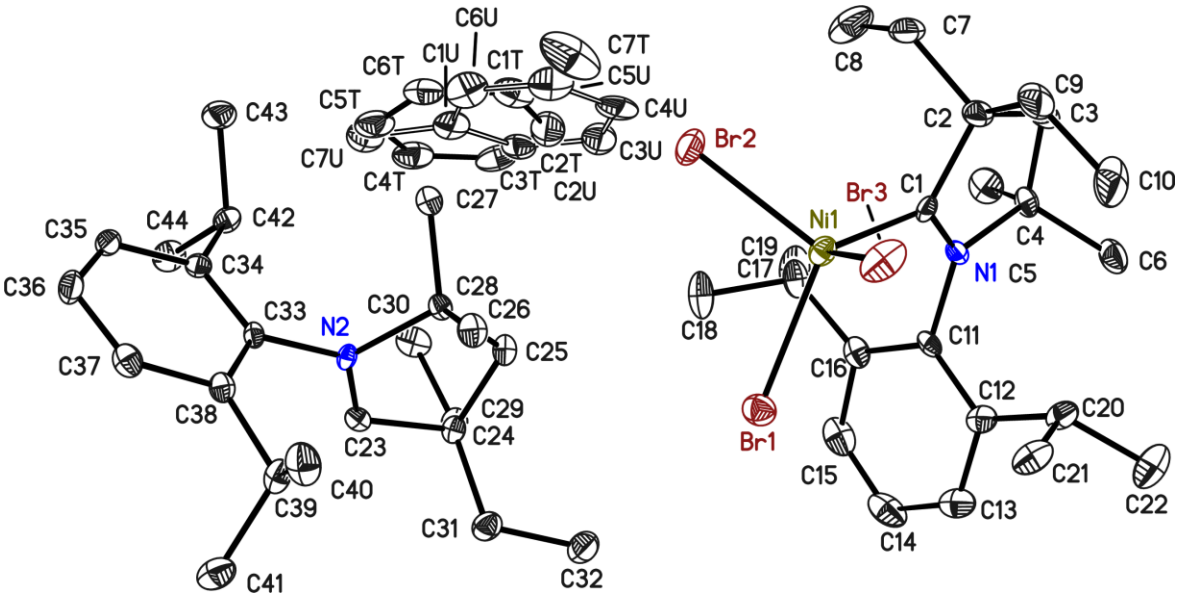

Figure 5.2.6: Asymmetric unit of [$C_{51}H_{79}Br_3N_2Ni$]. The anisotropic displacement parameters are depicted at the 50 % probability level. The hydrogen atoms are omitted for clarity.

structure code	PST_KCM_302	Z	4
Empirical formula	$C_{51}H_{79}Br_3N_2NiO$	ρ_{calc} [Mg·m^{-3}]	1.350
Formula weight [g/mol]	1018.60	μ [mm^{-1}]	1.507
Temperature [K]	100(2)	F(000)	2128
Wavelength [Å]	0.56086	θ range [°]	1.828 to 20.535
Crystal system	Monoclinic	Reflections collected	85241
space group	$P2_1/n$	Independent reflections	10237
a [Å]	10.459(2)	R(int)	0.0887
b [Å]	14.393(2)	Max. / min transmission	0.6731 / 0.6364
c [Å]	33.361(3)	Restraints / parameter	483 / 596
α [°]	90	GooF	0.955
β [°]	93.53(3)	R1 /*w*R2 (I > 2σ(I))	0.0355 / 0.0639
γ [°]	90	R1/ *w*R2 (all data)	0.0631 / 0.0720
Volume [Å³]	5012.5(13)	max. diff peak / hole [e·Å^{-3}]	0.530 / -0.557

Table 5.2.3: Crystal data of [$C_{51}H_{79}Br_3N_2Ni$].

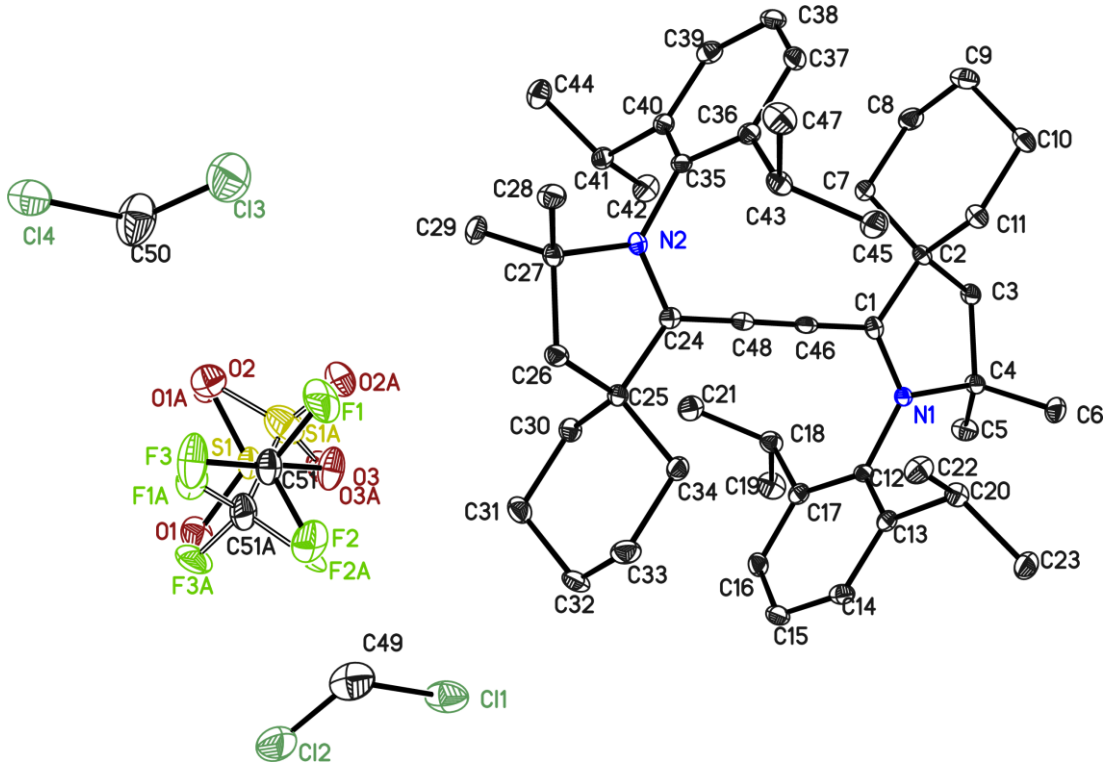

Figure 5.2.7. Asymmetric unit of [$C_{51}H_{74}Cl_4F_3N_2O_3S$]. The anisotropic displacement parameters are depicted at the 50 % probability level. The hydrogen atoms are omitted for clarity.

structure code	PST_KM221	Z	1
Empirical formula	$C_{51}H_{74}Cl_4F_3N_2O_3S$	ρ_{calc} [Mg·m^{-3}]	1.302
Formula weight [g/mol]	993.98	μ [mm^{-1}]	0.329
Temperature [K]	101(2)	F(000)	529
Wavelength [Å]	0.71073	θ range [°]	1.726 to 25.705
Crystal system	Triclinic	Reflections collected	23505
space group	$P\bar{1}$	Independent reflections	9482
a [Å]	9.412(2)	R(int)	0.0189
b [Å]	11.925(2)	Max. / min transmission	0.7453 / 0.6975
c [Å]	12.280(3)	Restraints / parameter	323 / 665
α [°]	76.140(10)	GooF	1.036
β [°]	78.247(10)	R1 /*w*R2 (I > 2σ(I))	0.0317 / 0.0838
γ [°]	73.181(10)	R1/ *w*R2 (all data)	0.0331 / 0.0849
Volume [Å³]	1267.5(5)	max. diff peak / hole [e·Å-^{3}]	0.439 / -0.347

Table 5.2.4: Crystal data of [$C_{51}H_{74}Cl_4F_3N_2O_3S$].

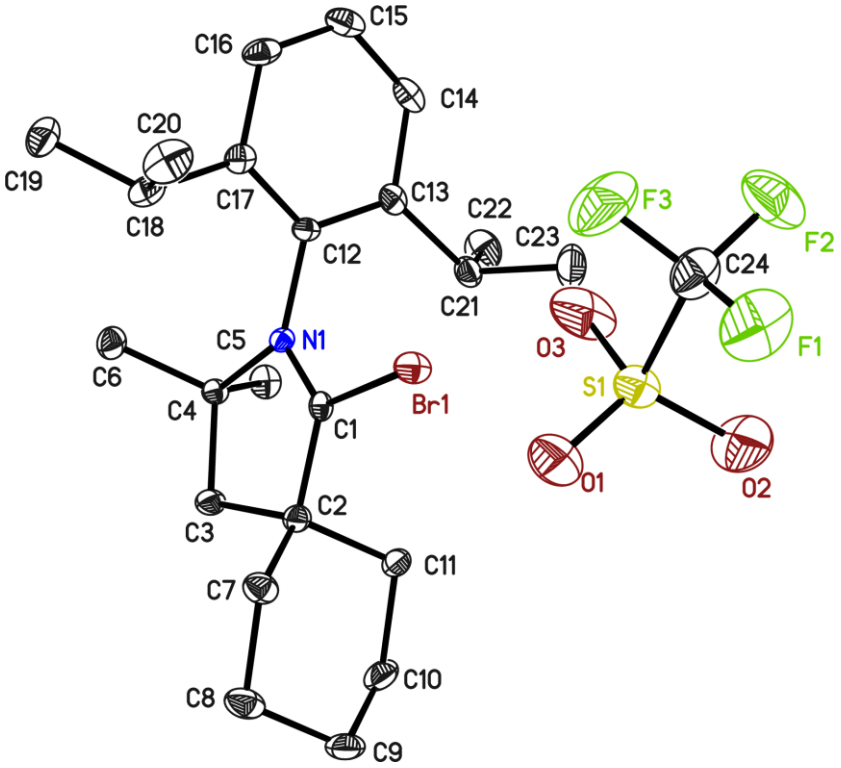

Figure 5.2.8: Asymmetric unit of [$C_{24}H_{35}BrF_3NO_3S$]. The anisotropic displacement parameters are depicted at the 50 % probability level. The hydrogen atoms are omitted for clarity.

structure code	PST_KM221b	Z	4
Empirical formula	$C_{24}H_{35}BrF_3NO_3S$	ρ_{calc} [Mg·m^{-3}]	1.438
Formula weight [g/mol]	554.50	μ [mm^{-1}]	1.734
Temperature [K]	101(2)	F(000)	1152
Wavelength [Å]	0.71073	θ range [°]	1.243 to 25.362
Crystal system	Monoclinic	Reflections collected	35777
space group	$P2_1/n$	Independent reflections	4684
a [Å]	10.647(2)	R(int)	0.0313
b [Å]	16.383(2)	Max. / min transmission	0.8201 / 0.7524
c [Å]	14.680(3)	Restraints / parameter	0 / 305
α [°]	90	GooF	1.106
β [°]	90.209(4)	R1 /*w*R2 (I > 2σ(I))	0.0304 / 0.0771
γ [°]	90	R1/ *w*R2 (all data)	0.0325 / 0.0783
Volume [Å³]	2560.6(8)	max. diff peak / hole [e·Å-^{3}]	0.595 / -0.661

Table 5.2.5: Crystallographic data of [$C_{24}H_{35}BrF_3NO_3S$].

5.2.2 Structures determined with Dr. Yan Li within the group of Prof. Dr. H. W. Roesky

CCDC number	Reference
944815 944816 944817 944818 944819	Li, Y.; Mondal, K. C.; Roesky, H. W.; Zhu, H.; Stollberg, P.; Herbst-Irmer, R.; Stalke, D.; Andrada, D. M., *Journal of the American Chemical Society* **2013,** *135* (33), 12422-12428.
953613 953614 953615 953616	Li, Y.; Mondal, K. C.; Stollberg, P.; Zhu, H.; Roesky, H. W.; Herbst-Irmer, R.; Stalke, D.; Fliegl, H., *Chemical Communications* **2014,** *50* (25), 3356-3358.

Table 5.2.6: Published structures in cooperation with Dr. Yan Li.

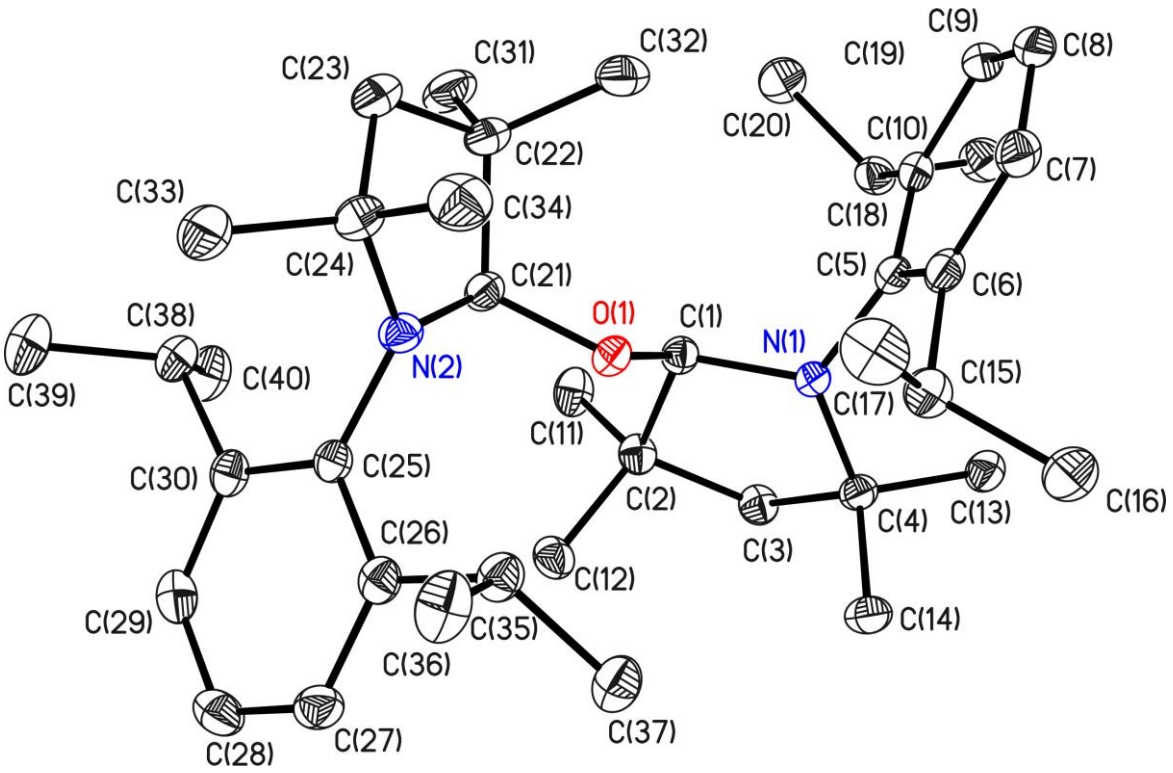

Figure 5.2.9: Asymmetric unit of CCDC no. 944815. The anisotropic displacement parameters are depicted at the 50 % probability level. The hydrogen atoms are omitted for clarity.

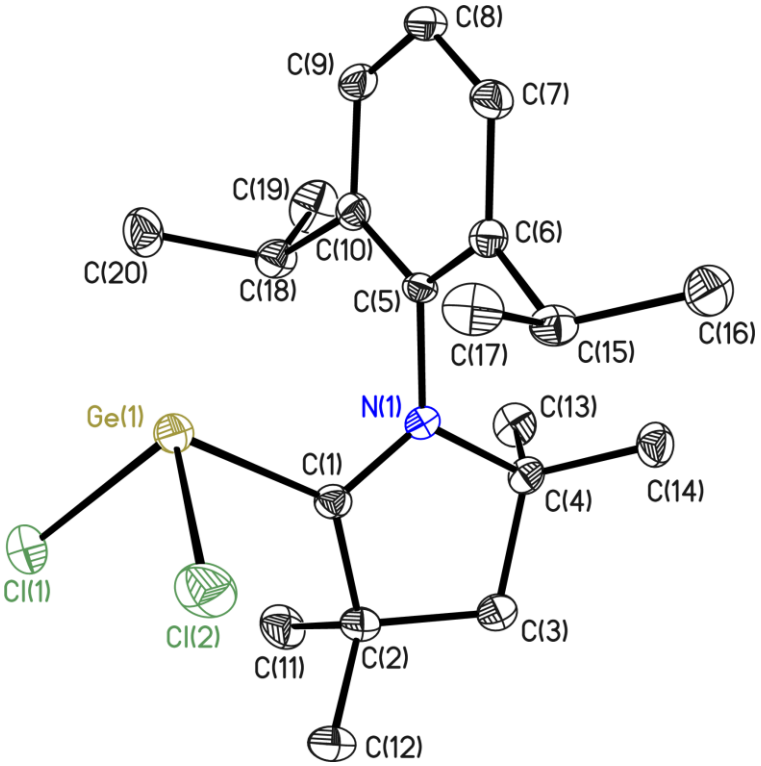

Figure 5.2.10: Asymmetric unit of CCDC no. 944816. The anisotropic displacement parameters are depicted at the 50 % probability level. The hydrogen atoms are omitted for clarity.

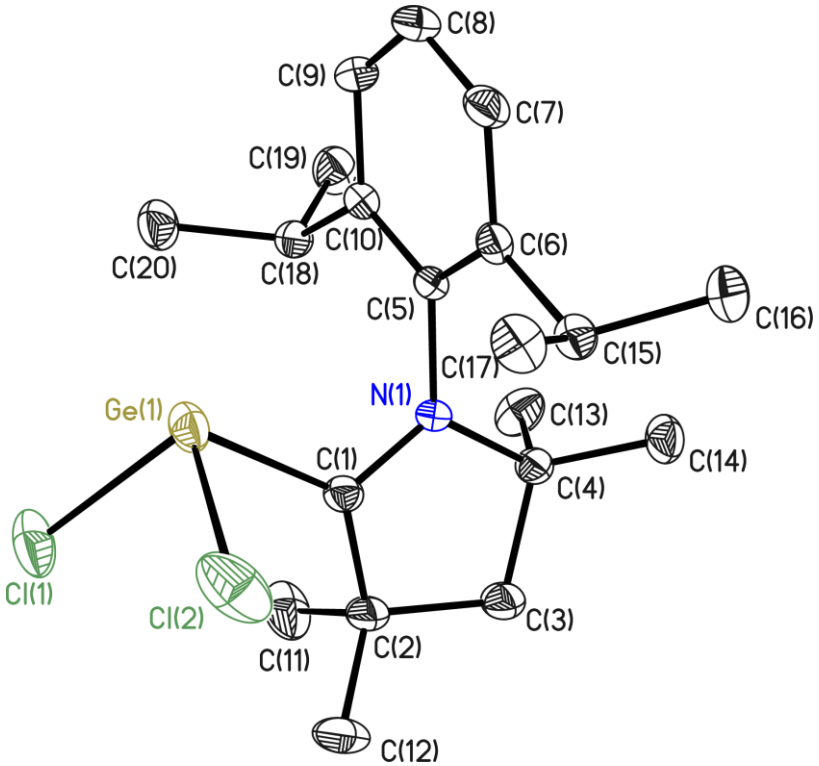

Figure 5.2.11: Asymmetric unit of CCDC no. 944817. The anisotropic displacement parameters are depicted at the 50 % probability level. The hydrogen atoms are omitted for clarity.

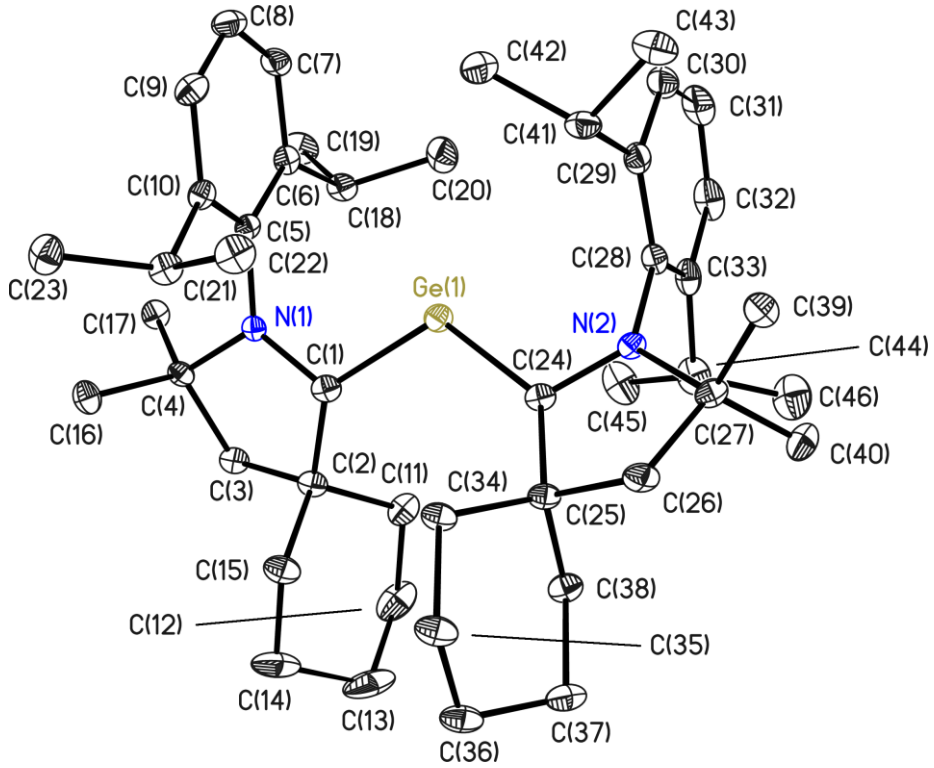

Figure 5.2.12: Asymmetric unit of CCDC no. 944818. The anisotropic displacement parameters are depicted at the 50 % probability level. The hydrogen atoms are omitted for clarity.

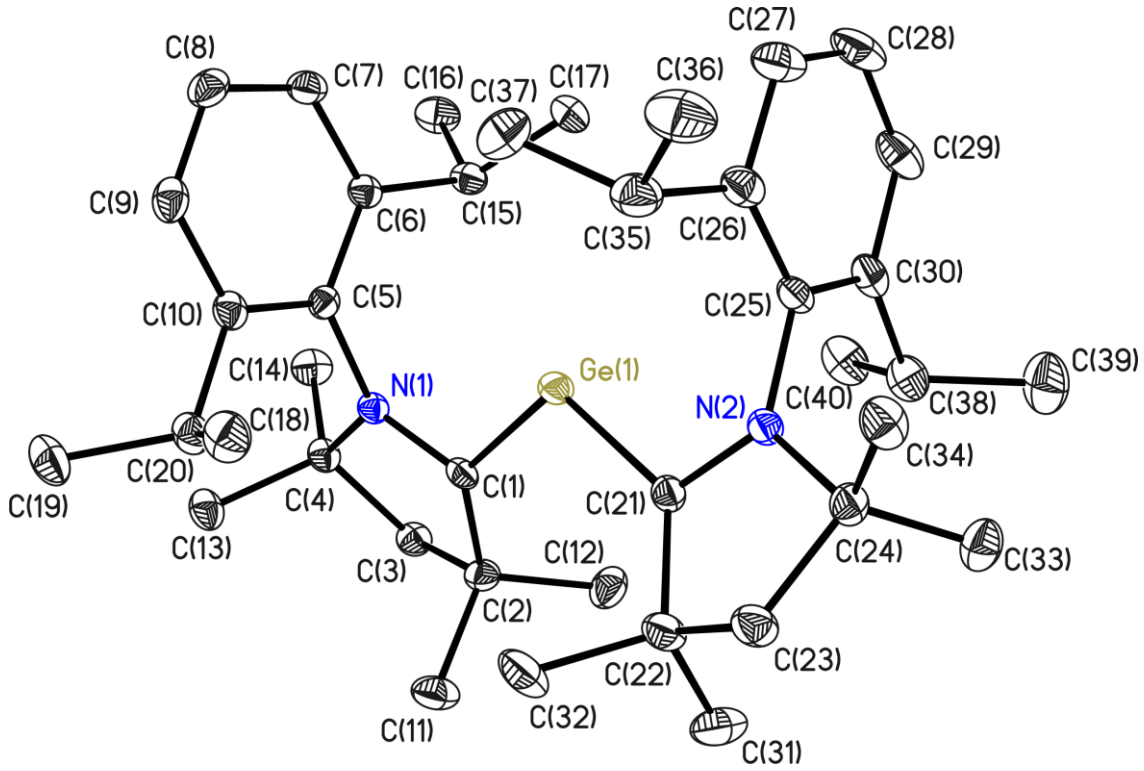

Figure 5.2.13: Asymmetric unit of CCDC no. 944819. The anisotropic displacement parameters are depicted at the 50 % prob-ability level. The hydrogen atoms are omitted for clarity.

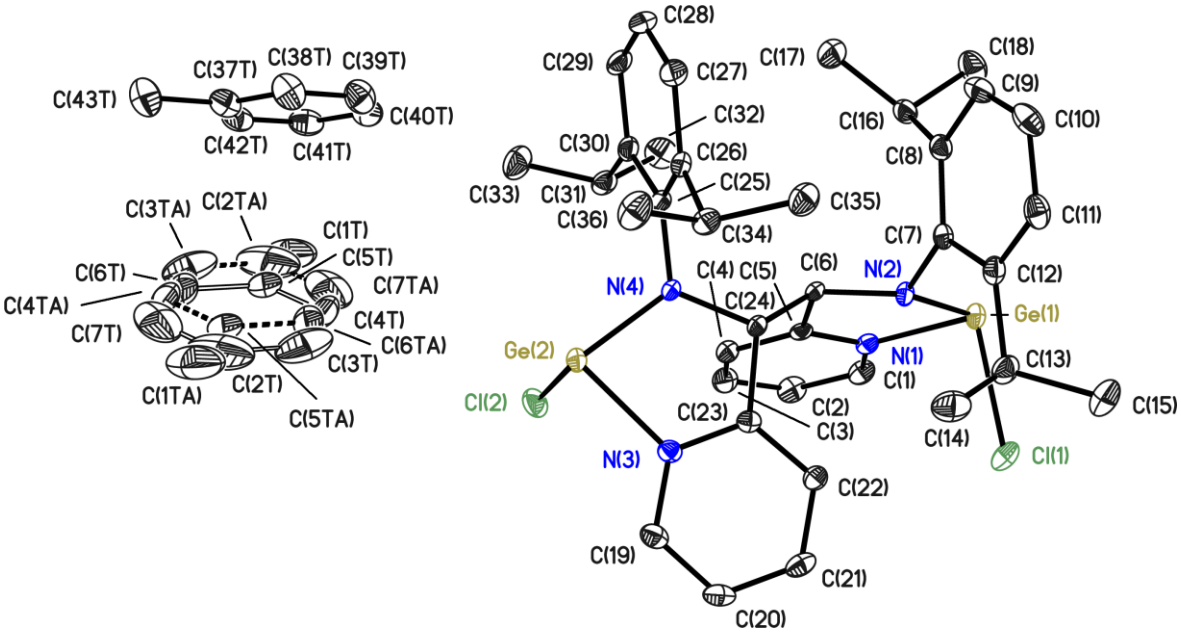

Figure 5.2.14: Asymmetric unit of CCDC no. 953613. The anisotropic displacement parameters are depicted at the 50 % probability level. The hydrogen atoms are omitted for clarity.

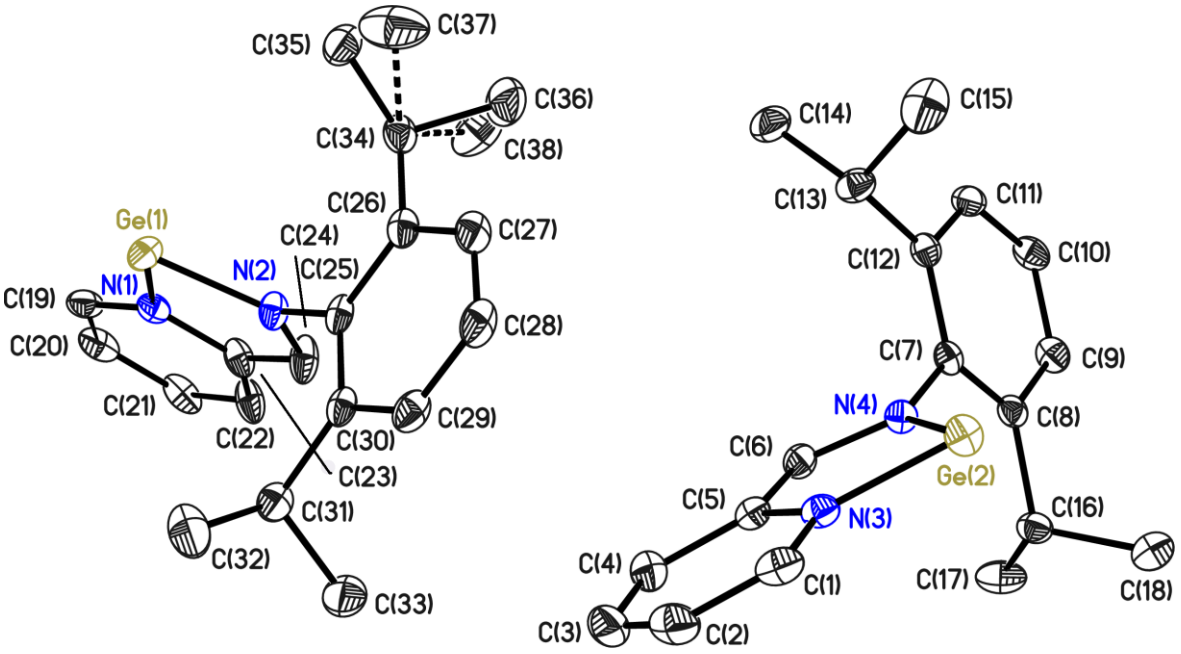

Figure 5.2.15: Asymmetric unit of CCDC no. 953614. The anisotropic displacement parameters are depicted at the 50 % probability level. The hydrogen atoms are omitted for clarity.

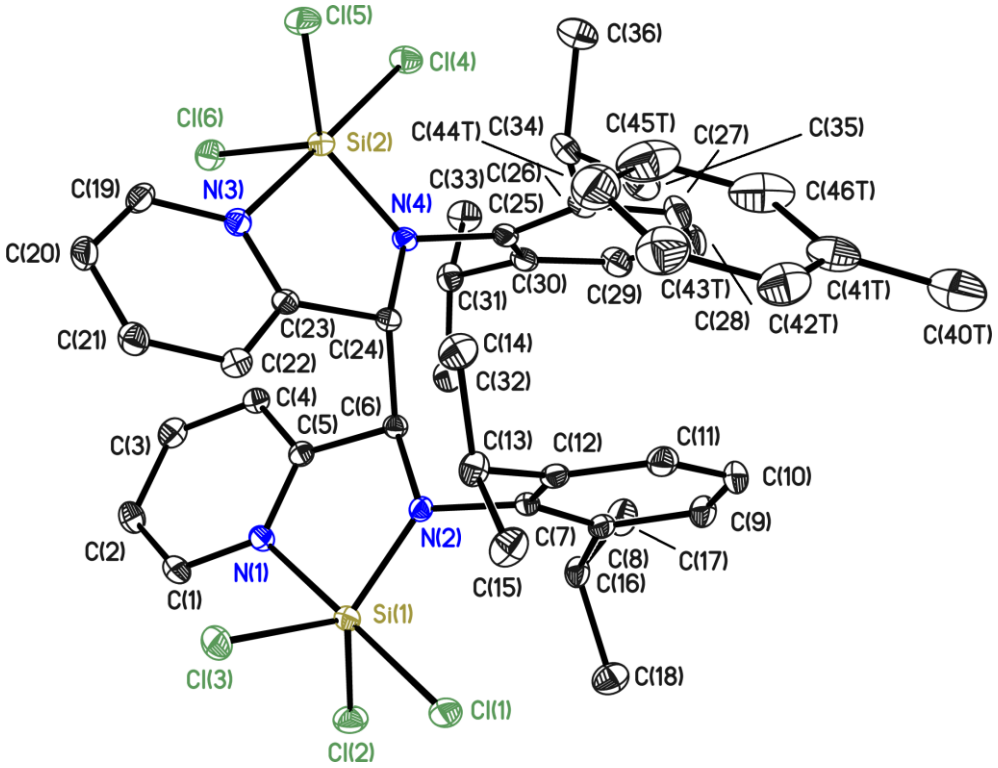

Figure 5.2.16: Asymmetric unit of CCDC no. 953615. The anisotropic displacement parameters are depicted at the 50 % probability level. The hydrogen atoms are omitted for clarity.

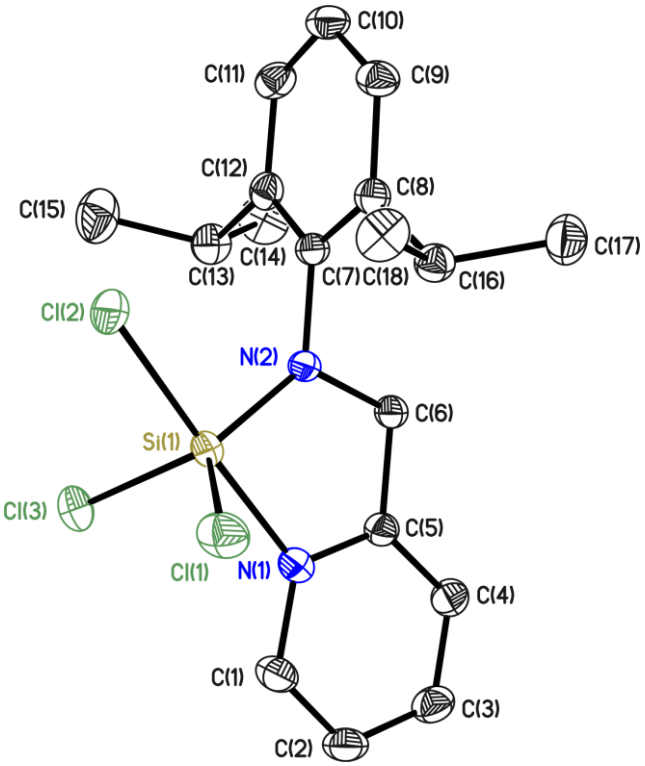

Figure 5.2.17: Asymmetric unit of CCDC no. 953616. The anisotropic displacement parameters are depicted at the 50 % probability level. The hydrogen atoms are omitted for clarity.

5.2.3 Structures determined with DR. M. G. SCHEIBEL within the group of PROF. DR. S. SCHNEIDER

CCDC number	Reference
930856	Scheibel, M. G.; Klopsch, I.; Wolf, H.; Stollberg, P.; Stalke, D.; Schneider, S., *European Journal of Inorganic Chemistry* **2013,** *2013* (20), 3454-3457.

Table 5.2.7: Published structures in cooperation with DR. M. G. SCHEIBEL.

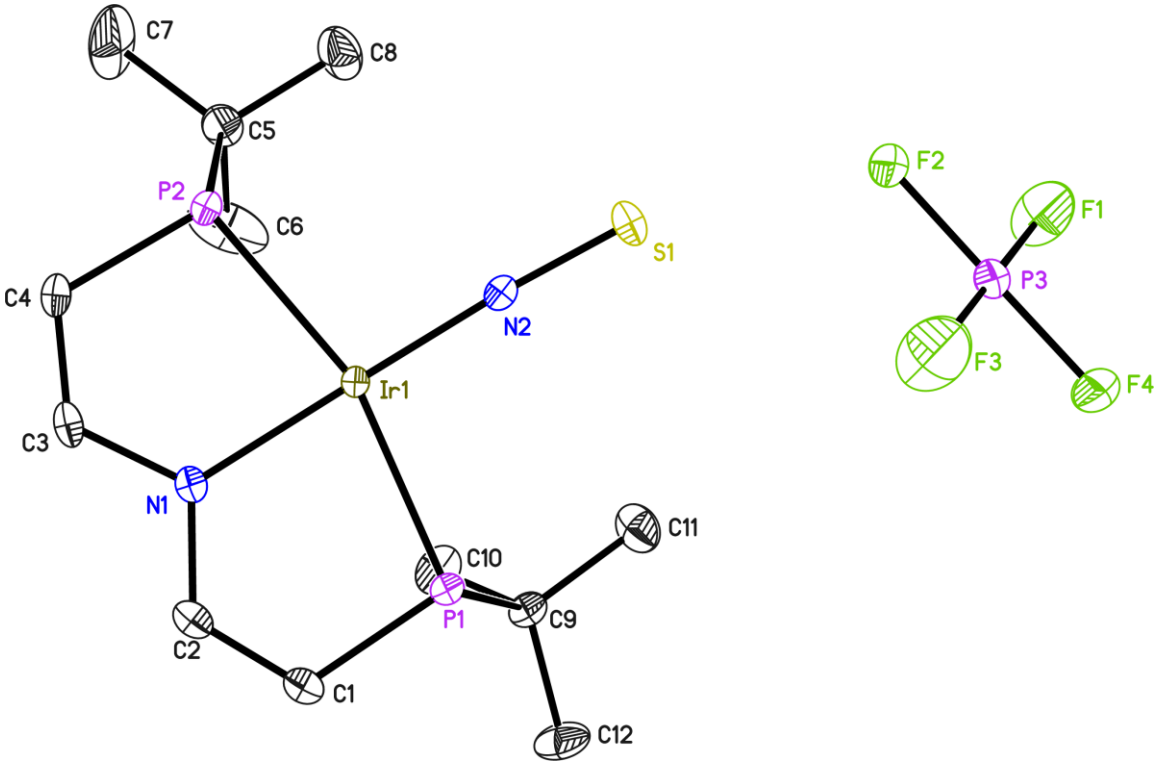

Figure 5.2.18: Asymmetric unit of CCDC no. 930856. The anisotropic displacement parameters are depicted at the 50 % probability level. The hydrogen atoms are omitted for clarity.

5.2.4 Strcutures determined with MARKUS KINAUER within the group of PROF. DR. S. SCHNEIDER

CCDC number	Reference
967913	Scheibel, M. G.; Klopsch, I.; Wolf, H.; Stollberg, P.; Stalke, D.; Schneider, S., *European Journal of Inorganic Chemistry* **2013,** *2013* (20), 3454-3457.

Table 5.2.8: Published structures in cooperation with MARKUS KINAUER.

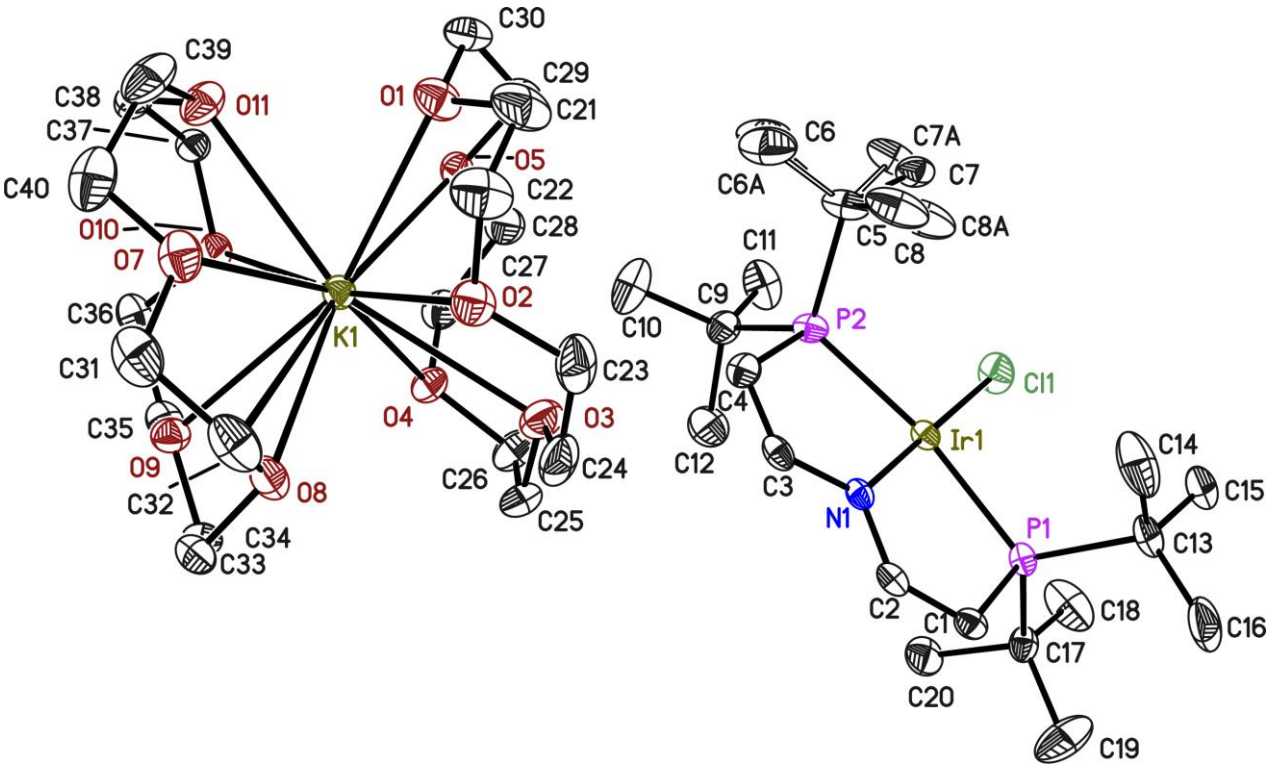

Figure 5.2.19: Asymmetric unit of CCDC no. 967913. The anisotropic displacement parameters are depicted at the 50 % prob-ability level. The hydrogen atoms are omitted for clarity.

5.2.5 Structures determined with FLAVIO FANELLI within the group of PROF. DEGENNARO LEONARDO, PH. D.

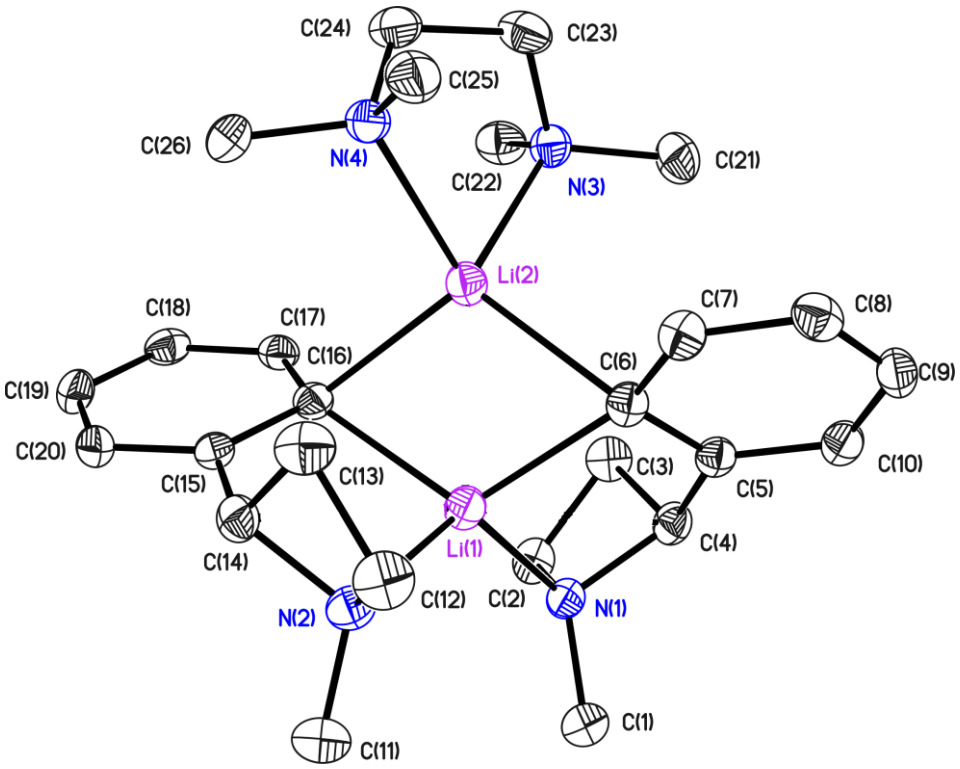

Figure 5.2.20: Asymmetric unit of [$C_{26}H_{40}Li_2N_4$]. The anisotropic displacement parameters are depicted at the 50 % probability level. The hydrogen atoms are omitted for clarity.

structure code	PST_FF_01	Z	8
Empirical formula	$C_{26}H_{40}Li_2N_4$	ρ_{calc} [Mg·m^{-3}]	1.078
Formula weight [g/mol]	422.50	μ [mm^{-1}]	0.063
Temperature [K]	100(2)	F(000)	1840
Wavelength [Å]	0.71073	θ range [°]	1.530 to 25.369
Crystal system	Orthorhombic	Reflections collected	56692
space group	Pbca	Independent reflections	4778
a [Å]	11.043(2)	R(int)	0.0625
b [Å]	17.723(3)	Max. / min transmission	
c [Å]	26.612(5)	Restraints / parameter	0 / 295
α [°]	90	GooF	1.044
β [°]	90	R1 /*w*R2 (I > 2σ(I))	0.0438 / 0.0948
γ [°]	90	R1/ *w*R2 (all data)	0.0633 / 0.1035
Volume [Å³]	5208.4(16)	max. diff peak / hole [e·Å-^{3}]	0.234 / -0.187

Table 5.2.9: Crystal data of [$C_{26}H_{40}Li_2N_4$].

5.2.6 Structures determined with DR. CHRISTIAN ROßNER within the group of PROF. DR. VANA

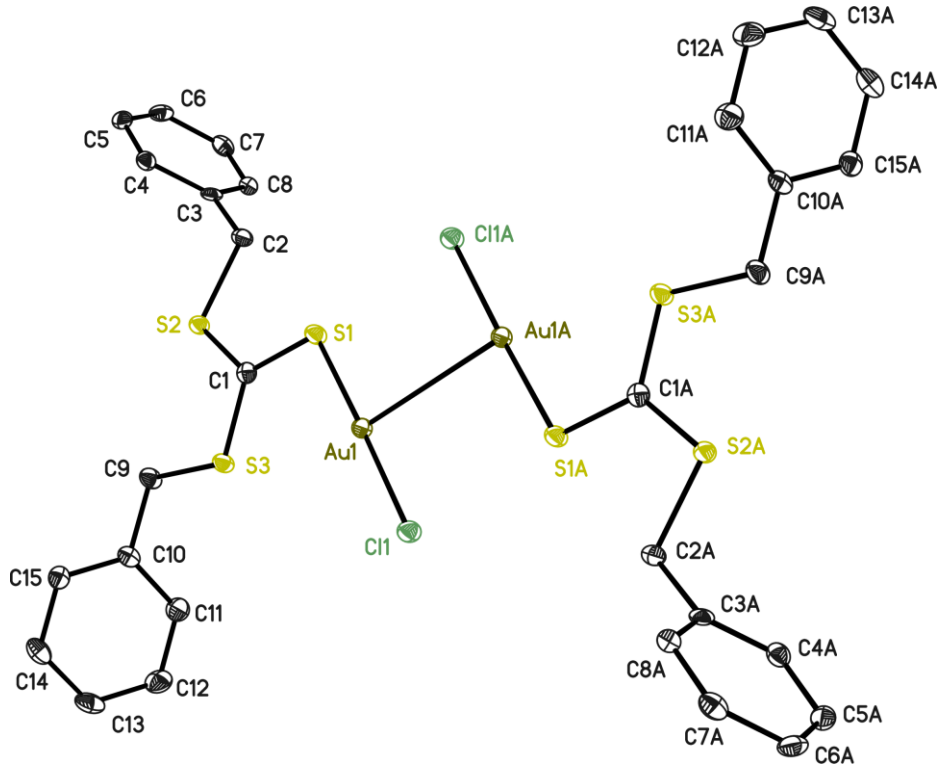

Figure 5.2.21: Asymmetric unit of $[C_{30}H_{28}Au_2Cl_2S_6]$. The anisotropic displacement parameters are depicted at the 50 % probability level. The hydrogen atoms are omitted for clarity.

structure code	PST_Vana_1	Z	2
Empirical formula	$C_{30}H_{28}Au_2Cl_2S_6$	ρ_{calc} [Mg·m^{-3}]	2.171
Formula weight [g/mol]	1045.72	μ [mm^{-1}]	9.739
Temperature [K]	100(2)	F(000)	992
Wavelength [Å]	0.71073	θ range [°]	0.870 to 25.354
Crystal system	Monoclinic	Reflections collected	23928
space group	$P2_1/c$	Independent reflections	2977
a [Å]	11.25(2)	R(int)	0.0287
b [Å]	6.08(2)	Max. / min transmission	0.3574 / 0.2575
c [Å]	23.43(3)	Restraints / parameter	0 / 182
α [°]	90	GooF	1.190
β [°]	92.933(2)	R1 /*w*R2 (I > 2σ(I))	0.0139 / 0.0311
γ [°]	90	R1/ *w*R2 (all data)	0.0152 / 0.0319
Volume [Å³]	1600(6)	max. diff peak / hole [e·Å^{-3}]	1.953 / -1.666

Table 5.2.10: Crystal data of $[C_{30}H_{28}Au_2Cl_2S_6]$.

5.2.7 Structures determined with JOHANNES KRETSCH within the group of PROF. DR. STALKE

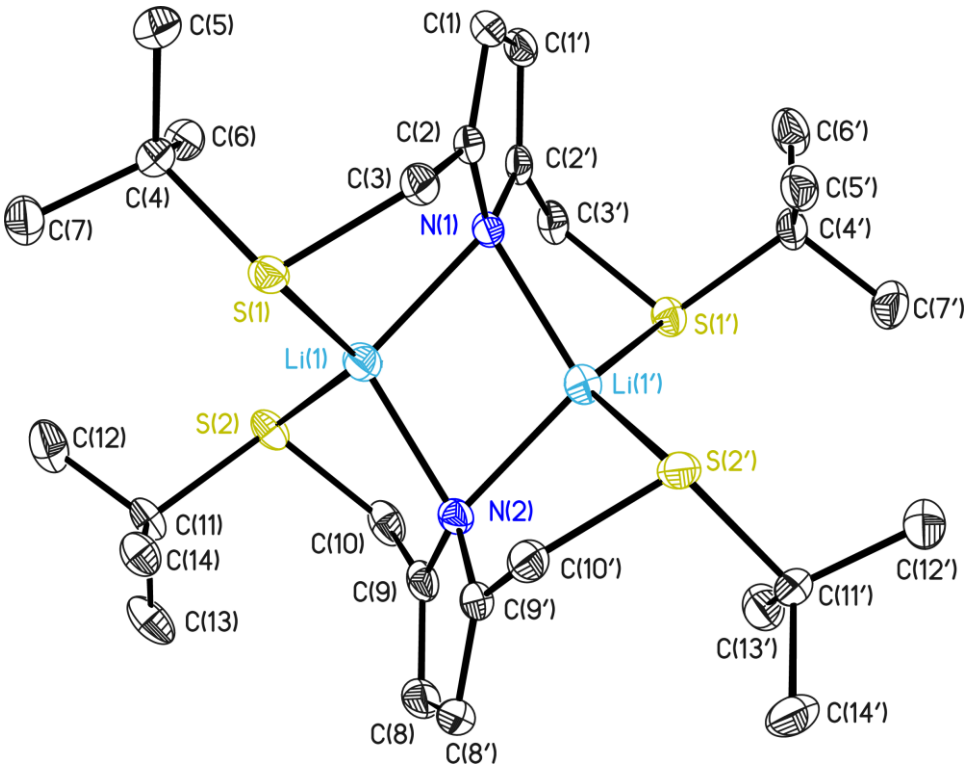

Figure 5.2.22: Asymmetric unit of [$C_{28}H_{48}Li_2N_2S_4$]. The anisotropic displacement parameters are depicted at the 50 % probability level. The hydrogen atoms are omitted for clarity.

structure code	PST_JK_Li	Z	4
Empirical formula	$C_{28}H_{48}Li_2N_2S_4$	ρ_{calc} [Mg·m^{-3}]	1.159
Formula weight [g/mol]	554.80	μ [mm^{-1}]	0.317
Temperature [K]	100(2)	F(000)	1200
Wavelength [Å]	0.71073	θ range [°]	1.346 to 25.363
Crystal system	Monoclinic	Reflections collected	45713
space group	$P2_1/n$	Independent reflections	5791
a [Å]	16.526(2)	R(int)	0.0307
b [Å]	10.186(2)	Max. / min transmission	0.9446 / 0.9224
c [Å]	20.608(3)	Restraints / parameter	0 / 337
α [°]	90	GooF	1.034
β [°]	113.5680(10)	R1 /*w*R2 (I > 2σ(I))	0.0278 / 0.0667
γ [°]	90	R1/ *w*R2 (all data)	0.0334 / 0.0698
Volume [Å³]	3179.7(9)	max. diff peak / hole [e·Å^{-3}]	0.262 / -0.195

Table 5.2.11: Crystal data of [$C_{28}H_{48}Li_2N_2S_4$].

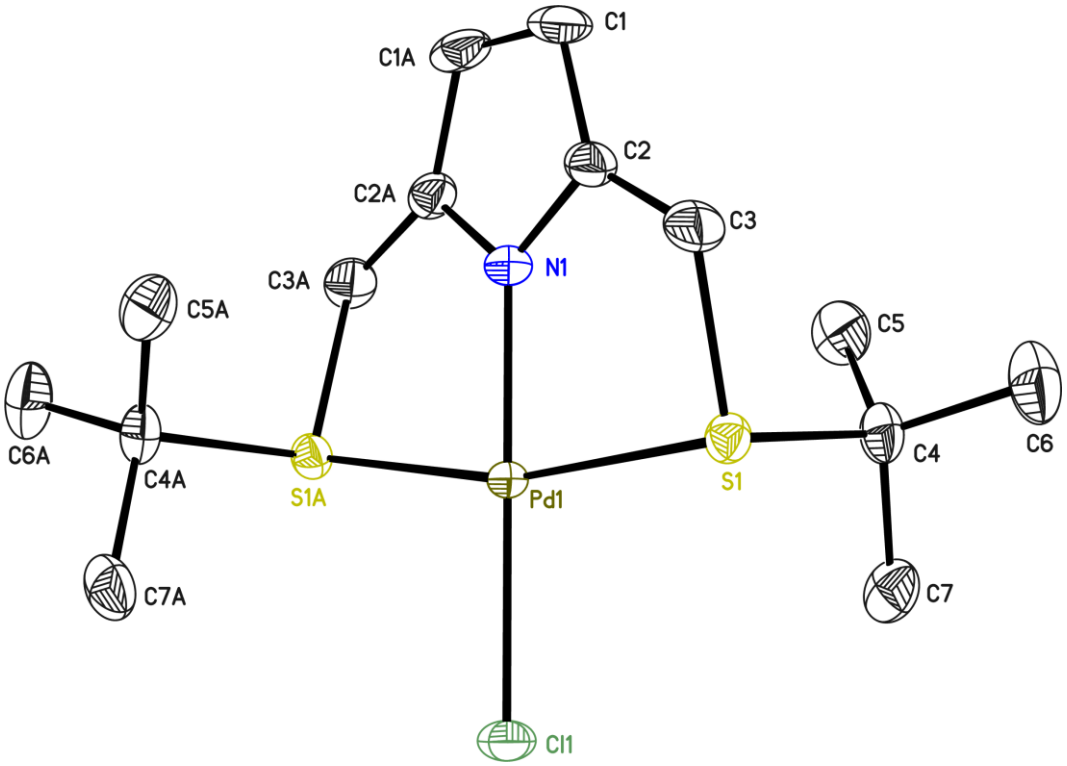

Figure 5.2.23: Asymmetric unit of [$C_{14}H_{24}ClNPdS_2$]. The anisotropic displacement parameters are depicted at the 50 % probability level. The hydrogen atoms are omitted for clarity.

structure code	PST_JK_Pd	Z	4
Empirical formula	$C_{14}H_{24}ClNPdS_2$	ρ_{calc} [Mg·m^{-3}]	1.619
Formula weight [g/mol]	412.31	μ [mm^{-1}]	1.489
Temperature [K]	100(2)	F(000)	840
Wavelength [Å]	0.71073	θ range [°]	2.564 to 25.359
Crystal system	Orthorhombic	Reflections collected	18305
space group	Pbcn	Independent reflections	1556
a [Å]	9.6011(10)	R(int)	0.0430
b [Å]	14.1382(15)	Max. / min transmission	
c [Å]	12.4604(13)	Restraints / parameter	0 / 91
α [°]	90	GooF	1.087
β [°]	90	R1 /*w*R2 (I > 2σ(I))	0.0196 / 0.0474
γ [°]	90	R1/ *w*R2 (all data)	0.0246 / 0.0499
Volume [Å³]	1691.4(3)	max. diff peak / hole [e·Å-^{3}]	0.359 / -0.607

Table 5.2.12: Crystal data of [$C_{14}H_{24}ClNPdS_2$].

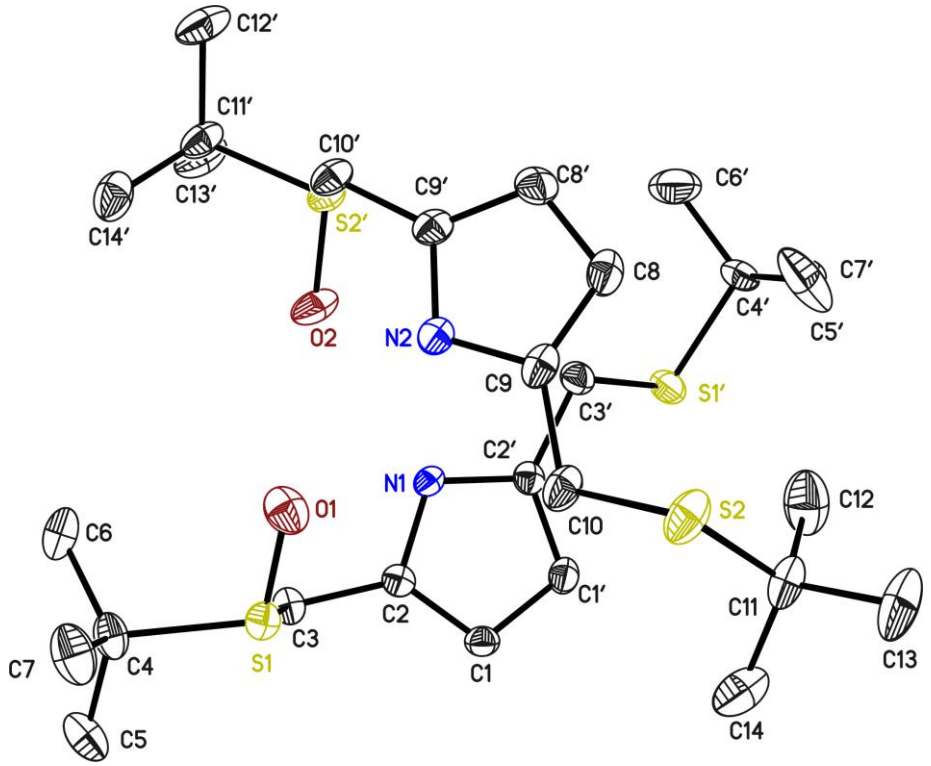

Figure 5.2.24: Asymmetric unit of [$C_{14}H_{25}NOS_2$]. The anisotropic displacement parameters are depicted at the 50 % probability level. The hydrogen atoms are omitted for clarity.

structure code	PST_JK_Ligand	Z	4
Empirical formula	$C_{14}H_{25}NOS_2$	ρ_{calc} [Mg·m^{-3}]	1.165
Formula weight [g/mol]	287.47	μ [mm^{-1}]	0.316
Temperature [K]	100(2)	F(000)	624
Wavelength [Å]	0.71073	θ range [°]	1.574 to 25.356
Crystal system	Triclinic	Reflections collected	24822
space group	$P\bar{1}$	Independent reflections	5993
a [Å]	11.189(2)	R(int)	0.0283
b [Å]	11.507(2)	Max. / min transmission	0.9583 / 0.9250
c [Å]	13.473(3)	Restraints / parameter	0 / 337
α [°]	90.3660(10)	GooF	1.034
β [°]	105.8660(10)	R1 /*w*R2 (I > 2σ(I))	0.0393 / 0.0903
γ [°]	100.3650(10)	R1/ *w*R2 (all data)	0.0478 / 0.0951
Volume [Å³]	1638.5(5)	max. diff peak / hole [e·Å^{-3}]	1.076 / -0.452

Table 5.2.13: Crystal data of [$C_{14}H_{25}NOS_2$].

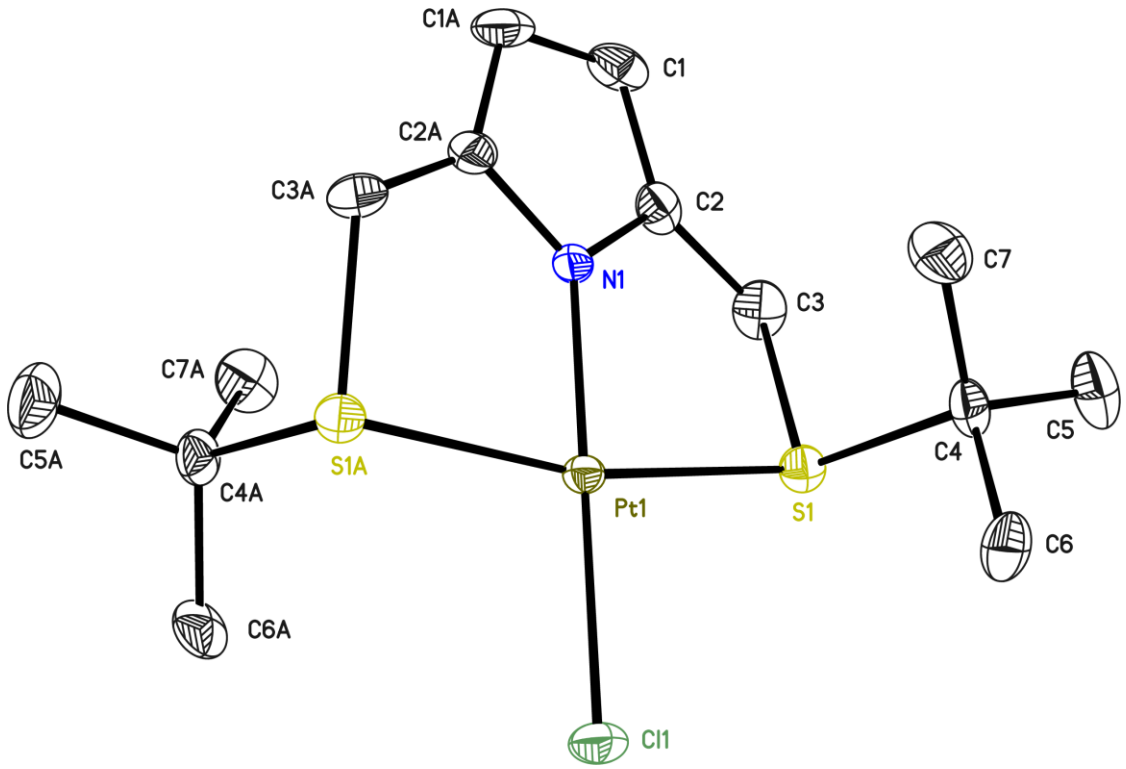

Figure 5.2.25: Asymmetric unit of [$C_{14}H_{24}ClNPtS_2$]. The anisotropic displacement parameters are depicted at the 50 % probability level. The hydrogen atoms are omitted for clarity.

structure code	PST_JK_Pt1	Z	4
Empirical formula	$C_{14}H_{24}ClNPtS_2$	ρ_{calc} [Mg·m^{-3}]	1.964
Formula weight [g/mol]	501.00	μ [mm^{-1}]	4.700
Temperature [K]	100(2)	F(000)	968
Wavelength [Å]	0.56086	θ range [°]	2.035 to 19.760
Crystal system	Orthorhombic	Reflections collected	24309
space group	Pbcn	Independent reflections	1564
a [Å]	9.492(2)	R(int)	0.0487
b [Å]	14.236(3)	Max. / min transmission	0.5511 / 0.4607
c [Å]	12.536(3)	Restraints / parameter	0 / 91
α [°]	90	GooF	1.047
β [°]	90	R1 /*w*R2 (I > 2σ(I))	0.0186 / 0.0365
γ [°]	90	R1/ *w*R2 (all data)	0.0301 / 0.0412
Volume [Å³]	1694.0(6)	max. diff peak / hole [e·Å-^{3}]	0.908 / -0.659

Table 5.2.14: Crystallographic data of [$C_{14}H_{24}ClNPtS2$].

5.2.8 Structures determined with LEONARDO ROJAS within the group of MAVIS MONTERO, PH.D.

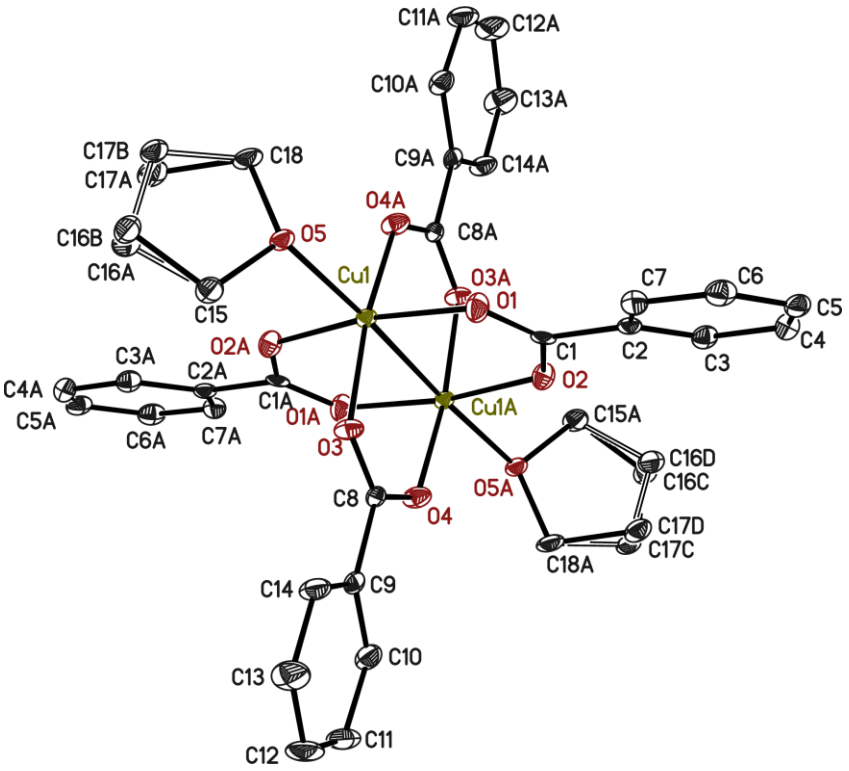

Figure 5.2.26: Asymmetric unit of [$C_{36}H_{36}Cu_2O_{10}$]. The anisotropic displacement parameters are depicted at the 50 % probability level. The hydrogen atoms are omitted for clarity.

structure code	3Y5_02_high	Z	2
Empirical formula	$C_{36}H_{36}Cu_2O_{10}$	ρ_{calc} [Mg·m^{-3}]	1.546
Formula weight [g/mol]	755.73	μ [mm^{-1}]	0.726
Temperature [K]	100(2)	F(000)	780
Wavelength [Å]	0.56086	θ range [°]	1.810 to 20.534
Crystal system	Monoclinic	Reflections collected	16520
space group	$P2_1/c$	Independent reflections	3330
a [Å]	9.079(2)	R(int)	0.0734
b [Å]	17.274(3)	Max. / min transmission	0.7445 / 0.5034
c [Å]	10.949(2)	Restraints / parameter	128 / 236
α [°]	90	GooF	1.035
β [°]	109.06(2)	R1 /*w*R2 (I > 2σ(I))	0.0427 / 0.1042
γ [°]	90	R1/ *w*R2 (all data)	0.0566 / 0.1118
Volume [Å³]	1623.0(6)	max. diff peak / hole [e·Å^{-3}]	0.887 / -0.858

Table 5.2.15: Crystallographic data of [$C_{36}H_{36}Cu_2O_{10}$].

REFERENCES

[1] Saouma, C. T.; Peters, J. C. *Coord. Chem. Rev.* **2011**, *255* (7), 920-937.

[2] G., B. A. *Eur. J. Inorg. Chem.* **2008**, *2008* (17), 2633-2647.

[3] Seebacher, J.; Vahrenkamp, H. *J. Mol. Struct.* **2003**, *656* (1), 177-181.

[4] Ruiz-Botella, S.; Vidossich, P.; Ujaque, G.; Peris, E.; Beer, P. D. *RSC Advances* **2017**, *7* (19), 11253-11258.

[5] Rodríguez, L.-I.; Roth, T.; Lloret Fillol, J.; Wadepohl, H.; Gade, L. H. *Chemistry – A European Journal* **2012**, *18* (12), 3721-3728.

[6] Hu, X.; Tang, Y.; Gantzel, P.; Meyer, K. *Organometallics* **2003**, *22* (4), 612-614.

[7] García-Álvarez, J.; García-Garrido, S. E.; Cadierno, V. *J. Organomet. Chem.* **2014**, *751* 792-808.

[8] Aizpurua, J. M.; Sagartzazu-Aizpurua, M.; Monasterio, Z. Mesoionic 1,2,3-Triazoles and 1,2,3-Triazole Carbenes In *Chemistry of 1,2,3-triazoles*; Dehaen, W., Bakulev, V. A., Eds.; Springer International Publishing: Cham, 2015, 211-267.

[9] Mathew, P.; Neels, A.; Albrecht, M. *J. Am. Chem. Soc.* **2008**, *130* (41), 13534-13535.

[10] Wanzlick, H. W. *Angew. Chem. Int. Ed.* **1962**, *1* (2), 75-80.

[11] Herrmann, W. A. *Angew. Chem. Int. Ed.* **2002**, *41* (8), 1290-1309.

[12] Bourissou, D.; Guerret, O.; Gabbaï, F. P.; Bertrand, G. *Chem. Rev.* **2000**, *100* (1), 39-92.

[13] Arduengo, A. J. *Acc. Chem. Res.* **1999**, *32* (11), 913-921.

[14] Trofimenko, S. *J. Am. Chem. Soc.* **1966**, *88* (8), 1842-1844.

[15] Trofimenko, S. *Chem. Rev.* **1972**, *72* (5), 497-509.

[16] Trofimenko, S. *Chem. Rev.* **1993**, *93* (3), 943-980.

[17] Bellemin-Laponnaz, S.; Gade, L. H. *Angew. Chem.* **2002**, *114* (18), 3623-3625.

[18] Whitesell, J. K. *Chem. Rev.* **1989**, *89* (7), 1581-1590.

[19] Rück-Braun, M. M. K. C3-Symmetric Ligands for Catalysis In *Organic Synthesis Highlights IV* 2000, 187-193.

[20] Burk, M. J.; Harlow, R. L. *Angew. Chem. Int. Ed.* **1990**, *29* (12), 1462-1464.

[21] Moberg, C. *Angew. Chem. Int. Ed.* **2006**, *45* (29), 4721-4723.

[22] Mata, J. A.; Poyatos, M.; Peris, E. *Coord. Chem. Rev.* **2007**, *251* (5–6), 841-859.

[23] Dias, H. V. R.; Jin, W. *Tetrahedron Lett.* **1994**, *35* (9), 1365-1366.

[24] Mas-Marzá, E.; Poyatos, M.; Sanaú, M.; Peris, E. *Inorg. Chem.* **2004**, *43* (6), 2213-2219.

[25] Schrock, R. R. *Acc. Chem. Res.* **1997**, *30* (1), 9-16.

[26] Hellmann, K. W.; Friedrich, S.; Gade, L. H.; Li, W.-S.; McPartlin, M. *Chem. Ber.* **1995**, *128* (1), 29-34.

[27] Gade, L. H. *Acc. Chem. Res.* **2002**, *35* (7), 575-582.

[28] Murso, A.; Stalke, D. *Z. Anorg. Allg. Chem.* **2004**, *630* (7), 1025-1030.

[29] Miyaura, N.; Yamada, K.; Suzuki, A. *Tetrahedron Lett.* **1979**, *20* (36), 3437-3440.

[30] Tamao, K.; Sumitani, K.; Kumada, M. *J. Am. Chem. Soc.* **1972**, *94* (12), 4374-4376.

[31] Sonogashira, K. *J. Organomet. Chem.* **2002**, *653* (1), 46-49.

[32] Hauwert, P.; Boerleider, R.; Warsink, S.; Weigand, J. J.; Elsevier, C. J. *J. Am. Chem. Soc.* **2010**, *132* (47), 16900-16910.

[33] Sprengers, J. W.; Wassenaar, J.; Clement, N. D.; Cavell, K. J.; Elsevier, C. J. *Angew. Chem.* **2005**, *117* (13), 2062-2065.

[34] Bortenschlager, M.; Schütz, J.; von Preysing, D.; Nuyken, O.; Herrmann, W. A.; Weberskirch, R. *J. Organomet. Chem.* **2005**, *690* (24), 6233-6237.

[35] Donnelly, K. F.; Petronilho, A.; Albrecht, M. *Chem. Commun.* **2013**, *49* (12), 1145-1159.

[36] Schreiner, P. R.; Reisenauer, H. P.; Pickard Iv, F. C.; Simmonett, A. C.; Allen, W. D.; Matyus, E.; Csaszar, A. G. *Nature* **2008**, *453* (7197), 906-909.

[37] IUPAC *Compendium of Chemical Terminology - Gold Book*; IUPAC, 2014; Vol. Version 2.3.3.

[38] Dorta, R.; Stevens, E. D.; Scott, N. M.; Costabile, C.; Cavallo, L.; Hoff, C. D.; Nolan, S. P. *J. Am. Chem. Soc.* **2005**, *127* (8), 2485-2495.

[39] de Frémont, P.; Scott, N. M.; Stevens, E. D.; Ramnial, T.; Lightbody, O. C.; Macdonald, C. L. B.; Clyburne, J. A. C.; Abernethy, C. D.; Nolan, S. P. *Organometallics* **2005**, *24* (26), 6301-6309.

[40] Richards, C. A.; Kim, S.-J.; Yamaguchi, Y.; Schaefer, H. F. *J. Am. Chem. Soc.* **1995**, *117* (40), 10104-10107.

[41] Myers, D. R.; Senthilnathan, V. P.; Platz, M. S.; Jones, M. *J. Am. Chem. Soc.* **1986**, *108* (14), 4232-4233.

[42] Boehme, C.; Frenking, G. *J. Am. Chem. Soc.* **1996**, *118* (8), 2039-2046.

[43] Wanzlick, H. W.; Schikora, E. *Angew. Chem.* **1960**, *72* (14), 494-494.

[44] Wanzlick, H. W.; Schönherr, H. J. *Angew. Chem. Int. Ed.* **1968**, *7* (2), 141-142.

[45] Arduengo, A. J.; Harlow, R. L.; Kline, M. *J. Am. Chem. Soc.* **1991**, *113* (1), 361-363.

[46] Arduengo, A. J.; Dias, H. V. R.; Harlow, R. L.; Kline, M. *J. Am. Chem. Soc.* **1992**, *114* (14), 5530-5534.

[47] Arduengo, A. J.; Goerlich, J. R.; Marshall, W. J. *Liebigs Annalen* **1997**, *1997* (2), 365-374.

[48] Alder, R. W.; Butts, C. P.; Orpen, A. G. *J. Am. Chem. Soc.* **1998**, *120* (44), 11526-11527.

[49] Lavallo, V.; Canac, Y.; Donnadieu, B.; Schoeller, W. W.; Bertrand, G. *Science* **2006**, *312* (5774), 722-724.

[50] Herrmann, W. A.; Köcher, C.; Gooßen, L. J.; Artus, G. R. J. *Chemistry – A European Journal* **1996**, *2* (12), 1627-1636.

[51] Magill, A. M.; Cavell, K. J.; Yates, B. F. *J. Am. Chem. Soc.* **2004**, *126* (28), 8717-8724.

[52] Huynh, H. V.; Han, Y.; Jothibasu, R.; Yang, J. A. *Organometallics* **2009**, *28* (18), 5395-5404.

[53] Tolman, C. A. *Chem. Rev.* **1977**, *77* (3), 313-348.

[54] Dröge, T.; Glorius, F. *Angew. Chem. Int. Ed.* **2010**, *49* (39), 6940-6952.

[55] Lever, A. B. P. *Inorg. Chem.* **1990**, *29* (6), 1271-1285.

[56] Enders, D.; Niemeier, O.; Henseler, A. *Chem. Rev.* **2007**, *107* (12), 5606-5655.

[57] Vougioukalakis, G. C.; Grubbs, R. H. *Chem. Rev.* **2010**, *110* (3), 1746-1787.

[58] Garber, S. B.; Kingsbury, J. S.; Gray, B. L.; Hoveyda, A. H. *J. Am. Chem. Soc.* **2000**, *122* (34), 8168-8179.

[59] Schuster, O.; Yang, L.; Raubenheimer, H. G.; Albrecht, M. *Chem. Rev.* **2009**, *109* (8), 3445-3478.

[60] Hollóczki, O.; Nyulászi, L. *J. Org. Chem.* **2008**, *73* (13), 4794-4799.

[61] Lavorato, D.; Terlouw, J.; McGibbon, G.; Dargel, T.; Koch, W.; Schwarz, H. *Int. J. Mass spectrom.* **1998**, *179-180* 7-14.

[62] Gründemann, S.; Kovacevic, A.; Albrecht, M.; Faller, J. W.; Crabtree, R. H. *J. Am. Chem. Soc.* **2002**, *124* (35), 10473-10481.

[63] Grundemann, S.; Kovacevic, A.; Albrecht, M.; Faller Robert, J. W.; Crabtree, H. *Chem. Commun.* **2001** (21), 2274-2275.

[64] Amyes, T. L.; Diver, S. T.; Richard, J. P.; Rivas, F. M.; Toth, K. *J. Am. Chem. Soc.* **2004**, *126* (13), 4366-4374.

[65] Massey, R. S.; Collett, C. J.; Lindsay, A. G.; Smith, A. D.; O'Donoghue, A. C. *J. Am. Chem. Soc.* **2012**, *134* (50), 20421-20432.

[66] Arnold, P. L.; Pearson, S. *Coord. Chem. Rev.* **2007**, *251* (5), 596-609.

[67] Lebel, H.; Janes, M. K.; Charette, A. B.; Nolan, S. P. *J. Am. Chem. Soc.* **2004**, *126* (16), 5046-5047.

[68] Aldeco-Perez, E.; Rosenthal, A. J.; Donnadieu, B.; Parameswaran, P.; Frenking, G.; Bertrand, G. *Science* **2009**, *326* (5952), 556-559.

[69] Heckenroth, M.; Kluser, E.; Neels, A.; Albrecht, M. *Dalton Trans* **2008** (44), 6242-6249.

[70] Guisado-Barrios, G.; Bouffard, J.; Donnadieu, B.; Bertrand, G. *Angew. Chem. Int. Ed. Engl.* **2010**, *49* (28), 4759-4762.

[71] Bouffard, J.; Keitz, B. K.; Tonner, R.; Lavallo, V.; Guisado-Barrios, G.; Frenking, G.; Grubbs, R. H.; Bertrand, G. *Organometallics* **2011**, *30* (9), 2617-2627.

[72] Canseco-Gonzalez, D.; Petronilho, A.; Mueller-Bunz, H.; Ohmatsu, K.; Ooi, T.; Albrecht, M. *J. Am. Chem. Soc.* **2013**, *135* (35), 13193-13203.

[73] Wright, J. R.; Young, P. C.; Lucas, N. T.; Lee, A.-L.; Crowley, J. D. *Organometallics* **2013**, *32* (23), 7065-7076.

[74] Maity, R.; van der Meer, M.; Hohloch, S.; Sarkar, B. *Organometallics* **2015**, *34* (12), 3090-3096.

[75] Hayes, J. M.; Viciano, M.; Peris, E.; Ujaque, G.; Lledós, A. *Organometallics* **2007**, *26* (25), 6170-6183.

[76] Beaufort, L.; Delaude, L.; Noels, A. F. *Tetrahedron* **2007**, *63* (30), 7003-7008.

[77] Kratzert, D. *Charge Density Distribution in Low-Valent Tetreles,* PhD Thesis, Georg-August-University, Göttingen, **2013**.

[78] Kratzert, D. *C3-Symmetrische Iminophosphoranliganden,* Diploma Thesis, Georg-August-University Göttingen, **2008**.

[79] Staudinger, H.; Meyer, J. *Helv. Chim. Acta* **1919**, *2* (1), 635-646.

[80] Kirsanov, A. V. *Zh. Obshch. Khim.* **1952**, *22* (1), 81-88.

[81] Allen, F. H.; Watson, D. G.; Brammer, L.; Orpen, A. G.; Taylor, R. Typical interatomic distances: organic compounds In *International Tables for Crystallography Volume C: Mathematical, physical and chemical tables*; Prince, E., Ed.; Springer Netherlands: Dordrecht, 2004, 790-811.

[82] Mantina, M.; Chamberlin, A. C.; Valero, R.; Cramer, C. J.; Truhlar, D. G. *The Journal of Physical Chemistry A* **2009**, *113* (19), 5806-5812.

[83] Cheng, F.; Hector, A. L.; Levason, W.; Reid, G.; Webster, M.; Zhang, W. *Angew. Chem. Int. Ed.* **2009**, *48* (28), 5152-5154.

[84] Steiner, A.; Stalke, D. *J. Chem. Soc., Chem. Commun.* **1993** (22), 1702-1704.

[85] Krummenacher, I.; Fernández, I.; Rüegger, H.; Weigend, F.; Breher, F. *Dalton Transactions* **2009** (27), 5335-5347.

[86] Krummenacher, I.; Oschwald, C.; Rüegger, H.; Breher, F. *Z. Anorg. Allg. Chem.* **2007**, *633* (13-14), 2354-2361.

[87] Huisgen, R. *Proceedings of the Chemical Society* **1961** (October), 357-396.

[88] Rostovtsev, V. V.; Green, L. G.; Fokin, V. V.; Sharpless, K. B. *Angew. Chem. Int. Ed.* **2002**, *41* (14), 2596-2599.

[89] Tornøe, C. W.; Christensen, C.; Meldal, M. *J. Org. Chem.* **2002**, *67* (9), 3057-3064.

[90] Himo, F.; Lovell, T.; Hilgraf, R.; Rostovtsev, V. V.; Noodleman, L.; Sharpless, K. B.; Fokin, V. V. *J. Am. Chem. Soc.* **2005**, *127* (1), 210-216.

[91] Kolb, H. C.; Finn, M. G.; Sharpless, K. B. *Angew. Chem. Int. Ed.* **2001**, *40* (11), 2004-2021.

[92] Mirjafari, A. *Chem. Commun.* **2018**, *54* (24), 2944-2961.

[93] Matthias, G.; A., L. S. *Angew. Chem. Int. Ed.* **2017**, *56* (49), 15504-15505.

[94] Pickens, C. J.; Johnson, S. N.; Pressnall, M. M.; Leon, M. A.; Berkland, C. J. *Bioconjugate Chem.* **2018**, *29* (3), 686-701.

[95] Steven, M.; O., H. J.; E., D. P. F. *Macromol. Rapid Commun.* **2017**, *38* (24), 1700469.

[96] Baixue, L.; Die, H.; Anjun, Q.; Zhong, T. B. *Macromol. Rapid Commun.*, *0* (0), 1800098.

[97] M. Begtrup, P. L. *Acta Chem Scand.* **1990** (44), 1050-1057.

[98] Abboud, J.-Luis M.; Foces-Foces, C.; Notario, R.; Trifonov, Rostislav E.; Volovodenko, Anna P.; Ostrovskii, Vladimir A.; Alkorta, I.; Elguero, J. *Eur. J. Org. Chem.* **2001**, *2001* (16), 3013-3024.

[99] Reichmann, S. O. **2016**.

[100] Jiang, Y. B.; Kuang, C. X.; Yang, Q. *Synlett* **2009**, *2009* (19), 3163-3166.

[101] Schwarze, E. *Mehrzähnige C3-symmetrische Liganden mit N-heterozyklischer Peripherie*, Georg-August-Universität, Göttingen, **2012**.

[102] Mahatthananchai, J.; Bode, J. W. *Chemical Science* **2012**, *3* (1), 192-197.

[103] Doisneau, G.; Balavoine, G.; Fillebeen-Khan, T. *J. Organomet. Chem.* **1992**, *425* (1), 113-117.

[104] Ciampi, S.; James, M.; Choudhury, M. H.; Darwish, N. A.; Gooding, J. J. *PCCP* **2013**, *15* (24), 9879-9890.

[105] Luo, S.-J.; Liu, Y.-H.; Liu, C.-M.; Liang, Y.-M.; Ma, Y.-X. *Synth. Commun.* **2000**, *30* (9), 1569-1572.

[106] Su, Z.-M.; Lin, C.-X.; Zhou, Y.-T.; Xie, L.-L.; Yuan, Y.-F. *J. Organomet. Chem.* **2015**, *788* 17-26.

[107] Shao, C.; Wang, X.; Xu, J.; Zhao, J.; Zhang, Q.; Hu, Y. *J. Org. Chem.* **2010**, *75* (20), 7002-7005.

[108] Kissinger, P. T.; Heineman, W. R. *J. Chem. Educ.* **1983**, *60* (9), 702.

[109] Noviandri, I.; Brown, K. N.; Fleming, D. S.; Gulyas, P. T.; Lay, P. A.; Masters, A. F.; Phillips, L. *The Journal of Physical Chemistry B* **1999**, *103* (32), 6713-6722.

[110] Choong, S. L.; Jones, C.; Stasch, A. *Dalton Transactions* **2010**, *39* (25), 5774-5776.

[111] Verkade, J. G. *Acc. Chem. Res.* **1993**, *26* (9), 483-489.

[112] Schrock, R. R.; Cummins, C. C.; Wilhelm, T.; Lin, S.; Reid, S. M.; Kol, M.; Davis, W. M. *Organometallics* **1996**, *15* (5), 1470-1476.

[113] Nugent, W. A.; Harlow, R. L. *J. Am. Chem. Soc.* **1994**, *116* (14), 6142-6148.

[114] Vennampalli, M.; Liang, G.; Webster, C. E.; Zhao, X. *Eur. J. Inorg. Chem.* **2014** (4), 715-721.

[115] Van der Made, A. W.; Van der Made, R. H. *J. Org. Chem.* **1993**, *58* (5), 1262-1263.

[116] Yamada, Y. M. A.; Sarkar, S. M.; Uozumi, Y. *J. Am. Chem. Soc.* **2012**, *134* (22), 9285-9290.

[117] Nasr-Esfahani, M.; Mohammadpoor-Baltork, I.; Khosropour, A. R.; Moghadam, M.; Mirkhani, V.; Tangestaninejad, S.; Amiri Rudbari, H. *J. Org. Chem.* **2014**, *79* (3), 1437-1443.

[118] Tavassoli, M.; Landarani-Isfahani, A.; Moghadam, M.; Tangestaninejad, S.; Mirkhani, V.; Mohammadpoor-Baltork, I. *ACS Sustainable Chemistry & Engineering* **2016**, *4* (3), 1454-1462.

[119] Albrecht, M. *Chem. Commun.* **2008** (31), 3601-3610.

[120] Yakelis, N. A.; Bergman, R. G. *Organometallics* **2005**, *24* (14), 3579-3581.

[121] Lin, I. J. B.; Vasam, C. S. *Coord. Chem. Rev.* **2007**, *251* (5), 642-670.

[122] Wang, H. M. J.; Lin, I. J. B. *Organometallics* **1998**, *17* (5), 972-975.

[123] Wang, H. A. J.; Vasam, C. S.; Tsai, T. Y. R.; Chen, S. H.; Chang, A. H. H.; Lin, I. J. B. *Organometallics* **2005**, *24* (4), 486-493.

[124] Lee, K. M.; Wang, H. M. J.; Lin, I. J. B. *J. Chem. Soc., Dalton Trans.* **2002** (14), 2852-2856.

[125] Lee, C. K.; Vasam, C. S.; Huang, T. W.; Wang, H. M. J.; Yang, R. Y.; Lee, C. S.; Lin, I. J. B. *Organometallics* **2006**, *25* (15), 3768-3775.

[126] de Frémont, P.; Scott, N. M.; Stevens, E. D.; Nolan, S. P. *Organometallics* **2005**, *24* (10), 2411-2418.

[127] Shen, H. C. *Tetrahedron* **2008**, *64* (34), 7847-7870.

[128] Manfred T., R.; Knut, S. *Eur. J. Org. Chem.* **2003**, *2003* (18), 3485-3496.

[129] Cristina, N. O.; Paz, M. M.; Elena, B.; Cristina, N.; J., C. D.; M., E. A. *Angew. Chem. Int. Ed.* **2004**, *43* (18), 2402-2406.

[130] Schmidbaur, H. *Gold Bulletin* **2000**, *33* (1), 3-10.

[131] Collins, C. L.; Dyall, K. G.; III, H. F. S. *J. Chem. Phys.* **1995**, *102* (5), 2024-2031.

[132] Cotton, F. A.; Feng, X.; Timmons, D. J. *Inorg. Chem.* **1998**, *37* (16), 4066-4069.

[133] Cotton, F. A.; Feng, X.; Matusz, M.; Poli, R. *J. Am. Chem. Soc.* **1988**, *110* (21), 7077-7083.

[134] Siemeling, U.; Vorfeld, U.; Neumann, B.; Stammler, H.-G. *Chem. Commun.* **1997** (18), 1723-1724.

[135] Jie-Peng, Z.; Yi-Bo, W.; Xiao-Chun, H.; Yan-Yong, L.; Xiao-Ming, C. *Chemistry – A European Journal* **2005**, *11* (2), 552-561.

[136] Pyykkö, P. *Chem. Rev.* **1997**, *97* (3), 597-636.

[137] Pekka, P. *Angew. Chem. Int. Ed.* **2004**, *43* (34), 4412-4456.

[138] D., K. R.; Guido, S.; Zhida, P.; F., M. M.; Gabriele, K. K. *Angew. Chem.* **2003**, *115* (7), 818-820.

[139] Chi-Ming, C.; Zhong, M.; M., M. V.; Man-Chung, T.; Chi-Keung, C.; Kung-Kai, C.; Lee, P. D.; King-Hung, L. *Angew. Chem. Int. Ed.* **2000**, *39* (22), 4084-4088.

[140] Satyachand, H. N. V.; Bo-Han, W.; Duan-Yen, L.; Ting-Shen, K.; I-Chia, C.; Yi-Chou, T. *Angew. Chem. Int. Ed.*, *0* (0).

[141] Fiorito, D.; Folliet, S.; Liu, Y.; Mazet, C. *ACS Catalysis* **2018**, *8* (2), 1392-1398.

[142] Tasker, S. Z.; Standley, E. A.; Jamison, T. F. *Nature* **2014**, *509* (7500), 299-309.

[143] David, R.; Yasuhiro, U. *Adv. Synth. Catal.* **2018**, *360* (4), 602-625.

[144] Molnár, Á. *Chem. Rev.* **2011**, *111* (3), 2251-2320.

[145] Hazari, N.; Melvin, P. R.; Beromi, M. M. *Nature Reviews Chemistry* **2017**, *1* 0025.

[146] Heck, R. F.; Nolley, J. P. *J. Org. Chem.* **1972**, *37* (14), 2320-2322.

[147] Frisch, A. C.; Zapf, A.; Briel, O.; Kayser, B.; Shaikh, N.; Beller, M. *J. Mol. Catal. A: Chem.* **2004**, *214* (2), 231-239.

[148] Dehimat, Z. I.; Yaşar, S.; Tebbani, D.; Özdemir, İ. *Inorg. Chim. Acta* **2018**, *469* 325-334.

[149] Wei, Y.; Petronilho, A.; Mueller-Bunz, H.; Albrecht, M. *Organometallics* **2014**, *33* (20), 5834-5844.

[150] Koszinowski, K.; Lissy, F. *Int. J. Mass spectrom.* **2013**, *354–355* 219-228.

[151] Fulmer, G. R.; Miller, A. J. M.; Sherden, N. H.; Gottlieb, H. E.; Nudelman, A.; Stoltz, B. M.; Bercaw, J. E.; Goldberg, K. I. *Organometallics* **2010**, *29* (9), 2176-2179.

[152] Kottke, T.; Stalke, D. *J. Appl. Crystallogr.* **1993**, *26* (4), 615-619.

[153] Kottke, T.; Stalke, D. *Angew. Chem. Int. Ed.* **1993**, *32* (4), 580-582.

[154] Kottke, T.; Lagow, R. J.; Stalke, D. *J. Appl. Crystallogr.* **1996**, *29* (4), 465-468.

[155] Schulz, T.; Meindl, K.; Leusser, D.; Stern, D.; Graf, J.; Michaelsen, C.; Ruf, M.; Sheldrick, G. M.; Stalke, D. *J. Appl. Crystallogr.* **2009**, *42* (5), 885-891.

[156] *APEX2 v2012/2*, Bruker AXS Inc.: Madison, USA, **2012**.

[157] *SAINT v8.30C*, Bruker AXS Inc.: Madison, USA, **2013**.

[158] Krause, L.; Herbst-Irmer, R.; Sheldrick, G. M.; Stalke, D. *J. Appl. Crystallogr.* **2015**, *48* (1), 3-10.

[159] Krause, L.; Herbst-Irmer, R.; Stalke, D. *J. Appl. Crystallogr.* **2015**, *48* (6), 1907-1913.

[160] Sheldrick, G. M., *XPREP in SHELXTL 2014/2*, USA, Madison, **2014**.

[161] Sheldrick, G. *Acta Crystallographica Section A* **2008**, *64* (1), 112-122.

[162] Hubschle, C. B.; Sheldrick, G. M.; Dittrich, B. *J. Appl. Crystallogr.* **2011**, *44* (6), 1281-1284.

[163] Sheldrick, G. M., *XP in SHELXTL v2008/2*, USA, Madison, **2008**.

ACKNOWLEDGEMENTS

Mein besonderer Dank gilt PROF. DR. DIETMAR STALKE für sein Vertrauen, die interessante Themenstellung, die stetige Hilfestellung bei zahlreichen technischen, wissenschaftlichen und sozialen Projekten, die gewährte wissenschaftliche Freiheit und die stetige Unterstützung während der gesamten Promotion.

Ebenso danke ich PROF. DR. SVEN SCHNEIDER für die Übernahmen des Korreferats und die gute wissenschaftliche Zusammenarbeit im Bereich der Kristallographie sowie die Unterstützung bei der Planung und Durchführung neuer Praktika.

PROF. DR. ULF DIEDERICHSEN, DR. FRANZISKA THOMAS, DR. CHRISTIAN SINDLINGER und DR. HEIDRUN SOWA, danke ich für Ihre Teilnahme an meiner Prüfungskommission.

Einen großen Beitrag zum Gelingen dieser Arbeit haben ebenso die folgenden Personen geleistet, denen ich auf diesem Wege danken möchte:

Bei den Angestellten der Feinmechanik-, Elektro- und Glaswerkstätten sowie den Hausmeistern des Instituts für Anorganische Chemie möchte ich mich besonders für die sehr gute Zusammenarbeit und vielseitige Unterstützung bei jeglichen technischen Projekten bedanken. Ein besonderer Dank gilt hier HA.JO. HEYMEL, BERND WICHMANN, BENJAMIN BOCK, MARIUSZ BURZYNSKI, HEIKO RENZIEHAUSEN, RAINER EHRHARDT, STEPHAN DULLNIG, ANNIKA VON RODEN, JOACHIM HILLE und UWE BECKMANN.

DR. REGINE HERBST-IRMER danke ich für ihre immerwährende Hilfe bei jeglichen kristallographischen Problemen sowie für die Weitergabe ihres umfangreichen Wissens in den vielfältigen Bereichen der Kristallographie.

Meinen Korrekturlesern ALEXANDER PAESCH, DR. FELIX ENGELHARDT, JOCHEN JUNG und DR. ULRIKE ROST für ihre konstruktiven Anmerkungen und Verbesserungen.

HEIKE TAPPE, MARTIN SCHLOTE und LAURA GARSKE möchte ich für ihre ausgezeichnete Organisation des Arbeitskreises, Bereitstellung von Chemikalien und Geräten sowie ihre anhaltende freundliche Hilfe im Laboralltag danken.

Meinem Laborpartner JOHANNES KRETSCH danke ich für die gelungene Arbeitsatmosphäre, die gegenseitige Unterstützung bei wissenschaftlichen Problemen und der Organisation und Durchführung des Praktikums für Materialwissenschaftler.

DR. SUSANN GRAUPNER gilt mein Dank für ihre stetige Unterstützung bei der Organisation der Grundvorlesung "Chemie für Landwirte" sowie dem Praktikum "Chemie für Studierende der Agrarwissenschaften". Darüber hinaus möchte ich ihr für ihre freundliche und motivierende Art danken und ihre Perspektive außerhalb der Fak. f. Chemie.

DR. DANIEL STERN möchte ich für die Zusammenarbeit und technische Unterstützung bei der Pflege und Wartung der Diffraktometer danken sowie der Schaffung anhaltender Kooperationen mit der Firma BRUKER.

Weiterhin danke ich den zahlreichen Kooperationspartner, Bachelorstudenten, Abteilungspraktikanten und Gaststudenten für die Zusammenarbeit und Unterstützung bei den verschiedenen Projekten und die große Freude daran. Genannt seien hier DR. NINA LOCK, NIKLAS FRERICHS, JOCHEN JUNG, JOHANNES KRETSCH, MIRCO WEBER, BASTIAN SCHLUSCHAß, BENJAMIN SCHMIDT, KATJA KOLOCAJ, ALEXANDER HECHT, MARTIN KLOOS, DR. ERANDI BERNABÉ-PABLO, LEONARDO ROJAS, DR. SUDIPTA ROY, DR. KARTIK CHANDRA MONDAL und DR. YAN LI.

Ein großer Dank gilt auch allen gegenwärtigen und ehemaligen Mitgliedern des Arbeitskreis STALKE für die stetige Unterstützung in allen Bereichen der wissenschaftlichen Arbeit, die freundliche und kollegiale Arbeitsatmosphäre als auch die vielen schönen Erlebnisse neben der wissenschaftlichen Arbeit.

Den Gründungsmitgliedern der Skedoches, ALEXANDER PAESCH und FELIX ENGELHARDT, danke ich für ihre Freundschaft, Hilfsbereitschaft und kreativen Pausen im Bastellabor. Das Experimentieren mit Glasfaser, Epoxidharz, Schnittgrößen und Oberflächenveredlung hat den Laboraltag deutlich aufgewertet. Die schönen Stunden beim Long-, Wake- und Kiteboarden möchte ich nicht missen.

Mein größter Dank gilt ULI für ihre immerwährende Liebe und Unterstützung in jeglicher Lebenslage. Mit der Geburt unserer Tochter LEONIE am 17.04.2017 hast du mir das größtmögliche Geschenk bereitet und ich freue mich gemeinsam mit dir die kleine Maus aufwachsen zu sehen.

Meiner gesamten Familie und im Besonderen meinen Eltern ANJA und KLAUS STOLLBERG danke ich für ihre stetige Unterstützung in allen Lebenslagen. Sich zu jedem Zeitpunkt auf die Hilfe und Unterstützung von euch verlassen zu können ist eine sehr große Bereicherung in meinem Leben.